UNIVERSITY OF OKLAHOMA

GRADUATE COLLEGE

A COMPREHENSIVE STUDY ON MOISTURE ABSORPTION OF THERMOSETTING POLYMERS, MICRO- AND NANOCOMPOSITES, AND FOAMS

A DISSERTATION

SUBMITTED TO THE GRADUATE FACULTY

in partial fulfillment of the requirements for the

Degree of

DOCTOR OF PHILOSOPHY

By

GORKEM EGEMEN GULOGLU
Norman, Oklahoma
2018

Downloaded from SHAREOK. Persistent Handle URL: https://hdl.handle.net/11244/316314

A COMPREHENSIVE STUDY ON MOISTURE ABSORPTION OF THERMOSETTING POLYMERS, MICRO- AND NANOCOMPOSITES, AND FOAMS

A DISSERTATION APPROVED FOR THE
SCHOOL OF AEROSPACE AND MECHANICAL ENGINEERING

BY

Dr. M. Cengiz Altan, Chair

Dr. Mrinal C. Saha

Dr. Zahed Siddique

Dr. Yingtao Liu

Dr. Shivakumar Raman

© Copyright by GORKEM EGEMEN GULOGLU 2018
All Rights Reserved.

I would like to dedicate this work to my family for all their support and motivation along the way.

Acknowledgements

First and foremost, I would like to express my deepest gratitude to my advisor, Dr. M. Cengiz Altan. His guidance, support, and encouragement from the first day made this research possible and allowed me to grow as a research scientist. I would also like to thank to my advisory committee, Dr. Mrinal C. Saha, Dr. Zahed Siddique, Dr. Yingtao Liu and Dr. Shivakumar Raman for their brilliant comments and suggestions.

A special thanks to my fellow researchers, Dr. Jacob Anderson, Dr. Levent Aktas, Dr. Orhan Ozcelik, Dr. Keith Hurdelbrink, Dr. M. Selim Demirtas, Dr. M. Akif Yalcinkaya, Dr. Youssef K. Hamidi, Dr. Hasan Baris Serce, Maya Pishvar and Mehrad Amirkhosravi for their support and help during my research. I would also like to express my gratitude to all of the AME faculty and staff especially to Mr. Billy Mays and Mr. Gregory Williams for their immense help at the machine shop.

Table of Contents

Acknowledgements……v

Table of Contents……...vi

List of Tables……x

List of Figures……...xii

Abstract……xix

Chapter 1. Introduction 1

1.1. Factors Effecting Liquid Absorption in Polymers and Polymer Composites 1

1.2. Adverse Effects of Liquid Penetrants on Polymers and Polymer Composites 4

i. Microstructural damage and changes induced by liquid absorption 4

ii. Reduction in thermomechanical properties.....5

1.3. Continuum Diffusion Models 7

i. Fickian Diffusion Model 8

ii. Langmuir-type Diffusion Model 9

iii. Anisotropic Diffusion Models 10

iv. Recovery of Diffusion Parameters 11

1.4. Effect of Inclusions and Voids on Diffusion Dynamics 13

1.5. Diffusion Dynamics in Closed-Cell Polymer Foams..... 16

Chapter 2. Moisture Absorption Modeling in Polymeric Composites..... 19

2.1. Fickian Diffusion Model..... 19

2.2. Langmuir-Type Diffusion Model 22

i. Effect of chemical interactions on moisture absorption kinetics 26

ii. Approximate Solutions.....31
iii. Non-dimensional Langmuir-type Diffusion Model.....32
2.3. Fickian and Non-Fickian Absorption in Polymers..... 33
2.4. Anisotropic Diffusion Models..... 37
i. Three-Dimensional Anisotropic Fickian Diffusion Model.....37
ii. Three-Dimensional Hindered Diffusion Model.....39
iii. Non-dimensional and Approximate Solution of 3D HDM.....47
2.5. Other Diffusion Models..... 48
i. Dual-Diffusivity Model.....48
ii. Time-Varying Diffusivity Model.....50
2.6. Model Parameter Recovery..... 51
i. Absorption parameters to be recovered.....53
2.7. Multilayer Hindered Diffusion Model..... 57
i. Initial and Boundary Conditions.....58
ii. Analytical Solution Procedure of Quadruple PDE of Multilayer Hindered Diffusion Model 60
2.8. Porous Media Diffusion Models..... 65
Chapter 3. Effects of Micro- and Nano-Filler Addition to Thermosetting Polymers on Moisture Absorption..... 68
3.1. Effect of Different Filler Content in Epoxy..... 71
i. Materials and Sample Preparation of I.30E Nanoclay/DGEBA Epoxy.....71
ii. Experimental Results of I.30E Nanoclay/DGEBA Epoxy and Discussion 71
iii. Materials and Sample Preparation of I.30E Nanoclay/EPON 862 Epoxy.....80

iv. Experimental Results of I.30E/EPON 862 and Discussion.....81
v. Effect of resin type on the molecular interactions between water molecules and epoxy 87
3.2. Effects of Interfaces and Filler Types..... 89
i. Materials and Sample Preparation of APS/DGEBA Epoxy and nBS/DGEBA Epoxy89
ii.Experimental Results of APS/DGEBA Epoxy and nBS/DGEBA Epoxy and Discussion 90
3.3. Hollow Micro Glass Sphere/Epoxy Composite Layer on Neat Epoxy..... 100
i. Materials and Sample Preparation of Micro Glass Sphere/EPON 862-EPON 862 Multilayer Composite.....101
ii. Moisture Absorption Test Results of Micro Glass Sphere/EPON 862-EPON 862 Multilayer Composite and Validation of Multilayer Absorption Model 103
3.4. Conclusion 112
Chapter 4. Moisture Absorption Modeling of Highly Porous Polymers and Polymer Composites 115
4.1. Void Filling Hindered Diffusion Model Development..... 116
4.2. Void Filling Hindered Diffusion Model Validation 122
i. Materials and Sample Preparation of Rohacell Closed-Cell Structural Foam.....123
ii. Characterization of as-received and heat treated foams.....124
4.3. Moisture Absorption into Foams 132
4.4. Foam Core Sandwich Composites..... 147
i. Materials and Sample Preparation of Rohacell Closed-Cell Structural Foam Core Sandwich Composite.....147

ii. Moisture Absorption into Foam Core Sandwich Composites.....147
4.5. Conclusion 149
Chapter 5. Effect of Moisture Absorption on Mechanical Properties of Polymer and Polymer Composites 153
5.1. Mechanical Property Loss due to Moisture Ingress..... 154
5.2. Moisture Absorption and Flexure Modulus Correlation Models..... 157
i. Reimschussell's glass transition temperature model.....157
ii. H-Bond dissociation model.....158
iii. Multiscale–Multiphysics computational model.....159
5.3. Concentration Dependent Modulus Model: Theory Development..... 160
i. Materials and Sample Preparation.....161
ii. EPON 862 moisture absorption results.....162
5.4. Concentration Dependent Modulus Model: Model Development..... 168
i. Tensile Modulus.....169
ii. Flexural Modulus.....169
5.5. Concentration Dependent Modulus Model: Validation..... 170
5.6. Conclusion 180
Chapter 6. Concluding Remarks 182
6.1. Research Proposals 188

List of Tables

Table 1. Absorption parameters of the concentration profiles in Figure 12. 45

Table 2. Diffusion parameters of the synthetic data, initial guess, and model prediction 54

Table 3. Moisture absorption parameters of DGEBA epoxy with different clay loading. 72

Table 4. Moisture absorption parameters of DGEBA epoxy with different clay loading (Change in $\boldsymbol{Dz}$ follows the rule of mixture)..... 73

Table 5. One-dimensional hindered diffusion moisture absorption parameters of EPON 862 epoxy with different clay loading where diffusion coefficient kept linearly decreasing.. 82

Table 6. Moisture absorption parameters of DGEBA epoxy with different APS treated glass loading where diffusion coefficient kept linearly decreasing. 92

Table 7. Moisture absorption parameters of DGEBA epoxy with different nBS treated glass loading where diffusion coefficient kept linearly decreasing. 94

Table 8. Moisture absorption parameters of glass sphere/epoxy layer and neat epoxy layer. 105

Table 9. Moisture absorption parameters of dispersed 21% and 40% vol. glass sphere/epoxy laminates 108

Table 10. Sample Dimensions and Abbreviations of Rohacell Foams..... 124

Table 11. VFHDM absorption parameters for untreated and heat treated Rohacell foams 134

Table 12. Diffusion rate comparison between heat treated under 50 psi, 30 psi and as-received foams 136

Table 13. 1DHDM absorption parameters of EPON 862 at different relative humidity 163

Table 14. Fiber contents and matrix type of the samples[154]..... 176

Table 15. Absorption parameters of polymers used to validate the elastic modulus models 204

List of Figures

Figure 1. Typical Fickian moisture uptake curve. 21

Figure 2. Typical Langmuir-type moisture uptake curve showing bound, unbound and total mass gain. 25

Figure 3. The effect of change in $\boldsymbol{\beta}$, rate of bound molecule to become unbound, on moisture absorption. 27

Figure 4. The effect of change in $\boldsymbol{\beta}$, rate of bound molecule to become unbound, on bound and unbound moisture absorption 28

Figure 5. The effect of change in $\boldsymbol{\gamma}$, rate of unbound molecule to become bound, on moisture absorption 29

Figure 6. The effect of change in $\boldsymbol{\gamma}$, rate of unbound molecule to become bound, on bound and unbound moisture absorption 30

Figure 7. Effect of rate of conversion (bound⇔unbound) on time to reach the equilibrium for the same hindrance coefficient (μ=0.143). 31

Figure 8. Experimental moisture absorption data of quartz/epoxy composite laminate of 6 months, Fickian and hindered diffusion model predictions 34

Figure 9. Experimental moisture absorption data of quartz/epoxy composite laminate of 3 years, Fickian and hindered diffusion model predictions 35

Figure 10. Comparison between the first and second predictions of Fickian and hindered diffusion model 36

Figure 11. The representative figure for finite slab and the three-dimensional Fickian model geometry. 38

Figure 12. Concentration profile of anisotropic, isotropic, and one-dimensional quartz/BMI laminate at t=96, 384, and 864 days 46

Figure 13. Two stages of dual diffusivity model on non-Fickian mass gain 49

Figure 14. Absorption parameter recovery from thermo-gravimetric synthetic data. 55

Figure 15. Variation in the least square error per data point during absorption parameter recovery 56

Figure 16. The representation of the model geometry (a) for a single coating layer of thickness $\boldsymbol{a}$. The total sample thickness is $\boldsymbol{b}$. (b) for a symmetric coating layer of thickness a. The total sample thickness is $\boldsymbol{2b}$ 58

Figure 17. Representative volume element of porous media 66

Figure 18. Linear change of diffusion coefficients with nanoclay volume fraction 73

Figure 19. Clay loading effect on moisture absorption of I.30E nanoclay/DGEBA epoxy composite. 74

Figure 20. Effect of nanoclay loading in DGEBA epoxy on hindrance coefficient. 75

Figure 21. Effect of nanoclay loading in DGEBA epoxy on maximum moisture content. 76

Figure 22. Total, unbound, and bound moisture absorption of 2 wt.% I.30E/DGEBA composite 78

Figure 23. Effect of nanoclay loading in DGEBA epoxy on maximum unbound moisture content. 78

Figure 24. Effect of nanoclay loading in DGEBA epoxy on maximum bound moisture content. 79

Figure 25. Linear change of diffusion coefficients of I.30E/EPON862 composite with nanoclay volume fraction..... 82
Figure 26. Clay loading effect on moisture absorption of I.30E nanoclay/EPON 862 epoxy composite and the hindered diffusion fit while keeping the diffusion coefficient constant. 83
Figure 27. Effect of nanoclay loading in EPON 862 epoxy on hindrance coefficient. 84
Figure 28. Effect of nanoclay loading in EPON 862 epoxy on maximum moisture content. 85
Figure 29. Effect of nanoclay loading in EPON 862 epoxy on maximum unbound moisture content..... 86
Figure 30. Effect of nanoclay loading in EPON 862 epoxy on maximum bound moisture content..... 87
Figure 31. Schematics of a) Bisphenol-A and b) Bisphenol-F 87
Figure 32. Linear change of diffusion coefficients of APS glass/DGEBA and nBS glass/DGEBA composite with glass volume fraction..... 91
Figure 33. APS glass sphere loading effect on moisture absorption of DGEBA epoxy and the hindered diffusion recovery while keeping the diffusion coefficient linearly decreasing. 93
Figure 34. nBS glass sphere loading effect on moisture absorption of DGEBA epoxy and the hindered diffusion recovery while keeping the diffusion coefficient linearly decreasing. 95
Figure 35. Effect of APS and nBS glass sphere loading in DGEBA epoxy on hindrance coefficient. 96

Figure 36. Effect of APS and nBS glass sphere loading in DGEBA epoxy on maximum moisture content. 97

Figure 37. Effect of APS and nBS glass sphere loading in DGEBA epoxy on maximum unbound moisture content. 98

Figure 38. Effect of APS and nBS glass sphere loading in DGEBA epoxy on maximum bound moisture content. 99

Figure 39. 2D chemical representation of a) APS, aminopropyltrimethoxysilane and b) nBS, n-butyltrimethoxysilane. 100

Figure 40. Representative SEM image of glass spheres *a)* as received *b)* sieved. 102

Figure 41. Hollow glass sphere size distribution. 102

Figure 42. *a)* Optical microscopy image of 6 immersion samples showing multilayer of 31% thick glass sphere/epoxy, and 69% thick epoxy *b)* a representative SEM image of a sample. 104

Figure 43. *a)* Optical microscopy image of 5 immersion samples showing multilayer of 57% thick glass sphere/epoxy, and 43% thick epoxy *b)* a representative SEM image of a sample. 104

Figure 44. *a)* Optical microscopy image of 6 immersion samples of 100% thick glass sphere/epoxy *b)* a representative SEM image of a sample. 104

Figure 45. Experimental mass uptake data of 31%, 57%, and 100% thick glass sphere/epoxy layer-epoxy multilayer laminates and multilayer hindered diffusion model predictions. 106

Figure 46. Multilayer HDM and 1D HDM predictions of 1mm thick 21% and 40% vol. glass sphere/epoxy layer-epoxy multilayer laminates and dispersed 21% and 40% vol. glass sphere/epoxy laminates, respectively..... 109

Figure 47. Concentration profiles of *a)* 31% thick glass sphere/epoxy layer-epoxy multilayer composite (21% vol. glass sphere), *b)* 57% thick glass sphere/epoxy layer-epoxy multilayer composite (40% vol. glass sphere), *c)* dispersed 21% vol. glass sphere/epoxy composite, and *d)* dispersed 40% vol. glass sphere/epoxy composite after 10 days of fully saturation..... 111

Figure 48. Illustration of the proposed moisture absorption and desorption mechanism of voids..... 117

Figure 49. Representative 2D solid slab having *a)* no void *b)* void with a volume of $\boldsymbol{Vv}$ 118

Figure 50. Moisture desorption steps in a representative water filled void..... 120

Figure 51. ROHACELL® WF-71 Foam 122

Figure 52. Measured densities of untreated and heat treated Rohacell foams..... 125

Figure 53. Representative SEM images of foam samples - as-received *a)* 3mm *b)* 6mm *c)* 9mm 127

Figure 54. Representative SEM images of foam samples – heat treated under 30 psi *a)* 3mm *b)* 6mm *c)* 9mm..... 128

Figure 55. Representative SEM images of foam samples – heat treated under 50 psi *a)* 3mm *b)* 6mm *c)* 9mm..... 129

Figure 56. Average cell sizes of as-received and heat treated Rohacell foams 130

Figure 57. %Porosity of untreated and heat treated Rohacell foams (Calculated from density measurements). 131
Figure 58. %Porosity of untreated and heat treated Rohacell foams (Image Analysis). 131
Figure 59. Moisture uptake mass gain data of foams: *a)* as-received *b)* heat treated under 30 psi *c)* heat treated under 50 psi 133
Figure 60. Mass gain data and VFHDM predictions of 3mm, 6mm, and 9mm as-received Rohacell foams. 137
Figure 61. VFHDM predictions of *a)* unbound *b)* bound and *c)* trapped moisture absorption into as-received Rohacell foams. 139
Figure 62. Mass gain data and VFHDM predictions of 3mm, 6mm, and 9mm Rohacell foams heat treated under 30 psi. 140
Figure 63. VFHDM predictions of *a)* unbound *b)* bound and *c)* trapped moisture absorption into Rohacell foams heat treated under 30 psi. 142
Figure 64. Mass gain data and VFHDM predictions of 3mm, 6mm, and 9mm Rohacell foams heat treated under 50 psi. 144
Figure 65. VFHDM predictions of *a)* unbound *b)* bound and *c)* trapped moisture absorption into Rohacell foams heat treated under 50 psi 146
Figure 66. Mass gain data of Rohacell foam core sandwich composite manufactured under 30 psi pressure 148
Figure 67. Mass gain data of Rohacell foam core sandwich composite manufactured under 50 psi pressure 149
Figure 68. Mass gain data and 1DHDM predictions of EPON 862 at Different Relative Humidity 164

Figure 69. Change of diffusion coefficients with relative humidity 164
Figure 70. Change in maximum moisture content with relative humidity 165
Figure 71. Change in *a)*the rate of bound molecule to become unbound *b)*the rate of unbound molecule to become bound *c)*hindrance coefficient with relative humidity 166
Figure 72. Flexural modulus of samples conditioned at different relative humidity levels 167
Figure 73. The correlation between the flexural modulus and maximum moisture content 168
Figure 74. Maximum moisture content of samples conditioned at 20%, 50% and 80% relative humidity on the mass uptake cure of immersed samples 171
Figure 75. Comparison between the transient and saturation moisture concentration ... 173
Figure 76. Comparison between the modulus distribution during moisture absorption and at corresponding saturation level 173
Figure 77. Variation in elastic modulus and mass gain due to moisture absorption into EPON 862 174
Figure 78. Variation in elastic modulus and mass gain due to moisture absorption into polyamide-6.6 175
Figure 79. Mass gain data and 1DHDM predictions of BFRP and BGRP samples. 177
Figure 80. Transient elastic modulus data and model prediction of BFRP and BGRP composites..... 178
Figure 81. Variation in elastic modulus and mass gain due to moisture absorption into nylon 6 179

Abstract

Molecular diffusion is the transfer or movement of individual molecules through a fluid or a solid by means of random, individual movements of the molecules. Even though moisture can diffuse into all materials above the absolute zero temperature, polymers are particularly susceptible to moisture ingress in highly humid environments. Fickian or non-Fickian diffusion models have often been utilized to characterize the effect of moisture absorption. Type, orientation, and homogeneity of reinforcement and type, microstructure, and dimensions of polymer control the effectiveness of each model on describing the moisture absorption dynamics.

In Chapter 3 of this dissertation, effects of additive content in I.30E nanoclay/DGEBA epoxy and I.30E nanoclay/DGEBF epoxy (EPON 862) nanocomposites, and APS or nBS treated glass sphere/DGEBA epoxy composites are investigated using moisture absorption data and one-dimensional hindered diffusion model. Impermeable additives in epoxy resulted in a linear decrease in diffusion coefficient with respect to the additive content following the rule of mixture. Impermeable additives also caused a linear decrease in the maximum moisture content of the composites. I.30E nanoclay addition into DGEBA epoxy lead to a more-Fickian absorption whereas increasing additive content in I.30E nanoclay/DGEBF epoxy (EPON 862) nanocomposite, and APS or nBS treated glass sphere/DGEBA epoxy composites shifted the absorption behavior to a more non-Fickian behavior.

In Chapter 3, capabilities of multilayer hindered diffusion model, a modified version of hindered diffusion model considering the discrete change in absorption properties, are tested by using the moisture absorption mass gain data of hollow glass sphere/EPON 862-

EPON 862 multilayer composites. It was shown that the multilayer hindered diffusion model accurately recovered the absorption behavior of multilayer composites having different layer thicknesses.

In Chapter 4, hindered diffusion model was extended to a new *void filling* hindered diffusion model to illustrate the effect of porosity and microstructure on moisture absorption. Moisture absorption tests on ROHACELL® WF-71 closed-cell foam showed up to 62% change in the maximum absorbed moisture due to the effect of thickness of the foam. Thickness of closed-cell foams changes the foam porosity by the open-cells on the surface to the closed-cell ratio. The distinct absorption behaviors due to the thickness of foams are accurately predicted by the void filling hindered diffusion model by defining the moisture absorbed by the pores as trapped moisture. Effects of heat treatment and pressure on moisture absorption behavior of foams are also investigated. Results of void filling hindered diffusion model predictions are found to be consistent with the experimental observation such as decrease in cell size, porosity, and thickness.

Moisture induced damage such as swelling, micro cracks, delamination, residual stresses, and plasticization of the polymer limit the intended design life due to subsequent electrical, optical, thermal, and mechanical property changes. In Chapter 5, a new comprehensive modulus degradation model where the modulus varies inversely linear with the moisture concentration is introduced and validated by experimental data of tensile or flexural modulus and moisture absorption from three different published studies.

Chapter 1. Introduction

Thermal motion of all fluid particles above absolute zero is called molecular diffusion. Diffusion helps to define the flow of particles from a low concentration medium to high concentration one when there is a concentration difference between systems. When the concentration gradient between the systems is zero, diffusion is reduced to self-diffusion which is random molecular motion (Brownian motion) where the net flux is zero. In this case, the penetrating molecules are uniformly distributed in the medium and the system is in equilibrium. The rate of movement of fluid particles depends on the viscosity of the fluid, temperature and molecular size of the particles. Thus, penetrating molecules and environmental conditions result in distinctive molecular diffusion for each medium.

1.1. Factors Effecting Liquid Absorption in Polymers and Polymer Composites

Polymers and polymer composites are well-known for their susceptibility to absorb different types of liquids due to their organic molecular structure. Water molecules are one of the smallest and readily available liquid penetrant. Utilization of polymers in wet and humid environment results in water absorption into the various polymers, ranging from 0.1 wt.% to more than 1000 wt.% [1–18]. A number of researchers have reported the amount of moisture absorption by such polymers and their composites over long periods of time. In many cases, the test samples are exposed to a humid environment or immersed into water until the maximum amount of water intake is achieved for that particular material. Popineau et al. [10] reported that EC2216 epoxy resin absorbs 8.9-10.2 wt.% moisture in equilibrium. A long-term study is recently published by Grace [19], where he investigated the moisture absorption behavior of quartz/BMI composite laminates. It was reported that

6-ply, 12-ply, and 40-ply quartz/BMI composites absorbed 1.7 wt.%, 1.7 wt.%, and 1.8 wt.% moisture in 5 years. Joliff et al. [20] studied the molecular diffusion kinetics of water molecules into DGEBA epoxy and glass/epoxy composite. The researchers stated that resin absorbed 2.3 wt.% water whereas the composite absorbed 0.6 wt.% water at full saturation (i.e., absorption equilibrium).

In addition to susceptibility to water, polymers are also known to absorb different types of liquids such as alcohol, hydraulic fluid, and anti-icing fluid. Scott and Lees [14] investigated the absorption of water, salt water, and alkaline solution into thin EPR4434/EPH943 epoxy plates. Salt water absorption and alkaline solution absorption are reported to be almost identical at 20℃. The epoxy plates absorbed 3.9 wt.% saltwater in 500 days. In addition, they reported that the epoxy plates absorbed 4% more water than alkaline solution and salt water. Helmroth et al. [21], reported that LDPE absorbs almost 30% of cyclohexane, 14% of n-heptane, and 12% of isooctane by weight in 32 hours at 40℃. Absorption of other types of liquids such as No. 2 diesel fuel [15,22], jet fuel [15,22,23], de-icing fluid [22,23], hydraulic fluid [23], and aviation oil [15,22] were also investigated. It is observed that each penetrant/medium pair has distinctive diffusion kinetics.

The medium that the molecules are diffusing into also affects the absorption kinetics. Dana et al. [16] reported that ortho-phtalic polyester resin absorbs 0.73 wt.% of moisture at 23℃ and 80% RH, whereas addition of 53% and 41% E-glass fibers by volume into the matrix lead to decrease in absorbed moisture by 59% and 72%, respectively. Moreover, Dhakal et al. [17] investigated the effect of fiber type in bio-based epoxy resin (Super Sap TM100/1000) to illustrate the change in moisture absorption due to modification of the

resin. Addition of flux, jute, and glass fiber into bio-based epoxy matrix resulted in 9.6%, 14.41% and 0.99% moisture absorption by weight, respectively. Other researchers also experimented on moisture absorption into various mediums such as vinyl ester [3,18], nylon 6 [4], polyester [5], polypropylene [6–8] and reported distinct moisture absorption kinetics.

Furthermore, diffusion is influenced by the environmental effects as well. Relative humidity and temperature are among the most important and influential environmental effects. Jia et al. [4] researched on the moisture absorption kinetics of nylon 6 in various temperatures and relative humidity. They reported that fully immersed nylon 6 absorbs 8.9 wt.% water at 100℃ whereas only 1.4 wt.% at 23℃ in 11 hrs. Moreover, Jia et al. also investigated the effect of relative humidity on moisture absorption into the nylon 6 and reported that fully immersed samples absorbed 11.0% water by weight while samples kept at 50% relative humidity absorbed only 1.5% water by weight in 1050 hrs. Yu et al. [9] also state that carbon fiber reinforced vinyl ester composite absorbs 1.05 wt.% water at 95℃ as it only absorbs 0.77 wt.% water at 65℃. Loos and Springer [15] presented results of absorption of 4 different liquids — distilled water, a saturated salt water solution, No. 2 diesel fuel, jet A fuel, and aviation oil — into three different commonly used graphite/epoxy composites. They showed that the diffusivity decreases with decreasing conditioning temperature and maximum moisture content increases with increasing relative humidity for all cases. Test temperature affects the kinetic energy of the penetrating particle which in turn influence the diffusion rate and the amount of molecule that can diffuse into the medium. Furthermore, increasing relative humidity causes an increase in the number of penetrating molecules (concentration) to diffuse into the medium. Increasing

the amount of penetrating molecules in contact with the available surface of the medium, escalates the flux resulting in faster diffusion.

Many factors affect the absorption kinetics of polymers. Knowing that the liquid absorption causes damages on the medium, diverse absorption kinetics will result in different type and level of degradation on the polymer. Degree and type of the damage depend on the amount of moisture absorbed, penetrating liquid and the polymer.

1.2. Adverse Effects of Liquid Penetrants on Polymers and Polymer Composites

i. Microstructural damage and changes induced by liquid absorption

Due to their high performance, polymer composites have been gaining wide industrial use in commercial, military, and space applications [24,25]. Moisture susceptibility of polymers lead researchers to investigate the moisture induced degradation in polymer and polymer composites. Microstructural changes due to moisture absorption results in plasticization of the polymer, swelling, and residual stresses [11,26–31].

Visco et al. [31] investigated the degradation effects of seawater on polyester and vinyl ester and reported that the seawater causes microcracks and voids in polyester and marine salt deposition in vinyl ester. Sugita et al. [27] immersed carbon fiber (10 ply T300 plain weave) reinforced epoxy (Proset 117 LV/Proset 237) composite into water, anti-icing solution, jet fuel, and hydraulic fluid and reported that the composite swell by absorption of all the liquid investigated. Additionally, composites absorbing anti-icing solution started to swell earlier than the others and broke into pieces in 5000 hours. Akil et al. [28] stated that water immersion into jute/glass fiber reinforced hybrid composites plasticizes and changes the mechanical properties of the resin matrix. In addition, the researchers observed degradation of the fiber/matrix interface and jute fibers, swelling of jute fibers and stress

corrosion on the glass fibers due to water ingress. Adhikary et al. [29] investigated the long-term water absorption and swelling properties of wood flour filled recycled/virgin polyolefin composites. They observed increasing swelling with increasing equilibrium moisture content in the composite. Similarly, Hu et al. [11] investigated the moisture induced damage in used jute fiber reinforced polyactide composite. The researchers observed pore formation on the surface after 4 days, microcracks along the fibers after 5 days, and swelling and delamination after 6 days of moisture absorption.

Absorption of liquid in polymers and composites causes changes in the microstructure. These microstructural changes result in mechanical damages and property loss in the material. Mechanical property loss due to liquid absorption limits the design and use of composites in environmentally harsh conditions.

ii. Reduction in thermomechanical properties

The mechanical integrity of polymers has been well-known to suffer significantly when exposed to moisture [32–34], to which they are typically exposed during their service life. Selzer and Friedrich [35], among many others, showed that the tensile strength of polymers is degraded by 52% to 66% by the absorption of moisture. Perez-Pacheco et al. [32] reported that 0.75 wt.% moisture absorption resulted in reduction of the tensile strength, elastic modulus, and interfacial shear strength of a carbon/epoxy composite by 25%, 38%, and 11%, respectively. Pomies and Carlsson [36] stated that 1.21% absorbed water in carbon/epoxy and 0.63% absorbed water in carbon/BMI-resin reduced the transverse tensile strength by 66% and 41%, respectively. They also stated that the transverse tensile strength of glass/epoxy with 1.08 wt.% water and glass/PPS with 0.18 wt.% water are reduced by 45% and 86%, respectively. Additionally, microstructural changes in jute fiber

reinforced polyactide composite due to water ingress resulted in 75% reduction in the tensile strength of the composite [11].

In a recently published article, Regazzi et al. [37] investigated the mechanical property degradation in PLA bio-resin and flax/PLA bio-composite due to moisture absorption. PLA and PLA composites were subjected to various environmental condition until saturation which resulted in distinctive saturation moisture contents for each condition. Their results showed that the elastic modulus decreases by increasing the saturation moisture content. The researchers also studied the change in elastic modulus during the moisture absorption. They reported that elastic modulus exponentially decreases to an asymptotical value in transient moisture absorption. Likewise, experiments on carbon fiber/epoxy composites by Perez-Pacheco et al. [32] showed that elastic modulus, tensile strength, interlaminar sheer strength, and glass transition temperature rapidly drop and slowly reach to an equilibrium when exposed to moisture. Initial fast water uptake in polymers results in high moisture concentration at the edges decreasing towards the mid-plane. Higher water concentration at the edges and surfaces results in greater degradation in those areas and resulting in fast drop in overall mechanical properties. Likewise, researchers [4,38] also showed that both elastic modulus and tensile strength of thermoplastics nylon 6 and polyamide-6.6 decrease fast and gradually reach an equilibrium.

Knowing that absorbed moisture degrades the polymer, researchers investigated transient hygro-elastic behavior of polymers. Peret et al. [39] modeled composite matrix and use finite element methods to solve uncoupled mechanical-water diffusion boundary problems. In addition, Reimschuessel [40] reported an exponential decrease of the glass transition temperature to an asymptotic value. An analytical model was also developed,

showing the change in glass transition temperature as a function of water content in the polymer. A relation between the glass transition temperature and the elastic modulus was established to successfully predict the property loss in glass transition temperature and elastic modulus due to water ingress.

Consequently, preventing in-service failure of structures with polymer composite parts would require their moisture absorption behavior to be fully characterized prior to the design phase. Such accurate characterization can enable a wider usage of polymer composites in structural components. Once, the moisture absorption behavior of thermoset is characterized, one can predict moisture concentration within components with any geometry at all times under a given hygrothermal loading. In turn, the concentration profiles can be used to evaluate the induced alteration of physical and electrical properties [37,39,41]. A novel method to predict the transient elastic modulus degradation behavior using known diffusion models has been introduced in Chapter 5.

1.3. Continuum Diffusion Models

Environmental conditions experienced by polymers during their service life often consist of large variations of humidity and temperature over long periods of time. The deleterious effects of moisture on the mechanical behavior and durability of polymers and polymer composites underscore the need to accurately predict absorption behavior and moisture content, especially for structural load-bearing applications designed for long service life.

i. Fickian Diffusion Model

The one-dimensional Fickian diffusion model is most often used for predicting absorption behavior and moisture content due to its simplicity and mathematical tractability [42]. Adolf Fick described the diffusion process as the flux goes from high concentration region to low concentration region under the assumption of steady state flow. He proposed that the magnitude of the flux is proportional to the concentration gradient. Fick derived his famous Fick's second law, which is the rate of accumulation of concentration within the volume as proportional to the local curvature of the concentration gradient, using the flux-concentration proportion and continuity equation, assuming no chemical interactions. Some researchers successfully applied Fickian diffusion model to various polymers and polymer composites [2,43–48].

Although a primarily Fickian diffusion is often observed during the initial moisture uptake, most polymeric materials, in the long-term, exhibit a non-Fickian absorption behavior [49–55]. This non-Fickian behavior, also referred to as anomalous or hindered diffusion, is frequently observed after a pseudo equilibrium, where the high initial slope of moisture uptake is substantially reduced. Moreover, polymers may exhibit Fickian or non-Fickian behaviors at different temperatures, and/or when they are exposed to different hygrothermal history [56]. It is worth noting here that the common practice for absorption characterization is to adhere to the ASTM standard, which is based on the Fickian diffusion model. However, a priori assumption of Fickian behavior may lead to: (a) premature termination of the thermogravimetric absorption experiments, (b) missing the non-Fickian behavior which often becomes apparent in the long-term absorption experiments, and (c)

inaccurate estimates of the maximum moisture absorption, which is critical in determining the reduction of thermomechanical properties.

Recognizing the limitations of Fickian theory, several researchers have proposed different models for moisture absorption, in order to account for the anomalous, or hindered diffusion behavior. These models include time-varying diffusion coefficient models [49]; two-phase polymer dual-diffusivity models, also known as Jacobs-Jones models [50,51]; coupled diffusion-relaxation models [52,53]; as well as dual-mode sorption models, referred to as the Langmuir-type or hindered diffusion models [54,55,57] and will be further discussed in Chapter 2.

ii. Langmuir-type Diffusion Model

Langmuir-type diffusion model is based on the assumption that moisture absorption in polymeric materials is partially related to the availability of molecular-sized interstice in the polymer structure and the polymer-water affinity. The availability of interstice, or free volume, within the polymer depends on its molecular structure, microstructural morphology and crosslink density [58]. Polymer-water affinity, on the other hand, is related to the availability of certain hydrophilic functional groups such as hydroxyl or amine within polymer chains. Part of the absorbed water molecules would be inclined to strongly couple with polar groups or hydrogen bonding sites within the polymer. These molecules would cease to be a part of the ongoing diffusion and are often considered as bound, or immobile. On the other hand, water molecules that are free to move through the interstice are often called unbound, or mobile. Presence of other storage sites for moisture such as fiber-matrix interphase or micro- and nano-scale voids may also be considered as part of the bound, immobile moisture from a phenomenological perspective.

In thermogravimetric experiments of polymeric materials, Fickian diffusion dominated initial fast moisture uptake is often followed by a slower absorption rate, where the diffusion is hindered by the increase in bound water molecules. The time required to reach moisture equilibrium can be considerably delayed and depends on the exchange rates between the bound and unbound water. The difference in these rates can describe a vast range of absorption behavior in two distinct time scales and can be accurately captured by the hindered diffusion model.

iii. Anisotropic Diffusion Models

Although useful in characterizing accurately the absorption behavior of isotropic polymers, neither the Langmuir model nor any other one-dimensional diffusion model account for anisotropy or edge effects. Fiber reinforced composite materials, on the other hand, often exhibit pronounced anisotropy. For instance, the diffusion rate of moisture absorption along the fiber/matrix interphase in glass-reinforced polymers has been reported to be about 450 times greater than that through the thickness [59]. Planar diffusivities of woven carbon/epoxy composites are also reported to be 2- to 4-fold higher than through-thickness diffusivity [60]. In addition, it may not be possible to obtain accurate diffusion coefficients from methods based on a one-dimensional characterization due to the errors associated with sample anisotropy [61]. Therefore, using one-dimensional isotropic models could yield distorted characterization of their absorption kinetics if the material is highly anisotropic.

A number of researchers attempted to prevent these potential characterization inaccuracies in moisture absorption models. For Fickian absorption behaviors, Aktas et al. [61] offered a technique to account for edge effect and anisotropy based on the three-

dimensional Fickian model. For non-Fickian absorption behaviors in anisotropic polymeric materials, on the other hand, Grace and Altan [55] recently proposed a three-dimensional Hindered Diffusion Model (3D HDM). Building on the established Langmuir framework, the HDM offers the possibility to describe both three-dimensional anisotropic diffusion and the interactions between water molecules and polymer chains. In addition, the 3D HDM can be simplified to the Langmuir model in one-dimensional cases. In addition, Grace and Altan [55] developed an approximate solution to the 3D HDM. A five-year validation study showed that the hindered diffusion model parameters recovered from two-year long absorption experiments allowed accurate prediction of five-year absorption behavior of 6-, 12-, and 40-ply, quartz/BMI composites [19]. An approximate analytical solution derived by Grace and Altan [57] can predict the comprehensive, anomalous liquid absorption behavior when $2\gamma, 2\beta \ll K$. More recently, exact analytical solution for three-dimensional hindered diffusion model is developed by Guloglu et al. [62] and will be further discussed later in Chapter 2.

iv. Recovery of Diffusion Parameters

The characterization of the absorption behavior of a specific polymeric material by using any one of the models mentioned earlier would require experimental identification of a set of material properties, generally referred to as diffusion or absorption parameters. For Fickian diffusion, Shen and Springer [43] suggests that the approximate diffusion coefficient can be obtained rapidly from the experimental data by using the saturation moisture content and the initial slope of the percent mass gain vs. square root of time curve. The disadvantage of this method is determination of the initial slope and maximum moisture content can be misleading. In a comparative study, Glaskova et al. [63]

investigated the effectiveness of these models in representing the non-Fickian behavior of an epoxy system. The authors reported the Langmuir model to be particularly effective. Other researchers [2,10,14,19,20,55,57,64–67] also found the one-dimensional hindered diffusion model to better describe the anomalous deviation from a Fickian behavior, and has demonstrated the ability to successfully predict both short- and long-term moisture absorption in polymeric materials.

Carter and Kibler [54] developed an exact analytical solution of the one-dimensional hindered diffusion model (1D HDM). They also proposed an approximate analytical solution and two "useful" approximate solutions for two distinct regions of the moisture uptake curve: (a) for the initial absorption region, and (b) for the long term absorption region. Because of their relative simplicity compared to the exact solution, the majority of researchers have used these "useful" approximate solutions to recover the absorption parameters [2,3,14,20,23,64,65,68–70]. However, the approximate solutions of the 1D HDM are valid only under certain conditions. In addition, the procedure suggested by Carter and Kibler [54] to recover the absorption parameters, explicitly summarized by other authors [20], can be inaccurate and lead to incorrect characterization of the absorption. For example, if the final thermogravimetric data point (i.e., last weight gain data) is used as the maximum moisture intake as suggested [20], any additional moisture absorption cannot be accounted for. Consequently, premature termination of absorption experiments will be detrimental to the accurate characterization of all absorption parameters, including erroneously reporting a much lower value for the maximum moisture absorption. Instead, the maximum moisture absorption should be left as an unknown parameter and obtained

from the theoretical model parameters that yield the best match to the experimental data [57].

It needs to be emphasized that very few researchers have used the exact solution of the hindered diffusion model — or any other Fickian and non-Fickian model — to characterize the absorption behavior [62,66]. This might be due to the mathematical difficulty and considerable computational effort involved in the recovery of absorption parameters. Using the exact solution would also require solving the classical inverse problem by developing a search algorithm to determine the set of absorption parameters which generate the absorption curve that matches the collected experimental thermogravimetric data with the minimum error. Searching for this set of absorption parameters may require a large number of iterations, depending on the initial guess and the convergence rate of the search algorithm. Within this framework, a robust and faster computational method for the recovery of the absorption parameters using the exact analytical solution of the absorption models is developed and introduced in Chapter 2.

1.4. Effect of Inclusions and Voids on Diffusion Dynamics

Often, thermosets would contain fillers or inclusions at different concentrations to help with cost, mechanical, and/or other property enhancement. The integration of these fillers can be cost-driven, non-structural applications [24,71]. However, for specific high-end applications, inclusions are used to further improve the mechanical [72,73], electrical [74–76], and/or barrier [73,77–80] properties of the final product. A variety of micro- and nano-scale fillers have been used, including micromica [77], glass spheres [81], carbon nanotubes [73,76], nanoclay [78,80,82], carbon nanofibers [83], and nanographene [79]. Type (i.e. nanofibers, nanoclay, and nano-glass spheres), amount of nano-filler, and

polymer usually determine the extent of enhancement in material properties. Researchers reported that nanoclay addition increases Young's modulus, tensile strength, and hardness in nylon 6-6 [84] and in epoxy [26], interlaminar sheer strength, flexural strength, and modulus in S2-glass/epoxy composite [85], flexural strength and modulus, storage and loss modulus, and glass transition temperature in SC15 epoxy [86] and flexural strength and modulus, tensile strength and modulus in HDPE/pine bio composite [87]. Addition of nanoclay in polymers may improve properties in short term but may cause further degeneration in long term due to environmental damage.

Absorption behavior of nano-inclusion reinforced polymers might give insight on the degree of degradation. However, diffusion kinetics of the composite depend on the type of polymer and nano-inclusion. Gauvin and Robert [82] state that equilibrium moisture content of vinyl ester increased by 110% and 10% by the addition of 5 wt.% synthetic fluorinated silicate mica nanoclay and ODA-modified nanoclay, respectively. In contrast, Kim and Kim [26] show that 1 wt.% surface-modified montmorillonite nanoclay addition in epoxy resin results in 44.3% less moisture absorption than neat epoxy in 250 hours. Likewise, nanoclay inclusion in polymer has varying effects on diffusivity. Cloisite 30B in bio-resin [88] and 5 wt.% Cloisite 15A in epoxy [3] results in a decrease in diffusivity; on the other hand, 5 wt.% Cloisite Na in epoxy increases diffusivity by 71% [3]. Effects of nano-inclusion on moisture absorption is further investigated and modeled in Chapter 3.

Curing of thermosetting polymers involves chemical reaction in a multiphase system with time-dependent material properties and heat, mass, and momentum transfer. This complex fabrication process leads to void formation in the course of gelation and curing [89,90]. Void morphology, content and distribution depend on the manufacturing process

and the relevant parameters [89–91]. Introduction of voids into a polymer medium would result in a nonhomogeneous structure. The discontinuity in the polymer induces localized stresses and microcracks leading to property loss [89,91–95]. Harper et al. [91] investigated the effect of voids upon the ply moduli E_1, E_2, and G_{12} of AS4/3502 graphite/epoxy composites. The researchers observed no effect on E_1 which is a fiber dominated property while significant loss in E_2 and G_{12} is observed with 6% increase in void content. Formation of voids in the polymer matrix results in degradation of matrix dominated properties. Costa et al. [89] reported that no change in tensile, flexural, and interlaminar shear stresses up to critical void content in T700/TDE85 carbon fiber reinforced epoxy composites. As the void content exceeds the critical void content, the researchers observed significant matrix dominated property loss on the samples.

In addition to the negative effect of voids on the mechanical properties of the polymer, voids lead to increase in absorbed moisture resulting in further degradation and property loss [91,96]. Lu et al. [96] experimented on thermally aged basalt fiber-reinforced polymers to investigate the effect of aging on water uptake. They reported that the void content in the composite laminate increased along with the aging temperature. The results showed an increase in water uptake with increasing void content. Harper et al. [91] showed that AS4/3502 graphite/epoxy composites with 5% void absorbed 27%, 26%, 43%, and 42% more moisture than graphite/epoxy composites with 1% void at 40%, 60%, 75%, and 100% relative humidity, respectively. Even though the penetrating liquid and medium may be the same, voids change the microstructure of the medium and result in distinctive absorption behavior. Bao and Yee [97] claims that the voids can be filled instantly if close to the surface and considerably alters the diffusion behavior. Generally, voids change the

characteristic of absorption to more non-Fickian. Thus, Bao and Yee successfully applied dual diffusivity model to investigate moisture absorption behavior of carbon/BMI composites with varying ply stacking. Even though, Bao and Yee efficaciously recovered the overall absorption behavior using dual diffusivity model, they assumed that the voids were interconnected. Thus, they were able to attribute the initial fast absorption to filling of voids. However, in closed-cell porous structures, effect of voids/pores on moisture absorption cannot be considered just as fast filling of voids. Since the voids are separated by polymer membranes, liquid diffusion into voids may not be analyzed extrinsically.

1.5. Diffusion Dynamics in Closed-Cell Polymer Foams

Although voids in polymers have negative effects on the material performance in general, pores may be introduced purposefully. These polymers with high porosity (foams) are mostly used as thermal [98,99] and electrical [98,100] insulation in many application areas [101] such as sports, civil infrastructure, interiors, chemical/electrical, naval, aerospace, automotive, and rail transportation. Presence of voids dispersed in the polymer matrix may lead to substantial reduction in density depending on the ratio of empty space to the solid matrix.

Mouritz et al. [102] investigated the effect of pore content on mechanical properties of glass fiber/epoxy composites. The researchers controlled the pore size and content by introducing hollow polymer spheres into the resin when manufacturing the composite. They reported that the interlaminar shear strength and Mode I fracture toughness deteriorated with increasing pore content. It should be noted here that Mode I fracture toughness remained practically constant as pore content goes above 15%. Although, increasing pore content leads to inferior mechanical properties, foams are also used as core

in continuous fiber polymer composites to reduce the weight of the composite while increasing the mechanical performance. By increasing the core thickness, the flexural stiffness of the sandwich laminate improves without substantially increasing weight and cost [101].

Foams used in highly humid environments absorbs extreme amount of liquid due to available vacant sites, pores, in foams [103]. Huo et al. [103] investigated the moisture absorption behavior of closed-cell rigid PU foam core, woven E-glass fiber-reinforced thermoset PU, and their sandwich composites. They showed that neat PU resin, face sheets, PU foam, and foam core sandwich composite absorbed ~2.5 wt.%, ~1 wt.%, ~75 wt.%, and ~10 wt.%, respectively.

Some researchers not only investigated, but also modeled the molecular diffusion into foams and porous structures [104–108]. Gueribiz et al. [104] used micro-modeling of the composite medium with homogenous microstructure (uniformly distributed pores) to find an effective diffusivity using the diffusivities of the constituents (matrix and void). Likewise, Youssef et al. [105] also used microstructural approach to find effective diffusion coefficient using electrical analogy model [109]. Prakotmak et al. [107] numerically modeled the pores in banana foam mat using 2-D stochastic pore network. They used finite difference method to solve the convective mass transfer model. Moisture absorption behavior of foams was successfully predicted with different foam density by using this numerical approach. Chen et al. [108] derived a convection-diffusion model that couples the vapor transport and water diffusion. They stated the water molecules diffuse into the solid matrix whereas vapor flows through the pore network assuming Fickian diffusion and vapor transport following Darcy's law. The researchers reported that the

convection–diffusion model is able to accurately recover the diffusion mechanism in highly porous polymers by combining both diffusion and convection mechanisms. Diffusion into foams and transport phenomena in porous structures will be further discussed in Chapter 4.

Chapter 2. Moisture Absorption Modeling in Polymeric Composites

2.1. Fickian Diffusion Model

Molecular diffusion process was first introduced in 1885 by A. Fick, assuming steady flow of molecules from high concentration to low concentration region. Fick's first law of diffusion relates the mass flux to the change in concentration and is given as:

$$J = D\frac{\partial C}{\partial \mathrm{x}} \tag{1}$$

where D is the diffusion coefficient, C is the concentration and x is the position.

Fick also formulated the relation between change of concentration in time and concentration curvature in space, using his first law in Eq. (1) and conservation of mass. Fick's formulation for diffusion, known as Fick's second law, assumes no chemical interactions and reactions during diffusion process. Fick's second law is given in Eq. (2).

$$\frac{\partial C}{\partial t} = D\frac{\partial^2 C}{\partial x^2} \tag{2}$$

where, t is the time.

Well-known Fick's second law, which governs the time-dependent change in concentration, can be advanced to describe the one-dimensional mass diffusion process. The classical Fickian model [110] is one of the most widely used model that utilizes the governing differential equation of the Fick's second law to predict the moisture mass gain in polymers [2,43–48]. The classical Fickian model gives an analytical solution of concentration for a fully immersed thin plate:

$$\frac{C - C_i}{C_m - C_i} = 1 - \frac{4}{\pi}\sum_{j=0}^{\infty}\frac{1}{2j+1}sin\frac{(2j+1)\pi x}{h}exp\left[-\frac{(2j+1)^2\pi^2 Dt}{h^2}\right] \tag{3}$$

where C_i is the initial moisture concentration, C_m is the maximum moisture concentration and h is the thickness of the plate. Solution for the concentration profile can illustrate the dynamics of the entire diffusion process until the plate absorbs the maximum amount of moisture. However, it is not the most suitable tool for experimental validation. Integrating the function of concentration over the plate thickness would yield the change of mass in time which can easily be used for validation purposes. The total moisture content in a fully immersed thin plate is

$$\frac{m - m_i}{m_\infty - m_i} = 1 - \frac{8}{\pi^2} \sum_{j=1}^{\infty} \frac{1}{(2j+1)^2} exp\left[-\frac{(2j+1)^2 \pi^2 D t}{h^2} \right] \tag{4}$$

where m_i is the initial weight of the moisture, m_∞ is the weight of the maximum moisture that material can absorb.

The mass absorption equation, Eq. (4), shows the mass gain of a fully immersed thin plate as a function of time. This one-dimensional solution assumes that the absorption through the edges is negligible. Although, Eq. (4) is an absolutely effective tool to characterize the moisture absorption behavior, the infinite sum in the solution may require computational effort. It has been observed that the effect of each term of the summation over the total sum decreases as number of terms, j, increases. Adding a stopping criterion to the solution may better manage the computational efforts. Our experiments indicated that $j \approx 10000$ yields accurate predictions over the entire time scale.

A typical classical Fickian moisture absorption curve is illustrated in Figure 1. Absorption starts with initial fast moisture uptake with a constant slope and slows down to reach an equilibrium moisture content.

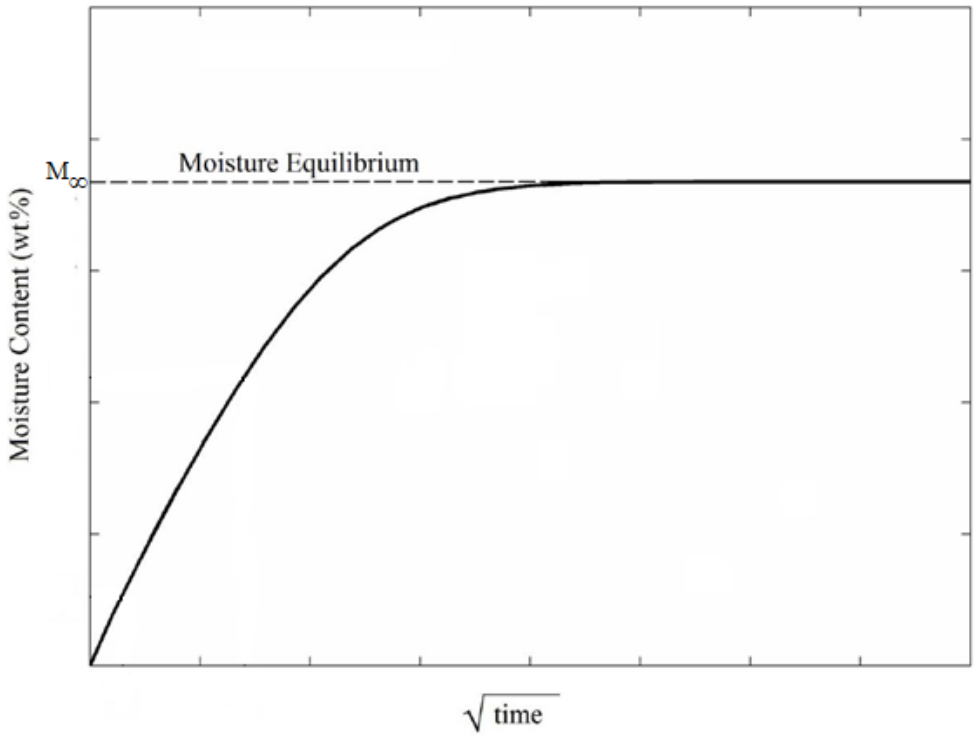


Figure 1. Typical Fickian moisture uptake curve.

Shen and Springer [43] also suggested a useful approximation that the maximum moisture content and diffusivity can be quickly found. Researchers [43] proposed to set the maximum moisture content to the last data point where the absorption reached an equilibrium. Using the maximum moisture content and the initial slope of the absorption curve diffusivity can be found using:

$$D = \pi \left[\left(\frac{M_2 - M_1}{\sqrt{t_2} - \sqrt{t_1}} \right) \frac{h}{4M_\infty} \right]^2 \tag{5}$$

where $\left(\frac{M_2 - M_1}{\sqrt{t_2} - \sqrt{t_1}} \right)$ is the initial slope of moisture absorption curve.

Shen and Springer also provided an approximation for the mass gain function in Eq. (3):

$$\frac{m - m_i}{m_\infty - m_i} = 1 - exp\left[-7.3 \left(\frac{Dt}{h^2} \right)^{0.75} \right] \tag{6}$$

It should be noted here that the approximate methods for classical Fickian model, Eqs. (5-6), may not yield accurate results since it highly depends on the maximum moisture content selection and experimental error in initial slope determination.

2.2. Langmuir-Type Diffusion Model

Polymers and polymer composites mostly display non-Fickian moisture absorption behavior where Fickian model is not sufficiently accurate [49–55]. The Langmuir model, proposed by Carter and Kibler [54], essentially modifies the Fickian diffusion kinetics by accounting for the hindrance introduced by chemical interactions between the penetrant and the medium. The model considers the chemical interactions by separating the diffused moisture molecules into two categories: *i)* unbound moisture molecules and *ii)* bound moisture molecules. Water molecules diffuse into the material as unbound moisture can either remain as unbound moisture or interact with polymer chain and become bound moisture. Likewise, bound moisture can transform back to unbound moisture. The rate of exchange between bound and unbound molecules, which sets the speed of moisture absorption, gradually decreases and reaches zero; whereas, only the diffusing molecules set the speed of absorption in Fickian diffusion. This ongoing transformation between the bound and unbound moisture hinders the absorption behavior. Corollary to this, the time required to reach moisture equilibrium is often much longer compared to a pure Fickian absorption. The governing set of differential equations of the one-dimensional hindered diffusion is written as:

$$D\frac{\partial^2 n}{\partial x^2} = \frac{\partial n}{\partial t} + \frac{\partial N}{\partial t} \tag{7a}$$

$$\frac{\partial N}{\partial t} = \gamma n - \beta N \tag{7b}$$

where n represents the unbound molecules per unit volume, N represents the bound molecules per unit volume, γ is the rate at which unbound molecules become bound, and β is the rate of bound molecules becoming unbound.

The hindered diffusion model expresses the total concentration as the sum of two terms: bound moisture concentration $N(x,t)$ and unbound moisture concentration $n(x,t)$, proportional to material parameters γ and β at equilibrium. The Fickian diffusion model does not consider bound molecules, and thus the total concentration is expressed in terms of $C(x,t)$. In the hindered diffusion model, if the rate of unbound molecules becoming bound, γ, is equal to zero, $N(x,t)$, the concentration of bound molecules goes to zero, and thus, $n(x,t)$, the concentration of unbound molecules, becomes equivalent to $C(x,t)$. In other words, the hindered diffusion simplifies to Fickian behavior, if there are no bound molecules. The ability to simplify to Fickian behavior is an additional advantage of the hindered diffusion model, where a priori knowledge of the absorption behavior is not needed.

Hindered diffusion model states that the moisture absorption continues until the dynamic equilibrium is reached. Dynamic equilibrium is where the rate of exchange between the unbound and bound molecule is the same. In other words, for every unbound molecule becoming bound, a bound molecule will become unbound. The equation describing this equilibrium condition can be written as:

$$N_\infty/n_\infty = \gamma/\beta = \mu \tag{8}$$

where N_∞ and n_∞ are the equilibrium bound and unbound moisture contents, respectively. Eq. (8) indicates that the ratio of the bound to unbound equilibrium moisture becomes constant throughout the sample, regardless of the location. In other words, Eq. (8) suggests that when the moisture equilibrium is reached, there is a generalized microstructural ratio between the bound and unbound molecules at any location within the material.

The analytical solutions of bound moisture concentration $N(x,t)$ and unbound moisture concentration $n(x,t)$ are given in Eqs. (9a-b).

$$N(z,t) = \frac{\gamma}{\beta} n_\infty \left\{ 1 - \frac{4}{\pi} \sum_{i=1}^{\infty(odd)} (-1)^{\frac{i-1}{2}} \frac{r_i^+ exp(-r_i^- t) - r_i^- exp(-r_i^+ t)}{\mathrm{i}(r_i^+ - r_i^-)} \cos\left(\frac{\pi i x}{2\delta}\right) \right\} \tag{9a}$$

$$n(z,t) = n_\infty \left\{ \begin{array}{l} 1 - \frac{4}{\pi} \sum_{i=1}^{\infty(odd)} (-1)^{\frac{i-1}{2}} \frac{r_i^+ exp(-r_i^- t) - r_i^- exp(-r_i^+ t)}{\mathrm{i}(r_i^+ - r_i^-)} \cos\left(\frac{\pi i x}{2\delta}\right) + \\ \frac{4}{\pi\beta} \sum_{i=1}^{\infty(odd)} (-1)^{\frac{i-1}{2}} (r_i^+ r_i^-) \frac{exp(-r_i^- t) - exp(-r_i^+ t)}{\mathrm{i}(r_i^+ - r_i^-)} \cos\left(\frac{\pi i x}{2\delta}\right) \end{array} \right\} \tag{9b}$$

where

$$r_i^\pm = \frac{1}{2}\left[(Ki^2 + \gamma + \beta) \pm \sqrt{(Ki^2 + \gamma + \beta)^2 - 4K\beta i^2}\right] \tag{9c}$$

$$K = \frac{\pi^2 D}{h^2}$$

When the sum of the bound moisture concentration $N(x,t)$ and the unbound moisture concentration $n(x,t)$ is integrated over the thickness, the resulting exact analytical solution gives the mass fraction of the absorbed moisture, and is expressed as:

$$M(t) = M_\infty \left\{ \begin{array}{l} 1 - \frac{8}{\pi^2} \sum_{i=1}^{\infty(odd)} \frac{r_i^+ exp(-r_i^- t) - r_i^- exp(-r_i^+ t)}{i^2 (r_i^+ - r_i^-)} + \\ \frac{8}{\pi^2} \left(K \frac{\beta}{\beta + \gamma} \right) \sum_{i=1}^{\infty(odd)} \frac{exp(-r_i^- t) - exp(-r_i^+ t)}{(r_i^+ - r_i^-)} \end{array} \right\} \quad (10)$$

$M(t)$ is the weight percent of absorbed moisture at time t and M_∞ is the equilibrium moisture weight percent. A typical hindered moisture absorption curve is illustrated in Figure 2.

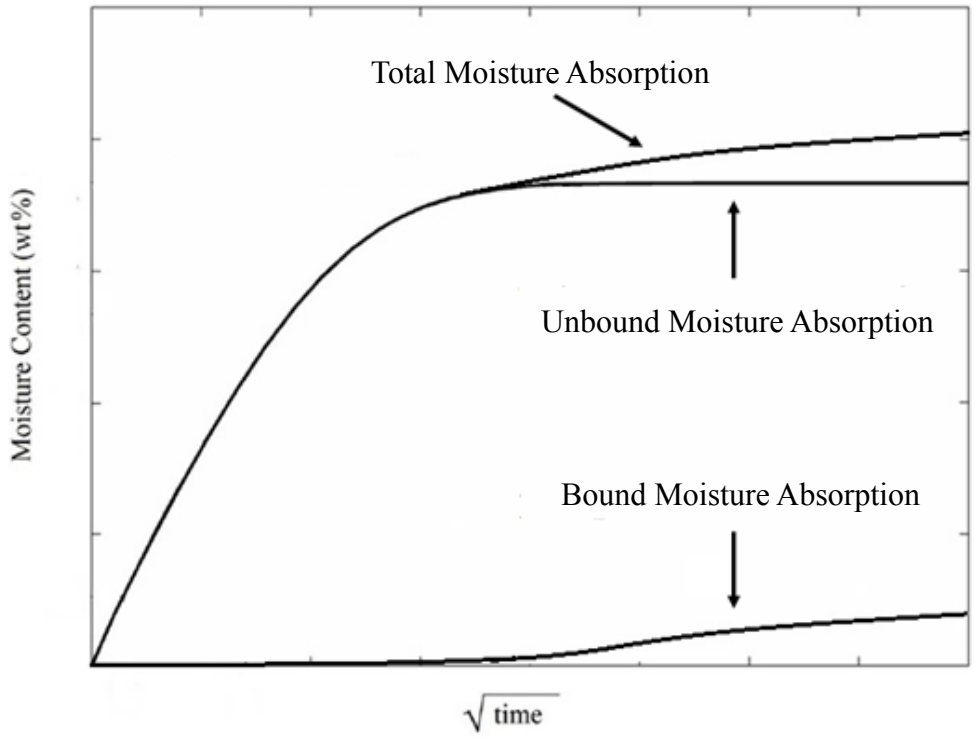


Figure 2. Typical Langmuir-type moisture uptake curve showing bound, unbound and total mass gain.

Overall moisture absorption starts with fast mass gain as in Fickian, followed by secondary slower absorption. As can be seen from Figure 2, secondary slower absorption is due to bound moisture absorption. The rate of transformation between the unbound and bound molecules determines the behavior of the secondary absorption kinetics. Due to ongoing transformation, hindered diffusion takes more time to reach equilibrium than the Fickian diffusion.

i. Effect of chemical interactions on moisture absorption kinetics

Addition of two absorption parameters to Fickian diffusion model, γ and β, to consider the chemical interaction between the penetrant and medium institute new absorption kinetics in polymers. Depending on the polymer-water affinity, rate of exchange between the bound and unbound molecules results in distinct absorption behavior.

Figure 3 illustrates the effect of rate of bound molecule to become unbound on overall moisture absorption kinetics of a representative mass gain curve. The representative curve illustrated as the red line uses the absorption parameters $\begin{bmatrix} D \\ \gamma_0 \\ \beta_0 \\ M_\infty \end{bmatrix} = \begin{bmatrix} 1.4 \times 10^{-3} \\ 1.0 \times 10^{-4} \\ 7.0 \times 10^{-4} \\ 2.2 \end{bmatrix}$. The other curves in Figure 3 use the same absorption parameters except β_0. As the rate of transformation from bound to unbound molecule, β, increases, time to reach the equilibrium decreases. In other words, decreasing β results in more non-Fickian absorption behavior.

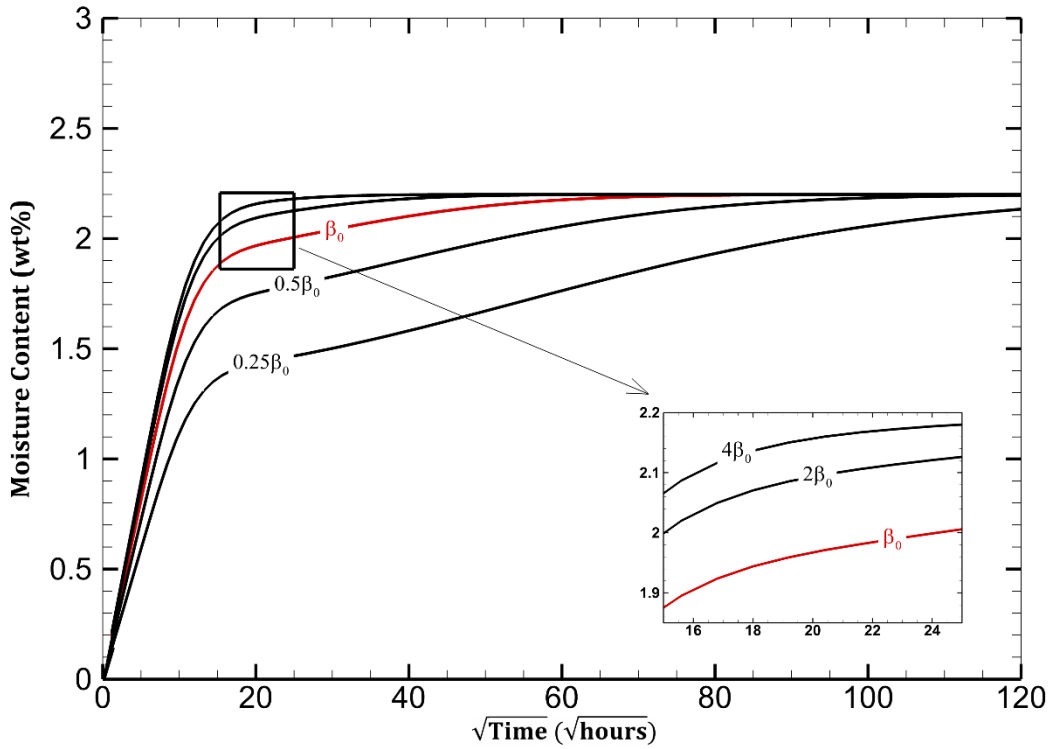


Figure 3. The effect of change in β, rate of bound molecule to become unbound, on moisture absorption ($\beta_0 = 7.0 \times 10^{-4}$).

In addition, Figure 4 shows the change in bound and unbound moisture absorption by the rate of bound molecule to become unbound. Increasing β means that more bound molecule will be transformed to unbound per unit time. Thus, unbound moisture content increases with β. As more bound molecule is transformed to unbound, the equilibrium bound molecule content decreases with increasing β.

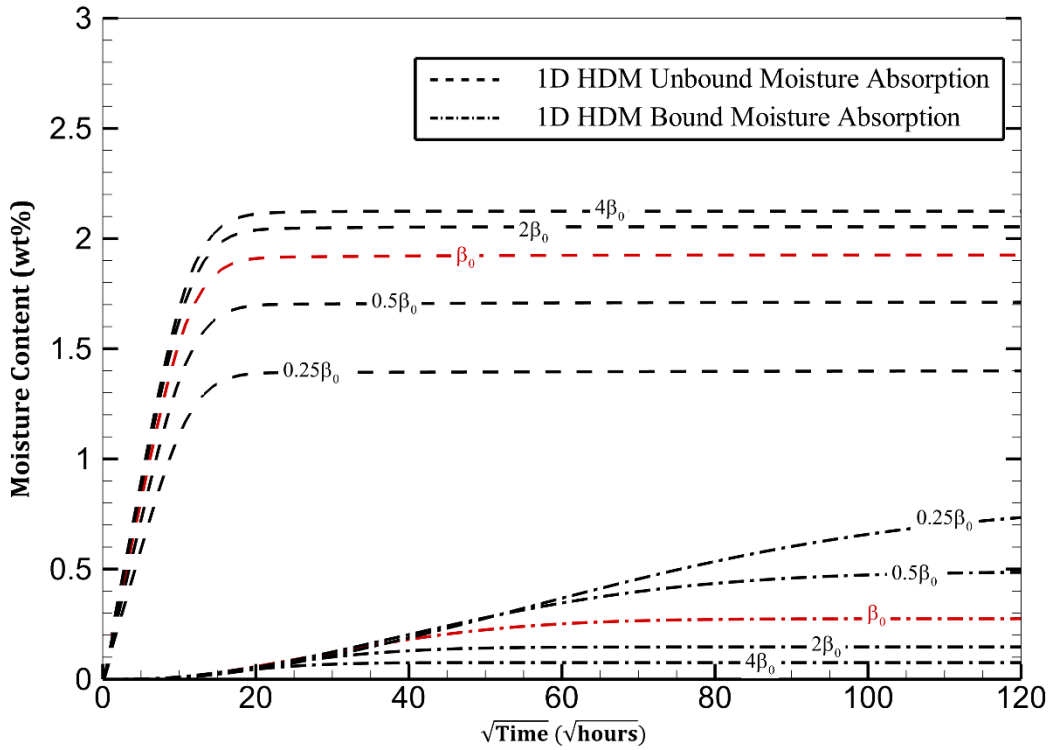


Figure 4. The effect of change in β, rate of bound molecule to become unbound, on bound and unbound moisture absorption ($\beta_0 = 7.0 \times 10^{-4}$).

Figure 5 shows the effect of rate of unbound molecule to become bound, γ, on overall moisture absorption. Change in γ has similar effect on overall moisture like β such as retardation in reaching the equilibrium. However, effect of β on time to reach equilibrium is significantly higher than the effect of γ. Smaller γ and β mean that the rate of chemical interaction is slow which leads to longer time to reach the equilibrium. However, decreasing γ/β ratio results in more Fickian behavior. Thus, overall effect of γ on hindrance is lower than the effect of β.

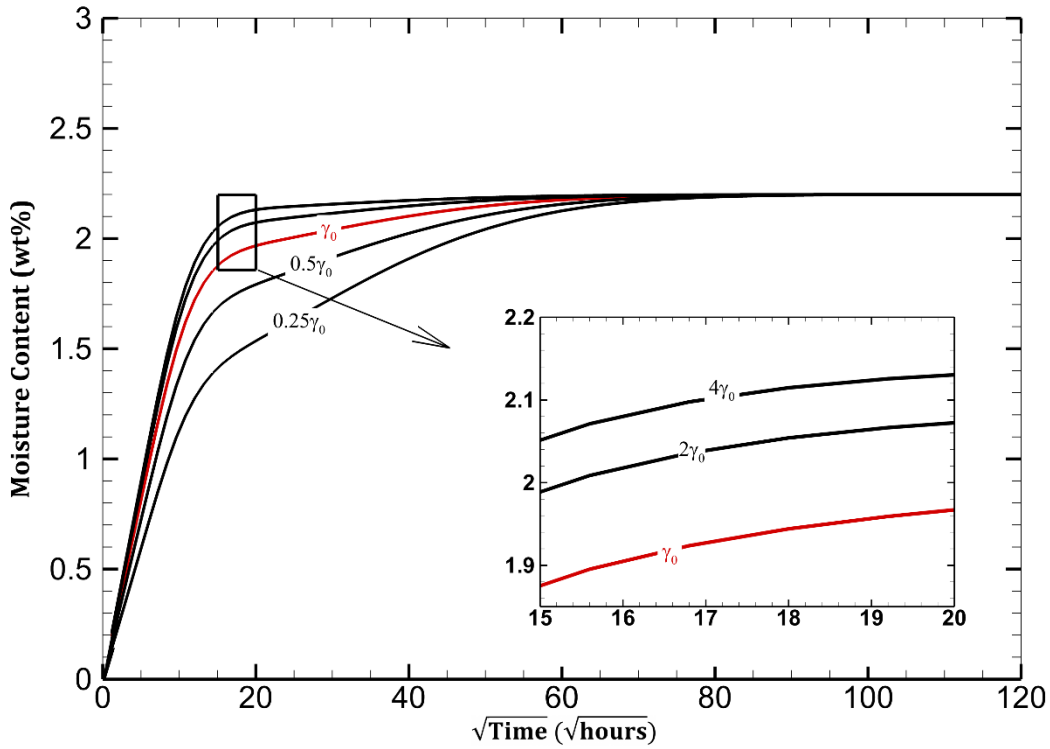


Figure 5. The effect of change in γ, rate of unbound molecule to become bound, on moisture absorption ($\gamma_0 = 1.0 \times 10^{-4}$).

Figure 6 portrays the change in unbound and bound moisture mass gain for various values of γ. The comparison of unbound moisture content of mediums with distinct rate of unbound molecule to become bound yields inverse relation between the unbound moisture content and the γ. As the rate of unbound molecule to become bound increases more unbound molecule will be transformed to bound molecule leading to escalation in overall bound moisture.

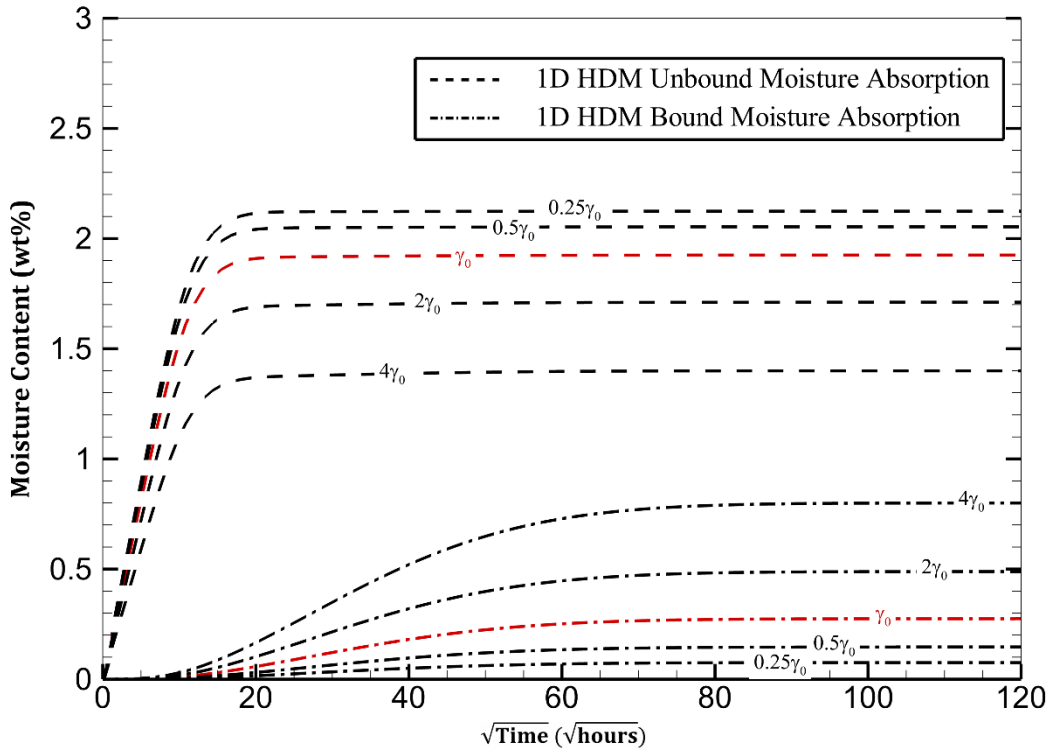


Figure 6. The effect of change in γ, rate of unbound molecule to become bound, on bound and unbound moisture absorption ($\gamma_0 = 1.0 \times 10^{-4}$).

Last, the effect of γ and β on moisture absorption of a medium having the same hindrance coefficient, $\gamma/\beta = 1/7$, is investigated and illustrated in Figure 7. Even though all the absorption curves on Figure 7 have the same hindrance coefficient, they have distinctive absorption behavior. Smaller γ and β retard reaching to equilibrium while the bound, unbound, and overall maximum moisture content does not change. Moreover, for a constant hindrance coefficient, kinetics of unbound moisture absorption is identical.

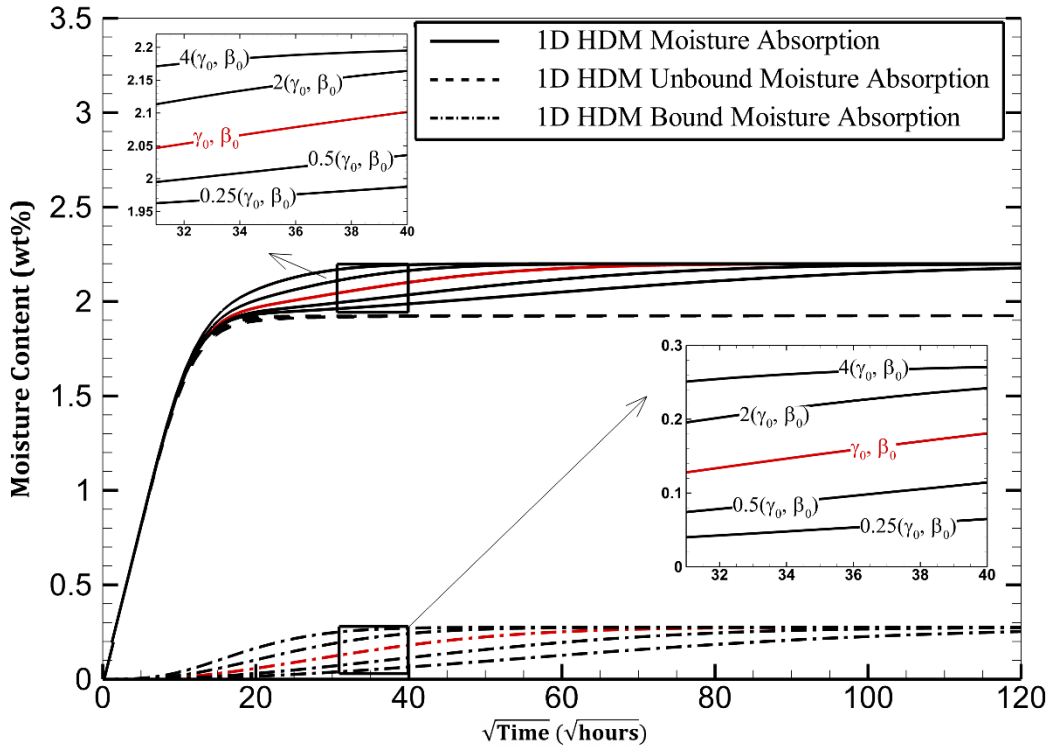


Figure 7. Effect of rate of conversion (bound⇔unbound) on time to reach the equilibrium for the same hindrance coefficient (μ=0.143).

ii. Approximate Solutions

The one-dimensional hindered diffusion model has an analytical approximation for cases where 2β and 2γ are very small when compared to K [54]:

$$M(t) = M_\infty \left\{ \begin{array}{c} \dfrac{\beta}{\gamma+\beta} e^{-\gamma t} \left(1 - \dfrac{8}{\pi^2} \sum_{i=1}^{\infty(odd)} \dfrac{1}{i^2} e^{-\left(\frac{\pi\, t\, D\, i^2}{h^2}\right)} \right) + \\ \dfrac{\beta}{\gamma+\beta}\left(e^{-\beta t} - e^{-\gamma t}\right) + \left(1 - e^{-\beta t}\right) \end{array} \right\} \tag{11}$$

Eq. (11) may be further simplified into "useful" approximations both for very short or very long times [54].

$$M(t) = \frac{4}{\pi^{\frac{3}{2}}} \left(\frac{\beta}{\beta+\gamma}\right) M_\infty \sqrt{Kt}\,, \qquad 2\gamma, 2\beta \ll K\,, \qquad t < \frac{0.7}{K} \tag{12}$$

$$M(t) = M_\infty \left[1 - \left(\frac{\gamma}{\beta+\gamma}\right) \exp[-\beta t]\right], \qquad 2\gamma, 2\beta \ll K\,, \qquad t \gg \frac{1}{K} \tag{13}$$

When the required conditions for Eqs. (11-13) are satisfied, these approximations can be used to recover the absorption parameters faster and without any iterative process. However, the accuracy of parameters determined from these approximations may change depending on the extent of experimental data available. In addition, these approximations are only valid when 2β and 2γ are much smaller than $K = (\pi^2\ D)/h^2$. The validity of the assumptions for Eq. (12) and Eq. (13) is not known a priori, and thus, indiscriminate use of these approximations without any justification may lead to erroneous results. Therefore, using the exact analytical solution given in Eq. (10) might be essential for the identification of absorption parameters as the accuracy of approximate solutions are not known.

iii. Non-dimensional Langmuir-type Diffusion Model

A non-dimensional form of Langmuir-type diffusion model is derived for further use of the model. Non-dimensional form of the model for a fully immersed thin plate is:

$$\frac{\partial^2 n^*}{\partial z^{*2}} = \frac{\partial n^*}{\partial t^*} + \mu^* \frac{\partial N^*}{\partial t^*} \tag{14a}$$

$$\frac{\partial N^*}{\partial t^*} = \beta^*(n^* - N^*) \tag{14b}$$

where

$$z^* = \frac{z}{h} \qquad t^* = \frac{D}{h^2} t$$

$$\beta^* = \frac{h^2}{D}\beta \qquad \gamma^* = \frac{h^2}{D}\gamma$$

$$n^* = \frac{n}{n_\infty} \qquad N^* = \frac{N}{N_\infty}$$

$$\mu^* = \frac{\gamma^*}{\beta^*}$$

The non-dimensional form of an equation can be particularly useful since it does not include any dimensional variable property and mostly useful to handle more complex systems governed by multiple dimensional variables. It can be utilized to uncover new physical phenomena that depends on the nondimensional properties or better describe the absorption behavior, revealing underlying principles. The non-dimensional form of Langmuir-type diffusion model, Eqs. (14), will be adopted to derive a convenient approximate solution for three-dimensional hindered diffusion model.

2.3. Fickian and Non-Fickian Absorption in Polymers

The moisture absorption in most polymers starts with fast unbound moisture uptake and continues until all vacant sites are filled with unbound moisture. For a Fickian diffusion that describes the whole absorption process which can be seen in Figure 1. However, in non-Fickian case, the moisture absorption does not stop here. As can be seen in Figure 2, during the unbound moisture uptake that some unbound molecules interact with the polymer medium and slowly become bound. Even though all the vacant sites are filled with unbound moisture, the polymer will continue to absorb since conversion from unbound moisture to bound remains. Moisture absorption reaches an equilibrium once the number of bound moisture does not change in time. In other words, the exchange rate between the bound and unbound moisture is equal. It should be noted here that bound moisture cannot diffuse into the polymer. Only the diffused unbound moisture can turn into bound moisture.

Figure 8 illustrates gravimetric moisture absorption data of quartz/epoxy composite laminate. The fabrication process of the laminate and procedure for moisture absorption test will be further discussed in Chapter 5. Figure 8 also demonstrates the moisture absorption prediction of Fickian and hindered diffusion model. Both Fickian and hindered

diffusion model correlate well with the initial thermo-gravimetric data. However, their future absorption behavior predictions differ.

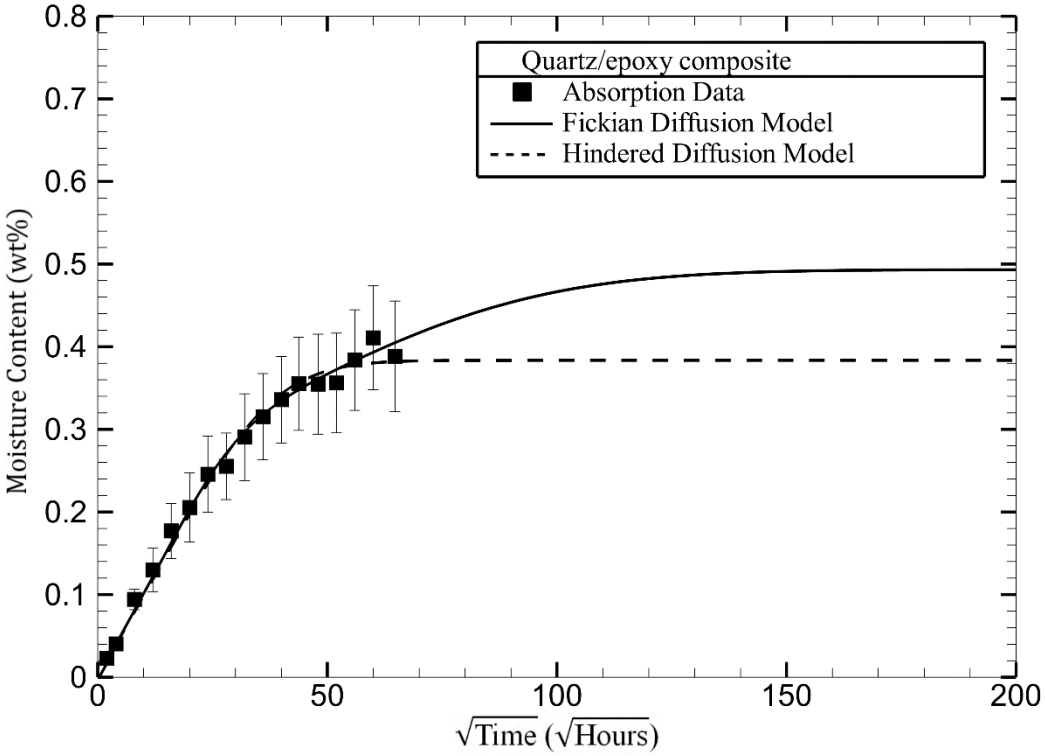


Figure 8. Experimental moisture absorption data of quartz/epoxy composite laminate of 6 months, Fickian and hindered diffusion model predictions

Figure 9 also shows the moisture absorption data of the same samples; however, the data is gathered from three-year measurement. It also depicts the Fickian and hindered diffusion model predictions using three-year test data. Hindered diffusion model is in well agreement with the moisture absorption data. However, Fickian model could not recover the absorption behavior of the samples. Chemical interactions between the polar water molecules and polymer chains lead to slower secondary absorption. Fickian model assumes that after the initial uptake, the absorption slows down and immediately stops. Hindered diffusion model accounts for those chemical interactions thus is able to capture the absorption behavior.

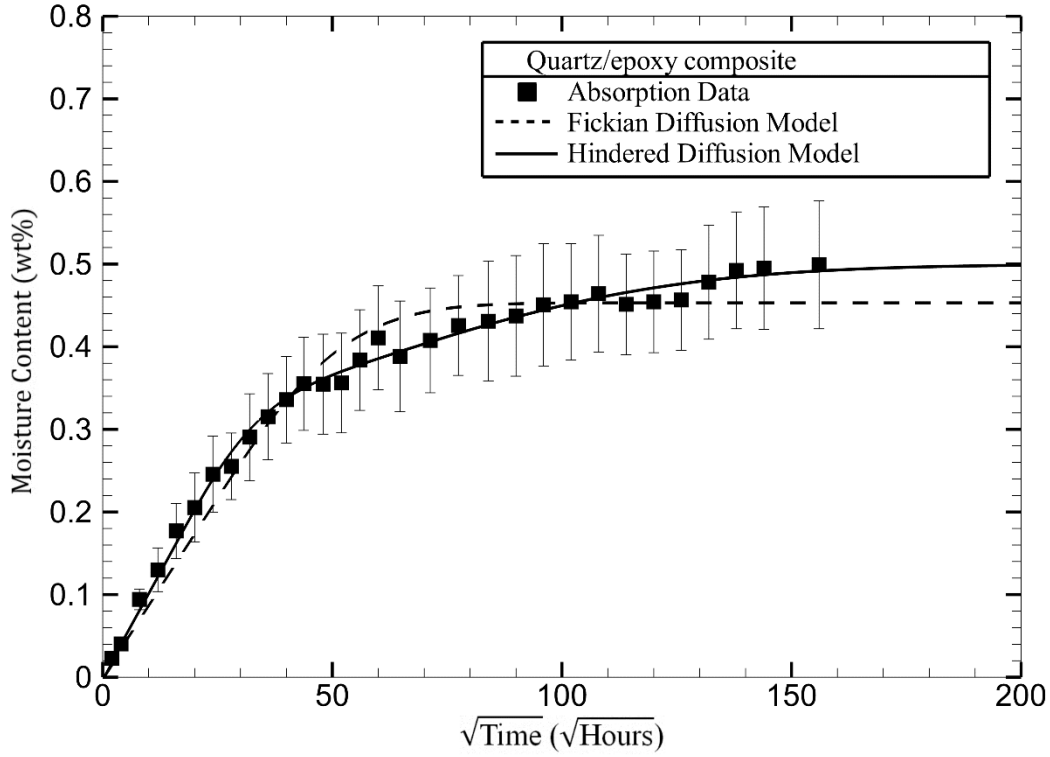


Figure 9. Experimental moisture absorption data of quartz/epoxy composite laminate of 3 years, Fickian and hindered diffusion model predictions

The comparison of first and second predictions of the diffusion models and how well they correlate with the absorption data is illustrated in Figure 10. Both the first and second predictions of Fickian absorption reflect the absorption behavior due to no chemical interaction assumption of the model. The second prediction of the hindered diffusion model fully represents the absorption behavior of the samples. Moreover, the first prediction of the hindered diffusion model is only 21% off from the second prediction which shows the early predictive capability of hindered diffusion model.

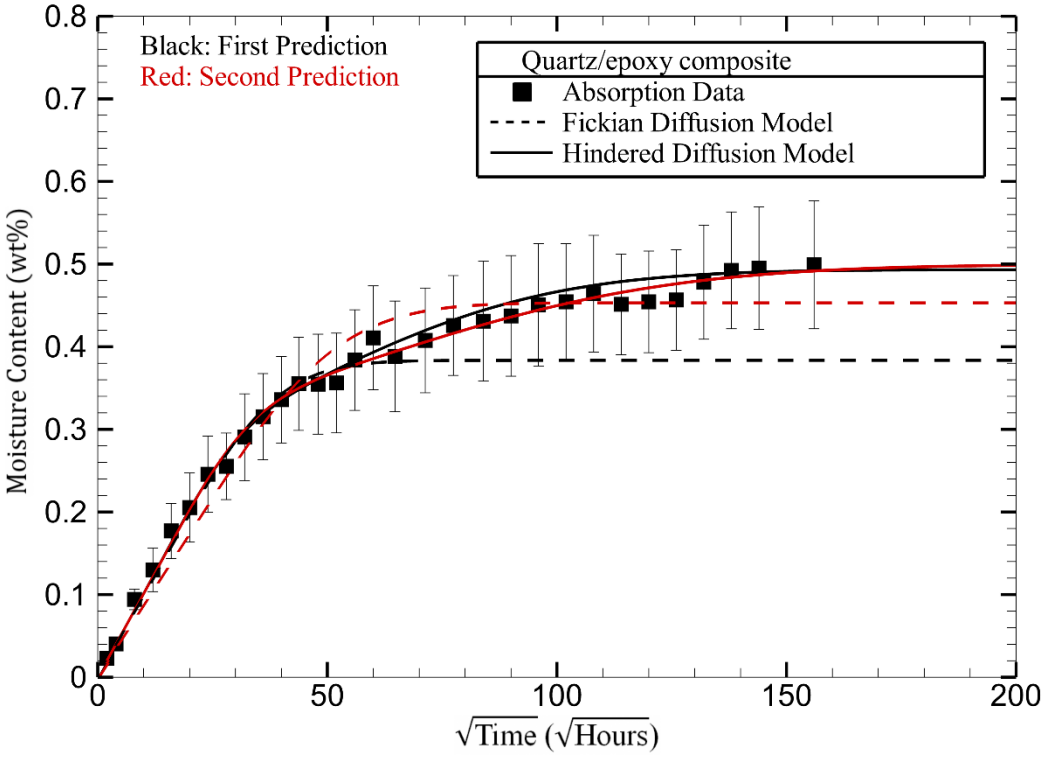


Figure 10. Comparison between the first and second predictions of Fickian and hindered diffusion model

2.4. Anisotropic Diffusion Models

One-dimensional diffusion models are widely used to study the absorption behavior of polymers and polymer composites. However, one-dimensional models may not fully capture the diffusion kinetics of an anisotropic slab. Aronhime et al. [17] reported that diffusion along the fiber in unidirectional Kevlar/epoxy is 3-100 times faster, depending on the fiber volume fraction, than diffusion transverse to the fiber. Likewise, Blikstad [16] stated that the diffusivity in the fiber direction is more than ten times larger than the through-thickness diffusivity for graphite/epoxy laminate. When material anisotropy exists and/or planar sizes are comparable to the thickness, three dimensional effects must be taken into consideration for accurate characterization of moisture absorption behavior. The existence of anisotropic three-dimensional diffusion in fiber-reinforced composites is well-documented and has been studied thoroughly [60,61,111–113].

i. Three-Dimensional Anisotropic Fickian Diffusion Model

The three-dimensional form of the Fickian diffusion model is basically an expansion of classical Fickian model to account for anisotropic diffusion. The model considers three distinct flux of moisture in three principal directions of a finite slab and is given by,

$$D_x \frac{\partial^2 C}{\partial x^2} + D_y \frac{\partial^2 C}{\partial y^2} + D_z \frac{\partial^2 C}{\partial z^2} = \frac{\partial C}{\partial t} \tag{15}$$

where D_x, D_y, and D_z are diffusion coefficients in the direction of x, y, and z, respectively. A finite slab, (e.g. Figure 11), will absorb moisture through all the surfaces which are in contact with the water. The flux of moisture basically depends on the area of contact. For a thin plate, the area of contact at the side surfaces is negligible compared to the top and bottom surface. However, for a thick slab, the flux through the side surfaces may significantly contribute to the absorption. Expansion of classical Fickian diffusion model

to three-dimension lead to grasp the moisture absorption through the edges. The model not only considers the change in absorption kinetics due to edge effects but also capture the material anisotropy using three diffusivities, D_x, D_y, and D_z.

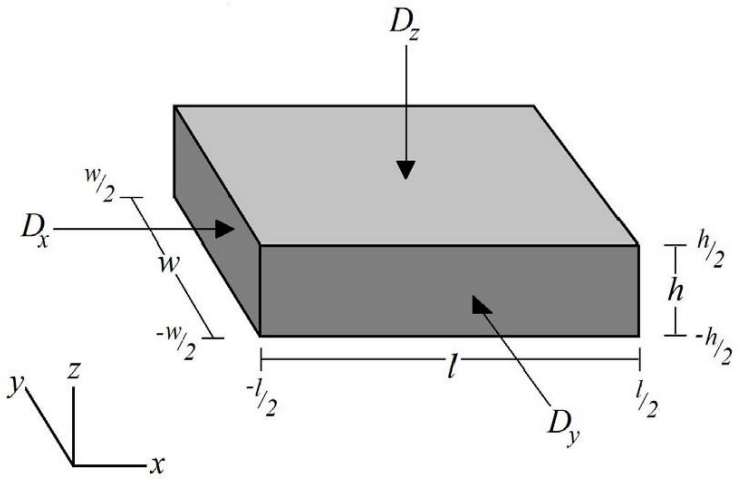


Figure 11. The representative figure for finite slab and the three-dimensional Fickian model geometry.

Assuming an initially dry slab of dimensions $h \times w \times l$ which is fully immersed in water, the analytical solution for concentration is given as:

$$C(\mathrm{x},\mathrm{y},\mathrm{z},t) = C_\infty - \frac{64C_\infty}{\pi^3}\sum_{i=0}^{\infty}\sum_{j=0}^{\infty}\sum_{k=0}^{\infty}\frac{sin\frac{(2i+1)\pi x}{l}}{(2\mathrm{i}+1)}\frac{sin\frac{(2j+1)\pi y}{w}}{(2\mathrm{j}+1)}\frac{sin\frac{(2k+1)\pi z}{h}}{(2\mathrm{k}+1)} exp\left[-(\frac{D_x(2i+1)^2}{l^2}+\frac{D_y(2j+1)^2}{w^2}+\frac{D_z(2k+1)^2}{h^2})\pi^2 t\right] \quad (16)$$

The total mass gain is determined by integration of moisture concentration over the volume:

$$M(t) = M_\infty - \frac{512M_\infty}{\pi^6}\sum_{i=0}^{\infty}\sum_{j=0}^{\infty}\sum_{k=0}^{\infty}\frac{1}{(2i+1)^2}\frac{1}{(2j+1)^2}\frac{1}{(2\mathrm{k}+1)^2} exp\left[-(\frac{D_x(2i+1)^2}{l^2}+\frac{D_y(2j+1)^2}{w^2}+\frac{D_z(2k+1)^2}{h^2})\pi^2 t\right] \quad (17)$$

where $M(t)$ is the moisture weight percent at time t and M_∞ is the equilibrium moisture weight percent of a sample.

ii. Three-Dimensional Hindered Diffusion Model

Although the 1D HDM helps depict the non-Fickian behavior of isotropic polymers, it fails to account for the edge and anisotropy effects commonly observed in composites. Characterizing the absorption behavior of a geometrically complex, anisotropic composite part is compromised when a one-dimensional, isotropic model is used. The absorption parameters obtained would not be scalable to actual parts. Building on the Langmuir approach, Grace and Altan [30] recently proposed a three-dimensional hindered diffusion model (3D HDM). This model has extended the Langmuir-type diffusion model by accounting for diffusion anisotropy and edge effects as well as the Fickian and anomalous moisture uptake behavior. In comparison to 3D Fickian model, 3D HDM can capture the non-Fickian effects by considering chemical interactions between the penetrant and the medium. Following the 3D HDM model development, Grace and Altan [65] validated the predictive capabilities of their model using moisture intake data of 6-, 12-, and 40-ply, quartz/BMI composite laminates. The modification of the one-dimensional model yields the following governing equations for hindered diffusion model:

$$D_x \frac{\partial^2 n}{\partial x^2} + D_y \frac{\partial^2 n}{\partial y^2} + D_z \frac{\partial^2 n}{\partial z^2} = \frac{\partial n}{\partial t} + \frac{\partial N}{\partial t} \tag{18a}$$

$$\frac{\partial N}{\partial t} = \gamma n - \beta N \tag{18b}$$

where $n(x, y, z, t)$ represents the unbound molecules per unit volume, $N(x, y, z, t)$ represents the bound molecules per unit volume. Again, β is the rate of bound molecules

becoming mobile, and γ is the rate of mobile molecules becoming bound. D_x, D_y, and D_z are the diffusion coefficients in the x, y, and z directions, respectively.

In addition, Grace and Altan [30] developed an approximate solution to the three-dimensional hindered diffusion model (3D HDM) that would simplify to Eq. (11) for one-dimensional cases. The approximate solution was obtained by solving the set of coupled partial differential equations given in Eqs. (18a-b) for the case where $2\gamma, 2\beta \ll K$:

$$\frac{M(t)}{M_\infty} = 1 - \frac{512\Xi}{\pi^6}\sum_{i=0}^{\infty}\sum_{j=0}^{\infty}\sum_{k=0}^{\infty}\frac{1}{(2i+1)^2}\frac{1}{(2j+1)^2}\frac{1}{(2\mathrm{k}+1)^2}e^{-\alpha t} - (1-\Xi)e^{-\beta t} \tag{19}$$

where

$$\alpha = \left(\frac{D_x(2i+1)^2}{l^2} + \frac{D_y(2j+1)^2}{w^2} + \frac{D_z(2k+1)^2}{h^2}\right)\pi^2$$

$$\Xi = \frac{\beta}{\beta+\gamma}$$

However, this approximation does not hold for all polymer composite systems. Thus, there is a need for the exact analytical solution of the three-dimensional hindered diffusion model.

To find an analytical solution of the coupled differential equations shown in Eqs. (18a-b), the following initial and boundary conditions are used:

- Slab is fully immersed in water,
- Initially no moisture presents in the slab.

To solve the coupled differential equations shown in Eqs. (18a-b), the separation of variables technique is applied. It is assumed that the variables $x, y, z,$ and t in $n(x, y, z, t)$

and $N(x, y, z, t)$ are independent, and hence the solution for concentrations n and N can be expressed as:

$$n(x, y, z, t) = \sigma_i(x)\, \varepsilon_i(y)\, \varphi_i(z)\, \tau(t)$$
$$N(x, y, z, t) = \sigma_i(x)\, \varepsilon_i(y)\, \varphi_i(z)\, \rho(t) \tag{20}$$

Substituting Eq. (20) in Eqs. (18a-b) and simplifying results in:

$$D_{x,i}\frac{1}{\sigma_i(x)}\frac{\partial^2\sigma_i(x)}{\partial x^2} + D_{y,i}\frac{1}{\varepsilon_i(y)}\frac{\partial^2\varepsilon_i(y)}{\partial y^2} + D_{z,i}\frac{1}{\varphi_i(z)}\frac{\partial^2\varphi_i(z)}{\partial z^2} = \frac{1}{\tau(t)}\frac{\partial\tau(t)}{\partial t} + \frac{1}{\tau(t)}\frac{\partial\rho(t)}{\partial t} = -\delta^2 \tag{21a}$$

$$\frac{\partial\rho(t)}{\partial t} = \gamma\tau(t) - \beta\rho(t) \tag{21b}$$

Separating independent functions and simplifying Eq. (21a) further leads to:

$$D_{x,i}\frac{\partial^2\sigma_i(x)}{\partial x^2} = -\bar{X}^2\sigma_i(x) \tag{22a}$$

$$D_{y,i}\frac{\partial^2\varepsilon_i(y)}{\partial y^2} = -\bar{Y}^2\varepsilon_i(y) \tag{22b}$$

$$D_{z,i}\frac{\partial^2\varphi_i(z)}{\partial z^2} = -\bar{Z}^2\varphi_i(z) \tag{22c}$$

$$\frac{\partial\tau(t)}{\partial t} + \frac{\partial\rho(t)}{\partial t} = -\delta^2\tau(t) \tag{22d}$$

where $\bar{X}$, $\bar{Y}, \bar{Z}$ and δ are constants that verify:

$$\delta^2 = \bar{X}^2 + \bar{Y}^2 + \bar{Z}^2 \tag{23}$$

Laplace transformation of Eq. (21b) yields:

$$s\bar{\tau}(s) - \tau(0) + s\bar{\rho}(s) - \rho(0) = -\delta^2\bar{\tau}(s) \tag{24}$$

A correlation between $\tau(t)$ and $\rho(t)$ is needed in order to solve this system of equations. The correlation can is developed using Laplace transformation of Eq. (21b):

$$\mathcal{L}\left\{\frac{\partial\rho(t)}{\partial t}\right\} = \mathcal{L}\{\gamma\tau(t)\} - \mathcal{L}\{\beta\rho(t)\} \tag{25}$$

Eq. (25) can be written as:

$$-s\,\bar{\rho}(s) = \gamma\bar{\tau}(s) - \beta\bar{\rho}(s) \tag{26a}$$

Reorganizing Eq. (26a) gives:

$$\bar{\rho}(s) = \frac{\gamma\bar{\tau}(s)}{\beta + s} \tag{26b}$$

Inserting Eq. (26b) into Eq. (24) yields:

$$s\bar{\tau}(s) - \tau(0) + \frac{\gamma\bar{\tau}(s)s}{\beta + s} = -\delta^2\bar{\tau}(s) \tag{27}$$

The only variable in Eq. (27) is $\bar{\tau}(s)$, thus can easily be solved using the initial conditions. For a non-trivial solution, eigenvalues of Eq. (27) can be found by using the residue theorem. The eigenvalues for a non-trivial solution are given in Eq. (29). Furthermore, Eqs. (22a-c) are second order ordinary differential equations which have a general solutions: $A_1 \sin Kx_i + A_2 \cos Kx_i$ which can be solved using the boundary conditions. Hence, the set of coupled differential equations of the 3D HDM are solved analytically for the both bound and unbound moisture concentrations $n(x, y, z, t)$ and $N(x, y, z, t)$ of a fully immersed slab.

The developed analytical solution, given in Eqs. (18a-b), describes the concentration of the bound, $N(x, y, z, t)$, and unbound, $n(x, y, z, t)$, moisture concentrations as a function of time and space.

$$N(x,y,z,t) = \frac{\gamma}{\beta} n_{\infty}$$

$$\left\{1 - \frac{64}{\pi^3} \sum_{i=1}^{\infty(odd)} \sum_{j=1}^{\infty(odd)} \sum_{m=1}^{\infty(odd)} (-1)^{\frac{i-1}{2}} (-1)^{\frac{j-1}{2}} (-1)^{\frac{m-1}{2}} \frac{r_{i,j,m}^{+}\, exp\left(-r_{i,j,m}^{-} t\right) - r_{i,j,m}^{-} \exp\left(-r_{i,j,m}^{+} t\right)}{\mathrm{ijm}\left(r_{i,j,m}^{+} - r_{i,j,m}^{-}\right)} \cos\left(\frac{\pi i x}{L}\right) \cos\left(\frac{\pi j y}{W}\right) \cos\left(\frac{\pi m z}{H}\right)\right\}$$

(28a)

$$n(x,y,z,t)$$

$$= n_{\infty} \left\{ \begin{array}{l} 1 - \frac{64}{\pi^3} \sum_{i=1}^{\infty(odd)} \sum_{j=1}^{\infty(odd)} \sum_{m=1}^{\infty(odd)} (-1)^{\frac{i-1}{2}} (-1)^{\frac{j-1}{2}} (-1)^{\frac{m-1}{2}} \frac{r_{i,j,m}^{+}\, exp\left(-r_{i,j,m}^{-} t\right) - r_{i,j,m}^{-} \exp\left(-r_{i,j,m}^{+} t\right)}{\mathrm{ijm}\left(r_{i,j,m}^{+} - r_{i,j,m}^{-}\right)} \cos\left(\frac{\pi i x}{L}\right) \cos\left(\frac{\pi j y}{W}\right) \cos\left(\frac{\pi m z}{H}\right) \\ + \\ \frac{64}{\pi^3 \beta} \sum_{i=1}^{\infty(odd)} \sum_{j=1}^{\infty(odd)} \sum_{\mathrm{m}=1}^{\infty(odd)} (-1)^{\frac{i-1}{2}} (-1)^{\frac{j-1}{2}} (-1)^{\frac{m-1}{2}} \left(r_{i,j,m}^{+} r_{i,j,m}^{-}\right) \frac{exp\left(-r_{i,j,m}^{-} t\right) - \exp\left(-r_{i,j,m}^{+} t\right)}{\mathrm{ijm}\left(r_{i,j,m}^{+} - r_{i,j,m}^{-}\right)} \cos\left(\frac{\pi i x}{L}\right) \cos\left(\frac{\pi j y}{W}\right) \cos\left(\frac{\pi m z}{H}\right) \end{array} \right\}$$

(28b)

where

$$r_{i,j,m}^{\pm} = \frac{1}{2}\left[(K_{i,j,m} + \gamma + \beta) \pm \sqrt{(K_{i,j,m} + \gamma + \beta)^2 - 4K_{i,j,m}\beta}\right]$$
$$K_{i,j,m} = \frac{\pi^2 D_x}{L^2} i^2 + \frac{\pi^2 D_y}{W^2} j^2 + \frac{\pi^2 D_z}{H^2} m^2 \tag{29}$$

The total mass gain is determined by integration of the sum of bound and unbound moisture concentration over the volume and is given in Eq. (30).

$$M(t) = M_\infty \left\{ \begin{array}{l} 1 - \frac{512}{\pi^6} \sum_{i=1}^{\infty(odd)} \sum_{j=1}^{\infty(odd)} \sum_{m=1}^{\infty(odd)} \frac{r_{i,j,m}^{+} \, exp\left(-r_{i,j,m}^{-} t\right) - r_{i,j,m}^{-} exp(-r_{i,j,m}^{+} t)}{i^2 j^2 m^2 (r_{\mathrm{i,j,m}}^{+} - r_{\mathrm{i,j,m}}^{-})} \\ + \frac{512\mu}{\pi^6} \sum_{i=1}^{\infty(odd)} \sum_{j=1}^{\infty(odd)} \sum_{m=1}^{\infty(odd)} K_{i,j,m} \frac{exp\left(-r_{i,j,m}^{-} t\right) - exp(-r_{i,j,m}^{+} t)}{i^2 j^2 m^2 (r_{\mathrm{i,j,m}}^{+} - r_{\mathrm{i,j,m}}^{-})} \end{array} \right\} \tag{30}$$

It is worth noting that the analytical solution of the 3D HDM given in Eq. (30) simplifies to Eq. (10) for the one-dimensional case. In addition, both the expressions of bound and unbound moisture concentrations given in Eqs. (28a-b) simplify to the corresponding equations developed by Carter and Kibler [54] for the one-dimensional case.

Analytical solution of the hindered diffusion model in Eqs. (28) allows to illustrate the edge effects and anisotropy in moisture absorption. Absorption parameters of quartz/BMI samples [19] are used to construct moisture concentration profiles (*Case i*). To compare anisotropic and isotropic absorption, the planar diffusion coefficient is set to the through-the-thickness diffusion coefficient (*Case ii*). Moreover, effect of finite material dimension on moisture absorption exemplified by setting the planar diffusion coefficient to zero (*Case iii*). Table 1 shows the absorption parameters used to create the concentration profiles for a 30 × 30 × 10.55 mm sample.

Table 1. Absorption parameters of the concentration profiles in Figure 12.

	i) 40-ply Quartz/BMI	*ii*) Isotropic	*iii*) One-dimensional
Through-the-thickness Diffusion Coefficient, D_z	3.94×10^{-4}	3.94×10^{-4}	3.94×10^{-4}
Planar Diffusion Coefficient, $D_x = D_y$	4.04×10^{-3}	3.94×10^{-4}	-
Bound→Unbound, β	5.64×10^{-5}	5.64×10^{-5}	5.64×10^{-5}
Unbound→Bound, γ	2.74×10^{-5}	2.74×10^{-5}	2.74×10^{-5}
Maximum Moisture Content, M_∞	1.80	1.80	1.80

Figure 12 illustrates the concentration profile of three cases given in Table 1 at 96 days, 384 days and 864 days. The two-dimensional concentration profiles are taken from the mid-plane of a three-dimensional slab illustrated in Figure 12. In all three cases, moisture content in the slabs increases over time. Between the *case i* and *ii*, the only difference is the planar diffusion coefficient. In the isotropic case, the planar diffusion coefficient is set to through-the-thickness diffusion coefficient which has a lower value. Smaller planar diffusion coefficient in *case ii* yields slower absorption through the side surfaces. At 864 days, average concentration in *case ii* is 25% lower than the *case i*.

In *case iii*, the absorption through the side surfaces are negligible. Thus, no concentration gradient in the x and y direction is observed. Diffusion flux is only through the thickness (z direction). Case iii absorbed 42% and 22% less amount of water at 864 days than *case i* and *ii*, respectively. Comparing *case ii* and *iii* indicates that having a finite dimensions causes a faster moisture intake. For an accurate characterization of the absorption behavior, three dimensional effects must be considered when material anisotropy exist and/or planar sizes are comparable to the thickness.

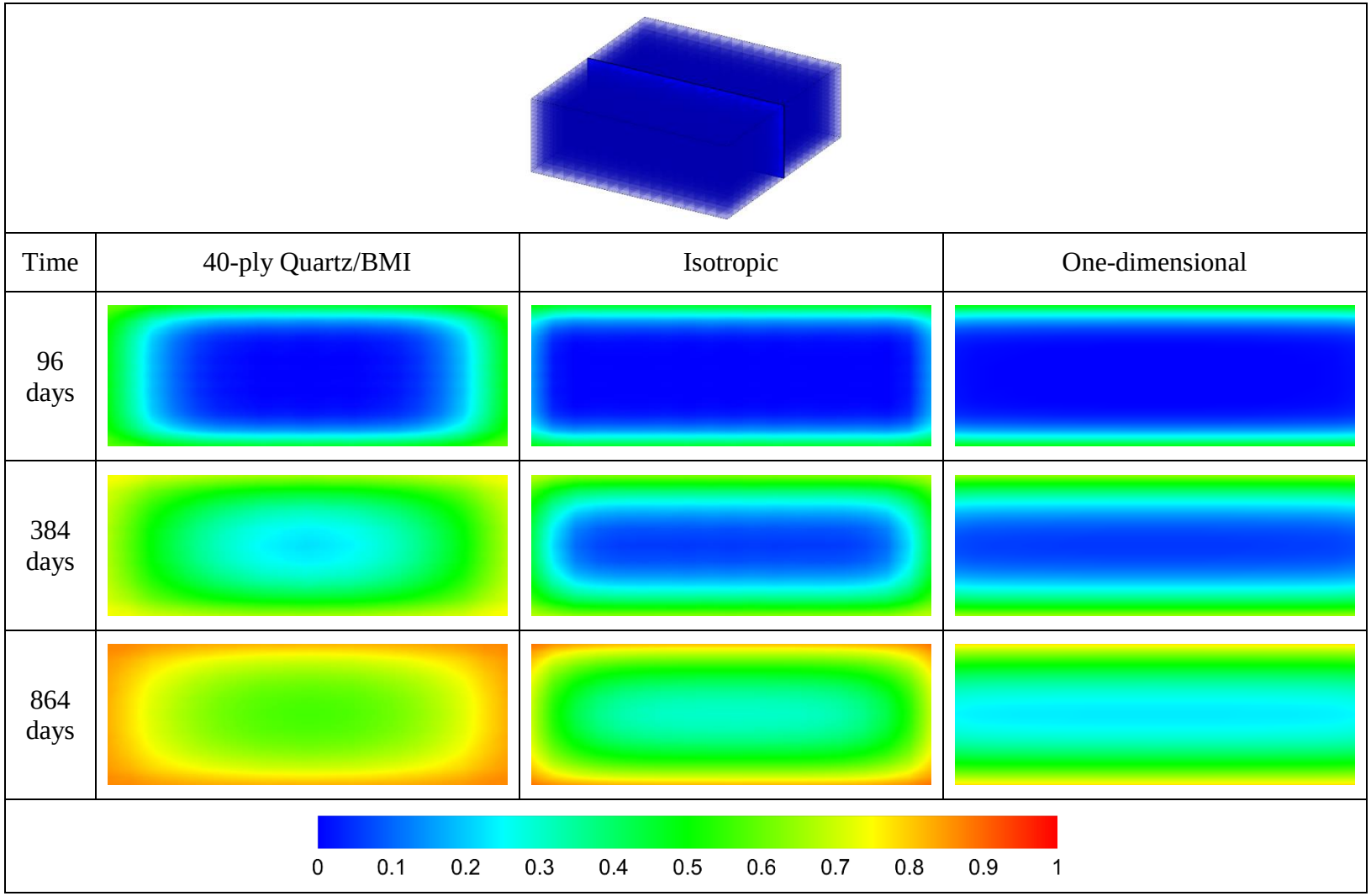


Figure 12. Concentration profile of anisotropic, isotropic, and one-dimensional quartz/BMI laminate at t=96, 384, and 864 days

iii. Non-dimensional and Approximate Solution of 3D HDM

To further investigate the capabilities of 3D HDM, non-dimensional solution is also obtained for a fully immersed slab. A new coordinate system x_1, y_1, and z_1 is defined as

$$x_1 = \sqrt{\frac{D}{D_x}}x,\ y_1 = \sqrt{\frac{D}{D_y}}y,\ z_1 = \sqrt{\frac{D}{D_z}}z$$

Original space $dxdydz$ transforms to $\frac{\sqrt{D_x D_y D_z}}{D^{3/2}}dx_1 dy_1 dz_1$

$$D = \sqrt[3]{D_x D_y D_z} \tag{31}$$

Using Eqs. (18) and (31), the non-dimensional form of 3D HDM becomes:

$$\Delta n^* = \frac{\partial n^*}{\partial t^*} + \mu^* \frac{\partial N^*}{\partial t^*} \tag{32a}$$

$$\frac{\partial N^*}{\partial t^*} = \beta^*(n^* - N^*) \tag{32b}$$

where:

$$x^* = \frac{x_1}{h} \qquad y^* = \frac{y_1}{h} \qquad z^* = \frac{z_1}{h}$$

$$\beta^* = \frac{h^2}{D}\beta \qquad \gamma^* = \frac{h^2}{D}\gamma \qquad \mu^* = \frac{\gamma^*}{\beta^*}$$

$$n^* = \frac{n}{n_\infty} \qquad N^* = \frac{N}{N_\infty} \qquad t^* = \frac{D}{h^2}t$$

Non-dimensional form of 3D HDM is similar to the non-dimensional form of 1D HDM. The only difference that 3D HDM has the spatial Laplacian of the unbound concentration instead of curvature of the unbound concentration. Having a similar non-dimensional formula allows transformation between the non-trivial solutions of the models. Seeking an approximate analytical solution for 3D HDM is found to be mathematically challenging. Non-dimensional solution similarity yielded that the 3D HDM and 1D HDM have the same approximate solution shown in Eqs. (12-13). It should

be noted here that the diffusivity used for 3D HDM should be the average diffusivity in Eq. (31). The approximate solution of 3D HDM can be utilized to find initial guesses in absorption parameter recovery.

2.5. Other Diffusion Models

i. Dual-Diffusivity Model

Jacobs and Jones [50] proposed a dual-diffusivity model describing the moisture absorption behavior of a polymer with two phases. Two-phase polymer is assumed to consist of dense and less dense polymer phases which have different diffusivity and maximum moisture content. Thus, both phases absorb water in different rates.

Figure 13 shows a typical non-Fickian type uptake behavior of moisture absorption and different regions of dual diffusivity model. Region I is the initial absorption where diffusion takes place in both phases. In Region II, only dense phase continues absorption whereas the less dense phase assumed to be saturated

Each phase has own diffusion coefficient and equilibrium moisture content. The equilibrium moisture content of less dense phase, M_l, is found by extrapolating the slope of the absorption curve in Region II to moisture content axis. Subtracting M_l from maximum moisture content, M_∞, gives the equilibrium moisture content of dense phase, M_d. Using the equilibrium moisture contents and the initial slope, s_1, and the slope of Region II, s_d, average diffusion coefficient, D_z, and diffusion coefficients of dense phase, D_d, and less dense phase, D_l can be found using Eqs. (33a-c).

$$D_z = \pi \left[\frac{s_1 h}{4M_\infty}\right]^2 \tag{33a}$$

$$D_d = \pi \left[\frac{s_d h}{4M_d}\right]^2 \tag{33b}$$

$$D_l = \pi \left[\frac{(s_1 - s_d) h}{4M_l}\right]^2 \tag{33c}$$

The normalized moisture absorption curve is represented by Eq. (34).

$$M(t) = V_d \left\{1 - exp\left[-7.3\left(\frac{D_d t}{h^2}\right)^{0.75}\right]\right\} + (1 - V_d)\left\{1 - exp\left[-7.3\left(\frac{D_l t}{h^2}\right)^{0.75}\right]\right\} \tag{34}$$

where V_d is the volume fraction of the dense phase relative to the total system.

$$V_d = \frac{\left(\frac{D_d}{D_l} + 2\right)\left(\frac{D_z}{D_l} - 1\right)}{\left(\frac{D_d}{D_l} - 1\right)\left(\frac{D_z}{D_l} + 2\right)} \tag{35}$$

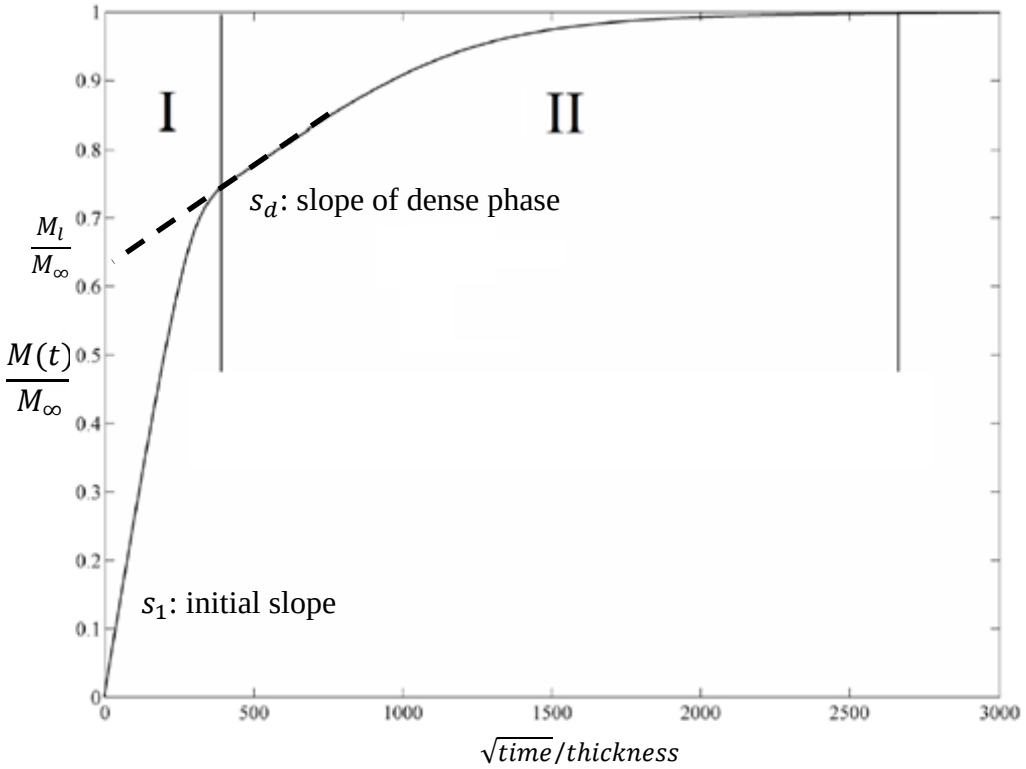


Figure 13. Two stages of dual diffusivity model on non-Fickian mass gain

ii. Time-Varying Diffusivity Model

Weitsman [114] developed a one-dimensional diffusion model with time-varying diffusivity. The diffusion model is same as the classical Fickian model but the diffusion coefficient is assumed to be a function of temperature. Weitsman [114] states that if the material is subjected to time-varying temperature, the diffusivity will be a function of time. Governing equation of time-varying diffusivity model is given in Eq. (36).

$$\frac{\partial C}{\partial t} = D_0 exp\left[-\frac{B}{\theta(t)}\right]\frac{\partial^2 C}{\partial x^2} \tag{36}$$

where, D_0, B are material constants and $\theta(t)$ is the absolute temperature function.

The solution of differential equation in Eq. (36) is given in Eq. (37).

$$C(x,t) = C_0\left\{1 + \frac{4}{\pi}\sum_{n=1}^{\infty}\frac{(-1)^n}{2n-1}Cos\left[\frac{(2n-1)\pi x}{2L}\right]exp\left[-\left(\frac{(2n-1)\pi}{2}\right)^2 t^*\right]\right\} \tag{37}$$

where

$$t^* = \frac{D_0\int_0^t exp\left[-\frac{B}{\theta(s)}\right]ds}{L^2} \tag{38}$$

If the integral in Eq. (38) is equal to t, diffusion is not time dependent and reduced to the classical Fickian diffusion.

2.6. Model Parameter Recovery

Both the Fickian and hindered diffusion models contain a model specific set of material properties generally referred to as "absorption parameters" or "diffusion parameters" which are needed for the characterization of liquid absorption in a particular polymer or composite. The one-dimensional Fickian diffusion model uses only two distinctive absorption parameters: through-the-thickness diffusion coefficient, D, and the maximum amount of penetrant that the material can absorb, M_∞, often given in terms of weight percentage. In the event that edge effects and/or anisotropy are present, different directions might have different diffusion coefficients, usually referred to as: through-the-thickness diffusion coefficient, D_z, and planar diffusion coefficients, D_x and D_y in the direction of x and y, respectively. When the diffusion is non-Fickian, the hindered diffusion model introduces two additional parameters to the ones used in the Fickian model: the rate of bound molecules becoming mobile per unit time, β, and the rate of mobile molecule becoming bound per unit time, γ. Bound molecule means that the liquid penetrant is chemically interacts and binds the medium, whereas in the case of unbound molecule penetrant is mobile and free to diffuse into the medium.

The most accurate and versatile method available to recover the absorption parameters is the one proposed by Aktas et al. [61]. The absorption parameters of a material can be recovered simultaneously from experimental moisture absorption data by using a gradient optimization method to match the data with either the exact analytical or the approximate solution. The error to be minimized in the matching algorithm is:

$$E(t) = \sum_{j}^{n} [M_j(t) - M_{exp,j}(t)]^2 \tag{39}$$

where $M(t)$ and $M_{exp}(t)$ are theoretically predicted and experimentally measured mass gains, respectively. The error function, $E(t)$, is calculated via the summation of the errors from each one of the n data points on the thermogravimetric curve.

A modified version of the steepest descent method [61] is used to iteratively find the set of absorption parameters that minimize the function $E(t)$. The gradient vector in the steepest descent optimization method is always towards the local maximum. Therefore, the model parameters are adjusted in the opposite direction of the gradient vector at each k^{th} iteration in order to find the minimum as given in Eqs. (40-41).

$$[U_i]_{k+1} = [U_i]_k - [\rho_i \nabla \bar{E}. U_i]_k \tag{40}$$

$$\nabla \bar{E} = \frac{\frac{\partial E}{\partial U_i}}{\sqrt{\sum_{i=1}^{n} \left(\frac{\partial E}{\partial U_i}\right)^2}} \tag{41}$$

where ρ_i is a vector of parameters chosen to accelerate the minimization of $E(t)$, k is the number of iterations, U_i is the absorption parameter to be recovered (e.g., $D, \beta, \gamma,$ and M_∞ for Langmuir diffusion model), and n is the number of absorption parameters (e.g. n=2 for Fickian and n=4 for Langmuir diffusion model).

To start the algorithm, initial values should be assigned to unknown absorption parameters. Selection of the initial guess should be performed carefully, as the rate of convergence is highly sensitive to these values. Consequently, absorption parameters of a similar material systems could be useful in this selection. A recent approach developed by Guloglu et al. [1] is to use the parameters obtained from the approximate solutions as

the initial guess. This novel approach could serve as excellent initial values and likely reduce the number of iterations needed, thus leading to the rapid recovery of parameters as demonstrated later in this section.

The minimization algorithm recalculates each of the absorption parameters based on the normalized gradient of the previous iteration. Using this algorithm, the set of absorption parameters that minimizes the function $E(t)$ can be found after the specified error convergence is achieved. Minimizing $E(t)$ results in the best possible match between the model prediction and each data point, and thus generates the best possible set of absorption parameters that represent the thermogravimetric experimental data.

The main advantage of this optimization method is that it minimizes $E(t)$ using all parameters simultaneously by changing their values at each iteration according to their individual effect on the error function $E(t)$. An advantage of the steepest descent optimization method is that when the function is differentiable and convex, this method is convergent. However, the number of iterations required and the convergence rate highly depend on the initial values supplied by the user.

i. Absorption parameters to be recovered

- Classical Fickian Model

$$[U_i] = \begin{bmatrix} D \\ M_\infty \end{bmatrix}$$

- Langmuir-type Diffusion Model (1D Hindered Diffusion Model)

$$[U_i] = \begin{bmatrix} D \\ \gamma \\ \beta \\ M_\infty \end{bmatrix}$$

- 3D Fickian Diffusion Model

$$[U_i] = \begin{bmatrix} D_x \\ D_y \\ D_z \\ M_\infty \end{bmatrix}$$

- 3D Hindered Diffusion Model

$$[U_i] = \begin{bmatrix} D_x \\ D_y \\ D_z \\ \gamma \\ \beta \\ M_\infty \end{bmatrix}$$

To illustrate the recovery mechanism, a representative thermo-gravimetric data is generated. No approximate solution is used to get the initial guesses. In order to demonstrate the predictive capabilities of modified steepest descent method, initial guesses are deliberately chosen not to represent the generated moisture mass gain curve. Table 2 presents the one-dimensional hindered diffusion model absorption parameters used to generate the synthetic data, initialing parameters and final recovered parameters.

Table 2. Diffusion parameters of the synthetic data, initial guess, and model prediction

	Synthetic Data	Initial Guess	Recovered
Through-the-thickness Diffusion Coefficient, D_z	7.00×10^{-4}	1.00×10^{-4}	6.86×10^{-4}
Bound→Unbound, β	1.00×10^{-3}	4.00×10^{-3}	9.72×10^{-4}
Unbound→Bound, γ	4.00×10^{-4}	1.00×10^{-4}	3.82×10^{-4}
Maximum Moisture Content, M_∞	2.00	3.00	2.00

The recovery starts with the initial guesses given in Table 2 and continues until the least square error between the model prediction and generated data is minimized. To show how the recovery method minimizes the error, synthetic mass gain data, initial guess, 100^{th}, 250^{th}, 500^{th}, and 750^{th} iteration predictions, and final prediction is illustrated in

Figure 14. The initial guess has completely different absorption kinetics than the generated data. Figure 14 shows that the model prediction quickly approaches to the synthetic data and slows down to fine-tune the absorption parameters.

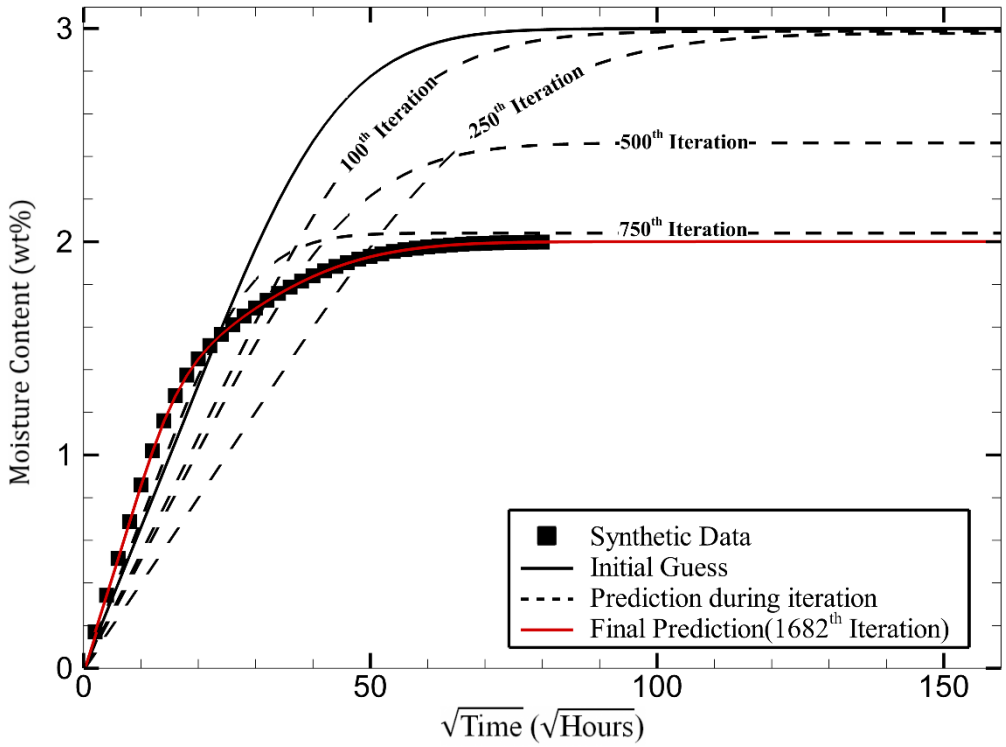


Figure 14. Absorption parameter recovery from thermo-gravimetric synthetic data.

Figure 15 illustrates how the least square error per data point changes during the recovery mechanism. The error between the model prediction and the data quickly decreases. Once the model prediction and the mass gain data start to overlap, the error starts oscillating. Even though the direction of the error gradient is towards to a local maximum, high local error gradient of an absorption parameter may lead to overshooting the absorption parameter in the next iteration. Thus, once the error is low, it starts oscillating towards to local minima. Moreover, two separate plateaus can be observed in Figure 15 around iteration number ~300 and ~800. These two plateaus are due to the error

gradient domination. Right after the first plateau, error gradient of M_∞ and D_z becomes the prevailing force to minimize the error. In the beginning of the second plateau, the recovery method already found the maximum moisture content of the synthetic data. The error gradient of M_∞, $\frac{\partial E}{\partial M_\infty}$, is no longer contributing to the recovery method as much as before. After 800 iteration, error gradient of γ, β, and D_z drives the recovery. It should be noted here that dominance of the error gradient of a constituent depends on the initial guesses and chosen vector parameters.

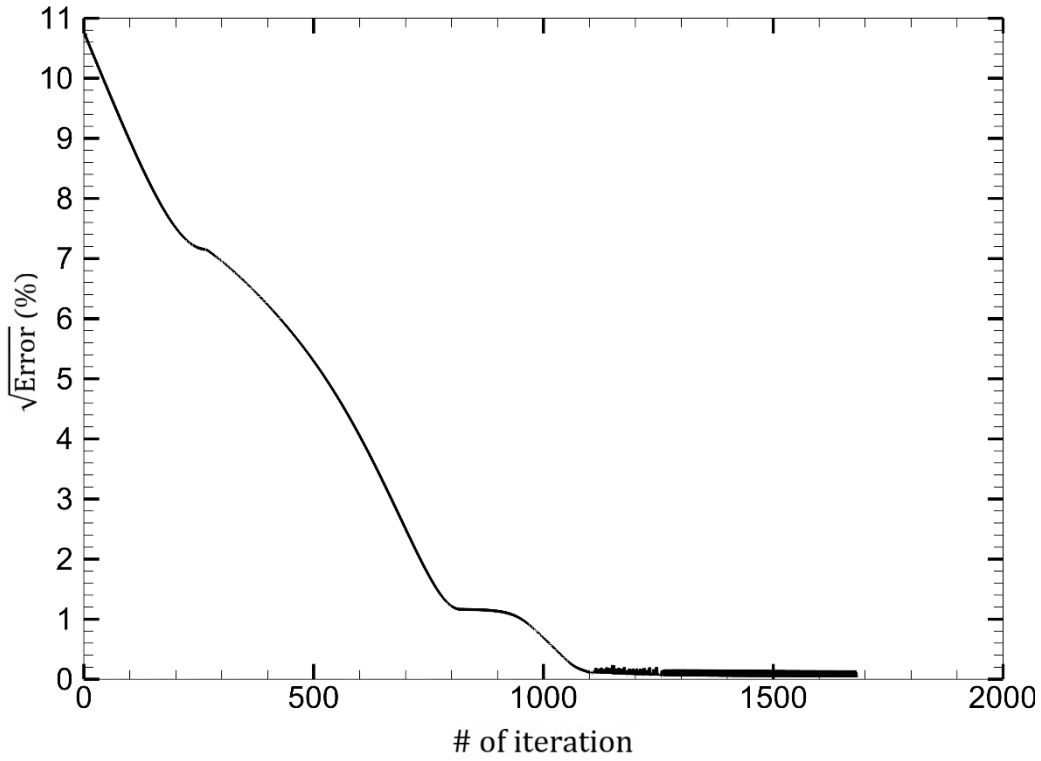


Figure 15. Variation in the least square error per data point during absorption parameter recovery

2.7. Multilayer Hindered Diffusion Model

To improve quality and service life, many engineering polymers are subjected to various protective coatings and processes prior to use. Although three-dimensional hindered diffusion model can account for material anisotropy, edge effects, and non-Fickian behavior, it cannot predict the multilayer effects on absorption behavior. Thus, 3D HDM is modified to consider a continuous absorption with the discrete changes in material properties. This modification yields the following governing equations for multilayer, three-dimensional, and anisotropic hindered diffusion model:

$$D_{x,i}\frac{\partial^2 n_i}{\partial x^2} + D_{y,i}\frac{\partial^2 n_i}{\partial y^2} + D_{z,i}\frac{\partial^2 n_i}{\partial z^2} = \frac{\partial n_i}{\partial t} + \frac{\partial N_i}{\partial t} \tag{42a}$$

$$\frac{\partial N_i}{\partial t} = \gamma n_i - \beta N_i \tag{42b}$$

The analytical solution of the differential equations shown in Eqs. (42a-b) yields the concentration of the bound, N_i, and unbound, n_i, moisture molecules as a function of time and space, where the subscript, i, represents the number of layers.

An analytical solution of multilayer hindered diffusion model can be derived for any number of layers. However, the analytical solution of only two separate cases (Figure 16a-b), will be derived. In first case, the substrate is coated by a single layer of thickness, a, on one surface (Figure 16a). In the second case, the substrate is coated by a single layer of thickness, a, on both sides (Figure 16b). The coupled system of partial differential equations given in Eqs. (42a-b) are solved analytically by applying the initial and boundary conditions given in Eqs. (43a-d).

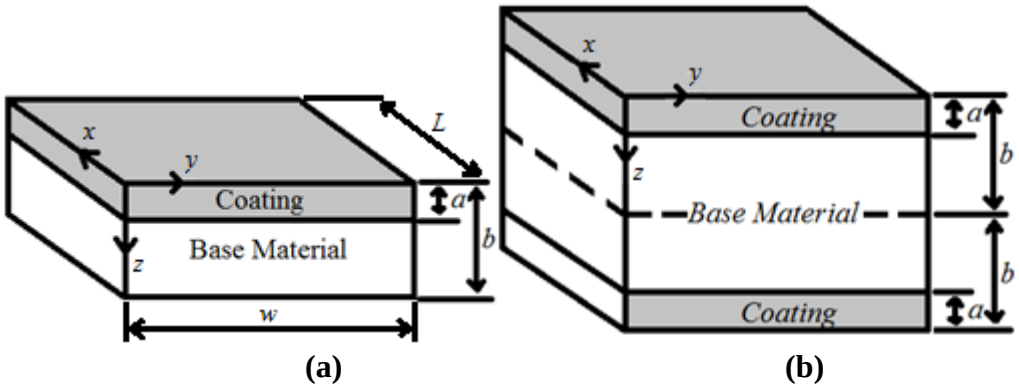


Figure 16. The representation of the model geometry (a) for a single coating layer of thickness a. The total sample thickness is b. (b) for a symmetric coating layer of thickness a. The total sample thickness is $2b$.

i. Initial and Boundary Conditions

Initially, at time, $t = 0$, the coating and the substrate are taken to be completely dry.

$$N_1(x, y, z, 0) = n_1(x, y, z, 0) = N_2(x, y, z, 0) = n_2(x, y, z, 0) \tag{43a}$$

The coating is designated by subscript 1 and substrate is designated by subscript 2.

The solution is derived for a fully immersed slab. For the three-dimensional samples shown in Figure 16a-b common boundary conditions become:

$$n_1(0, y, z, t) = n_1(x, 0, z, t) = n_1(x, y, 0, t) = n_2(L, y, z, t)$$
$$= n_2(x, w, z, t) = \frac{\beta}{\beta + \gamma} C_0 = n_\infty \tag{43b}$$

$$N_1(0, y, z, t) = N_1(x, 0, z, t) = N_1(x, y, 0, t) = N_2(L, y, z, t)$$
$$= N_2(x, w, z, t) = \frac{\gamma}{\beta + \gamma} C_0 = N_\infty \tag{43c}$$

The total moisture concentration is the summation of bound and unbound moisture and is equal to C_0 in equilibrium.

Interface conditions between the coating and the substrate can be written as:

$$D_1 \frac{\partial n_1(x,y,a,t)}{\partial z} = D_2 \frac{\partial n_2(x,y,a,t)}{\partial z}$$
$$n_1(x,y,a,t) = n_2(x,y,a,t) \tag{43d}$$
$$N_1(x,y,a,t) = N_2(x,y,a,t)$$

At an ideal interface, the flux from the substrate to coating is equal to the flux from the coating to substrate. Moreover, the moisture concentration at the interface between the coating and the substrate must be equal. Eq. (43d) represents idealized interface conditions which indicate a perfect contact without interfacial resistance or delamination which may behave as a moisture accumulation site.

$$n_2(x,y,b,t) = \frac{\beta}{\beta+\gamma} C_0 \qquad N_2(x,y,b,t) = \frac{\gamma}{\beta+\gamma} C_0 \tag{43e}$$

Eq. (43e) shows boundary conditions specific to the one layer coating shown in Figure 16a. The boundary conditions represents the unbound, n_2, and bound, N_2, maximum moisture content at the free edge of b that the material can absorb.

$$D_1 \frac{\partial n_1(x,y,b,t)}{\partial z} = 0 \tag{43f}$$

Eq. (43f) shows boundary conditions specific to the both layer symmetric coating shown in Figure 16b. Eq. (43f) expresses that moisture flux is zero at the centerline, b, of the both layer symmetric coated sample. The centerline is also the symmetry line and the boundary, interface conditions, and moisture concentrations are also symmetric around the symmetry axis.

ii. Analytical Solution Procedure of Quadruple PDE of Multilayer Hindered Diffusion Model

Separation of variables technique is applied to Eq. (42a) by assuming that the variables x, y, z and t in $n_{\mathrm{i}}(x,y,z,t)$ and $N_{\mathrm{i}}(x,y,z,t)$ are independent. Hence the solution for n_{i} and N_{i} can be expressed as:

$$\begin{aligned} n_{\mathrm{i}}(x,y,z,t) &= \sigma_i(x)\varepsilon_i(y)\varphi_i(z)\tau(t) \\ N_{\mathrm{i}}(x,y,z,t) &= \sigma_i(x)\varepsilon_i(y)\varphi_i(z)\rho(t) \end{aligned} \tag{44}$$

Applying Eq. (44) to Eqs. (42a-b) and simplifying result in,

$$\begin{aligned} &D_{x,i}\frac{1}{\sigma_i(x)}\frac{\partial^2\sigma_i(x)}{\partial x^2} + D_{y,i}\frac{1}{\varepsilon_i(y)}\frac{\partial^2\varepsilon_i(y)}{\partial y^2} + D_{z,i}\frac{1}{\varphi_i(z)}\frac{\partial^2\varphi_i(z)}{\partial z^2} \\ &= \frac{1}{\tau(t)}\frac{\partial\tau(t)}{\partial t} + \frac{1}{\tau(t)}\frac{\partial\rho(t)}{\partial t} = -\delta^2 \end{aligned} \tag{45a}$$

$$\frac{\partial\rho(t)}{\partial t} = \gamma\tau(t) - \beta\rho(t) \tag{45b}$$

where

$$-\delta^2 = -\bar{X}^2 - \bar{Y}^2 - \bar{Z}^2$$

Eq. (45a) can also be written as follows,

$$D_{x,i}\frac{\partial^2\sigma_i(x)}{\partial x^2} = -\bar{X}^2\sigma_i(x) \tag{46a}$$

$$D_{y,i}\frac{\partial^2\varepsilon_i(y)}{\partial y^2} = -\bar{Y}^2\varepsilon_i(y) \tag{46b}$$

$$D_{z,i}\frac{\partial^2\varphi_i(z)}{\partial z^2} = -\bar{Z}^2\varphi_i(z) \tag{46c}$$

$$\frac{\partial\tau(t)}{\partial t} + \frac{\partial\rho(t)}{\partial t} = -\delta^2\tau(t) \tag{46d}$$

Inserting Eq. (45b) into Eq. (46d) yields,

$$\frac{\partial \tau(t)}{\partial t} + \gamma\tau(t) - \beta\rho(t) = -\delta^2\tau(t) \tag{47}$$

There needs to be a correlation between $\tau(t)$ and $\rho(t)$ in order to solve the system of equations. The correlation can be found by Laplace transformation of Eq. (45b).

$$\mathcal{L}\left\{\frac{\partial \rho(t)}{\partial t}\right\} = \mathcal{L}\{\gamma\tau(t)\} - \mathcal{L}\{\beta\rho(t)\} \tag{48}$$

Eq. (48) gives,

$$-s\,\bar{\rho}(s) = \gamma\bar{\tau}(s) - \beta\bar{\rho}(s) \tag{49a}$$

Reorganizing and inverse Laplace transformation of Eq. (49a) results,

$$\rho(t) = \mathcal{L}^{-1}\left\{\frac{\gamma\bar{\tau}(s)}{\beta - s}\right\} = \frac{1}{2\pi i}\int_{\bar{\gamma}-i\infty}^{\bar{\gamma}+i\infty} \frac{\gamma\bar{\tau}(s)}{\beta - s} e^{st} ds \tag{49b}$$

where $\bar{\gamma}$ is a vertical contour in the complex plane chosen so that all singularities of $\frac{\bar{\tau}(t)}{\beta - s}$ are to the left of it.

Eq. (47) becomes,

$$\frac{\partial \tau(t)}{\partial t} + \gamma\tau(t) - \frac{\beta\gamma}{2\pi i}\int_{\bar{\gamma}-i\infty}^{\bar{\gamma}+i\infty} \frac{\bar{\tau}(s)}{\beta - s} e^{st} ds = -\delta^2\tau(t) \tag{50}$$

Eq. (50) becomes only the function of $\tau(t)$. The inverse Laplace transformation is solved by using Residue Theorem.

Eqs. (46a-b) are second order ordinary differential equations which can be solved easily. However, Eq. (46c) is solved using Orthogonal Expansion Technique because there is a discreet property change in x direction. The boundary conditions are regenerated according to the new functions. The solution is found for homogenous boundary conditions, and then the non-homogenous boundary conditions are introduced.

$$\varphi_{1n}(0) = 0 \tag{51a}$$

$$\varphi_{1n}(a) = \varphi_{2n}(a) \tag{51b}$$

$$D_{z,1}\frac{\partial\varphi_{1n}(a)}{\partial \mathrm{x}} = D_{z,2}\frac{\partial\varphi_{2n}(a)}{\partial \mathrm{x}} \tag{51c}$$

$$\varphi_{2n}(b) = 0 \tag{51d}$$

$$D_{z,2}\frac{\partial\varphi_{2n}(b)}{\partial \mathrm{x}} = 0 \tag{51e}$$

The general solution for the Eq. (46c) eigenvalue problem is,

$$\varphi_i(x) = \sum_{n=1}^{\infty} c_n \varphi_{in}(x) \tag{52}$$

where

$$\varphi_{in}(x) = A_{in}\sin\frac{\bar{Z}_n}{\sqrt{D_{z,in}}}x + B_{in}\cos\frac{\bar{Z}_n}{\sqrt{D_{z,in}}}x \tag{53}$$

and c_n is the coefficient and can be found by utilizing the orthogonality relation.

To determine the eigenvalues and A_{in} and B_{in}, the boundary conditions are applied to Eq. (53),

For one-layer coating;

$$\begin{bmatrix} sin\left(a\frac{\bar{Z}_n}{\sqrt{D_{z,1}}}\right) & -sin\left(a\frac{\bar{Z}_n}{\sqrt{D_{z,2}}}\right) & -cos\left(a\frac{\bar{Z}_n}{\sqrt{D_{z,2}}}\right) \\ \left(\sqrt{\frac{D_{z,1}}{D_{z,2}}}\right)cos\left(a\frac{\bar{Z}_n}{\sqrt{D_{z,1}}}\right) & -cos\left(a\frac{\bar{Z}_n}{\sqrt{D_{z,2}}}\right) & sin\left(a\frac{\bar{Z}_n}{\sqrt{D_{z,2}}}\right) \\ 0 & sin\left(b\frac{\bar{Z}_n}{\sqrt{D_{z,2}}}\right) & cos\left(b\frac{\bar{Z}_n}{\sqrt{D_{z,2}}}\right) \end{bmatrix}\begin{bmatrix} 1 \\ A_{2n} \\ B_{2n} \end{bmatrix} = \begin{bmatrix} 0 \\ 0 \\ 0 \end{bmatrix} \tag{54a}$$

For symmetric two-layer coating;

$$\begin{bmatrix} sin\left(a\frac{\bar{Z}_n}{\sqrt{D_{z,1}}}\right) & -sin\left(a\frac{\bar{Z}_n}{\sqrt{D_{z,2}}}\right) & -cos\left(a\frac{\bar{Z}_n}{\sqrt{D_{z,2}}}\right) \\ \left(\sqrt{\frac{D_{z,1}}{D_{z,2}}}\right)cos\left(a\frac{\bar{Z}_n}{\sqrt{D_{z,1}}}\right) & -cos\left(a\frac{\bar{Z}_n}{\sqrt{D_{z,2}}}\right) & sin\left(a\frac{\bar{Z}_n}{\sqrt{D_{z,2}}}\right) \\ 0 & cos\left(b\frac{\bar{Z}_n}{\sqrt{D_{z,2}}}\right) & -sin\left(b\frac{\bar{Z}_n}{\sqrt{D_{z,2}}}\right) \end{bmatrix} \begin{bmatrix} 1 \\ A_{2n} \\ B_{2n} \end{bmatrix} = \begin{bmatrix} 0 \\ 0 \\ 0 \end{bmatrix} \quad (54b)$$

Equating the determinant of the matrix in Eq. (54) to zero gives the eigenvalues, $\bar{Z}_n$, for both cases.

When the solutions of $\sigma_i(x)\ \varepsilon_i(y)\ \varphi_i(z)$ and $\tau(t)$ and $\rho(t)$ are combined, the result gives the analytical solution of the multi-layer hindered diffusion model.

The total moisture concentration $n_{\mathrm{i}}(x,y,z,t)$+$N_{\mathrm{i}}(x,y,z,t)$ is

$$n_{\mathrm{i}}(x,y,z,t) + N_{\mathrm{i}}(x,y,z,t)$$

$$= \left\{ \begin{array}{l} 1 - \frac{16}{\pi^2} \sum_{i=1}^{\infty(odd)} \sum_{j=1}^{\infty(odd)} \sum_{m=1}^{\infty(odd)} \frac{L_{1,i,j,m} Int_m}{\mathrm{ij}N_m} \varphi_{1m}(z) \sin(\frac{i\pi x}{L}) \sin(\frac{i\pi y}{w}) + \\ \frac{16}{\pi^2} \sum_{i=1}^{\infty(odd)} \sum_{j=1}^{\infty(odd)} \sum_{m=1}^{\infty(odd)} \frac{L_{2,i,j,m} Int_m}{\mathrm{ij}N_m} \varphi_{2m}(z) \sin(\frac{i\pi x}{L}) \sin(\frac{i\pi y}{w}) \end{array} \right\} \quad (55)$$

The total mass gain is determined by integration of the sum of bound and unbound moisture concentration over the total sample volume and is given in Eq. (56).

$$M(t)=\left\{\begin{array}{l} M_{1,\infty}-\dfrac{64M_{1,\infty}}{a\pi^4}\sum_{i=1}^{\infty(odd)}\sum_{j=1}^{\infty(odd)}\sum_{m=1}^{\infty(odd)}\dfrac{L_{1,i,j,m}Int_m}{i^2j^2N_m}\int_{z=0}^{a}\varphi_{1m}(z)+ \\ M_{2,\infty}-\dfrac{64M_{2,\infty}}{b\pi^4}\sum_{i=1}^{\infty(odd)}\sum_{j=1}^{\infty(odd)}\sum_{m=1}^{\infty(odd)}\dfrac{L_{2,i,j,m}Int_m}{i^2j^2N_m}\int_{z=a}^{b}\varphi_{2m}(z) \end{array}\right\} \quad (56)$$

where

$$r_{1,i,j,m}^{\pm}=\frac{1}{2}[(K_{1,i,j,m}+\gamma+\beta)\pm\sqrt{(K_{1,i,j,m}+\gamma+\beta)^2-4K_{1,i,j,m}\beta}]$$

$$r_{2,i,j,m}^{\pm}=\frac{1}{2}[(K_{2,i,j,m}+\gamma+\beta)\pm\sqrt{(K_{2,i,j,m}+\gamma+\beta)^2-4K_{2,i,j,m}\beta}]$$

$L_{1,i,j,m}$

$$=\frac{(\mu_1K_{1,i,j,m}-r_{1,i,j,m}^{-})\,exp(-r_{1,i,j,m}^{+}t)-(\mu_1K_{1,i,j,m}-r_{1,i,j,m}^{+})\,exp(-r_{1,i,j,m}^{-}t)}{(r_{1,i,j,m}^{+}-r_{1,i,j,m}^{-})}$$

$L_{2,i,j,m}$

$$=\frac{(\mu_2K_{2,i,j,m}-r_{2,i,j,m}^{-})\,exp(-r_{2,i,j,m}^{+}t)-(\mu_2K_{2,i,j,m}-r_{2,i,j,m}^{+})\,exp(-r_{2,i,j,m}^{-}t)}{(r_{2,i,j,m}^{+}-r_{2,i,j,m}^{-})}$$

$$U=\frac{L_{1,i,j,m}}{L_{2,i,j,m}}$$

$$A_{2m}=U(-\sin a\frac{\varepsilon_m}{\sqrt{D_{z,1}}}\sin a\frac{\varepsilon_m}{\sqrt{D_{z,2}}}-\sqrt{\frac{D_{z,1}}{D_{z,2}}}\cos a\frac{\varepsilon_m}{\sqrt{D_{z,1}}}\cos a\frac{\varepsilon_m}{\sqrt{D_{z,2}}})$$

$$B_{2m}=U(-\sin a\frac{\varepsilon_m}{\sqrt{D_{z,1}}}\cos a\frac{\varepsilon_m}{\sqrt{D_{z,2}}}+\sqrt{\frac{D_{z,1}}{D_{z,2}}}\cos a\frac{\varepsilon_m}{\sqrt{D_{z,1}}}\sin a\frac{\varepsilon_m}{\sqrt{D_{z,2}}})$$

$$N_m = \int_{\acute{z}=0}^{a} \varphi_{1m}^2(\acute{z})\, F_1(\acute{z}) d\acute{z} + \int_{\acute{z}=a}^{b} \varphi_{2m}^2(\acute{z})\, F_2(\acute{z}) d\acute{z}$$

$$Int_m = \int_{\acute{z}=0}^{a} \varphi_{1m}(\acute{z})\, F_1(\acute{z}) d\acute{z} + \int_{\acute{z}=a}^{b} \varphi_{2m}(\acute{z})\, F_2(\acute{z}) d\acute{z}$$

$$F_1 = F_2 = -1$$

$$\varphi_{1m}(z) = \sin\left(\frac{\varepsilon_m}{\sqrt{D_{z,1}}} z\right)$$

$$\varphi_{2m}(z) = A_{2m} \sin\left(\frac{\varepsilon_m}{\sqrt{D_{z,2}}} z\right) + B_{2m} \cos\left(\frac{\varepsilon_m}{\sqrt{D_{z,2}}} z\right)$$

$$K_{1,i,j,m} = \frac{\pi^2 D_{x,1}}{L^2} i^2 + \frac{\pi^2 D_{y,1}}{W^2} j^2 + \varepsilon_m$$

$$K_{2,i,j,m} = \frac{\pi^2 D_{x,2}}{L^2} i^2 + \frac{\pi^2 D_{y,2}}{W^2} j^2 + \varepsilon_m$$

Applications and validation of multilayer hindered diffusion model will be further discussed in Chapter 3.

2.8. Porous Media Diffusion Models

Presence of voids in the polymer matrix may result in substantial reduction in mechanical, electrical, and optical properties. Voids may also be purposefully introduced as pores for application specific purposes. When porous foams are used in wet environment, they absorb excessive amount of moisture due to presence of voids acting as free space.

Gueribiz et al. [104] investigated and modeled the change in diffusivity due to presence of voids. The researchers introduced a representative void into infinite matrix as seen in Figure 17. They assumed the voids are diluted in the matrix.

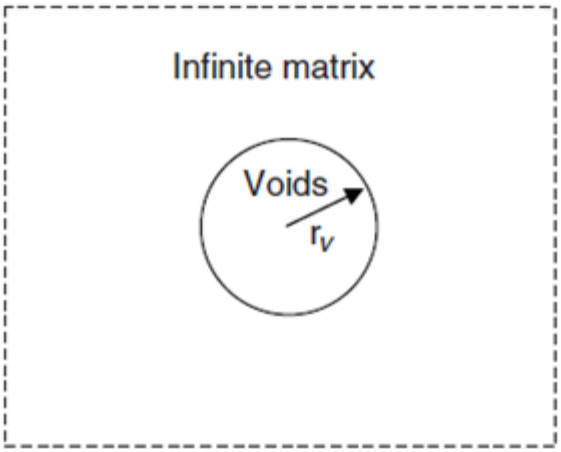


Figure 17. Representative volume element of porous media

The moisture content field solution of the unit cell problem is:

$$C(r\theta) = A_v r Cos\theta \tag{57a}$$

$$C(r\theta) = \left(Gr + \frac{B_m}{r}\right) Cos\theta \tag{57b}$$

where A_v, B_m, and G are unknown constants.

The homogeneous equivalent behavior is defined as follows:

$$D_{eff}^{m} \Delta\bar{C} = v_v D_v \Delta\bar{C}_{v_v} + v_m D_m \Delta\bar{C}_{v_m} \tag{58}$$

where D_{eff}^{m} is effective diffusivity, D_v is the diffusivity of voids, D_m is the diffusivity of matrix, and $\Delta\bar{C}$ average concentration gradients over the volume.

For continuous diffusion, the moisture content and moisture flux in/out of void/matrix at the interface must be equal. Applying the boundary conditions to Eqs. (57a-b) and solving Eq. (58) for A_v, B_m, and G yields:

$$\frac{D_{eff}}{D_m} = \left[1 + 2\frac{\rho_w}{M_m \rho_m (1 - v_v)} v_v \frac{\left({}^{D_v}/_{D_m}\right) - 1}{\left({}^{D_v}/_{D_m}\right) + 1}\right] \frac{1 - v_f}{1 + v_f} \tag{59}$$

Effective diffusivity in Eq. (59) can be used to predict the diffusivity of porous media with different void content. Increasing void content in a polymer matrix would result in extra new free volume that unbound moisture can diffuse into. Unbound moisture mostly diffuse into the polymer during the first initial uptake. Thus, a faster initial absorption rate is expected with increasing void content. In Eq. (59), higher void content increases the effective diffusivity which correlates well with the theory.

The micromechanical model [104] is a very useful tool to understand the diffusion behavior in porous structures. However, its predictive capabilities are only limited to diffusivity. The model cannot elucidate additional mass gain and non-Fickian behavior.

Bao and Yee [97] successfully used Dual Diffusivity Model [50] to predict the moisture absorption in interconnected porous polymer. Bao and Yee wisely assumed that the interconnected voids are the less dense phase and polymer matrix is the dense phase. In dual diffusivity, less dense phase contributes to only initial fast uptake and dense phase governs the non-Fickian secondary absorption. Thus, the voids have no effect on the non-Fickian behavior of the polymer.

Dual diffusivity model can be effectively used for polymers with interconnected voids. In closed-cell polymers, however, ongoing binding/unbinding of moisture molecules to the void/matrix interface during filling of the voids requires a more comprehensive model that can consider the non-Fickian effect of voids. In Chapter 4, one-dimensional hindered diffusion model has been extended to newly developed Void Filling Hindered Diffusion Model to capture the moisture absorption behavior of highly porous, closed-cell foams.

Chapter 3. Effects of Micro- and Nano-Filler Addition to Thermosetting Polymers on Moisture Absorption

Along with fiber reinforced polymers, nano-filler reinforced polymers are among the most widely used composites due to their high specific properties (i.e. specific tensile strength, elastic modulus). A variety of nano-fillers (i.e. nanofibers, nanoclay, and nano-glass spheres) make these composites unique in a way that property enhancement or degradation depend on the nano-filler type and content. A study by Gauvin and Robert [82] indicates that the addition of 5 wt.% synthetic fluorinated silicate mica nanoclay increases the tensile strength of the vinyl ester by 40%, while ODA-modified nanoclay (Montmorillonite modified with Octadecylamine) induce 15% increase. On the other hand, both fluorinated silicate mica nanoclay and ODA-modified nanoclay enhance the elastic modulus of vinyl ester by 10%. The interaction of nanoparticles with polymer chains reduces the mobility of polymer chains under loading which in turn increases the mechanical properties [115,116].

The effect of nanoclay on a thermosetting polymer may not always have a positive impact on material properties. Kim and Kim [26] reported that the presence of 3 wt.% of surface-modified montmorillonite nanoclay (Nanomer 1.30E) in YD-128 epoxy resin caused an increase in the strength and stiffness by 61.7% and 47.2%, respectively. However, further increase in nanoclay content from 3 wt.% to 5 wt.% did not yield additional gain in elastic modulus. Kim and Kim argue that high amount of nanoclay (5 wt.%) addition resulted in agglomeration of nanoclays which in turn plasticize the epoxy resin, and decrease the crosslink density of the epoxy.

Although small amount of nanoclay addition in polymers generally enhances mechanical properties, wet and high humid environments decrease the effectiveness of those improvements. Agubra et al. [117] reported that 20 day rain exposure on an E-glass/epoxy composite reinforced with 2 wt.% nanoclay induces 4.4% additional voids whereas under the same conditions, only 0.6% additional voids are detected in the E-glass/epoxy composite. These microstructral changes are one of the primary sources of material property degradation. Gauvin and Robert [82] demonstrated that salt water immersion at 50℃ for 100 days decreased the tensile strength of 5 wt.% synthetic fluorinated silicate mica nanoclay/vinyl ester composite and 5 wt.% ODA-modified nanoclay/vinyl ester by 44% and 39%, respectively. Likewise, elastic modulus of nanoclay/vinyl ester decreases between 6%-15% [82]. Other researchers also have observed property loss in storage modulus [117], tensile strength [26,117,118], elastic modulus [26,117], microhardness [3], transverse tensile strength [36], interlaminar shear strength [119], and transverse flexural strength [120] of different composites.

Different kinds of nanoclays have diverse effects on moisture absorption. Gauvin and Robert [82] state that the addition of 5 wt.% synthetic fluorinated silicate mica nanoclay in vinyl ester increases the equilibrium moisture content up to 110% when compared to neat vinyl ester. However, the addition of 5 wt.% ODA-modified nanoclay in vinyl ester merely increases the maximum moisture content by 10%. On the other hand, Kim and Kim [26] show that 1 wt.% surface-modified montmorillonite nanoclay reinforced epoxy absorb 44.3% less moisture than neat epoxy in 250 hours.

Another aspect of moisture absorption that might be influenced by nano-filler addition is diffusivity. Haq et al. [88] investigated the effect of different clay loadings on

diffusivity and stated that increasing nanoclay content of Cloisite 30B in bio-resin decreases the diffusion coefficient. Similarly, Sridhar et al. [3] reported that the addition of 5 wt.% Cloisite 15A into vinyl ester slows down the diffusion by 71%. On the other hand, addition of 5 wt.% Cloisite Na increases the diffusivity by 33%. These conflicting results show that moisture absorption kinetics in nanoclay reinforced thermosets are highly dependent on the type of nanoclay/polymer pair.

In this study, the effect of nano-filler/epoxy type and nano-filler content on moisture absorption are investigated. Thermogravimetric moisture absorption data of I.30E/DGEBA epoxy [80], and glass sphere/DGEBA epoxy [81] are used to recover the absorption parameters by one-dimensional hindered diffusion model. In order to additional correlations between nano-filler content and moisture absorption, I.30E nanoclay/EPON 862 epoxy (DGEBF) composites with different clay loading (0.5, 1, 2, 3, and 5 wt.%) are manufactured and immersed in a water bath for a year. It is significant to note that, although three-dimensional hindered diffusion model is one of the most comprehensive diffusion model, one-dimensional hindered diffusion model is used to recover the absorption behavior because (i) the samples are extremely thin compared to their planar sizes and (ii) samples having different planar sizes are needed to fully utilize 3D-HDM.

Furthermore, fully saturated micro hollow glass sphere/EPON 862 composite layer has been formed on top of neat EPON 862 epoxy to investigate the effect of composite layer on overall absorption kinetics. Fully saturated glass sphere/epoxy composite layer thicknesses are chosen as 31%, 57%, and 100% of the overall composite thickness. Absorption parameters of the fully saturated glass sphere/epoxy layer have been

recovered by multilayer hindered diffusion model to construct concentration profiles. The effects of composite layer formation on moisture absorption kinetics are investigated by comparing concentration profiles of samples with different layer thicknesses.

3.1. Effect of Different Filler Content in Epoxy

i. Materials and Sample Preparation of I.30E Nanoclay/DGEBA Epoxy

In a recent study by Al-Qadhi et al. [80], moisture absorption experiments of 1, 2, and 5 wt.% (0.67, 1.34, and 3.39 vol%) I.30E nanoclay-DGEBA epoxy nanocomposite were conducted. Samples containing different clay loadings were prepared by manually mixing of DGEBA epoxy with the desired amount of nanoclay for 5 min to achieve good dispersion. For further dispersion of the nanoclay in the epoxy, a high sheer mixing of 6000 rpm was used for 60 minutes. A cold water bath kept the temperature of the mixture between 35 and 45℃ (95-113°F). Subsequently, the required amount of hardener was added and mixed for 5 min. The resulting mixture was then poured onto an aluminum mold, pre-cured at 100℃ (212°F) for one hour and post-cured at 170℃ (338°F) for another hour. The obtained 2.5-mm thick nanoclay/epoxy was cut into 76.2 × 25.4 mm panels for the moisture absorption experiments and immersed in tap water for 299 days.

ii. Experimental Results of I.30E Nanoclay/DGEBA Epoxy and Discussion

The gravimetric data obtained from the experimental work of Al-Qadhi et al. [80] is used to determine the absorption parameters of one-dimensional hindered diffusion model. The recovered absorption parameters ($D, \gamma, \beta,\ and\ M_\infty$) are given in Table 3. Comparison of the absorption parameters with respect to their nanoclay content may outline the change in moisture uptake kinetics. In Table 3, a decreasing trend on the diffusion coefficients by increasing amount of nanoclay content is observed. A decrease

in total diffusivity is expected as nanoclay content increases since moisture molecules have to transport through a more tortuous path around the nanoclay. The diffusion coefficient of a nanoclay can be taken as zero so that the diffusion coefficient of the matrix is expected to decrease with increasing nanoclay content. More interestingly, reduction in diffusivity values was observed to follow a trend very similar to the rule of mixture. Coefficient of determination of a linear trendline between the diffusivities and nanoclay loading is calculated as 0.90.

Table 3. Moisture absorption parameters of DGEBA epoxy with different clay loading.

Material Systems	D_z (mm^2/h)	β (hr^{-1})	γ (hr^{-1})	μ	M_∞ (wt.%)	RMSE (%)
Pure DGEBA	7.55×10^{-4}	1.22×10^{-2}	2.51×10^{-3}	0.205	2.18	0.40
1 wt.% I.30E-DGEBA	7.37×10^{-4}	5.62×10^{-4}	9.70×10^{-5}	0.173	2.05	0.23
2 wt.% I.30E-DGEBA	7.40×10^{-4}	7.02×10^{-4}	1.25×10^{-4}	0.178	2.00	0.43
5 wt.% I.30E-DGEBA	7.14×10^{-4}	7.30×10^{-5}	1.28×10^{-5}	0.175	1.91	0.50

Assuming the recovered diffusion coefficients were subjected to the experimental error, diffusion coefficients of nanoclay/epoxy composites with different nanoclay loading are calculated following the rule of mixture in order to investigate the trends of other absorption parameters with respect to the nanoclay content. Diffusion coefficients of nanoclay/epoxy composite laminates are determined by using the diffusion coefficient of pure epoxy and illustrated in Figure 18. The remaining absorption parameters ($\gamma, \beta,$ $and\ M_\infty$) are recovered by the steepest descent method. The resulting sets of absorption parameters are given in Table 4.

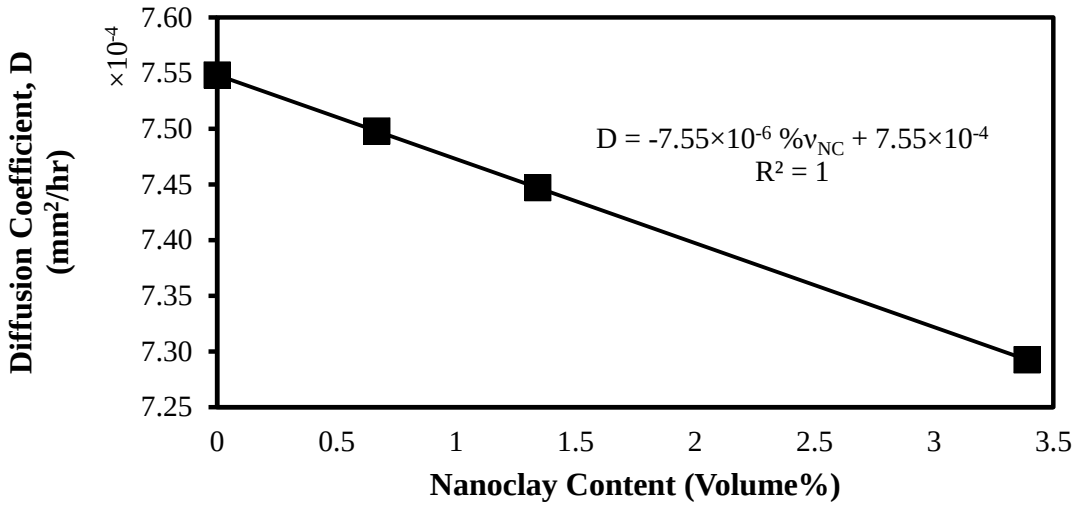


Figure 18. Linear change of diffusion coefficients with nanoclay volume fraction

Table 4. Moisture absorption parameters of DGEBA epoxy with different clay loading (Change in D_z follows the rule of mixture).

Material Systems	D_z (mm²/h)	β (hr^{-1})	γ (hr^{-1})	μ	M_∞ (wt.%)	RMSE (%)
Pure DGEBA	7.55×10^{-4}	1.22×10^{-2}	2.51×10^{-3}	0.205	2.18	0.40
1 wt.% I.30E-DGEBA	7.50×10^{-4}	5.96×10^{-4}	1.08×10^{-4}	0.181	2.05	0.22
2 wt.% I.30E-DGEBA	7.45×10^{-4}	7.22×10^{-4}	1.27×10^{-4}	0.176	1.99	0.43
5 wt.% I.30E-DGEBA	7.30×10^{-4}	1.62×10^{-4}	2.03×10^{-5}	0.125	1.80	0.48

As can be seen in Table 4, the maximum moisture content is observed to decrease with increasing nanoclay content. For example, 5 wt.% increase in nanoclay loading resulted in an 18% decrease in the maximum moisture content. Similarly, hindrance coefficients follow a decreasing trend. These changes in absorption parameters can also be observed in one-dimensional hindered diffusion model prediction in Figure 19.

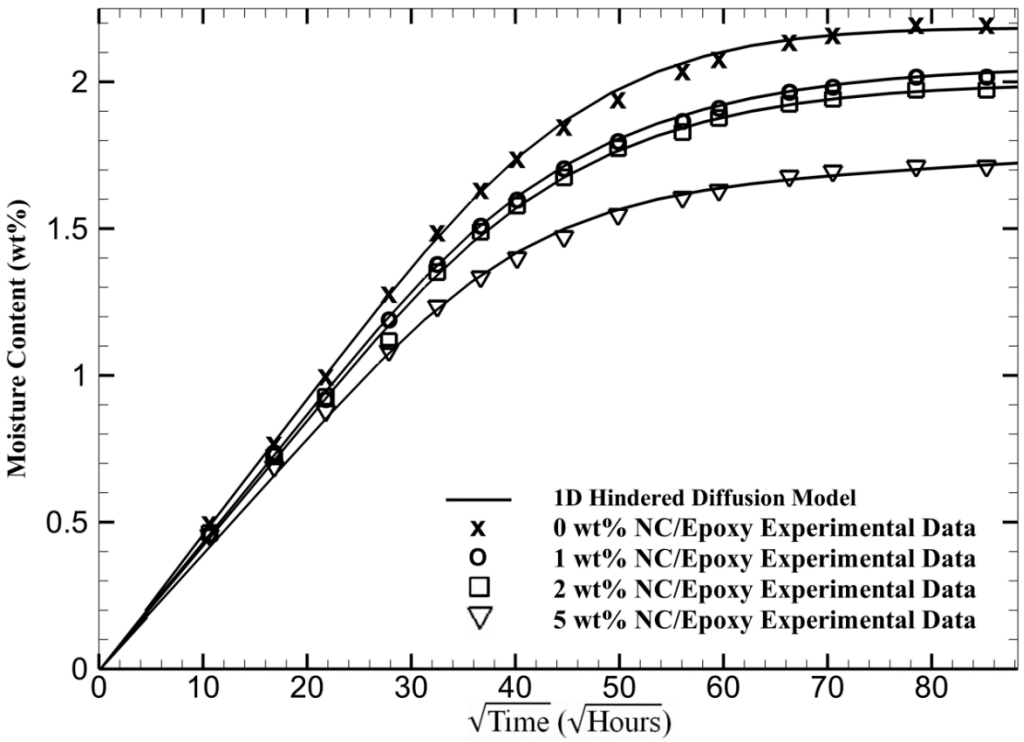


Figure 19. Clay loading effect on moisture absorption of I.30E nanoclay/DGEBA epoxy composite.

In Figure 19, the thermogravimetric data of 0, 1, 2, and 5 wt.% (0, 0.67, 1.34, and 3.39 vol%) I.30E nanoclay/DGEBA epoxy [80] and one-dimensional hindered diffusion model fits are shown. All the HDM moisture absorption curves match well their respective experimental gravimetric data. In addition, the RMS error per data point in Table 4 is fairly insignificant (in the order of 10^{-3}), which indicate that the recovered absorption parameters accurately represent the absorption behavior. Decrease in maximum moisture content with increasing clay content may also be observed in Figure 19. Despite the different maximum moisture content, the absorption curves of composites with different clay loading seems to have similar absorption kinetics. This similarity suggests a potential correlation between the clay content and the maximum moisture content and/or the hindrance coefficient. To investigate these correlations, the hindrance

coefficient, as well as the bound, unbound, and total maximum moisture content are presented with respect to clay volume fraction.

In Figure 20, hindrance coefficients of DGEBA epoxy with different clay loadings and their trendline with respect to the clay content are depicted. Remarkably, the hindrance coefficient is found to linearly decrease by nanoclay addition. Decreasing hindrance coefficient means that the absorption behavior is becoming more Fickian. When the hindrance coefficient, μ, equals to zero, the absorption is completely Fickian. Increase in the non-Fickian absorption behavior was expected by nanoclay addition due to creation of new interfacial surfaces between the nanoclay and epoxy. However, change in absorption towards Fickian suggests presence of strong nanoclay/epoxy interface where the water molecules could not interfere.

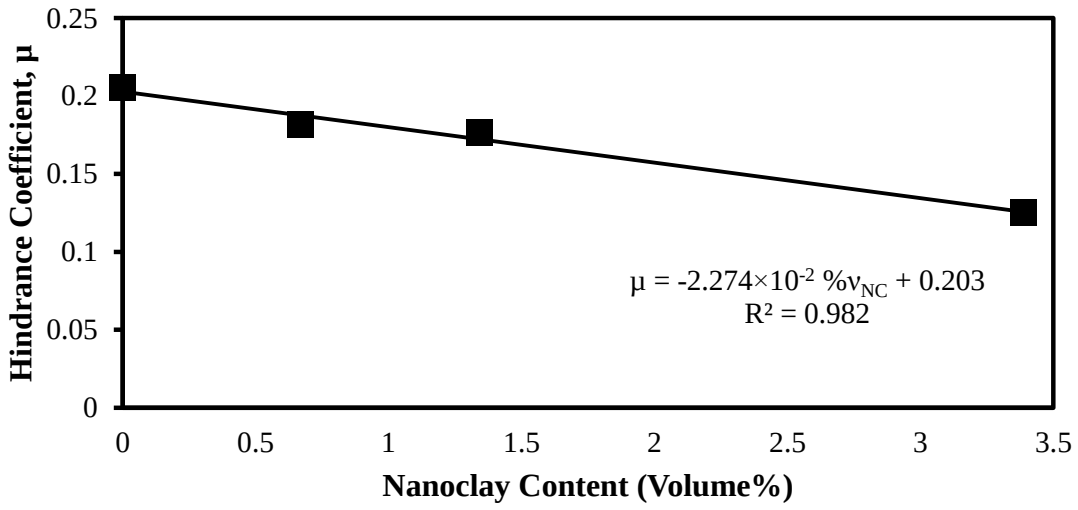


Figure 20. Effect of nanoclay loading in DGEBA epoxy on hindrance coefficient.

In Figure 21, the correlation between maximum moisture content and the nanoclay loading is shown. As the nanoclay content increases, the maximum moisture content decreases linearly. Since the nanoclay is assumed to be impermeable, or to have very low diffusion coefficient, the water does not diffuse into the nanoclay platelets. Moisture is

only absorbed by the matrix; hence, an increase in the nanoclay content in per unit volume would yield a drop in the maximum moisture content of the composite.

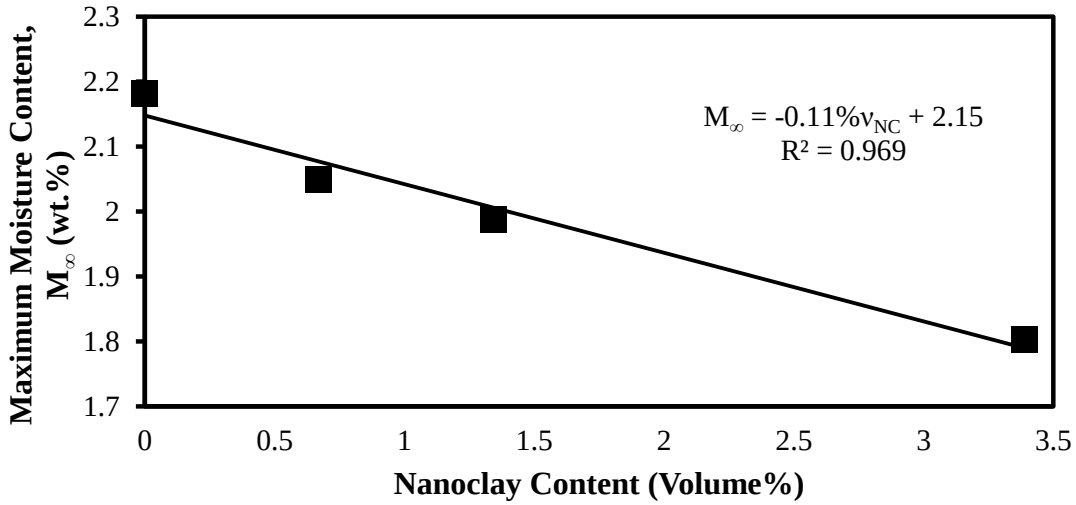


Figure 21. Effect of nanoclay loading in DGEBA epoxy on maximum moisture content.

Although the nanoclays absorb little to no moisture, they still affect the absorbed overall moisture content. Hindered diffusion model suggests that the total moisture content is aggregate of two types of moisture in polymers: bound moisture and unbound moisture. Unbound moisture is absorbed via diffusion by random molecular motion towards the low concentration. Added nanoclays occupy some amount of volume "free volume' where the moisture could have diffused, thus, presence of less free volume decreases the maximum unbound moisture content. Moreover, nanoclay addition may also decrease the binding sites in the medium by replacing the polymers resulting in a decrease of bound moisture. On the other hand, nanoclays create new interfaces which may increase the chemical interactions between the polar water molecules and the medium, resulting in an increase of bound moisture. Interface chemistry and type of nanoclay and epoxy determine the change in bound moisture.

One-dimensional hindered diffusion model can also predict the behavior of unbound and bound moisture absorption. In Figure 22, total, unbound, and bound moisture absorptions of 2 wt.% I.30E/DGEBA composite are illustrated. The total moisture is a combination of bound and unbound moisture. In most polymer, almost all the first initial moisture uptake is unbound moisture. After reaching pseudo-equilibrium phase, there is no additional unbound moisture uptake. Since unbound moisture is governed by diffusion by random molecular motion, it shows Fickian diffusion behavior. On the other hand, bound moisture is generally generated relatively later than the unbound moisture. Bound moisture is responsible for the delay in reaching equilibrium moisture content. Once the overall rate of transformation between bound and unbound reaches equilibrium, polymer would stop absorbing any additional water. Maximum bound and unbound moisture content is directly related to maximum moisture content and hindrance coefficient:

$$M_{\infty,bound} = \frac{\mu}{1+\mu} M_{\infty} \tag{60a}$$

$$M_{\infty,unbound} = \frac{1}{1+\mu} M_{\infty} \tag{60b}$$

In Figure 23, the relationship between equilibrium unbound moisture content and the volume fraction of nanoclay is illustrated. As in bound moisture vs. nanoclay content, the linearity is directly related to the linearity of both the hindrance coefficient and the maximum moisture vs. nanoclay content. The unbound moisture content decreases by 11% with the addition of 5 wt.% (3.5 vol%) nanoclay. As the nanoclay content increases, the amount of free volume in samples, which the water molecules can diffuse into, decreases. The free volume that was available in neat epoxy has now been occupied by the added nanoclay.

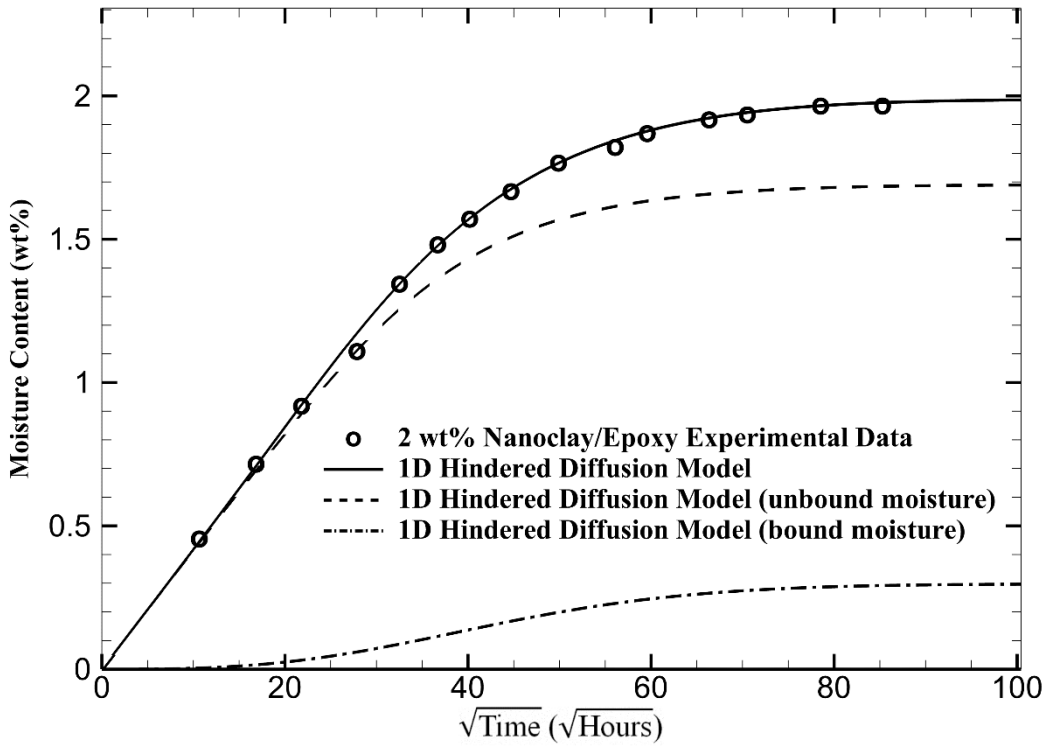


Figure 22. Total, unbound, and bound moisture absorption of 2 wt.% I.30E/DGEBA composite

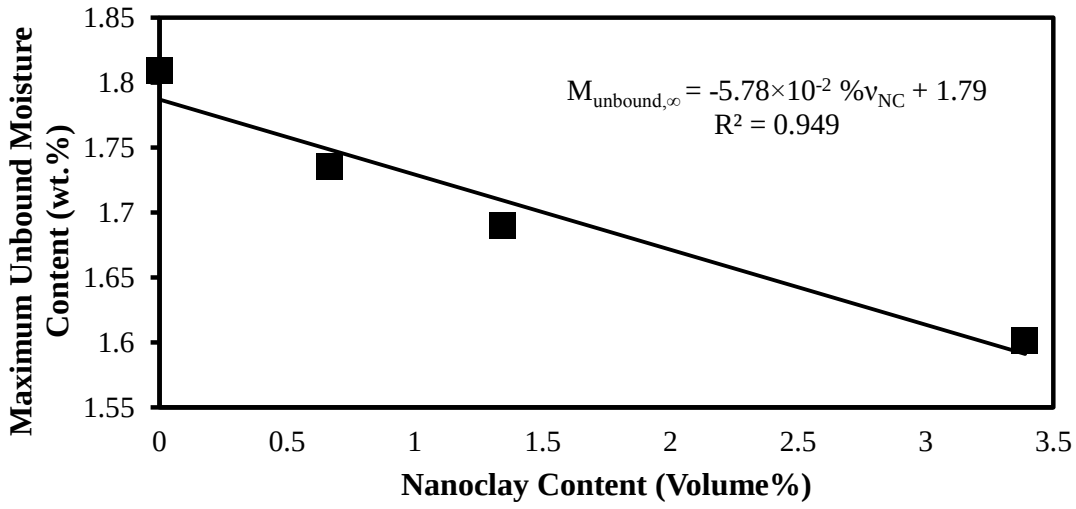


Figure 23. Effect of nanoclay loading in DGEBA epoxy on maximum unbound moisture content.

In Figure 24, the change of equilibrium bound moisture content is presented with respect to the nanoclay content. Since the equilibrium bound moisture content is directly

related to the maximum moisture content and hindrance coefficient, the linear trend was expected. However, the decrease in maximum bound moisture content was not expected. One would expect that addition of nanoclay would increase the interface in epoxy and creates new binding sites for moisture. The decrease in maximum bound moisture content suggests that addition of nanoclay might restrict the amount of binding sites previously available in the neat DGEBA epoxy.

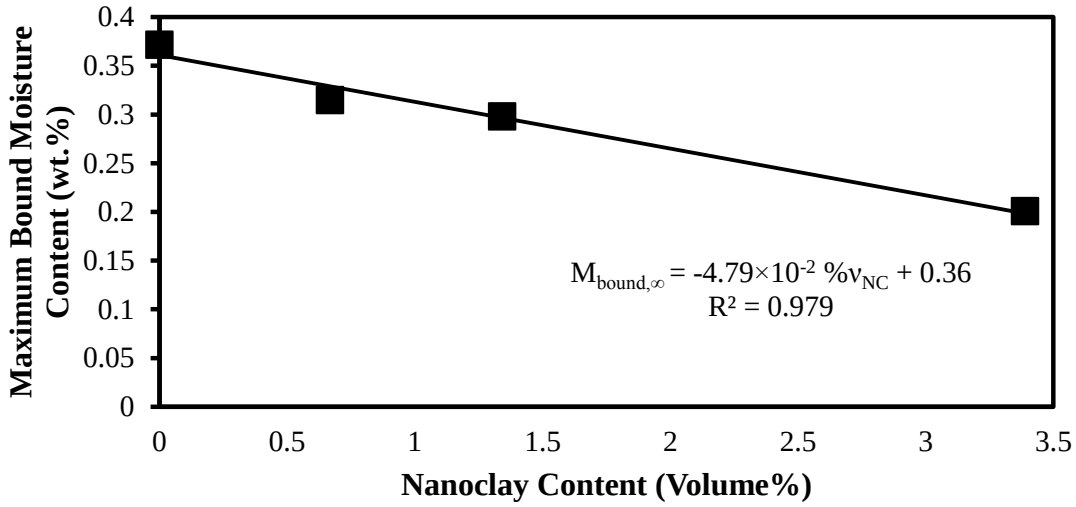


Figure 24. Effect of nanoclay loading in DGEBA epoxy on maximum bound moisture content.

The linear correlation between the hindrance coefficients, the maximum moisture content with respect to the nanoclay loading is an interesting phenomenon. Even though convincing linear trends between the 1D HDM absorption parameters and 3 different nanoclay loadings is observed, more data point would yield a more robust validation of these trends. In order to validate whether this linear correlation holds for other experiments and to develop a deeper understanding of moisture absorption behavior in nanoclay composites, a new set of material with 5 different clay loadings is manufactured and moisture absorption experiments were carried out.

iii. Materials and Sample Preparation of I.30E Nanoclay/EPON 862 Epoxy

The epoxy resin and curing agent used in this study is selected as EPON 862 and Epikure W (Momentive Performance Materials Inc.), respectively. Nanomer® I.30E nanoclay, a surface modified montmorillonite mineral, is used as the reinforcing material.

First, 0.5, 1, 2, 3, and 5 wt.% (0.35, 0.70, 1.40, 2.10, and 3.50 vol%) nanoclay is mixed with the epoxy resin at 100 RPM for 5 minutes. Then, the mixture is blended in high shear mixer at 5000 RPM for 30 minutes. It should be noted that high shear mixing generates heat, causing the mixture temperature to increase. Therefore, it is important to cool down the mixture. For cooling down, an alternating 5-minute mixing and 10-minute in the freezer procedure is implemented in order to keep the mixture below 70℃ (158℉).

After the high shear mixing, the mixture is sonicated at 42 kHz for 1 hour in 5 second on, 5 second off cycles. Throughout the sonication process, the mixture is kept in an icy water bath to eliminate the degradation due to high temperature at the tip of the sonicator.

After the sonication, the epoxy resin-nanoclay mixture and curing agent is mixed at a ratio of 100:26.4 by weight at 100 RPM for 15 minutes. The mixture is then degassed for 4 hours at room temperature to remove the trapped air. Subsequently, thin epoxy laminates are gravity-cast onto a 177.8x101.6 mm^2 aluminum mold, preheated to 100℃ (212℉). The mold is kept at 100℃ (212℉) for 1.5 hours and then heated to 179℃ (355℉) and held constant for 2 hours. After 2 hours, the part is cooled down to room temperature at approximately 2.8℃/min to complete the cure cycle. Eight 31.8 × 31.8 mm^2 specimens were cut from each laminate for water immersion experiments. The average thickness of the each set of eight specimens is 0.97 ± 0.02 mm.

To remove the initial moisture, the samples are placed in vacuum oven at 43℃ (110℉) for approximately 5 days. Dried samples are immersed in distilled water at 25℃ (77℉). Mass gain of samples due to moisture absorption is periodically measured for approximately 5 months and one final mass gain data collected at one year mark. The collected mass gain data of 5 months is used to recover absorption parameters of hindered diffusion model following the aforementioned recovery procedure in Chapter 2.

iv. Experimental Results of I.30E/EPON 862 and Discussion

In order to detect the effect of nanoclay content on the hindrance coefficient and maximum moisture content, the hindered diffusion model absorption parameters of pure epoxy are first found. It should be noted that the pure epoxy is also subjected to sonication and high sheer mixing. Thus, the absorption parameters and absorption behavior are slightly different from the regularly cured EPON 862. Using the diffusion coefficient of pure epoxy, the diffusion coefficients of nanoclay/epoxy composites with different nanoclay loading are calculated using the rule of mixture and shown in Figure 25. The remaining absorption parameters ($\gamma, \beta,\ and\ M_\infty$) are recovered by the steepest descent method. The resulting sets of absorption parameters are given in Table 5.

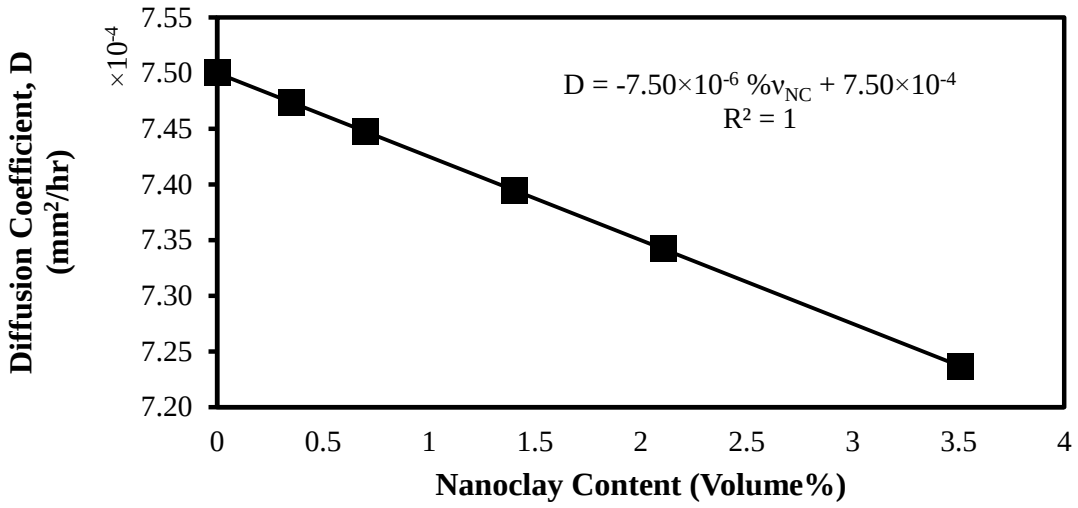


Figure 25. Linear change of diffusion coefficients of I.30E/EPON862 composite with nanoclay volume fraction

Table 5. One-dimensional hindered diffusion moisture absorption parameters of EPON 862 epoxy with different clay loading where diffusion coefficient kept linearly decreasing.

Material Systems	D_z (mm²/h)	β (hr^{-1})	γ (hr^{-1})	μ	M_∞ (wt.%)	RMSE (%)
Pure EPON 862	7.50×10^{-4}	6.50×10^{-4}	8.56×10^{-5}	0.132	2.242	0.45
0.5 wt.% I.30E-EPON 862	7.47×10^{-4}	1.03×10^{-3}	1.39×10^{-4}	0.134	2.238	0.44
1 wt.% I.30E-EPON 862	7.45×10^{-4}	6.96×10^{-4}	9.66×10^{-5}	0.139	2.211	0.44
2 wt.% I.30E-EPON 862	7.39×10^{-4}	4.82×10^{-4}	7.20×10^{-5}	0.149	2.198	0.43
3 wt.% I.30E-EPON 862	7.34×10^{-4}	7.20×10^{-4}	1.10×10^{-4}	0.153	2.181	0.44
5 wt.% I.30E-EPON 862	7.24×10^{-4}	5.84×10^{-4}	1.02×10^{-4}	0.174	2.126	0.44

Experimental gravimetric data and the hindered diffusion model prediction using the absorption parameters in Table 5 are shown in Figure 26. As in compliance with the root

mean square error per data point values in Table 5, one-dimensional hindered diffusion model has predicted each case successfully. Moreover, the last data points around $\sqrt{time} \approx 90$ shown in Figure 26 are not used to recover the absorption parameters. The prediction of long-term absorption behavior from short-term experiment shows the capabilities of one-dimensional hindered diffusion model.

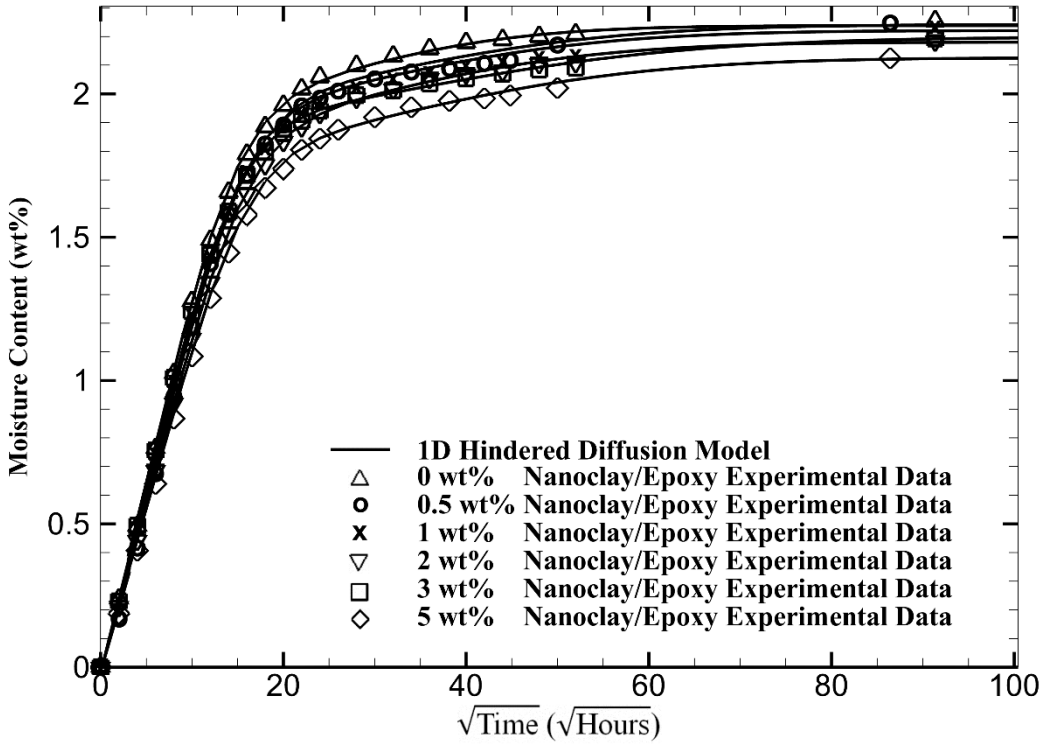


Figure 26. Clay loading effect on moisture absorption of I.30E nanoclay/EPON 862 epoxy composite and the hindered diffusion fit while keeping the diffusion coefficient constant.

Effect of nanoclay on degree of non-Fickian behavior is shown using the hindrance coefficient which describes the degree of hindered diffusion by $\mu = {}^{\gamma}/_{\beta}$. In addition, the hindrance coefficient also gives the ratio of maximum bound moisture to unbound moisture. When the hindrance coefficient is zero, the moisture absorption is pure Fickian. As the hindrance coefficient increases, the diffusion becomes more non-Fickian. Figure

27 shows the relationship between the hindrance coefficient and the nanoclay loading in EPON 862. Similar to the results depicted in Figure 20, a linear relationship is observed between the hindrance coefficient and the nanoclay loading. However, at this time, a linearly increasing trend is observed between the hindrance coefficient and the nanoclay loading, meaning that the diffusion becomes more non-Fickian with nanoclay addition. These opposing trends might originate from the type of the epoxy used. Epoxy used in this study, EPON 862, is DGEBF epoxy, which has Bisphenol-F group, whereas epoxy used by Al-Qadhi et al. [80], DGEBA, has Bisphenol-A group. These different chemical groups might interact differently with the I.30E nanoclay and effect the diffusion distinctively.

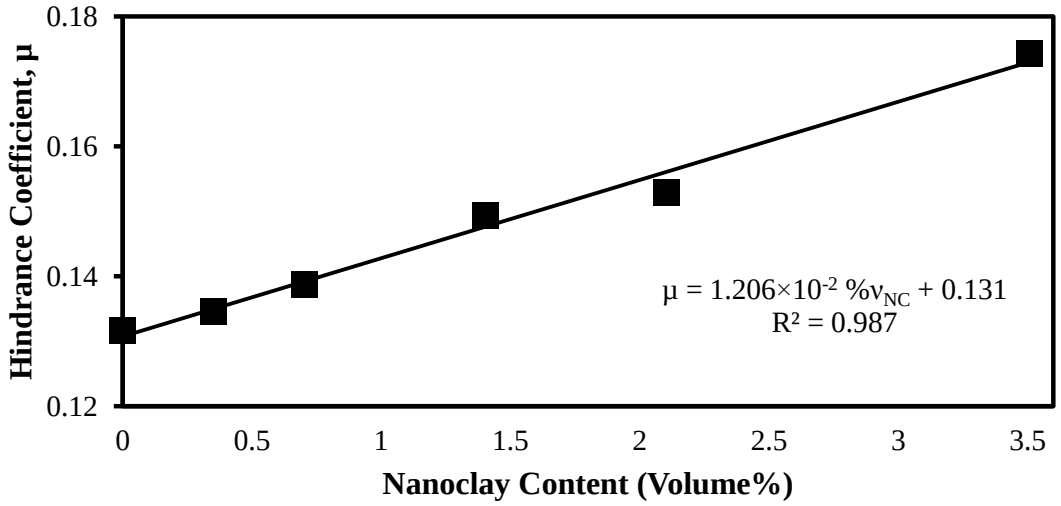


Figure 27. Effect of nanoclay loading in EPON 862 epoxy on hindrance coefficient.

The increase in non-Fickian behavior is believed to be due to generation of new surface areas by nanoclay addition. Additional interfaces between the EPON 862 and nanoclay may have relatively higher energy than its surrounding. Thus, polar water molecules would probably prefer to bind to the rather high energy surfaces resulting in increasing non-Fickian behavior.

In Figure 28, the effect of nanoclay content in EPON 862 on the maximum moisture content is shown. Addition of nanoclay in EPON 862 results in a linear decrease of maximum moisture that the polymer can absorb. The addition of 5 wt.% (3.5 vol%) I.30E nanoclay to EPON 862 is observed to decrease the maximum moisture content by 5%. The maximum moisture content, on the other hand, decreased by 17% when 5 wt.% I.30E nanoclay is added to the DGEBA epoxy. This result clearly shows that the presence of the same type of nanoclay can have different effects on different epoxy systems.

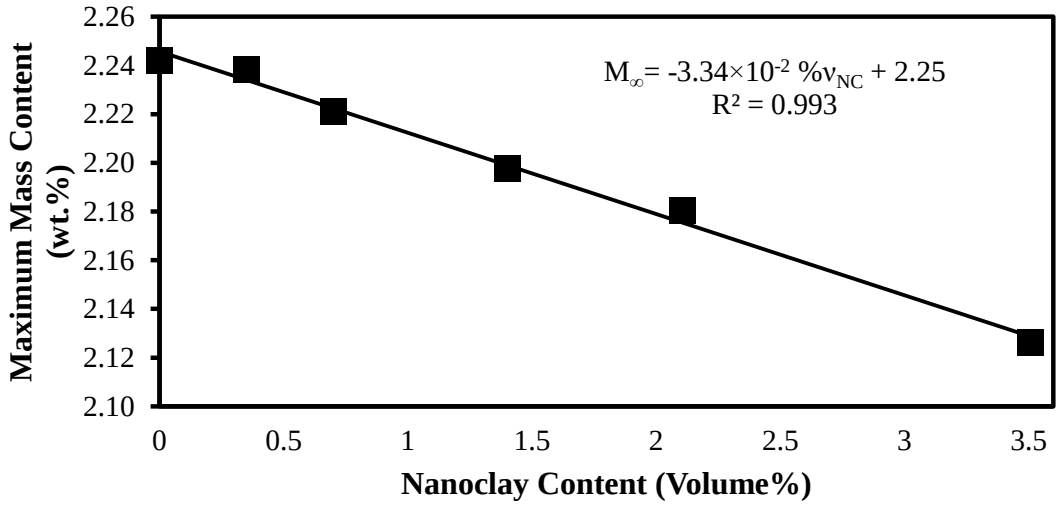


Figure 28. Effect of nanoclay loading in EPON 862 epoxy on maximum moisture content.

Figure 29 shows the decreasing linear trend of maximum unbound moisture content with increasing nanoclay content. The addition of 5 wt.% (3.5 vol%) of I.30E nanoclay to the DGEBF epoxy caused a decrease in the equilibrium unbound moisture content by 9%. The linear decrease is again conceivably related to the decrease in the free volume due to nanoclay addition.

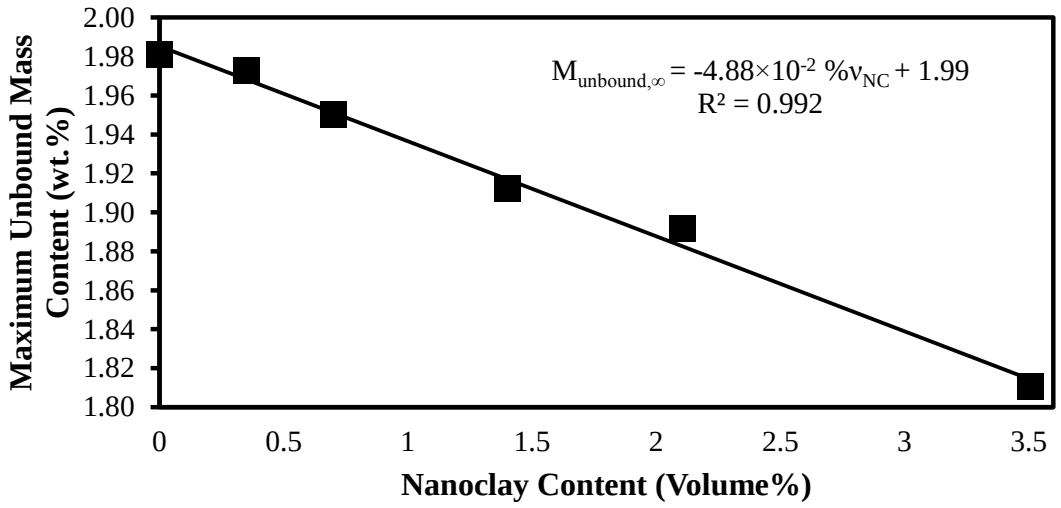


Figure 29. Effect of nanoclay loading in EPON 862 epoxy on maximum unbound moisture content.

Figure 30 shows the effect of nanoclay content on the equilibrium bound moisture content. As expected, due to the linearity of the change in maximum moisture content and the hindrance coefficient with respect to nanoclay content, the maximum bound moisture content shows a linear trend with the nanoclay content. Interestingly, the equilibrium bound moisture content increased with increasing nanoclay content, as opposed to a decreasing trend in I.30E/DGEBA epoxy system. The only difference between the two nanoclay/epoxy systems is the epoxy resin.

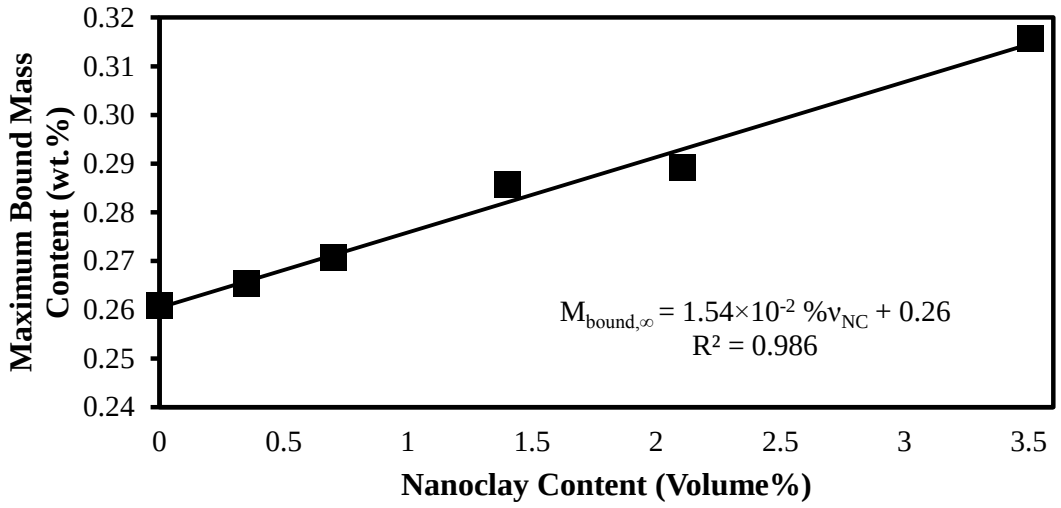


Figure 30. Effect of nanoclay loading in EPON 862 epoxy on maximum bound moisture content.

v. Effect of resin type on the molecular interactions between water molecules and epoxy

The DGEBA epoxy has bisphenol-A group, whereas EPON 862 is DGEBF epoxy, which has Bisphenol-F group. Reactants of Bisphenol-A are phenol and acetone while reactants of Bisphenol-F are phenol and formaldehyde. Schematics of the chemical formulas of both Bisphenol-A and Bisphenol-F are shown in Figure 31.

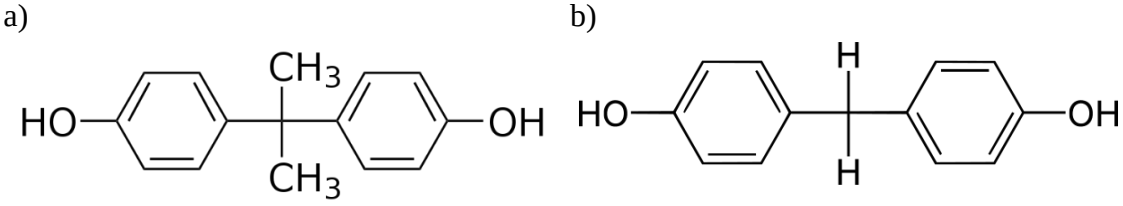


Figure 31. Schematics of a) Bisphenol-A and b) Bisphenol-F

As depicted in Figure 31, the only difference between Bisphenol-A and Bisphenol-F is in the group linked to Carbon (C) in the middle of the monomer. Bisphenol-A has two methyl groups linked to the Carbon atom in the middle, while Bisphenol-F has two

Hydrogen (H) atoms. Bentzl and Neville [121] reported that binding of the moisture molecule can be due to electromagnetic attractions between epoxy and water or residual attractive or repulsive forces between molecules or atomic groups. For both types of epoxy, OH group on the left end would be the preferential moisture molecule binding site due to possible hydrogen bond formation. Additional binding of water molecules may be governed by other weaker chemical interactions. Methyl group (CH_3^-) and Hydrogen (H^-) would have Van der Waals interactions with moisture molecules although not as strong as Hydroxyl (OH^-) groups. When comparing the Van der Waals interactions, Methyl groups have a higher Van der Waals force due to longer chain than hydrogen. Therefore, the DGEBA epoxy is expected to have a higher bound moisture content. The DGEBF epoxy has 30% less maximum bound moisture content than DGEBA epoxy, which is consistent with the theory.

Reynolds et al. [122] reported that any cation or cationic species can occupy the interlayer between the nanoclay layers and these cations have relatively high enthalpies of hydration. Consequently, to satisfy the hydration conditions of cations between nanoclay layers, water is preferentially absorbed into these layer resulting in an increase of bound moisture. Moreover, newly created surfaces between the nanoclay and epoxy would have higher energy levels than the surrounding. Since all systems try to achieve the lowest state of energy, depending on the surface chemistry, water molecules might wet the surface, as a result, increase bound moisture.

The increasing trend of maximum bound moisture content in I.30E/EPON862 nanoclay composites suggests that binding to interface between nanoclay and epoxy and to nanoclay interlayer overcomes the negative effects of decreasing polymer binding

sites. However, for I.30E/DGEBA nanoclay composites, as nanoclay content increases, the epoxy content per unit volume decreases. The decrease in polymer binding sites dominates over the water molecule binding to the nanoclay interlayers and nanoclay/epoxy interfaces. Thus, a decreasing trend of maximum bound moisture content is observed in I.30E/DGEBA as nanoclay content increases.

3.2. Effects of Interfaces and Filler Types

Further study about nano-fillers on epoxy is conducted to investigate the effects of interfaces and nano-filler types. Glass spheres are chosen due to their excellent water resistant properties. Using glass spheres as reinforcements would help characterize the effect of the interface on moisture absorption. For that purpose, experimental moisture gravimetric data of epoxy composites reinforced with different surface treated glass spheres [81] are used.

i. Materials and Sample Preparation of APS/DGEBA Epoxy and nBS/DGEBA Epoxy

Kawaguchi and Pearson [81] used diglycidyl ether of bisphenol-A (DGEBA) based epoxy resin (Dow Chemical DERw331) and bisphenol-A (resin modifier) cured with piperidine. Glass spheres from Potters Industry Spheriglass w2900 with mean diameter of 42μm were used as reinforcements.

The glass spheres were surface treated with 1 wt.% aminopropyltrimethoxysilane (APS) or 1 wt.% n-butyltrimethoxysilane (nBS) and rinsed with methanol. Amine compounds are commonly used as a curing agent for epoxy. Therefore, Kawaguchi and Pearson [81] expected high adhesion between APS treated glass which has amine compound and DGEBA epoxy due to covalent bond formation. Methyl group of nBS

does not chemically react with epoxy, thus, only Van der Waals interactions were expected between the nBS glass spheres and epoxy.

DGEBA epoxy and Bisphenol-A were mixed in a ratio of (100:24) at 180℃ (356°F) under vacuum and cooled down to 80℃ (176°F). Glass spheres of 10%, 20%, and 30% by volume is added to epoxy and mixed under vacuum. 5 wt.% Piperidine curing agent is added and mixed for 10 minutes. Resulting mixture is poured onto an aluminum mold at 160℃ (320°F) and cured for 6 hours. The cured composite is cut into 30.5 × 30.5 mm specimens having thickness of 6 mm.

ii. Experimental Results of APS/DGEBA Epoxy and nBS/DGEBA Epoxy and Discussion

Kawaguchi and Pearson [81] kept all samples in an environmental chamber at 85% relative humidity and 85℃ (185°F) for 1350 hours. Similar to I.30E/DGEBA and I.30E/EPON 862 composites, the diffusion coefficients of the epoxy with inclusions are calculated to linearly vary starting from the recovered diffusion coefficient of pure epoxy. The linear variation of diffusion coefficients is shown in Figure 32.

Using the diffusion coefficients in Figure 32 and Eqs. (39-41), remaining absorption parameters ($\gamma, \beta,\ and\ M_\infty$) of APS treated glass sphere/epoxy composite are recovered and given in Table 6.

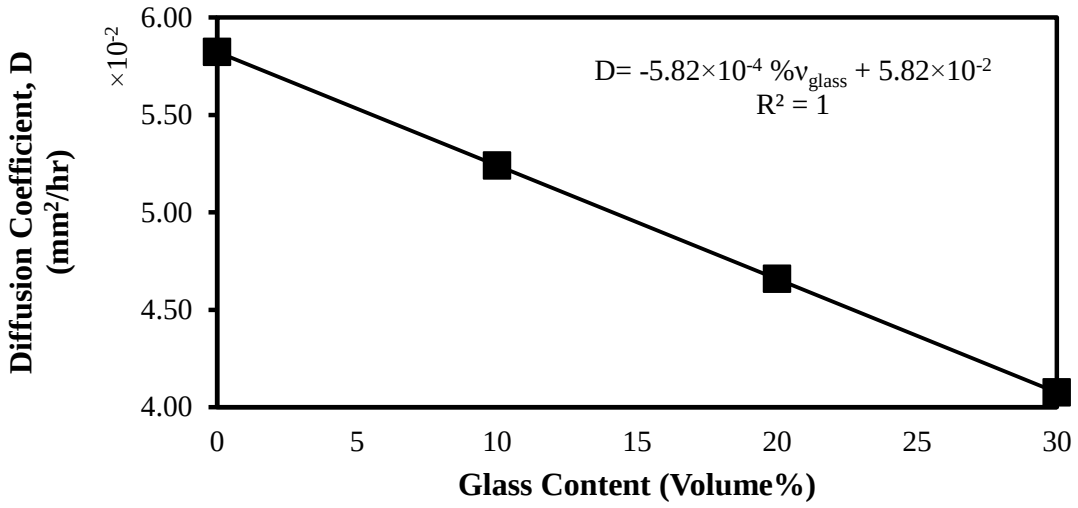


Figure 32. Linear change of diffusion coefficients of APS glass/DGEBA and nBS glass/DGEBA composite with glass volume fraction

In Table 6, through-the-thickness diffusion coefficients (already determined), the hindrance coefficients, the maximum moisture content of APS treated glass sphere/epoxy composites and the root mean square error between the experimental data and model prediction per data point are presented. In Table 6, the increase in hindrance coefficient and decrease in maximum moisture content can easily be seen. The addition of 30 vol% APS glass sphere in DGEBA epoxy induced in an 11% decrease in the maximum moisture content. Similarly, the addition of APS glass sphere in DGEBA epoxy caused a steady increase in the hindrance coefficient. Moreover, the root mean square error per data point is fairly small, indicating that the absorption parameters accurately represent the absorption behavior. The gravimetric experimental data and the one-dimensional hindered diffusion model predictions are illustrated in Figure 33.

Table 6. Moisture absorption parameters of DGEBA epoxy with different APS treated glass loading where diffusion coefficient kept linearly decreasing.

Material Systems	D_z (mm^2/h)	β (hr^{-1})	γ (hr^{-1})	μ	M_∞ (wt.%)	RMSE (%)
Pure DGEBA	5.82×10^{-2}	4.38×10^{-3}	9.10×10^{-4}	0.208	1.36	0.37
10 vol% APS Glass-DGEBA	5.24×10^{-2}	1.22×10^{-3}	4.43×10^{-4}	0.364	1.31	0.55
20 vol% APS Glass-DGEBA	4.66×10^{-2}	1.01×10^{-3}	5.51×10^{-4}	0.545	1.26	0.32
30 vol% APS Glass-DGEBA	4.08×10^{-2}	7.24×10^{-4}	5.59×10^{-4}	0.773	1.21	0.35

In Figure 33, the effect of glass spheres on diffusion kinetics can be depicted. Around $\sqrt{time} = 13$, the diffusion behavior begins to change for different glass volume fraction. For neat epoxy, the diffusion behavior after initial uptake shows more Fickian behavior where moisture diffusion extremely slows down right after the initial uptake. However, in the case of glass/epoxy composites, after the initial uptake, lower rate of deceleration of absorption is observed. This phenomenon is predicted by the increase of hindrance coefficient of the one-dimensional hindered model. Moreover, the decrease in the maximum moisture content can also be observed in Figure 33. Low RMS error values shown in Table 6 do also agree with the 1D-HDM recovery presented in Figure 33.

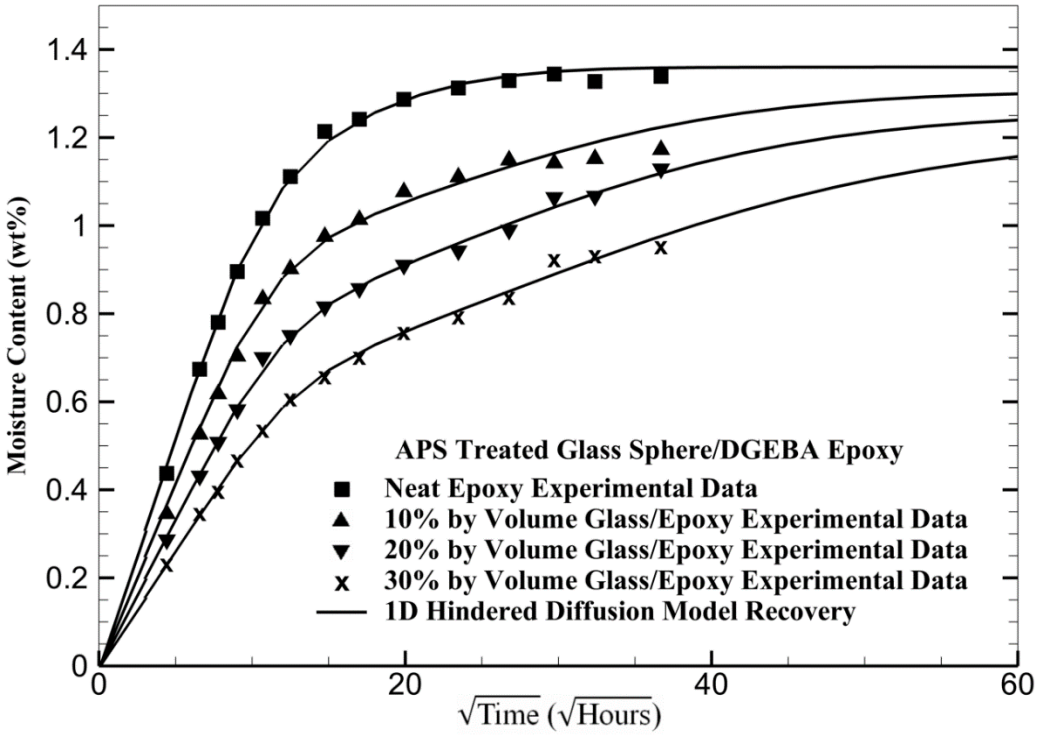


Figure 33. APS glass sphere loading effect on moisture absorption of DGEBA epoxy and the hindered diffusion recovery while keeping the diffusion coefficient linearly decreasing.

Once again, using the diffusion coefficients shown in Figure 32, the absorption parameters ($\gamma, \beta,\ and\ M_\infty$) of DGEBA epoxy reinforced with nBS surface-treated glass spheres are recovered and shown in Table 7. In Table 7, through-the-thickness diffusion coefficients (already determined), the hindrance coefficients, the maximum moisture content and the root mean square error per data point are presented. As in APS treated glass sphere/epoxy, decreasing trend for the maximum moisture content and increasing trend for the hindrance coefficient of nBS treated glass sphere/epoxy laminates are observed. Furthermore, small RMS error values (order of 10^{-3}) indicate an accurate recovery of the absorption parameters.

Table 7. Moisture absorption parameters of DGEBA epoxy with different nBS treated glass loading where diffusion coefficient kept linearly decreasing.

Material Systems	D_z (mm^2/h)	β (hr^{-1})	γ (hr^{-1})	μ	M_∞ (wt.%)	RMSE (%)
Pure DGEBA	5.82×10^{-2}	4.38×10^{-3}	9.10×10^{-4}	0.208	1.36	0.37
10 vol% nBS Glass-DGEBA	5.24×10^{-2}	3.34×10^{-3}	8.80×10^{-4}	0.264	1.17	0.36
20 vol% nBS Glass-DGEBA	4.66×10^{-2}	9.23×10^{-4}	3.19×10^{-4}	0.345	1.08	0.36
30 vol% nBS Glass-DGEBA	4.08×10^{-2}	6.32×10^{-4}	3.04×10^{-4}	0.482	0.98	0.33

In Figure 34, experimental mass gain data of nBS treated glass sphere/epoxy and 1D HDM model recovery is illustrated. As in Figure 33, the decrease in maximum moisture content and slight change in diffusion behavior can be observed. Comparing Figure 34 and Figure 33 yields that nBS treatment on glass sphere causes a higher reduction of maximum moisture content than APS treatment. Remarkably, the one-dimensional hindered diffusion model is shown to accurately represent the anomalous diffusion behavior for any glass content.

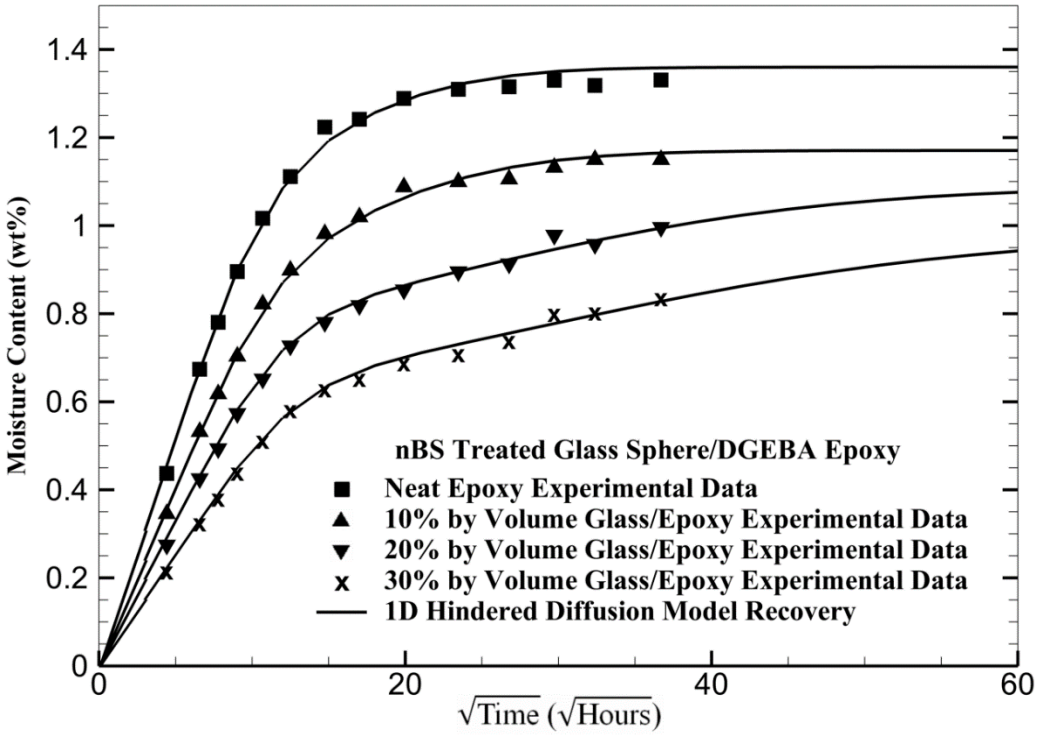


Figure 34. nBS glass sphere loading effect on moisture absorption of DGEBA epoxy and the hindered diffusion recovery while keeping the diffusion coefficient linearly decreasing.

In Figure 35, the linear increase in hindrance coefficient with increasing glass content can be seen. As shown in Figure 20 and Figure 27 the linear trend of the hindrance coefficients is consistent. As in the case of I.30E/EPON 862, the increasing linear trend is observed with increasing nanoclay content. Increasing linear trend shows that the absorption kinetics are governed not only by epoxy type, but the type of the nano-filler as well. The compatibility between the nano-filler and the epoxy is one of the most important influence on moisture absorption. Moreover, since the glass spheres are absolutely impermeable, the coefficient of determination, R^2, is exceptionally close to unity.

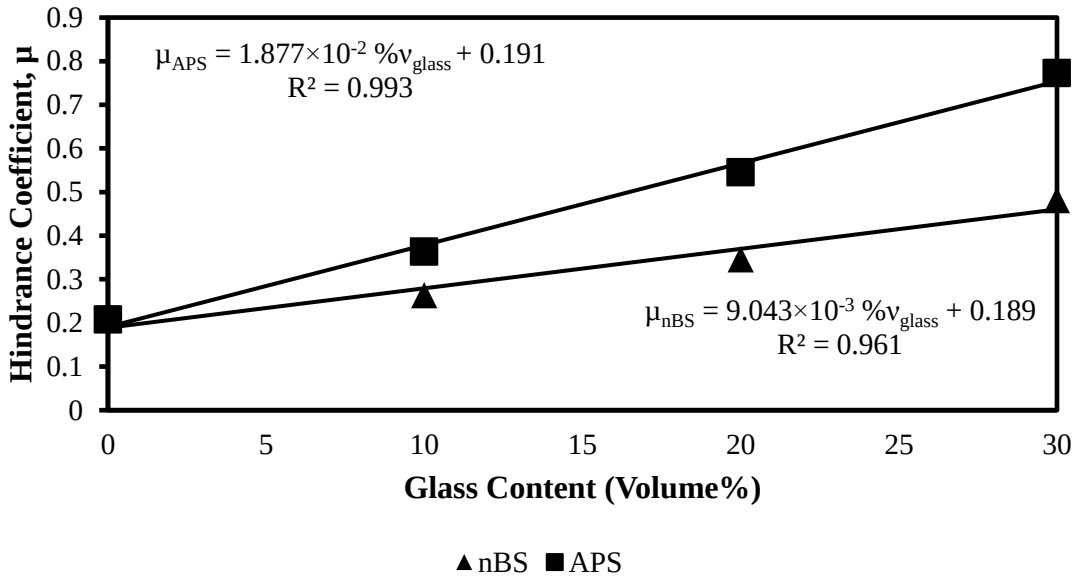


Figure 35. Effect of APS and nBS glass sphere loading in DGEBA epoxy on hindrance coefficient.

The addition of 30 vol% nBS-treated glass spheres to the DGEBA epoxy causes a 132% increase in the hindrance coefficient whereas 271% increase in hindrance coefficient is observed for the 30 vol% APS-treated glass case. When the nBS and APS treatments are compared, APS treated glass/epoxy causes 109% higher hindered diffusion than nBS treated glass/epoxy. The increase in the hindrance coefficient can be explained by the creation of new interfaces as glass content increases. These interfaces may act as binding zones for moisture molecules depending on the surface energy between glass/epoxy, glass/water and water/epoxy. As additional binding zones (i.e. glass/epoxy surfaces) exist in the material system, hindrance coefficient is expected to increase. Moreover, different surface chemistry due to surface coatings (i.e. nBS and APS) lead to distinct chemical interaction between the glass, water, and epoxy resulting in difference between the slopes of change in hindrance coefficient trends.

Figure 36 shows the decreasing linear trend of maximum moisture content with increasing glass content. In all four cases, I.30E/DGEBA, I.30E/EPON 862, APS glass sphere/DGEBA, and nBS glass sphere/DGEBA, the addition of fillers lead to decrease in the maximum moisture content. However, different slopes suggest that the decrease in maximum moisture content is not only governed by the amount of nano- micro- fillers. Type of epoxy and nano- micro- fillers may have various impact on the maximum moisture content.

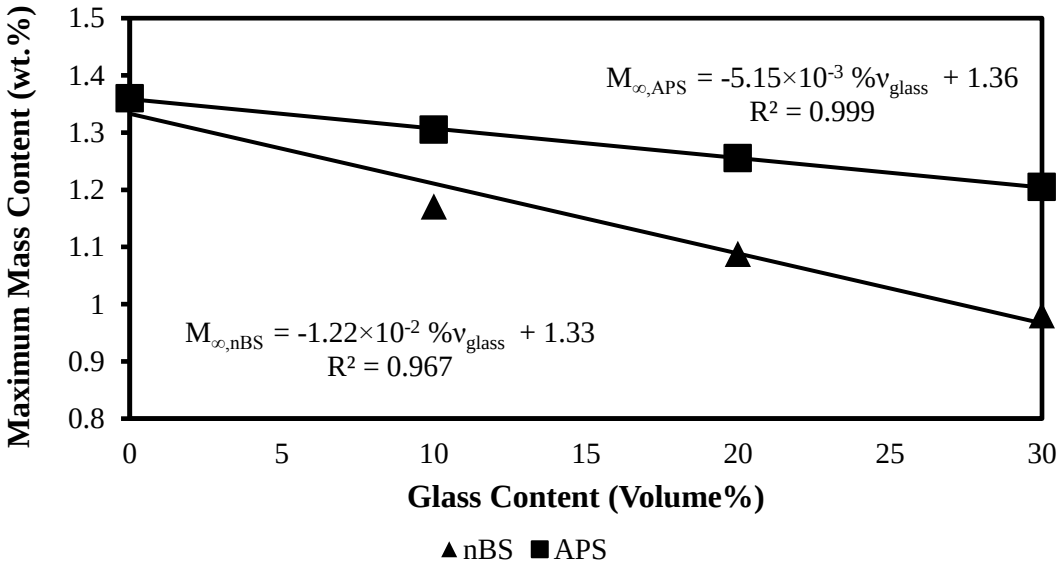


Figure 36. Effect of APS and nBS glass sphere loading in DGEBA epoxy on maximum moisture content.

Addition of 30 vol% glass into epoxy leads to 12% and 28% decrease in maximum moisture content for APS and nBS treated glass sphere epoxies, respectively. Comparing APS- and nBS-glass sphere/epoxy, the decrease in the maximum moisture content in the nBS-glass sphere/epoxy is 145% more than in the APS-glass sphere/epoxy. Although the same amount of nBS-glass sphere/epoxy can absorb less amount of moisture at

equilibrium than the APS-glass sphere/epoxy, reaching the equilibrium moisture content will be faster for nBS-glass sphere/epoxy due its higher hindrance coefficient.

Figure 37 shows the decreasing linear trend of maximum unbound moisture content with increasing glass volume fraction similar to the other two material systems (I.30E/DGEBA and I30.E/EPON 862). Enhancement on DGEBA epoxy by 30% vol. of APS and nBS glass results in a 40% decrease in equilibrium unbound moisture content. Glass sphere inclusion reduces the available free volume where normally epoxy would reside. Since the unbound moisture only diffuses through the epoxy, addition of any glass sphere or any nano-fillers will reduce the equilibrium unbound moisture content. Since the maximum unbound moisture content is directly related to the free volume, the same amount of glass should affect the maximum unbound moisture content the same.

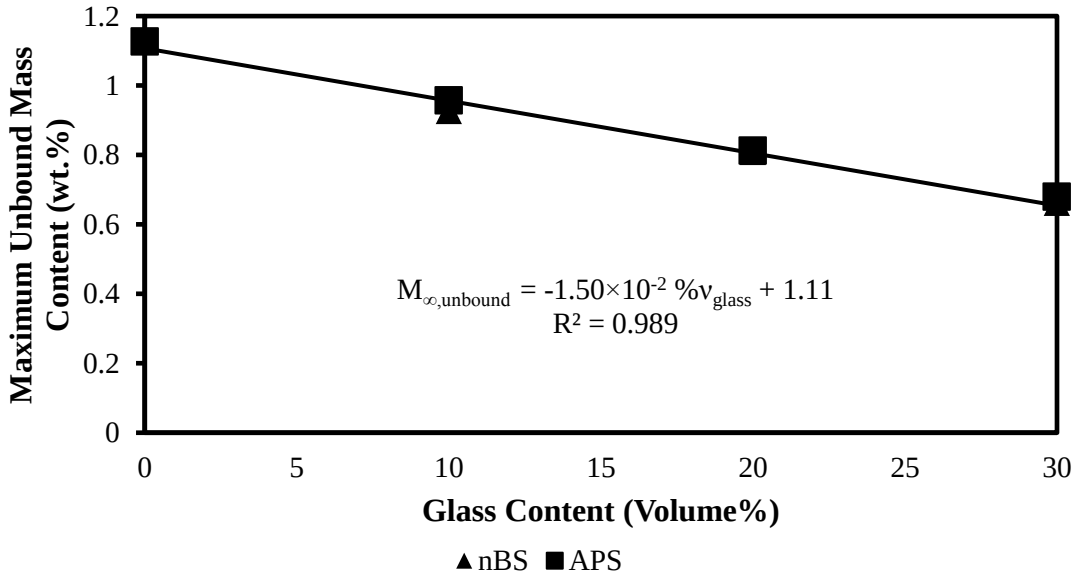


Figure 37. Effect of APS and nBS glass sphere loading in DGEBA epoxy on maximum unbound moisture content.

Figure 38 shows the trend of the bound equilibrium moisture content with respect to the glass sphere content. The addition of 30 vol% nBS-glass sphere causes 36% increase

in maximum bound moisture whereas 125% increase in maximum bound moisture content with 30 vol% APS glass addition is noticed which suggests that the APS glass spheres highly hinder the moisture intake. Comparison between the nBS-glass/epoxy and the APS-glass/epoxy shows a 242% higher increase in the maximum bound moisture content for the APS system. To reach the equilibrium shown in Eq. (8), continuous transformation of unbound moisture to bound moisture is required. The availability of additional binding sites also leads to longer period of time required to reach the equilibrium due to continuous transformation between the unbound and bound moisture.

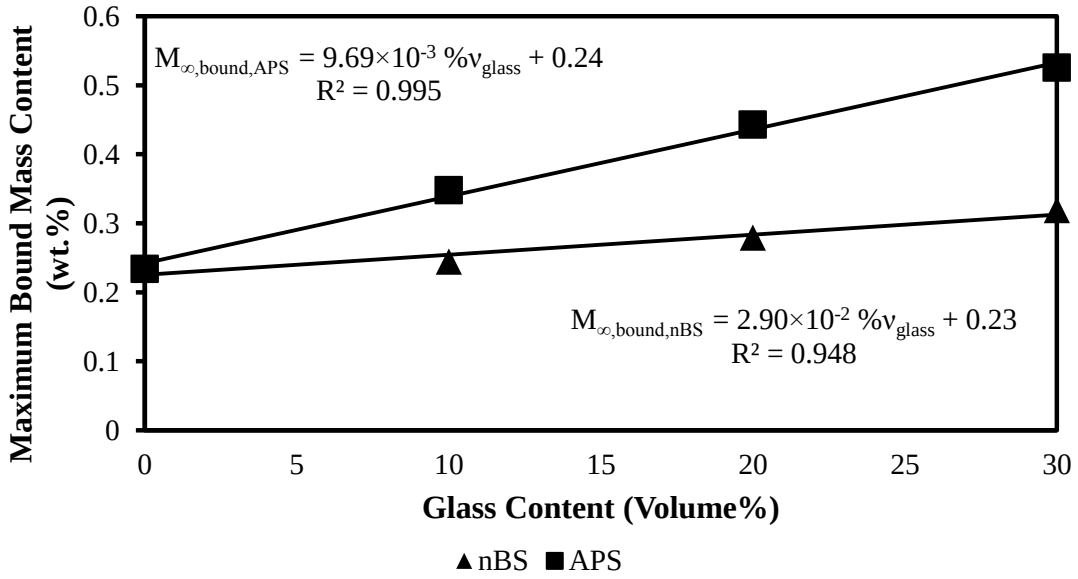
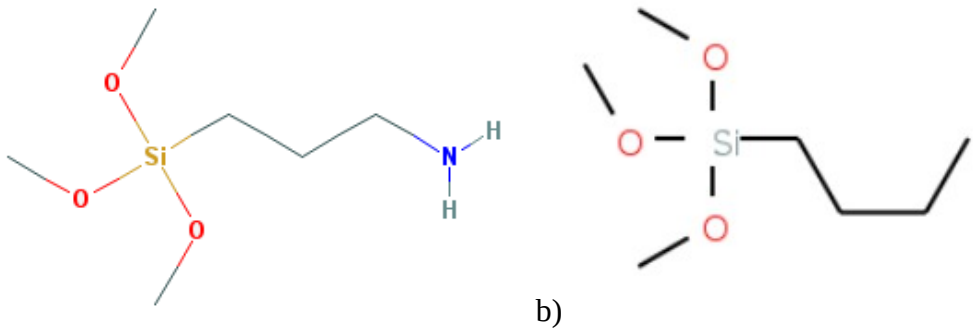


Figure 38. Effect of APS and nBS glass sphere loading in DGEBA epoxy on maximum bound moisture content.

Bentzl and Neville [121] reported that hydrogen bonding can hold water molecules. As shown in Figure 39-a, APS (aminopropyltrimethoxysilane) has an amine group (NH_2 group), which may create hydrogen bonding with H_2O molecules. On the other hand, nBS (n-butyltrimethoxysilane), shown in Figure 39-b, does not have any hydrogen bond. Hence, the epoxy/water interaction is assumed to be governed by the weak Van der Waals

interactions. Moreover, free electron of nitrogen of amine group of APS and hydrogen of the highly polarized water molecules may be electromagnetically bound and hold indefinite number of moisture molecules. Thus, addition of APS treated glass spheres are assumed to act as a better water bonding sites than nBS treated glass spheres. Additional bonding sites are anticipated to cause retardation in reaching the equilibrium; which in turn results in a higher increase in the hindrance coefficient. For the nBS case, weak Van der Waals attractions between the nBS and the moisture molecules create faster conversion between bound and unbound moisture. The fast transformation between bound and unbound moisture leads to early dynamic equilibrium, which can be seen in samples with lower hindrance coefficient.



a) b)

Figure 39. 2D chemical representation of a) APS, aminopropyltrimethoxysilane and b) nBS, n-butyltrimethoxysilane.

3.3. Hollow Micro Glass Sphere/Epoxy Composite Layer on Neat Epoxy

In this study, glass sphere/epoxy layer has been formed on epoxy to seek the moisture absorption kinetics of the layers and the composite and validate multilayer hindered diffusion model.

i. Materials and Sample Preparation of Micro Glass Sphere/EPON 862-EPON 862 Multilayer Composite

The epoxy resin and curing agent used in this study is selected as EPON 862 and Epikure W (Momentive Performance Materials Inc.), respectively. To produce a glass sphere/epoxy layer on top of the epoxy, 3M IM30K hollow micro glass spheres are chosen due to their low density ($\rho = 0.6\ g/cc$). First, SEM images of glass sphere powder are taken to observe the size distribution of the spheres. A representative SEM image of the glass sphere powder as received is shown in Figure 40a. As seen in Figure 40a, spheres have a wide range of size distribution which correlates well with the diameter distribution given by the manufacturer. To have a more uniform size distribution, the glass sphere powder is further sieved using a mechanical sieve shaker (Gilson Performer III). Glass spheres greater than 45μm and smaller than 20μm are discarded. The purpose is to better characterize the moisture absorption behavior by having more uniform glass sphere size. Figure 40b illustrates a representative SEM image of glass spheres after sieving. Sieved glass size distribution is estimated by using SEM images of approximately 500 spheres. Size histogram is illustrated in Figure 41. Sieved glass spheres have more concentrated size distribution having average sphere size of 25 ± 0.44 μm. Density of the sieved hollow glass spheres are measured using pycnometer as 0.44 g/cc.

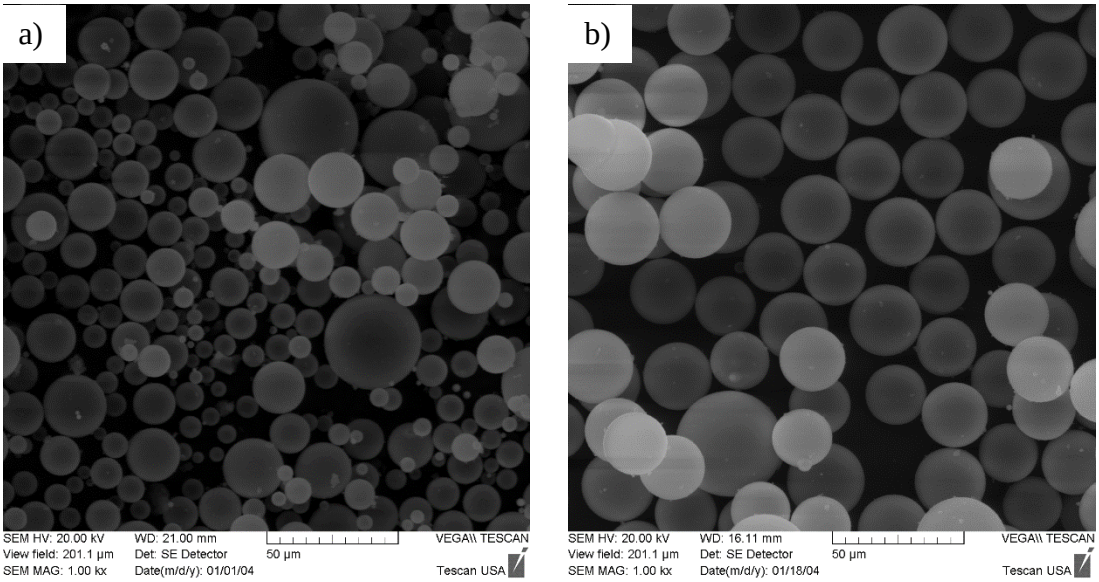


Figure 40. Representative SEM image of glass spheres *a)* as received *b)* sieved.

Glass spheres are mixed with epoxy at 100 RPM for 5 minutes to obtain 9.2, 19.7, and 50.0 wt.% (21, 40, and 71 vol%). Then, the mixture is sonicated at 42 kHz for 1 hour in 5 second on, 5 second off cycles. Throughout the sonication process, the mixture is kept in an icy water bath to eliminate the localized overheating or resin degradation.

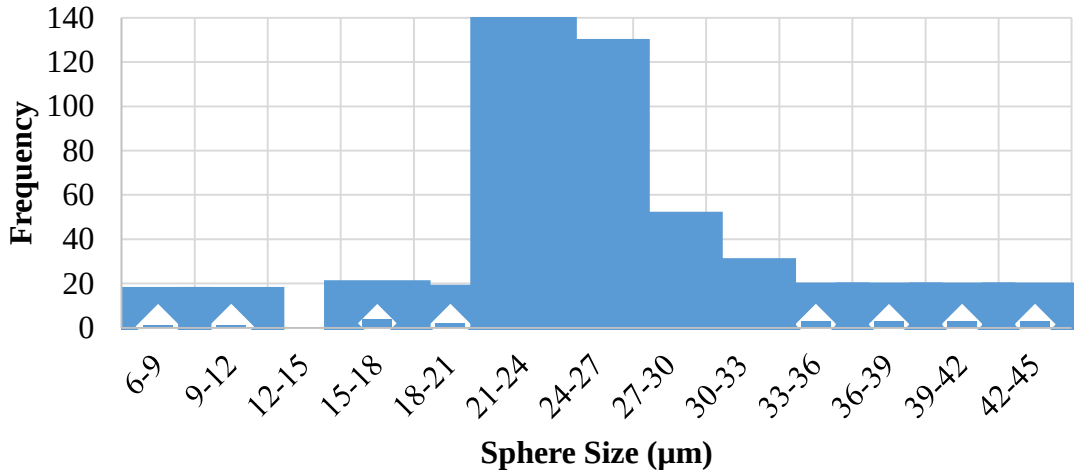


Figure 41. Hollow glass sphere size distribution.

After the sonication, the epoxy resin-nanoclay mixture and curing agent is mixed at a ratio of 100:26.4 by weight at 100 RPM for 15 minutes. The mixture is then degassed for 1 hour at room temperature to remove the trapped air. Subsequently, curing, cutting, drying, and moisture absorption testing procedures described in section 3.1.iii are applied. Average thickness of each set of samples with layer thickness of 31%, 57%, and 100% were measured as 1.15, 0.90, and 0.93 mm, respectively. The samples are thin enough to assume no moisture ingress through the much smaller side surfaces.

ii. Moisture Absorption Test Results of Micro Glass Sphere/EPON 862-EPON 862 Multilayer Composite and Validation of Multilayer Absorption Model

In order to utilize multilayer hindered diffusion model, thickness of the glass sphere layer in each laminate is determined using SEM imaging. In Figure 42Figure 44, glass sphere/epoxy layer formation on the neat epoxy can be observed. Due to its low density ($\rho = 0.44\ g/cc$), glass spheres float on the epoxy resin when gravity cast, thus forming a layer. Figure 42-Figure 44a illustrate the optical microscopy images of the multilayer composite samples for absorption experiments. White regions show the glass sphere/epoxy layer while grey regions are neat epoxy without glass spheres. It should be noted here that the glass sphere/epoxy layer formation caused slight bending of the laminates during cure due to non-zero coupling stiffness matrix. Figure 42Figure 44b show representative SEM images of the multilayer composite samples having glass sphere/epoxy layer thickness of 31%, 57%, and 100%, respectively. SEM images clearly show the highly-packed, uniform layer formation of the surface for each case. Thus, multilayer hindered diffusion model can be utilized to characterize the moisture absorption behavior of these laminates.

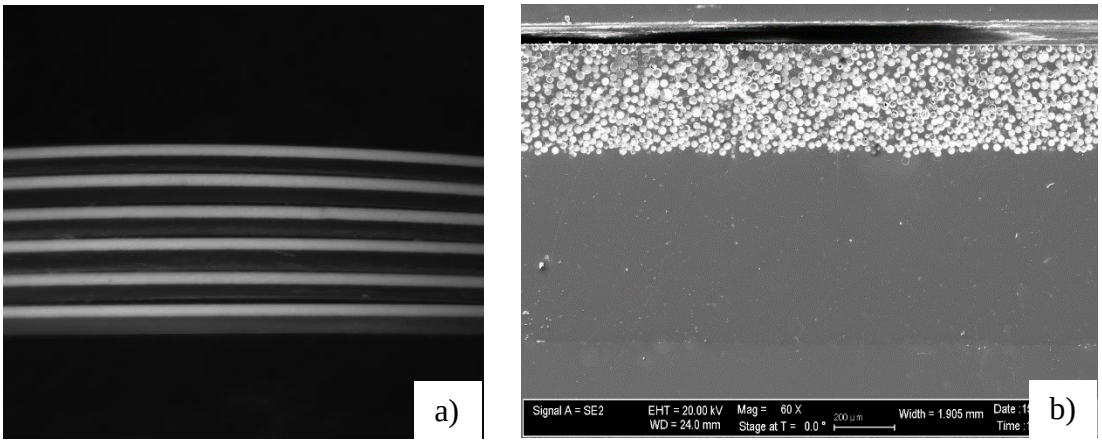


Figure 42. *a)* Optical microscopy image of 6 immersion samples showing multilayer of 31% thick glass sphere/epoxy, and 69% thick epoxy *b)* a representative SEM image of a sample.

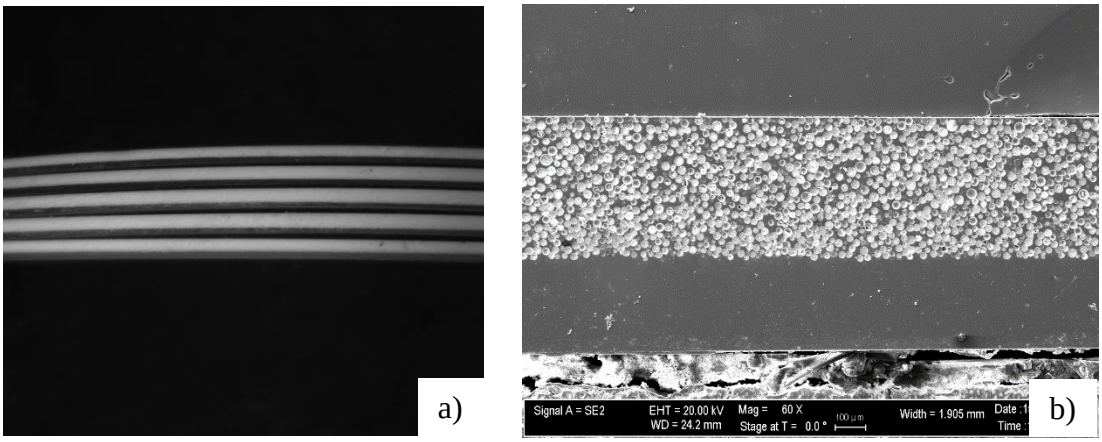


Figure 43. *a)* Optical microscopy image of 5 immersion samples showing multilayer of 57% thick glass sphere/epoxy, and 43% thick epoxy *b)* a representative SEM image of a sample.

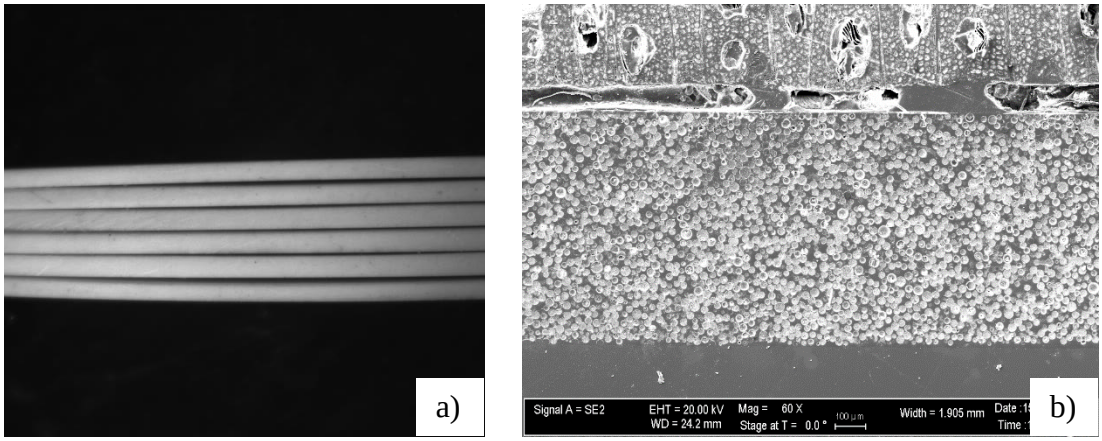


Figure 44. *a)* Optical microscopy image of 6 immersion samples of 100% thick glass sphere/epoxy *b)* a representative SEM image of a sample.

Multilayer hindered diffusion model is applied to recover the absorption parameters of the glass sphere/epoxy layer. If absorption parameters of both glass sphere/epoxy layer and neat epoxy layer were to be recovered simultaneously, eight absorption parameters would have needed to be recovered (i.e. $D_e, \gamma_e, \beta_e, M_{e,\infty}, D_{g/e}, \gamma_{g/e}, \beta_{g/e}, M_{g/e,\infty}$). Thus, absorption parameters of the neat epoxy layer have been found by hindered diffusion model in order to decrease computational cost, and tabulated in Table 8. Solving the eigenvalue problem for one-layer coating in Eq. (54a) and using the multilayer hindered diffusion model in Eq. (56), absorption parameters of the glass sphere/epoxy layer are recovered and tabulated in Table 8.

Table 8. Moisture absorption parameters of glass sphere/epoxy layer and neat epoxy layer.

Material Systems	D_z **(mm^2/h)**	β **(hr^{-1})**	γ **(hr^{-1})**	μ	M_∞ **(wt.%)**	**RMSE (%)**
Neat epoxy layer	8.59×10^{-4}	1.35×10^{-3}	2.59×10^{-4}	0.192	2.09	0.25
Glass sphere/epoxy layer	2.20×10^{-4}	3.03×10^{-4}	8.73×10^{-5}	0.288	2.98	2.75

Comparison between absorption parameters of the neat epoxy layer and glass sphere/epoxy layer show similar trends observed for previously analyzed micro glass and nanoclay reinforced epoxies. First, the change in the diffusion coefficient follows the rule of mixture. As previously stated, glass spheres do not absorb any moisture, accordingly has zero diffusivity. The diffusion coefficient of fully saturated glass sphere/epoxy layer (74 vol%) is calculated as 2.23×10^{-3} mm^2/h using rule of mixtures. The recovered diffusivity is only 1% off less than the theoretical diffusivity. Second, no significant change in γ, the rate of unbound moisture becoming bound is observed. However, the

decrease in β, the rate of bound moisture becoming unbound, suggests that the diffusion became more hindered by the addition of glass spheres. Lastly, glass addition increased the maximum moisture content by 31%. Even though the glass addition decreases the free volume that the moisture can diffuse into, glass sphere/epoxy interfaces increase the generation of bound moisture. Thus, the maximum moisture content increases. The effect of the glass sphere/epoxy layer formation and glass sphere saturated saturation in epoxy on moisture absorption kinetics is illustrated in Figure 45.

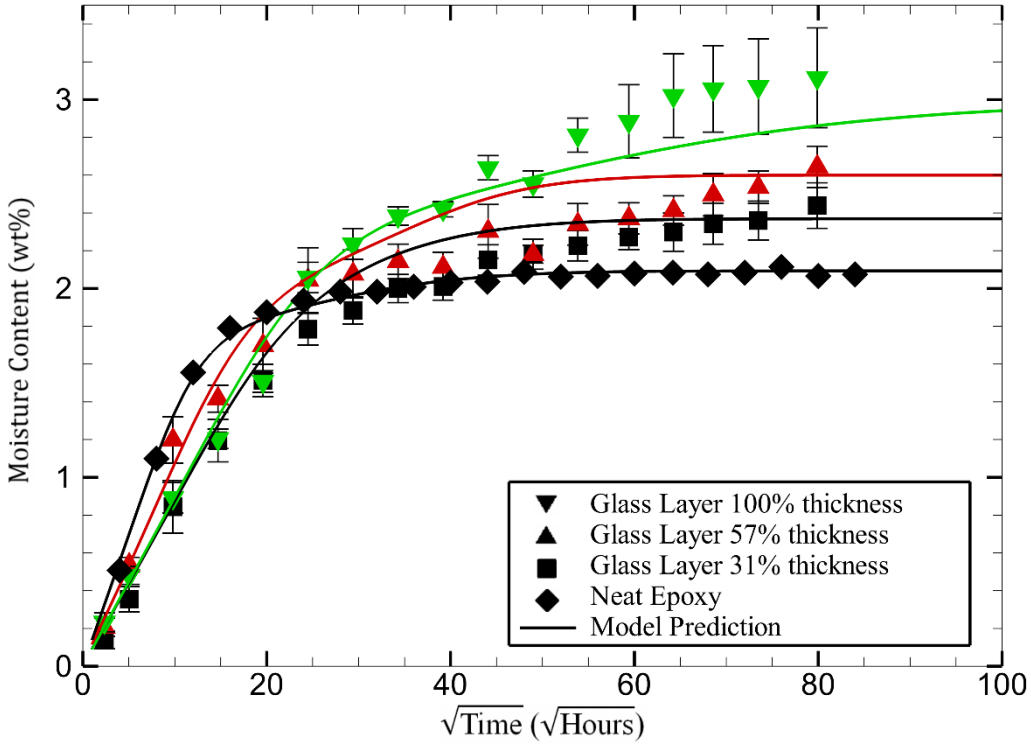


Figure 45. Experimental mass uptake data of 31%, 57%, and 100% thick glass sphere/epoxy layer-epoxy multilayer laminates and multilayer hindered diffusion model predictions.

In Figure 45, experimental mass gain data of neat epoxy, 31%, 57%, and 100% thick glass sphere/epoxy layer-epoxy multilayer composites and multilayer hindered diffusion model predictions are illustrated. Model prediction for neat epoxy laminate represents the experimental data smoothly in compliance with the root mean square error per data point

in Table 8. Even though the model predictions for 31% and 57% thick glass sphere/epoxy layer-epoxy laminates overshoot the experimental data a little, the hindered diffusion model was able to predict the moisture absorption behavior of three composites with different characteristics. It should be noted that variations in the average experimental mass gain data of glass sphere/epoxy-epoxy laminates are believed to be caused by non-uniform rate of chemical interaction between the water molecules and the glass sphere/epoxy interfaces. Increased fluctuation of the data with increasing glass content is considered to support this idea. Thus, a little overshoot of the multilayer hindered diffusion model prediction is expected. Regardless, multilayer hindered diffusion model is an effective tool to predict the absorption behavior of layered laminates.

To illustrate the effect of layer formation on moisture absorption kinetics, mass gain, and concentration profiles of multilayer glass sphere/epoxy-epoxy laminates and dispersed glass sphere/epoxy laminates are compared. It should be noted here that no dispersed glass sphere/epoxy laminate is manufactured or tested. The absorption parameters of the dispersed cases are deduced from the absorption parameters of neat epoxy and fully saturated glass sphere/epoxy laminates. Diffusion coefficient, maximum moisture content, and hindrance coefficient of dispersed glass sphere/epoxy laminates are assumed to follow the linear trend as observed for glass sphere/epoxy and nanoclay/epoxy laminates in previous sections. The diffusion coefficient of the 71% vol. glass sphere/epoxy laminate has already been detected to follow the rule of mixture. Thus, the diffusion coefficients of dispersed 21% and 40% vol. glass sphere/epoxy laminates are calculated using the rule of mixture. Diffusion coefficient, maximum moisture content, and hindrance coefficient is not enough to capture the absorption kinetics. Rates of

exchange between the bound and unbound moisture molecules, β and γ, are also required. The rate of unbound moisture to become bound, γ, has no significant change when glass added as shown in Table 8. Since hindrance coefficient is $\mu = {}^{\gamma}/_{\beta}$, assumed linear change in hindrance coefficient is attributed to β. Thus, change in γ and β are also assumed linear. The calculated absorption parameters of dispersed 21% and 40% vol. glass sphere/epoxy laminates are tabulated in Table 9.

Table 9. Moisture absorption parameters of dispersed 21% and 40% vol. glass sphere/epoxy laminates

Material Systems	D_z **(mm²/h)**	β **(hr⁻¹)**	γ **(hr⁻¹)**	μ	M_∞ **(wt.%)**
21% glass sphere/epoxy laminate	6.61×10^{-4}	1.03×10^{-3}	2.06×10^{-4}	0.201	2.37
40% glass sphere/epoxy laminate	4.95×10^{-4}	7.53×10^{-4}	1.61×10^{-4}	0.214	2.60

The comparison between the dispersed and layered glass sphere/epoxy laminates is illustrated in Figure 46 by using the absorption parameters in Table 8Table 9. Mass gain predictions of 21% and 40% vol. dispersed and layered glass sphere/epoxy laminates in Figure 46 demonstrates the change in absorption kinetics when glass spheres are dispersed or layered. For the same amount of glass addition, multilayer glass sphere/epoxy-epoxy and dispersed glass sphere/epoxy laminates absorb the same amount of maximum moisture content and reach to the maximum moisture content at the same time. Total moisture content is consist of unbound and bound moisture according to the hindered diffusion model. Same amount of glass, if not agglomerated, would induce the same amount of binding zone and occupy the same amount of free volume. Thus, no

change is expected in maximum bound and unbound moisture content of dispersed or layered glass/epoxy laminates.

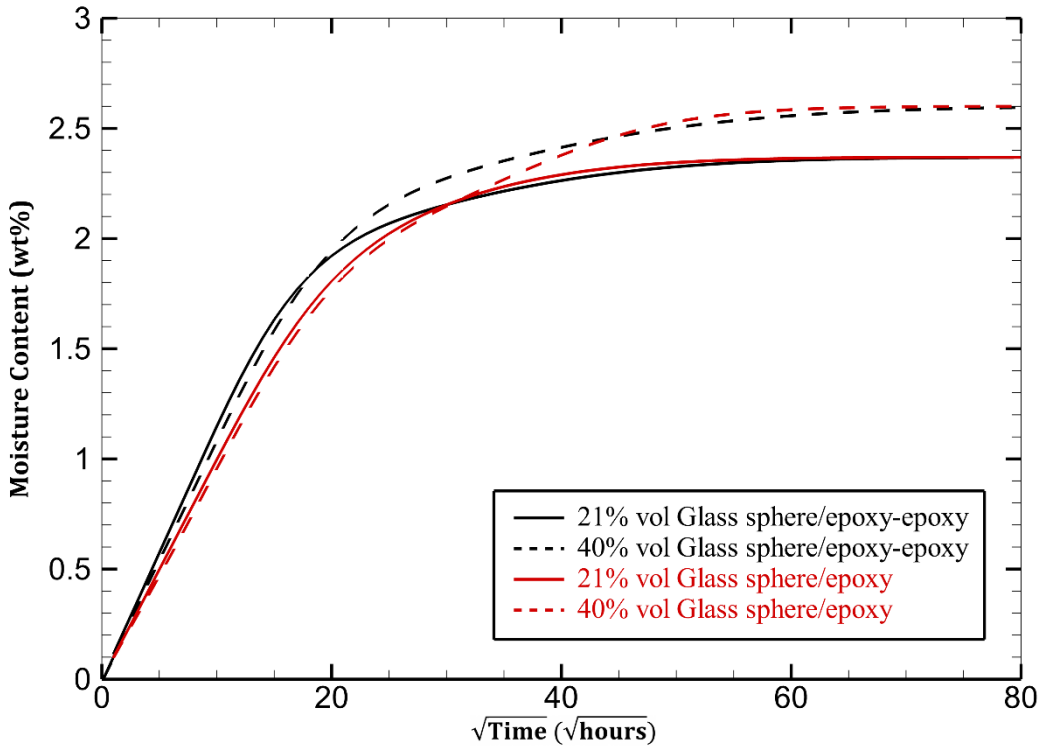


Figure 46. Multilayer HDM and 1D HDM predictions of 1mm thick 21% and 40% vol. glass sphere/epoxy layer-epoxy multilayer laminates and dispersed 21% and 40% vol. glass sphere/epoxy laminates, respectively.

Nonetheless, change in absorption kinetics is detected at initial moisture absorption where multilayer laminate absorbs moisture faster than the dispersed case. Multilayer laminate may be considered to be consist of fully saturated glass sphere/epoxy layer and neat epoxy layer. Even though moisture diffuse slower into the fully saturated glass sphere/epoxy layer, rate of binding of moisture molecules is very fast due to available binding sites per unit volume. In neat epoxy layer, no glass sphere obstructs the diffusion leading to fast diffusion into the laminate. In dispersed case, both diffusion and molecular binding rate are compromised. Fast binding rate in saturated glass sphere/epoxy layer and fast diffusion in neat epoxy layer of multilayer laminate result in faster initial moisture

uptake than the dispersed case where the diffusion and binding rate is average. To substantiate the change in absorption kinetics, concentration profiles of multilayer glass sphere/epoxy-epoxy laminates and dispersed glass sphere/epoxy laminates are demonstrated in Figure 47.

In Figure 47, each line separates equipotential surfaces separated by concentration of 2.5%. Frequency of these lines explains the change in the flux throughout the composite layers. Increasing frequency of the lines represents higher concentration gradient. On the other hand, the color gradient denotes the dimensional change in the moisture content. The non-dimensional concentration profiles are scaled to the maximum moisture content of the fully saturated glass sphere/epoxy composite laminate (i.e. 2.75 wt.%). Hence, the amount of absorbed moisture and change in absorption behavior in each layer can be distinguished. The boundaries of the different layers are separated by a red line in multilayer cases. All the two-dimensional concentration profiles are taken from the mid-plane of the laminate at $\sqrt{time} = 15$.

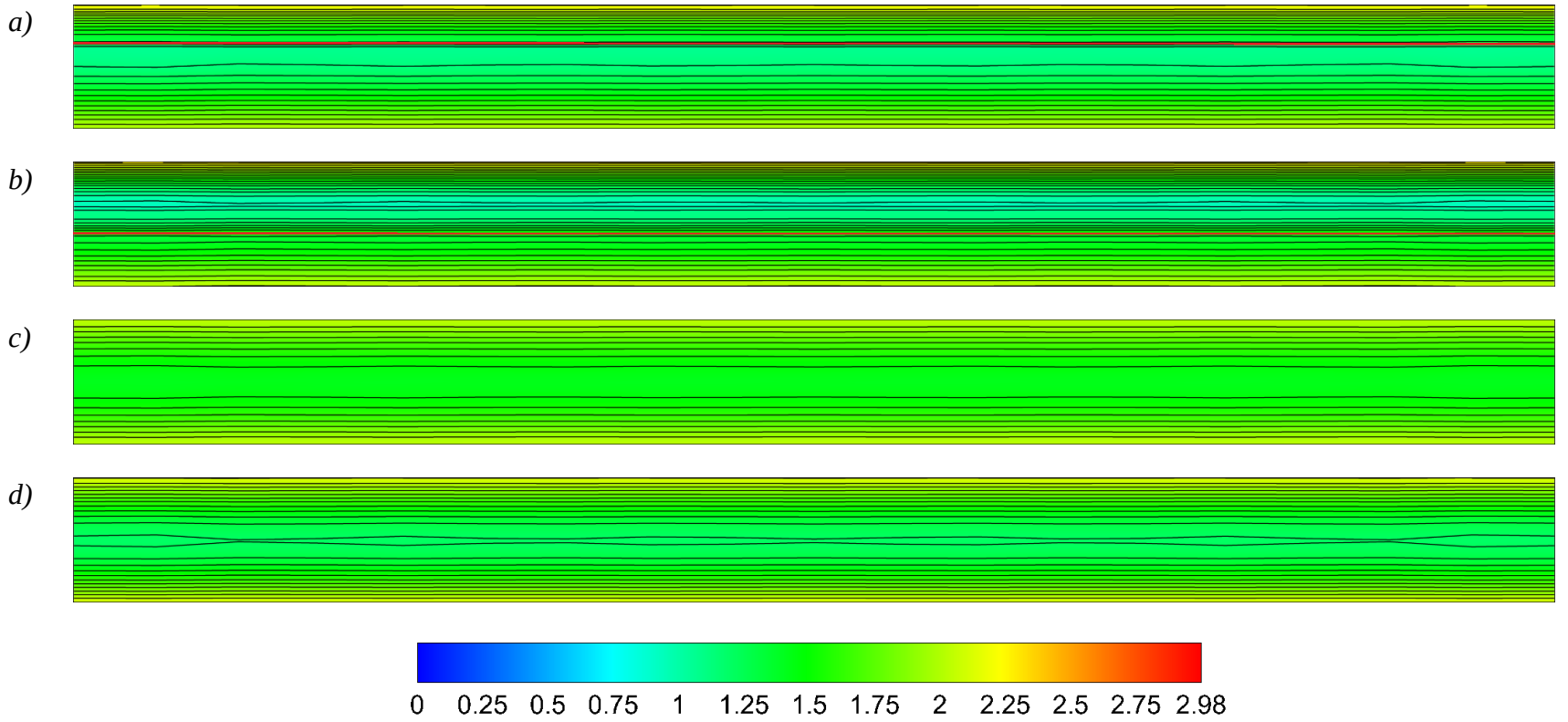


Figure 47. Concentration profiles of *a)* 31% thick glass sphere/epoxy layer-epoxy multilayer composite (21% vol. glass sphere), *b)* 57% thick glass sphere/epoxy layer-epoxy multilayer composite (40% vol. glass sphere), *c)* dispersed 21% vol. glass sphere/epoxy composite, and *d)* dispersed 40% vol. glass sphere/epoxy composite after 10 days of fully saturation.

For the cases of multilayer composites, *a)* and *b)*, higher concentration gradient is observed in the glass sphere/epoxy layer. Concentration profiles in the cases *a)* and *b)*, the neat epoxy layer absorbed more moisture than glass sphere/epoxy layer leading to shift of minimum concentration location towards the glass sphere/epoxy layer. Whereas, the minimum concentration is at the center of the laminate for the dispersed cases, *c)* and *d)*, due to uniform moisture absorption in through-the-thickness direction. Moreover, Figure 47 shows that the higher concentration in the neat epoxy layer of cases *a)* and *b)* is responsible for the higher initial uptake observed in mass gain predictions in Figure 46. Higher diffusivity of the neat epoxy result in faster initial uptake.

Finally, similar initial uptake of 21% and 40% vol. glass sphere/epoxy laminates in Figure 46 is not observed in Figure 47. Even though initial mass uptake of 21% and 40% vol. glass sphere/epoxy laminates are almost identical, the absorption kinetics differ. Higher diffusivity of 21% vol. glass sphere/epoxy laminate allows faster diffusion whereas higher binding rate of 40% vol. glass sphere/epoxy laminate increases the bound moisture content. Thus, overall initial mass gain of the cases, *c)* and *d)*, are similar.

3.4. Conclusion

Nano-filler addition in epoxy is observed to result in a linear relation between both the maximum moisture content and the hindrance coefficient with respect to the nanoclay content, when the diffusion coefficient linearly decreases following the rule of mixture.

The hindrance coefficient and maximum bound moisture content have a tendency to linearly increase with increasing nanoclay content in I.30E nanoclay/DGEBF epoxy and glass sphere/epoxy while they have a decreasing trend in I.30E nanoclay/DGEBA epoxy. Due to both theoretical groundwork and mathematical calculations, the trend of the

hindrance coefficient and maximum bound moisture content should be identical. Increasing binding sites would also hinder the moisture absorption due to an increase in continuous transformation between the unbound and bound molecules. Hydration of cations between the nanoclays, water binding to high energy surface areas, and intermolecular bonding between the water molecule and the epoxy are the main causes of hindrance in moisture absorption. Negative or positive slope of change in the hindrance coefficient and maximum bound moisture content with respect to nano-filler addition is governed by the compromise between the decreasing intermolecular bonding sites in epoxy and increasing binding sites due to inclusion addition.

Increasing inclusion content also affects the maximum unbound moisture content. Addition of inclusion decreases the epoxy content per unit volume - in other words, "free volume" in which the moisture can freely diffuse, when inclusions are impermeable. Since the unbound moisture is just a measure of the diffusing water, reducing the free volume with inclusion addition results in decreasing maximum unbound moisture content. The decrease in free volume depends upon the type of the inclusion and epoxy. Although the decrease in unbound maximum moisture content in DGEBA and DGEBF epoxies are not exactly the same, they are similar. Likewise, addition of 30% vol. APS and nBS treated glass spheres into DGEBA epoxy reduced the equilibrium unbound moisture content by 40% for both cases. Different surface treatment of glass spheres changes the outcome of bound moisture. Same glass spheres would still occupy the same effective volume. Therefore, different surface treatments on glass spheres did not affect the unbound moisture content as long as they are at the same size and amount.

The decrease in the maximum moisture content with increasing inclusion originates from the fact that the decrease in the maximum unbound moisture content is more dominant than the corresponding decrease/increase in the maximum bound moisture content.

Lastly, multilayer hindered diffusion model is successfully incorporated in multilayer glass sphere/epoxy-epoxy laminates. Same amount of glass sphere addition did not change the time to reach the equilibrium or the maximum moisture content whether glass sphere/epoxy layer is formed or glass spheres are dispersed. Layer formation changed the dynamics of the initial moisture intake when compared to corresponding dispersed case. Even though the glass sphere/epoxy layer formation decreased the barrier capabilities of EPON 862 epoxy, validation of multilayer hindered diffusion model may be used to predict what type of reinforcement or coating would be needed to improve the water resistance.

Chapter 4. Moisture Absorption Modeling of Highly Porous Polymers and Polymer Composites

Polymeric foams are lightweight cellular material containing numerous small voids filled with air or some gases. They are widely used for their unique properties such as thermal stability [98,99,123–125], electrical insulation [98,100], shock absorption [125], and acoustical dampening [125,126]. Polymeric foams are also frequently used in composite sandwich structures as core materials mainly to achieve reduction in the overall weight of the composite structure. Properties of the foam depend on not only the foam matrix polymer but also the foam density, cell size, and geometry [127–130].

Polymeric foams are commonly used in wet or highly humid environments. Use of polymeric foams in naval vehicles is of current interest due to their light-weight, buoyancy enhancement on submersible vessels, and ship stability improvement [131]. Besides, polymeric foams such as polyurethane and polyisocyanurate are in standard use in space launch vehicles as thermal insulation [132]. However, foams were found to gain excessive amount of moisture under naval and cryogenic conditions, leading to mechanical property degradation [133,134]. Utilization of foams in mission critical applications lead researchers to investigate the moisture absorption into polymeric foams [103,133,135–138].

Avilés and Aguilar-Montero [135] investigated moisture absorption into PVC foam and PVC foam core E-glass/polyester face sheets sandwich composites. Although researchers [135] used approximate three-dimensional Fickian diffusion model to recover the diffusivity and the maximum moisture content, they reported that using Langmuir type or multistep diffusion model would yield better agreement with the experimental data.

Nonetheless, they found the maximum moisture content of the foam core as 1.9 wt.% and 74.2 wt.% under 95% RH and in sea water, respectively. They also reported that the face sheets significantly limit water absorption into the sandwich structure. Similarly, Huo et al. [103] reported that neat PU resin, face sheets, PU foam, and foam core sandwich composite absorbed ~2.5 wt.%, ~1 wt.%, ~75 wt.%, and ~10 wt.%, respectively.

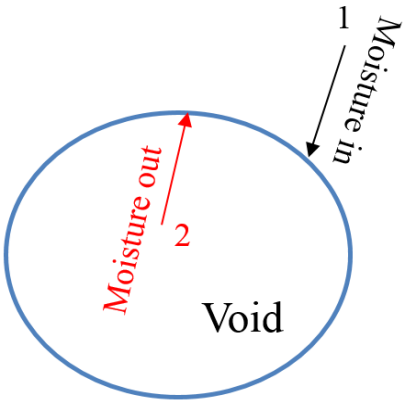
Some researchers investigated the effect of foam microstructure, geometry, and density on moisture absorption. Earl and Shenoi [136] studied the moisture uptake mechanism on closed-cell polyurethane foams. Their research showed that same type of foams with different thicknesses have diverse absorption kinetics. They concluded that the classical models cannot sufficiently describe the long-term absorption behavior. Li and Weitsman [137] observed that the less dense foam with larger cell size absorbed more water and claimed that major portion of the absorbed water goes into the pores.

A number of different models have been developed to identify the absorption kinetics into the foams [97,104–108]. These models have been briefly explained in Chapter 1.5 and Chapter 2.8. In this chapter, a new approach is presented to identify the moisture intake kinetics of closed-cell rigid polymeric foams. Effects of foam microstructure and porosity on absorption is sought. Within this framework, void filling hindered diffusion model is developed to illustrate the effect of porosity on moisture absorption.

4.1. Void Filling Hindered Diffusion Model Development

Void filling hindered diffusion model (VFHDM) has been developed as an expansion of hindered diffusion model. In addition to the bound and unbound moisture molecules, VFHDM considers stored (trapped) water inside the closed-cell pores. A concept similar to hindered diffusion model is used to describe the diffusion into the closed-cell pores.

Pores are assumed to be sources and sinks for diffusing moisture. The rates of going in and out of the voids have been used to identify the trapped water and illustrated in Figure 48. The rates of exchange between the medium and the pore depend on the diffusion mechanism. First, for a water molecule to diffuse into a pore, it should be a mobile (unbound) molecule. Unbound moisture penetrating into the pore occurs at a rate of, $n\gamma'$. Once inside the pore, the moisture molecule is assumed trapped. The stored (trapped) moisture, S, then, go out and become unbound at a constant rate of, $S\beta'$. Hence, the set of governing equations for VFHDM is given in Eqs. (61).



1: $\gamma' n$ 2: $-\beta' S$ Overall Rate (1+2):

$$\frac{\partial S}{\partial t} = \gamma' n - \beta' S$$

Figure 48. Illustration of the proposed moisture absorption and desorption mechanism of voids

$$D\frac{\partial^2 n}{\partial z^2} = \frac{\partial n}{\partial t} + \frac{\partial N}{\partial t} + \frac{\partial S}{\partial t} \tag{61a}$$

$$\frac{\partial N}{\partial t} = \gamma n - \beta N \tag{61b}$$

$$\frac{\partial S}{\partial t} = \gamma' n - \beta' S \tag{61c}$$

where n represents the unbound moisture per unit volume, N represents the bound moisture per unit volume, S is the stored moisture per unit volume, γ is the rate of an unbound moisture to become bound, β is the rate of bound moisture to become an unbound, γ' is the rate of an unbound moisture to become stored, and β' is the rate of stored moisture to become an unbound.

The formation of the trapped moisture is further investigated by quantifying the rate of exchanges between the unbound and trapped moisture. To characterize the effect of void volume fraction on the trapped moisture, a representative two-dimensional cross-section of a solid slab with and without void is illustrated in Figure 49.

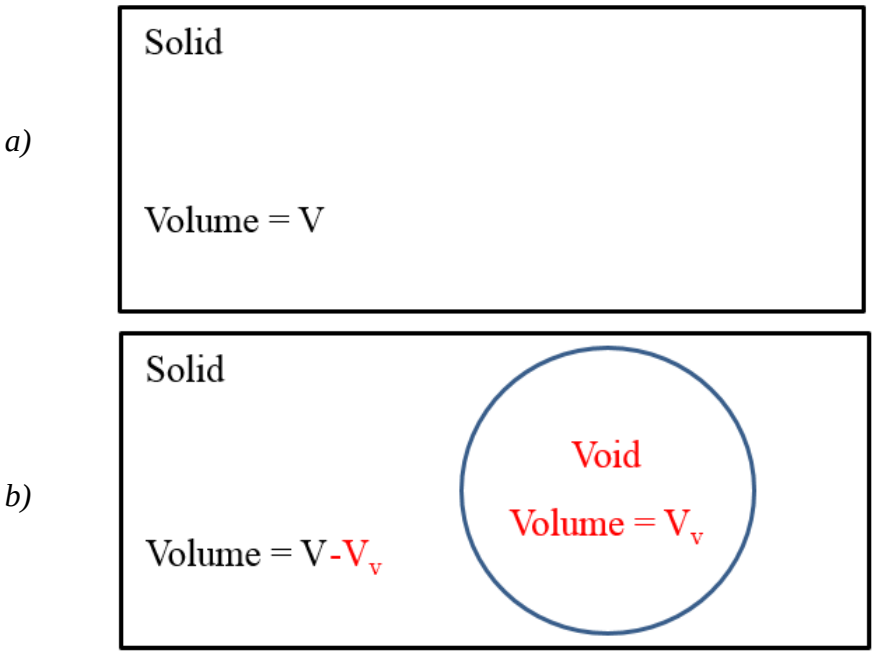


Figure 49. Representative 2D solid slab having *a)* no void *b)* void with a volume of V_v

Let amount of unbound moisture that the solid with no void *(a)* can absorb be n. The amount of unbound moisture that the solid with void can absorb will be $n\frac{V-V_V}{V} = nv_m$ where v_m is the matrix volume fraction.

When the v_m is smaller than void volume fraction, $v_v = 1 - v_m$, the rate of an unbound molecule to become trapped in the void should be higher than the rate of unbound molecule to become bound (If $v_m < v_v \xrightarrow{yields} \gamma' > \gamma$). Unbound moisture around the void can either bind to the matrix/void interface or diffuse into the void. If the rate of unbound moisture to become bound is higher than the rate of unbound moisture to be trapped, unbound moisture would prefer to bind to the interface instead of filling the void resulting in reaching an unbound-bound moisture equilibrium before unbound-trapped and bound-trapped moisture equilibrium. Hence, equilibrium condition between the unbound and trapped molecules, and bound and trapped molecules would not be satisfied. No unbound molecule would be left to fill the pores, causing intermittent diffusion. Thus, for a continuous diffusion:

$$\gamma' = \frac{v_v}{v_m}\gamma = \zeta\gamma \tag{62}$$

In Figure 50, a representative water-filled-void is illustrated to explain the moisture desorption process in VFHDM. The moisture exits the pores through the void/matrix interface in two stages: 2a) Moisture desorption into the void/matrix interface, and 2b) moisture desorption from the interface to the matrix. For high porosity cases, ($v_v > 0.5$), β' should be equal to β due to equilibrium constraints. If the rate of desorption to the interface from the pore is higher (2a>2b), the interface would reach equilibrium faster causing intermittent diffusion just like $\gamma' < \gamma$. On the other hand, higher rate of desorption from the interface to the matrix (2b>2a), pores would be left dry. Thus, $\beta' = \beta$. It should be noted here that the bound moisture absorbed by the matrix is assumed to be negligible compared to the interface bound moisture.

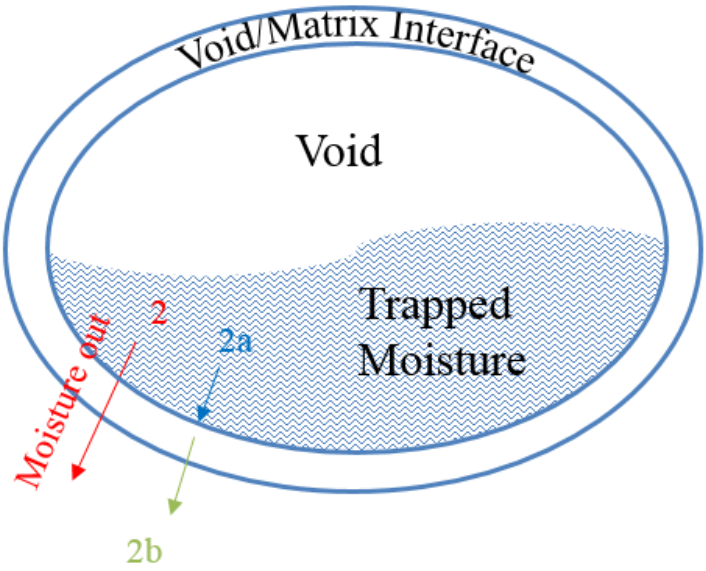


Figure 50. Moisture desorption steps in a representative water filled void

Resulting void filling model becomes:

$$D\frac{\partial^2 n}{\partial z^2} = \frac{\partial n}{\partial t} + \frac{\partial N}{\partial t} + \frac{\partial S}{\partial t} \tag{63a}$$

$$\frac{\partial N}{\partial t} = \gamma n - \beta N \tag{63b}$$

$$\frac{\partial S}{\partial t} = \zeta\gamma n - \beta S \tag{63c}$$

Void filling hindered diffusion model considers diffusion, chemical interaction between medium and penetrant, and storage of moisture in voids and porous structure. The model moderately assumes that there are two types of bound molecules. First type is the bound molecules which interact with the polymer chains, the polymer-inclusion, and/or polymer-void interface. This type of bound molecule absorption can be predicted by the unmodified, original hindered diffusion model. Second type of bound molecule is the one that penetrates the closed-cell pore and forms an accumulated amount of penetrant. In other words, diffusing molecules interacts with each other inside the pore to become a body of

liquid. Void filling hindered diffusion model basically extends the hindered diffusion model by introducing a new type of bound moisture which is stored in the voids.

Analytical solution of the set of differential equations of void filling hindered diffusion model is given in Eqs. (64).

$$n(z,t)$$

$$= n_\infty \left\{ \begin{array}{l} 1 - \frac{4}{\pi} \sum_{i=1}^{\infty(odd)} (-1)^{\frac{i-1}{2}} \frac{r_i^+ exp(-r_i^- t) - r_i^- exp(-r_i^+ t)}{\mathrm{i}(r_i^+ - r_i^-)} \cos\left(\frac{\pi i z}{2\delta}\right) + \\ \frac{4}{\pi\beta} \sum_{i=1}^{\infty(odd)} (-1)^{\frac{i-1}{2}} (r_i^+ r_i^-) \frac{exp(-r_i^- t) - exp(-r_i^+ t)}{\mathrm{i}(r_i^+ - r_i^-)} \cos\left(\frac{\pi i z}{2\delta}\right) \end{array} \right\} \quad (64a)$$

$$N(z,t) = \frac{\gamma}{\beta} n_\infty \left\{ 1 - \frac{4}{\pi} \sum_{i=1}^{\infty(odd)} (-1)^{\frac{i-1}{2}} \frac{r_i^+ exp(-r_i^- t) - r_i^- exp(-r_i^+ t)}{\mathrm{i}(r_i^+ - r_i^-)} \cos(\frac{\pi i z}{2\delta}) \right\} \quad (64b)$$

$$S(z,t) = \zeta \frac{\gamma}{\beta} n_\infty \left\{ 1 - \frac{4}{\pi} \sum_{i=1}^{\infty(odd)} (-1)^{\frac{i-1}{2}} \frac{r_i^+ exp(-r_i^- t) - r_i^- exp(-r_i^+ t)}{\mathrm{i}(r_i^+ - r_i^-)} \cos(\frac{\pi i z}{2\delta}) \right\} \quad (64c)$$

where

$$r_i^{\pm} = \frac{1}{2}[(Ki^2 + (1+\zeta)\gamma + \beta) \pm \sqrt{(Ki^2 + (1+\zeta)\gamma + \beta)^2 - 4K\beta i^2}]$$

$$K = \frac{\pi^2 D}{h^2}$$

When the sum of bound moisture concentration $N(z,t)$, unbound moisture concentration $n(z,t)$ and trapped moisture concentration $S(z,t)$ is integrated over the laminate thickness, the result is mass fraction of the absorbed moisture and expressed as:

$$M(t) = M_\infty \left\{ \begin{array}{c} 1 - \frac{8}{\pi^2} \sum_{i=1}^{\infty(odd)} \frac{r_i^+ exp(-r_i^- t) - r_i^- \exp(-r_i^+ t)}{i^2 (r_i^+ - r_i^-)} + \\ \frac{8}{\pi^2} \left(K \frac{\beta}{\beta + (1+\zeta)\gamma} \right) \sum_{i=1}^{\infty(odd)} \frac{exp(-r_i^- t) - \exp(-r_i^+ t)}{(r_i^+ - r_i^-)} \end{array} \right\} \quad (65)$$

4.2. Void Filling Hindered Diffusion Model Validation

ROHACELL® WF-71 (Figure 51) rigid foam plastic based on PMI (polymethacrylimide) is used to investigate the moisture absorption in closed-cell foams. It is primarily designed to be used in aerospace applications and satisfies MIL and CMS specifications for industry requirements.



Figure 51. ROHACELL® WF-71 Foam

ROHACELL® WF-71 structural foam can withstand curing temperatures up to 130℃ (266℉) and 0.7 MPa (102 psi) pressure. Heat treatment on the foam can change the cell structure to make it withstand up to 180℃ (356℉) at 0.7 MPa.

i. Materials and Sample Preparation of Rohacell Closed-Cell Structural Foam

To investigate the effect of porosity in absorption kinetics, three sheets of 625 mm × 1250 mm (25″ × 50″) ROHACELL® WF-71 (Evonik Industries) having 3mm, 6mm, and 9mm thicknesses are used in this study. Prior to absorption tests, eight samples of 51 mm × 51 mm (2″ × 2″) is cut from each foam sheet.

Remaining part of each foam sheets were heat treated to change their microstructure. Each sheet is cut into two 254 mm × 254 mm (10″ × 10″) panels. Cut panels were dried in vacuum oven at 40℃ (104°F). Then, panels were subjected to 21 MPa (30 psi) or 34 MPa (50 psi) at 127℃ (260°F) for 3 hours. Immediately, the panels are further processed at 176℃ (350°F) under the same pressures for 3 hours. Heat treated foams are cooled down to room temperature at a rate of 2℃/min (5°F/min). Heat treated panels are cut into 51 mm × 51 mm (2″ × 2″) specimens for absorption test.

Each specimen set contains eight foam samples to minimize the experimental uncertainty. The cut samples are dried in vacuum oven 43℃ (110°F) for approximately 5 days. Dried samples are immersed in distilled water at 25℃ (77°F). Final sample dimensions and their abbreviations are given in Table 10.

Table 10. Sample Dimensions and Abbreviations of Rohacell Foams

Sample	Thickness(mm)	Length(mm)	Width(mm)	Treatment
R3	3.070	50.616	49.598	-
R6	6.152	51.090	49.689	-
R9	8.930	50.319	49.324	-
R3-30	2.541	49.755	49.806	Heat treated @ 30 psi
R6-30	4.797	49.578	50.031	Heat treated @ 30 psi
R9-30	6.339	50.009	49.620	Heat treated @ 30 psi
R3-50	1.333	49.988	49.761	Heat treated @ 50 psi
R6-50	2.933	49.844	49.906	Heat treated @ 50 psi
R9-50	4.203	49.799	49.854	Heat treated @ 50 psi

ii. Characterization of as-received and heat treated foams

A quick glance on Table 10 yields a thickness reduction due to heat treatment on foams. Heat treatment under 30 psi and 50 psi lead to thickness reduction ranging from 17% to 29% and 67% to 75%, respectively. Thickness reduction suggests that the heat treatment has changed the microstructure of the foams as predicted. To analyze the effect of microstructural changes on moisture absorption, variations in the cell size, cell geometry, porosity, and density have been sought.

Density of as-received and heat treated foams are measured by Accupyc II 1340 gas pycnometer and given in Figure 52. The increase in density is observed to be consistent with the decrease in the thickness due to heat treatments. As the foams are compressed at

elevated temperature, pores shrink to smaller size resulting in thickness reduction. Since no chemical reaction occurs, the amount of polymeric matrix in the sample does not change. Reduced volume of a constant mass indicates an increase in density.

Change in density is not identical for foams with different thicknesses. For example, 30 psi pressure increased the density of 3 mm thick foams about 8.7% whereas for 6 mm and 9 mm thick foams, 27.5% and 47.0% density increase is measured, respectively. Moreover, more than twofold increase in density is observed when the foams are subjected to heat treatment under 50 psi pressure.

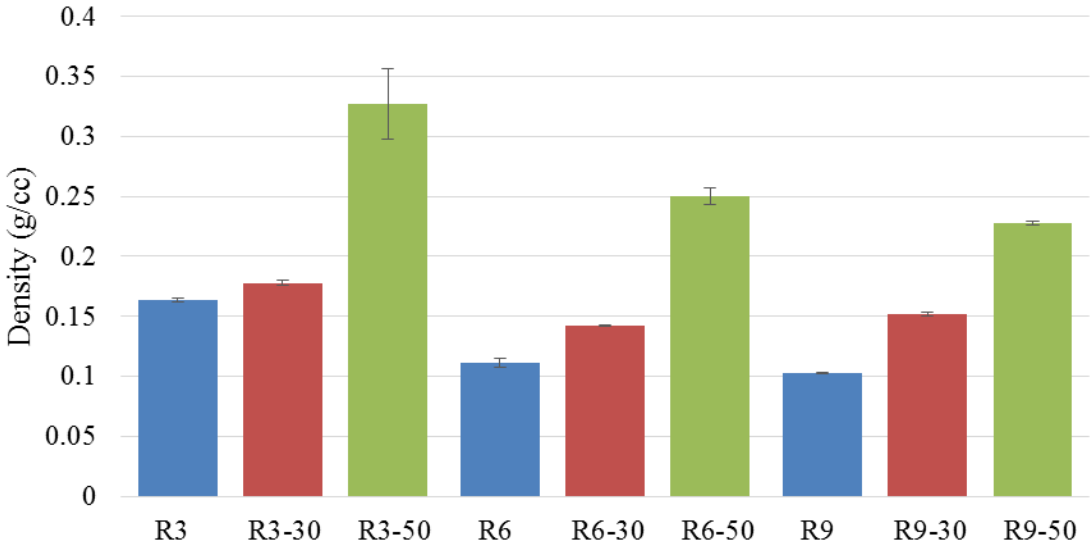
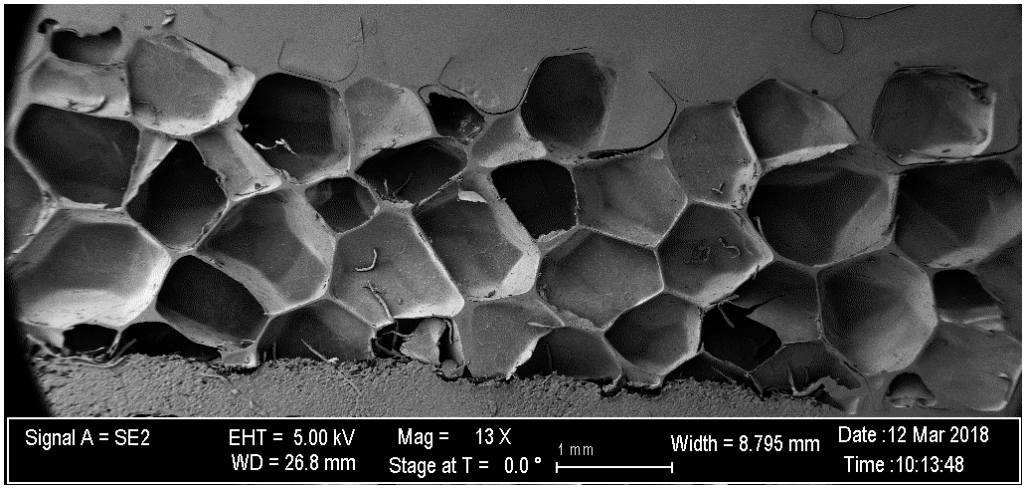


Figure 52. Measured densities of untreated and heat treated Rohacell foams.

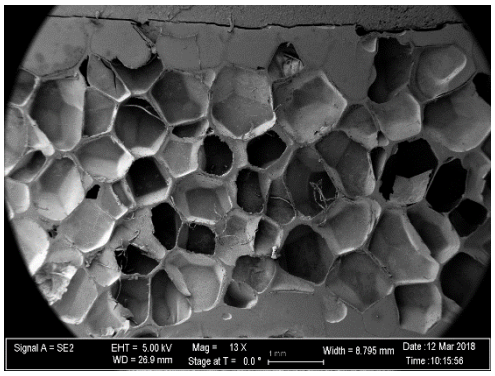
Comparison between the densities of the 3mm, 6mm, and 9mm as-received foams shows that as the foams get thinner they get denser. Even though the as-received foams was supposed to have identical properties, different densities lead to further investigate the microstructure of each foam. Hence, SEM images of as-received and heat treated foams are captured using Zeiss Neon high resolution SEM and demonstrated in Figure 53.

In Figure 53, representative through-the-thickness SEM images of 3mm, 6mm, and 9mm as-received foams are illustrated. Immediately, large cell sizes stand out in Figure 53. Even though the cell geometries and the cell sizes of foams with three different thicknesses are comparable, open large cells at the surfaces may be the reason of the density difference. Pycnometer basically measures the volume of a sample by pressurizing a cup of known volume (via calibration) with an inert gas, admitting the pressurized gas to the chamber containing the sample and measuring the pressure. Then using ideal gas equation it calculates the volume of the sample. While measuring the volume of the closed-cell porous media, open-cells at the surface would be filled with pressurized gas and will not be accounted as solid part. Thus, in thinner samples open-cell to closed-cell ratio would be higher, if the cell size is comparable to any dimension of the sample. For example, 2-3 closed-cell can fit through-the-thickness of 3mm foam while 6-7 closed-cell is observed through-the-thickness of 6mm foam. Open-cell to closed-cell ratio is higher in 3mm samples resulting in higher density.

a)



b)



c)

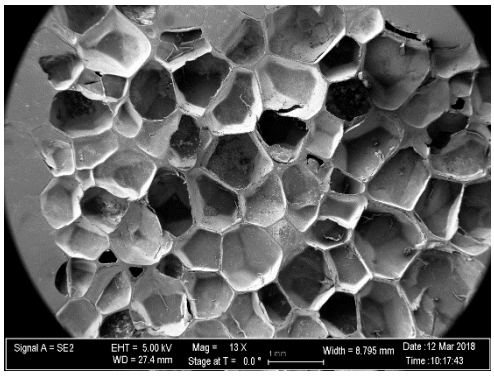
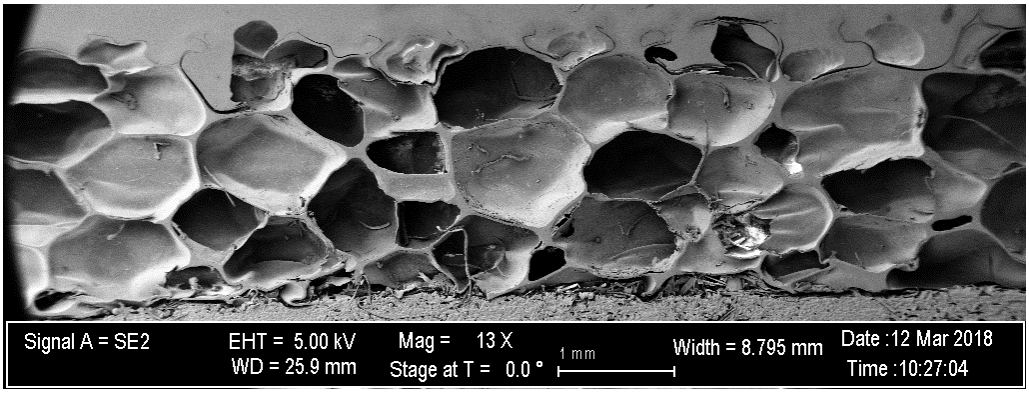


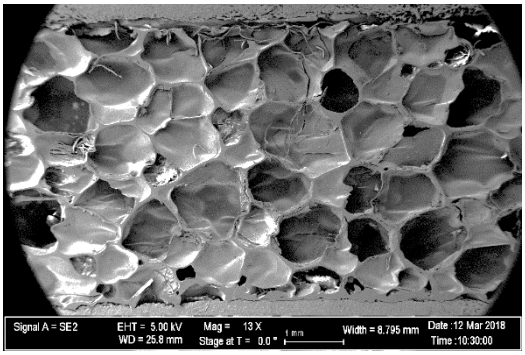
Figure 53. Representative SEM images of foam samples - as-received *a)* 3mm *b)* 6mm *c)* 9mm

Figure 54 illustrates through-the-thickness SEM images of 3mm, 6mm, and 9mm foams which are heat treated under 30 psi pressure. Smaller and slightly elongated cells are observed in Figure 54 as compared to the cell size and geometry of as-received foams. However, compared to the closed-cells in the matrix, open-cells on the surface are observed to be greatly squeezed causing the majority of thickness reduction. Moreover, squeezing of the surface cells resulted in less variation in open-cell volume to closed-cell volume ratio in samples with different thicknesses. In turn, density variation between the samples with different thicknesses is decreased compared to the as-received samples.

a)



b)



c)

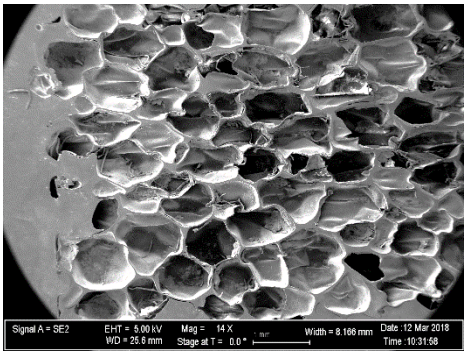
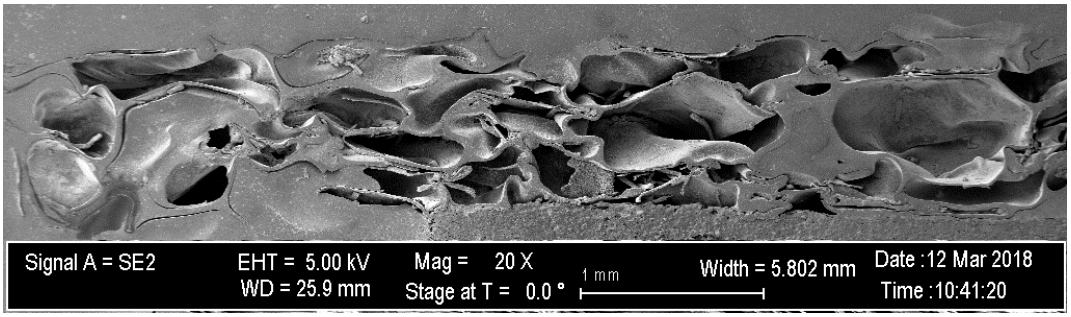


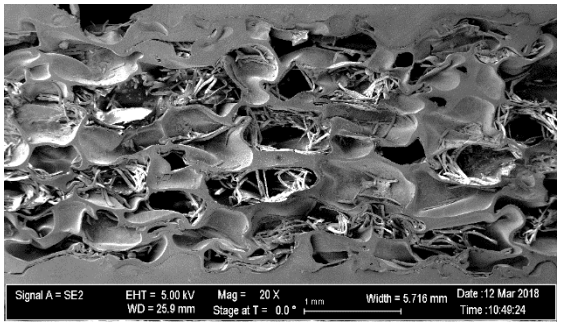
Figure 54. Representative SEM images of foam samples – heat treated under 30 psi *a)* 3mm *b)* 6mm *c)* 9mm

Figure 55 shows through-the-thickness SEM images of 3mm, 6mm, and 9mm foams which are heat treated under 50 psi pressure. Drastic changes in cell size and geometry may easily be observed in SEM images. Cells are extremely elongated. Cell coalescence can be observed. Some degraded and elongated cells reach to the surface becoming an open-cell resulting in substantial density increase observed in Figure 52.

a)



b)



c)

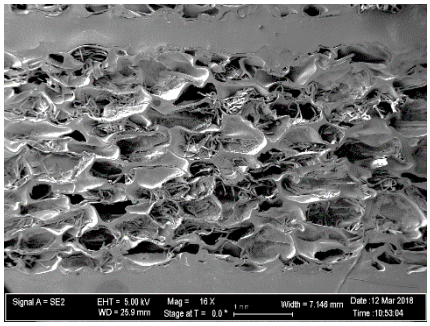


Figure 55. Representative SEM images of foam samples – heat treated under 50 psi *a)* 3mm *b)* 6mm *c)* 9mm

Cell sizes of as-received and heat treated foams are calculated using image processing tool ImageJ and shown in Figure 56. To calculate the cell size, average of the longest and shortest diagonals of approximately 100 hexagonal closed-cells per foam sample are used. As observed in SEM images, change in average cell size with heat treatment pressure has been quantified. Decrease in cell size due to heat treatment is slightly higher for 3mm samples because of extra compression of surface open-cells compared to the closed-cells. Moreover, all the as-received foams have the same average cell size. Even though the as-received foams have identical microstructure, their density is different due to open-cells on the surface. Since cell size for the as-received foams are approximately 1mm, open-cells on the surface have significant impact on the density of thin samples.

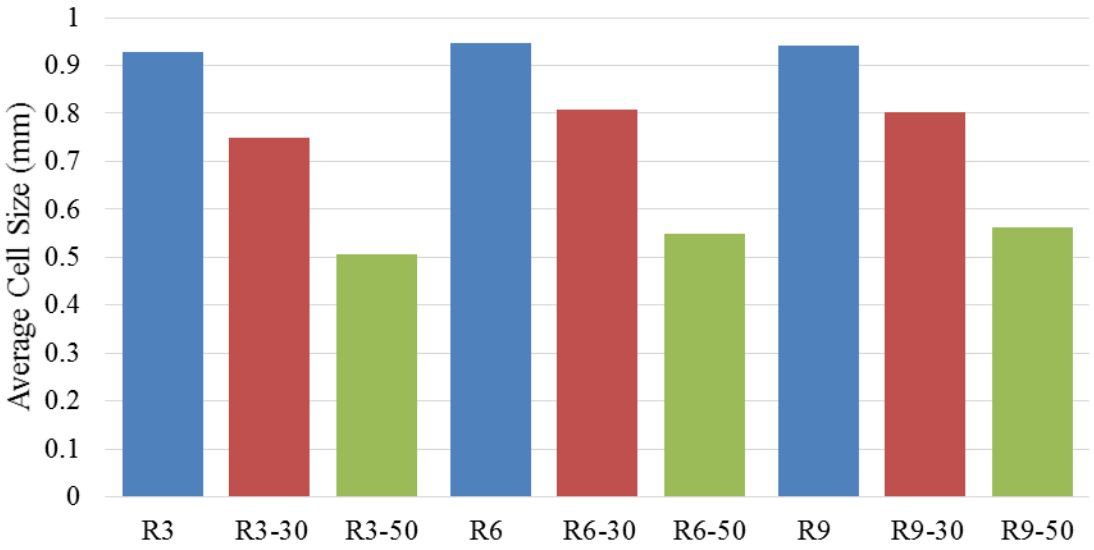


Figure 56. Average cell sizes of as-received and heat treated Rohacell foams

Each set of samples have three different thicknesses. If the samples had no pore, they would have the same absorption parameters and absorb the same amount of maximum moisture. However, pores absorbs and retains water. Different porosity results in distinctive maximum moisture content. To utilize the Void Filling Hindered Diffusion Model, porosity (p) of the foams must be identified to determine the ratio of pores to solid, $\zeta = \frac{v_v}{v_m}$. Ratio of pores to solid, ζ can be expressed in terms of porosity as $\zeta = \frac{p}{1-p}$.

Porosities of each foam are determined by two different methods. First, porosities are calculated by using the densities of the foams and the density of the polymer matrix (Polymethacrylimide) using Eq. (66).

$$p = 1 - \frac{\rho_{foam}}{\rho_{PMI}} \tag{66}$$

To find the density of PMI (Polymethacrylimide), a small sample of untreated foam is ground to obtain PMI powder. The density of the PMI powder is measured using pycnometer as 680 kg/m^3. Calculated porosities of the foams are charted in Figure 57.

Second, the porosities are determined by using the SEM images. Porosities by image process are demonstrated in Figure 58. Both calculated porosities and porosities gathered by image processing are in good agreement.

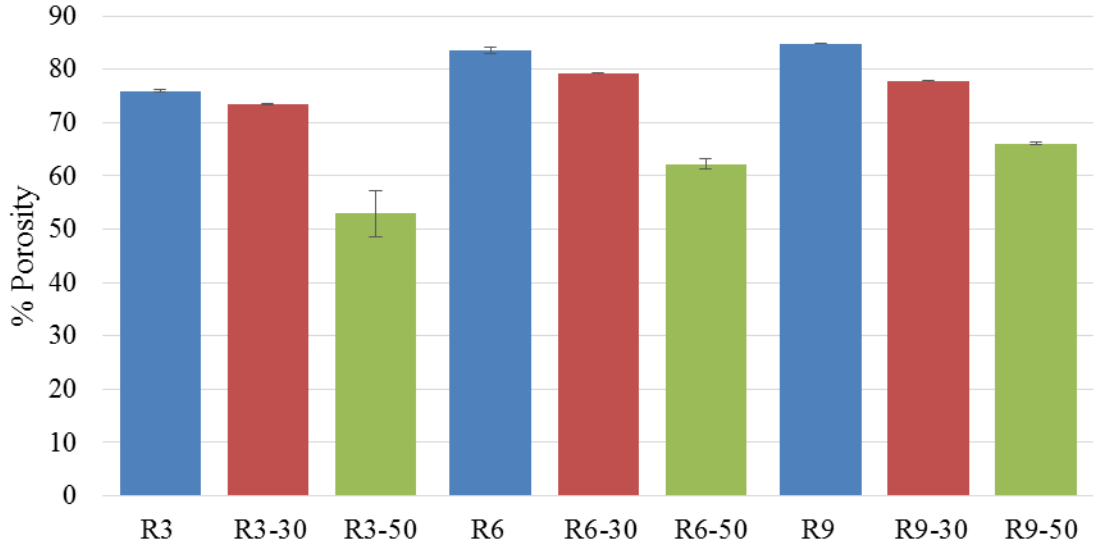


Figure 57. %Porosity of untreated and heat treated Rohacell foams (Calculated from density measurements).

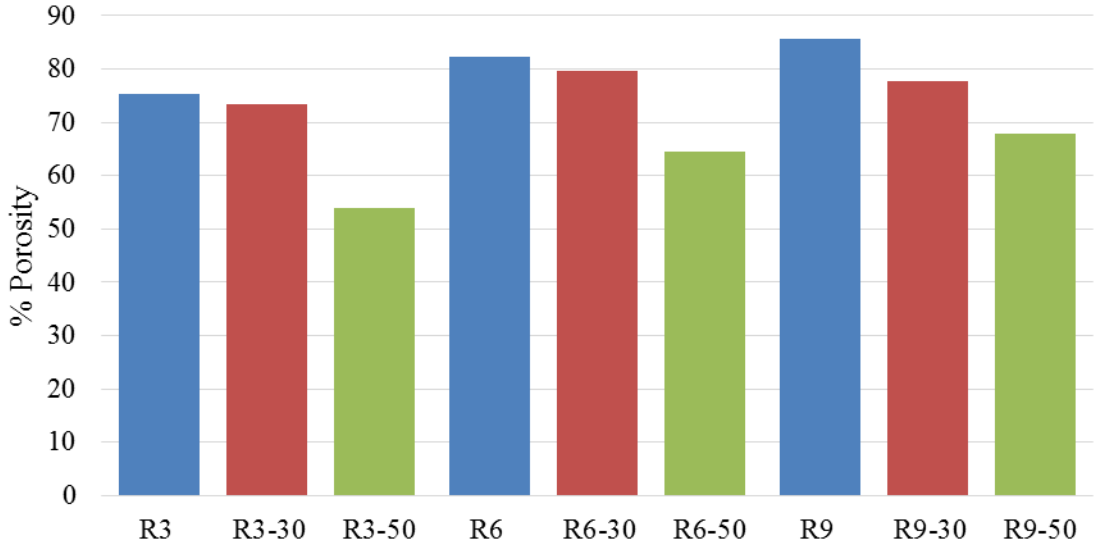


Figure 58. %Porosity of untreated and heat treated Rohacell foams (Image Analysis).

4.3. Moisture Absorption into Foams

Immersed samples are kept in water bath for approximately two years. During that time, their mass change is periodically measured in order to recover absorption parameters by using the Eq. (65). The mass gain data of as-received foams (R3, R6, R9), foams heat treated under 30 psi (R3-30, R6-30, R9-30), and foams heat treated under 50 psi (R3-50, R6-50, R9-50) are illustrated in Figure 59. First, difference in thickness has caused distinct variations in absorption behavior in foams with the same microstructure. This is attributed to filling of voids. Lower porosity in thinner samples leads to decrease in amount of absorbed moisture due to fewer amount of water-filled-voids. Proper application of the VFHDM should be able to explain and predict this phenomenon.

Change in absorption behavior due to heat treatment may also be observed in Figure 59. Modifications in cell size and geometry by temperature and pressure resulted in distinct absorption kinetics. Moreover, drastic and non-uniform changes in microstructure of foams due to heat treatment under 50 psi produced large variations within the same sample group evidenced by the higher confidence intervals in moisture absorption as in density and porosity. To further discuss the absorption behavior of the foams, absorption parameters of each set of samples are needed to be recovered.

Knowing the porosity of each set of sample and using the mass gain data from the immersed samples, void filling hindered diffusion model (VFHDM) is utilized to recover model parameters of Rohacell closed-cell foams. The resulting VFHDM absorption parameters are given in Table 11.

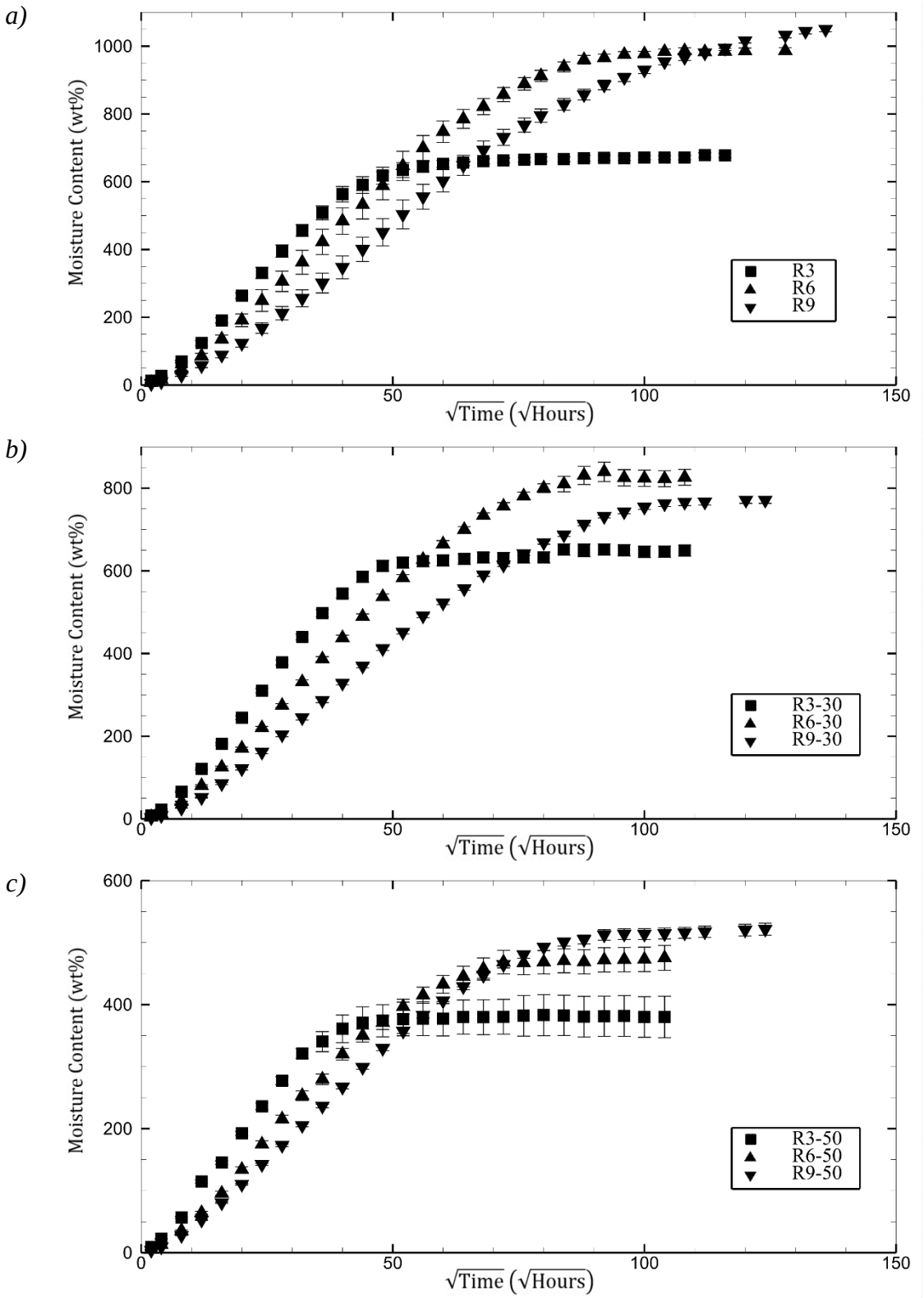


Figure 59. Moisture uptake mass gain data of foams: *a)* as-received *b)* heat treated under 30 psi *c)* heat treated under 50 psi

Table 11. VFHDM absorption parameters for untreated and heat treated Rohacell foams

	Untreated									
	$D(mm^2/hr)$ $x10^2$	$\beta(hr^{-1})$ $x10^3$	$\gamma(hr^{-1})$ $x10^2$	ζ	$\mu = \frac{\gamma}{\beta}$	$M_\infty(wt\%)$	$M_{\infty,unbound}$ $(wt\%)$	$M_{\infty,bound}$ $(wt\%)$	$M_{\infty,trapped}$ $(wt\%)$	RMS/data
R3	4.86	1.45	0.71	3.15	4.90	673.6	32.8	160.6	480.1	0.016
R6				5.05		1004.8			811.4	
R9				5.60		1092.4			899.0	
	@127 °C under 30 psi for 3hr @177 °C under 30 psi for 3hr									
	$D(mm^2/hr)$ $x10^2$	$\beta(hr^{-1})$ $x10^3$	$\gamma(hr^{-1})$ $x10^2$	ζ	μ	$M_\infty(wt\%)$	$M_{\infty,unbound}$ $(wt\%)$	$M_{\infty,bound}$ $(wt\%)$	$M_{\infty,trapped}$ $(wt\%)$	RMS/data
R3-30	3.64	1.66	1.02	2.75	6.13	663.6	27.7	169.6	466.4	0.016
R6-30				3.79		838.8			641.6	
R9-30				3.49		788.5			591.3	
	@127 °C under 50 psi for 3hr @177 °C under 50 psi for 3hr									
	$D(mm^2/hr)$ $x10^2$	$\beta(hr^{-1})$ $x10^3$	$\gamma(hr^{-1})$ $x10^2$	ζ	μ	$M_\infty(wt\%)$	$M_{\infty,unbound}$ $(wt\%)$	$M_{\infty,bound}$ $(wt\%)$	$M_{\infty,trapped}$ $(wt\%)$	RMS/data
R3-50	2.84	1.85	2.49	1.12	13.44	384.6	13.0	175.0	196.6	0.016
R6-50				1.65		476.0			288.1	
R9-50				1.94		528.0			340.0	

In Table 11, absorption parameters of as-received and heat treated foams are separately tabulated. Thickness dependence observed in mass gain data can be also noticed in absorption parameters. However, VFHDM resolves the thickness dependence by incorporating porosity and attributes the additional mass gain due void filling. In Table 11, for the foams with the same microstructure but different thicknesses, all absorption parameters are identical except porosity dependent parameters, $M_{\infty,trapped}$ and M_{∞}. Actually, thickness dependence of maximum moisture content, M_{∞}, is due to maximum trapped moisture content, $M_{\infty,trapped}$. Maximum moisture content in VFHDM is a combination of maximum bound, unbound, and trapped moisture content. Thus, variation in mass gain data due to foam thickness is credited to trapped moisture absorption into the pores. Pores-to-solid ratio, ζ basically scales the maximum moisture content of solid phase and unbound-to-bound transformation per unit time, in turn, generates distinctive moisture absorption.

Comparing foams heat treated under 30 psi and as-received foams reveals that as-received Rohacell foams and samples compressed under 30 psi seems to have similar absorption parameters- except diffusion coefficient. As the foam compressed, the cell size decreases and cell geometry changes. Since there is no material loss or gain, the diffusion path changes. Heat treatment would create a more complex closed-cell foam structure, thus creating a more tortuous path for penetrant. Even though compressed Rohacell have a more tortuous diffusion path, the length of the path is similar due to thickness reduction.

The diffusion process in VFHDM is governed by $K = \frac{\pi^2 D}{h^2}$. K values of foams compressed under 30 psi and as-received foams are compared in Table 12 and they are remarkably close. However, for Rohacell foam heat treated under 50 psi, this relation does

not hold. Rohacell foams compressed under 50 psi changed closed-cell foam structure drastically. Cells not only compressed but also coalesce. The drastic changes in microstructure of foam result in distinctive absorption parameters.

Table 12. Diffusion rate comparison between heat treated under 50 psi, 30 psi and as-received foams

	$K_{Rohacell}$	K_{30psi}	K_{50psi}
3mm	0.051	0.056	0.158
6mm	0.013	0.016	0.033
9mm	0.006	0.009	0.016

In Figure 60, the thermogravimetric moisture absorption data of 3mm, 6mm, and 9mm (R3, R6, and R9) as-received foams and one-dimensional void filling hindered diffusion model predictions are shown. All the VFHDM moisture absorption curves match well with their respective experimental gravimetric data as seen by the very small the root mean square error per data point values in Table 11. It should be noted here that the last data point taken after 3 years of immersion is not used for VFHDM recovery. VFHDM was able to predict the change in maximum moisture content along with the thickness of the sample. In spite of the distinct maximum moisture content in foams with different thickness, there should be similarities in moisture absorption kinetics according to the VFHDM absorption parameters in Table 11. To thoroughly investigate the absorption behavior of foams, unbound, bound, and trapped curves are illustrated in Figure 61.

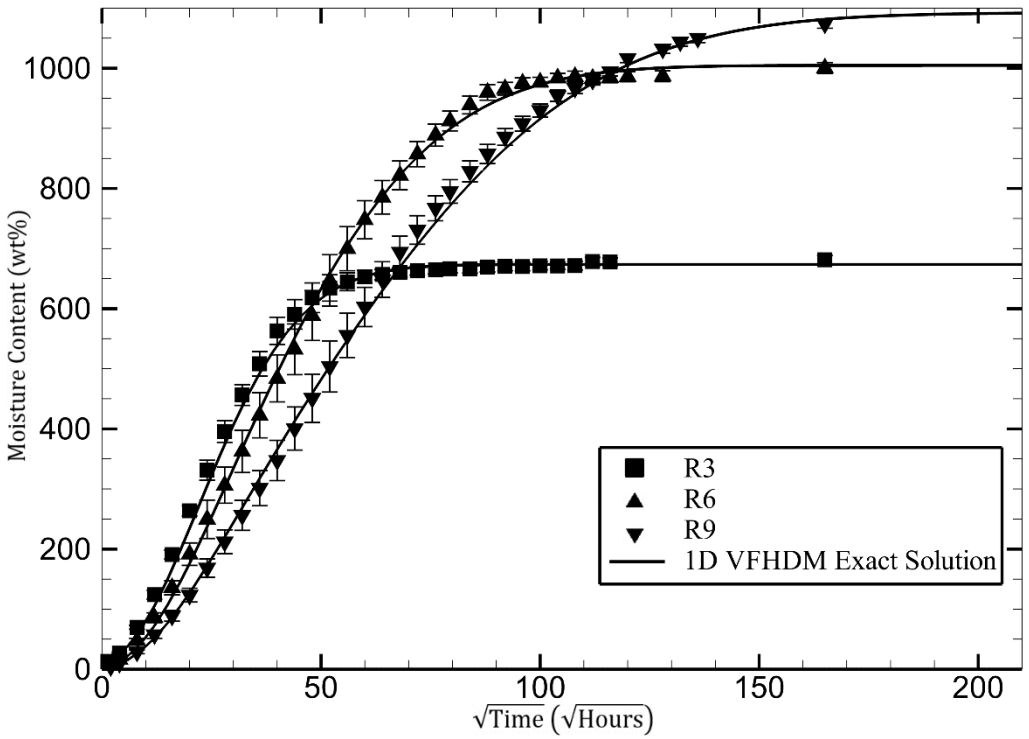


Figure 60. Mass gain data and VFHDM predictions of 3mm, 6mm, and 9mm as-received Rohacell foams.

In Figure 61a, unbound moisture absorption kinetics of as-received Rohacell foams are illustrated. Even though all three set of samples with different thicknesses have the same maximum unbound moisture content as observed in Table 11, they have distinct unbound moisture absorption kinetics due to change in porosity. In thick samples, unbound moisture must diffuse a longer path due to the thickness of the sample. Moreover, increased porosity causes faster unbound moisture to trapped moisture transformation. More unbound moisture transforms to trapped moisture per unit time causing hindrance in unbound moisture diffusion. Additionally, influence of porosity on bound moisture absorption may be observed in Figure 61b.

Similarly, thickest foam samples, which have the highest porosity, reach to bound moisture equilibrium later than thinner samples. Faster transformation from unbound

moisture to trapped moisture also affects the absorption kinetics of bound moisture. As more unbound moisture becomes trapped, less amount of unbound moisture remains per unit volume. Even though the rate of exchange between the unbound and bound moisture remains constant, quantitatively less amount of remaining unbound moisture becomes bound. Thus, bound moisture absorption is more hindered in high porosity samples.

In Figure 61c, trapped moisture absorption into as-received Rohacell foams are demonstrated. Both absorption kinetics and the maximum trapped moisture content for samples with different thicknesses have certain characteristics. The maximum trapped moisture content is related to the porosity of the samples. Highly porous samples absorbed more moisture compared to relatively less porous foams. In VFHDM theory, pores in the matrix are assumed to be fully occupied with water in equilibrium. In this extent, the amount of water trapped inside the pores has been experimentally investigated. All the pores of one of the samples are popped by a small needle to convert the closed-cells to open-cell and remove the trapped water. For fast removal of trapped water, open-cell foam is subjected to 6.5 psi pressure for 1 min. Removal of trapped water by vacuum or in standard conditions might result in removal of unbound and/or bound moisture therefore compression for a short period of time on the sample is chosen. After popping the pores and compression, weight of the sample reduced as 1.7432g (498.8 wt.%). The amount of trapped moisture in that sample is predicted by VFHDM as 1.6779g (480.1 wt.%). Slight difference between the predicted and measured weight gain by trapped moisture is possibly due to desorption of unbound and/or bound moisture in the sample during popping and compression. Regardless, 3% difference between the theoretical and experimental trapped moisture content substantiates the capabilities of void filling hindered diffusion model.

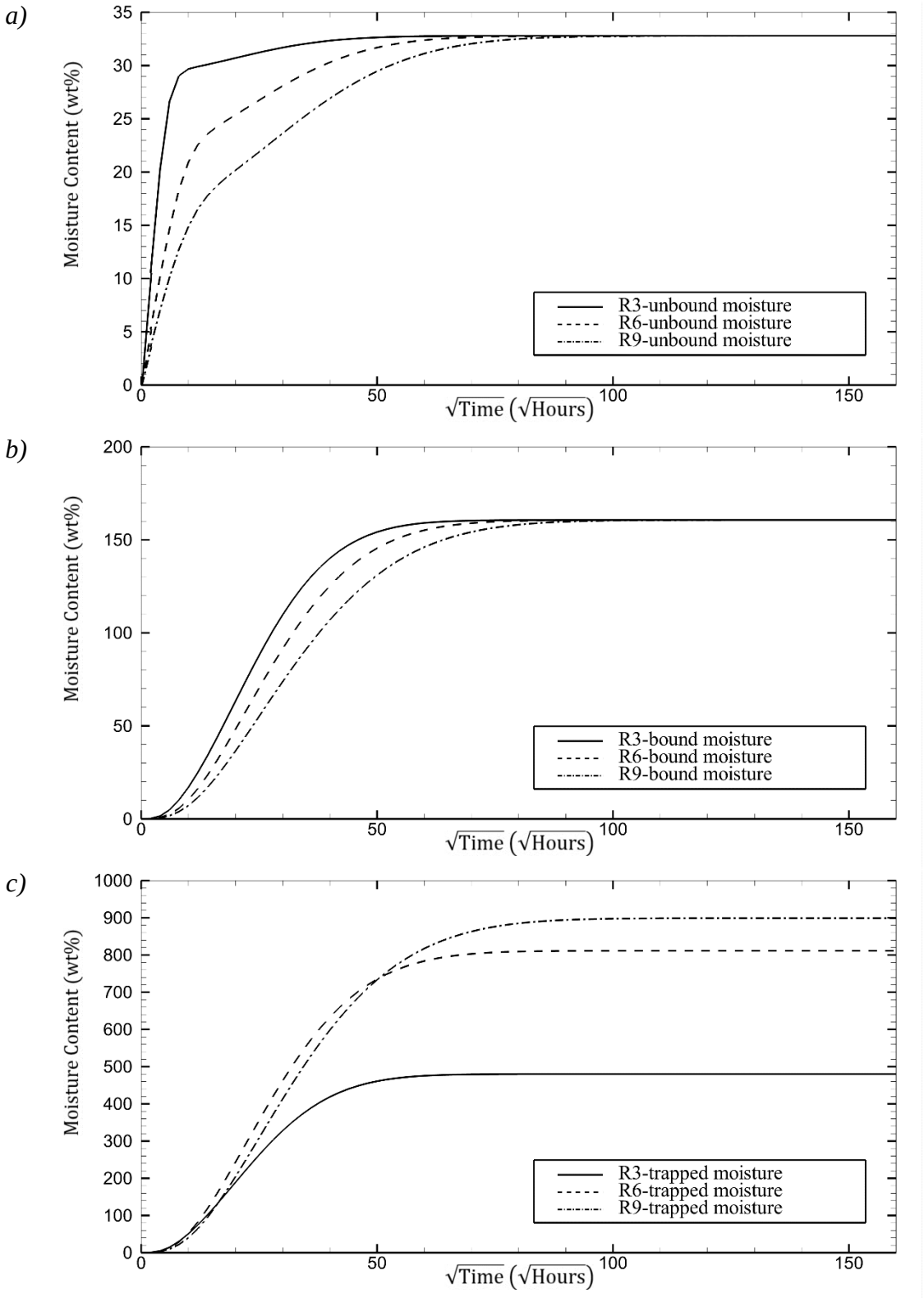


Figure 61. VFHDM predictions of *a)* unbound *b)* bound and *c)* trapped moisture absorption into as-received Rohacell foams.

In Figure 62, one-dimensional VFHDM predictions over mass gain data of foams heat treated under 30 psi (R3-30, R6-30, and R9-30) are illustrated. As in as-received foams, VFHDM was able to predict the absorption behavior of foams with different thicknesses. The last data point is not used for VFHDM recovery, only illustrated to show the capabilities of the model. The quality of the prediction can be observed both in Figure 62 and by the RMS/data pt. column of Table 11. Each set of samples heat treated under 30 psi foam absorbed less amount of water in comparison with the corresponding set of as-received foam samples. The decrease in maximum moisture content is associated with the decrease in porosity due to heat treatment and compression. Even though no significant change in microstructure other than cell shrinkage is observed in SEM images, change in absorption kinetics is investigated through the unbound, bound, and trapped moisture mass gain in Figure 63.

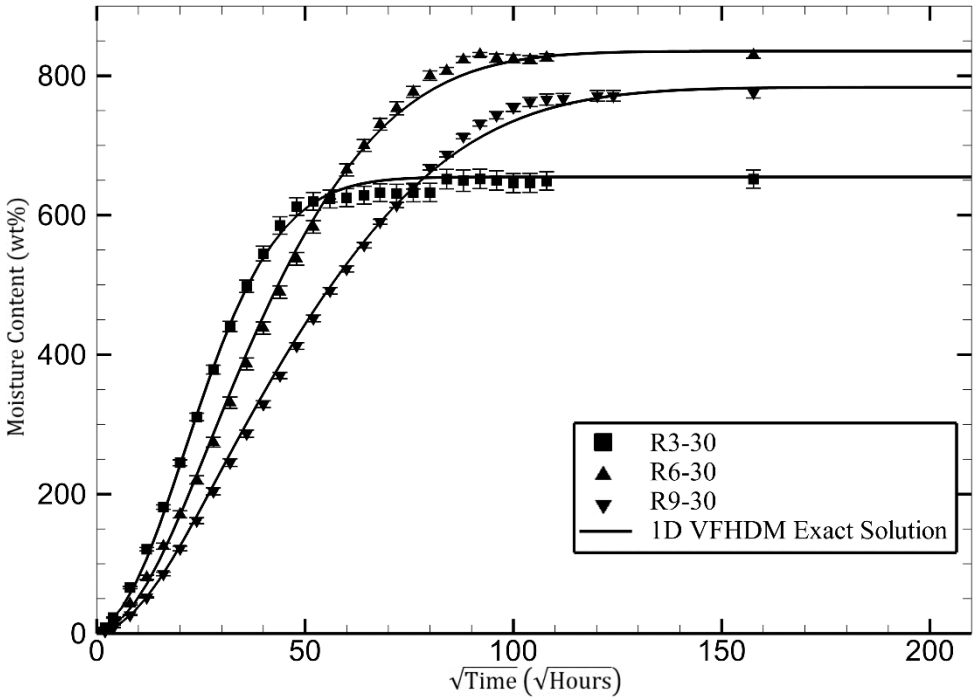


Figure 62. Mass gain data and VFHDM predictions of 3mm, 6mm, and 9mm Rohacell foams heat treated under 30 psi.

Effect of sample thickness on unbound moisture absorption dynamics of foams heat treated under 30 psi is illustrated in Figure 63a. As observed in Table 11, unbound moisture content does not change with the sample thickness. In contrast, heat treatment under 30 psi has caused 5.1 wt.% less unbound moisture absorption in Rohacell foams. The compaction under elevated temperature may have led to increase in crosslinking density in turn decrease in free volume where unbound moisture can diffuse into. Alternately, adjacent polymer chains might be compacted to get closer contributing to decrease in free volume. In addition, the change in thickness, thus porosity, resulted in change in absorption behavior similar to the absorption kinetic variation in as-received foam samples. Increasing porosity slows down the unbound mass gain because more unbound moisture becomes trapped in pores.

In Figure 63b, bound moisture absorption behavior of foams heat treated under 30 psi is presented. In terms of maximum bound moisture content and change in absorption kinetics, foam samples heat treated under 30 psi shows similar properties with as-received foams: i) thickness has no effect on maximum bound moisture content and ii) increased porosity/thickness decelerate the bound moisture absorption. On the other hand, comparison between bound moisture absorption of the as-received foams samples and foam samples heat treated under 30 psi shows that heat treated samples absorb 9 wt.% more bound moisture than as-received foams. This small difference in maximum bound moisture content may be also attributed to increasing crosslinking density due to heat treatment[139]. Increasing crosslinking density not only would decrease the unbound maximum moisture content due to decreasing free volume but also increase the maximum bound moisture content due to new crosslinks between the polymer chains.

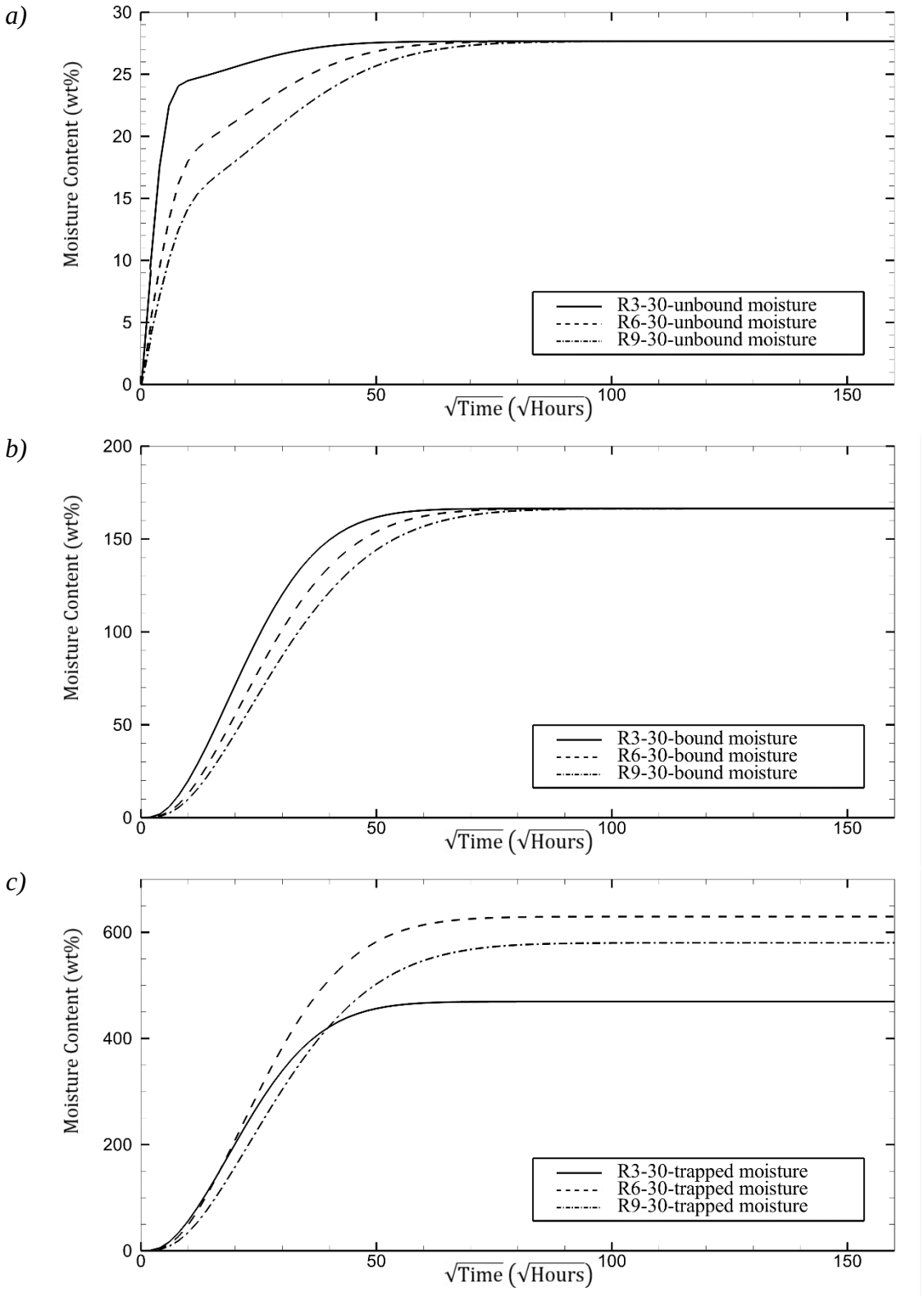


Figure 63. VFHDM predictions of *a)* unbound *b)* bound and *c)* trapped moisture absorption into Rohacell foams heat treated under 30 psi.

In Figure 63c, trapped moisture absorption into heat treated foams is illustrated. As VFHDM predicts, the amount of trapped water is directly related to the porosity of the foam. Thickness dependence of porosity caused different maximum trapped moisture content in sample. For example, R6-30 samples absorbed 37.6% more trapped moisture than R3-30 samples. Along the line, R6-30 samples are 37.6% more porous than R3-30 samples. In addition, the effect of decreasing porosity due to heat treatment can be observed in maximum trapped moisture content. Comparison between the as-received foam samples and foam samples heat treated under 30 psi yields that heat treatment compacted the pores and in turn decreased the trapped maximum moisture content.

In Figure 64, one-dimensional VFHDM predictions over thermogravimetric data foams heat treated under 50 psi (R3-50, R6-50, and R9-50) are demonstrated. As in as-received foam samples and foam samples heat treated under 30 psi, VFHDM successfully represented the overall moisture absorption behavior of foam samples heat treated under 50 psi in line with the root mean square error per data point values in Table 11. The last mass gain data is only given to show the predictive abilities, not used for recovery. To compare the absorption kinetics of foam samples heat treated under 50 psi with other foam samples, unbound, bound, and trapped moisture absorption curves are plotted and shown in Figure 65.

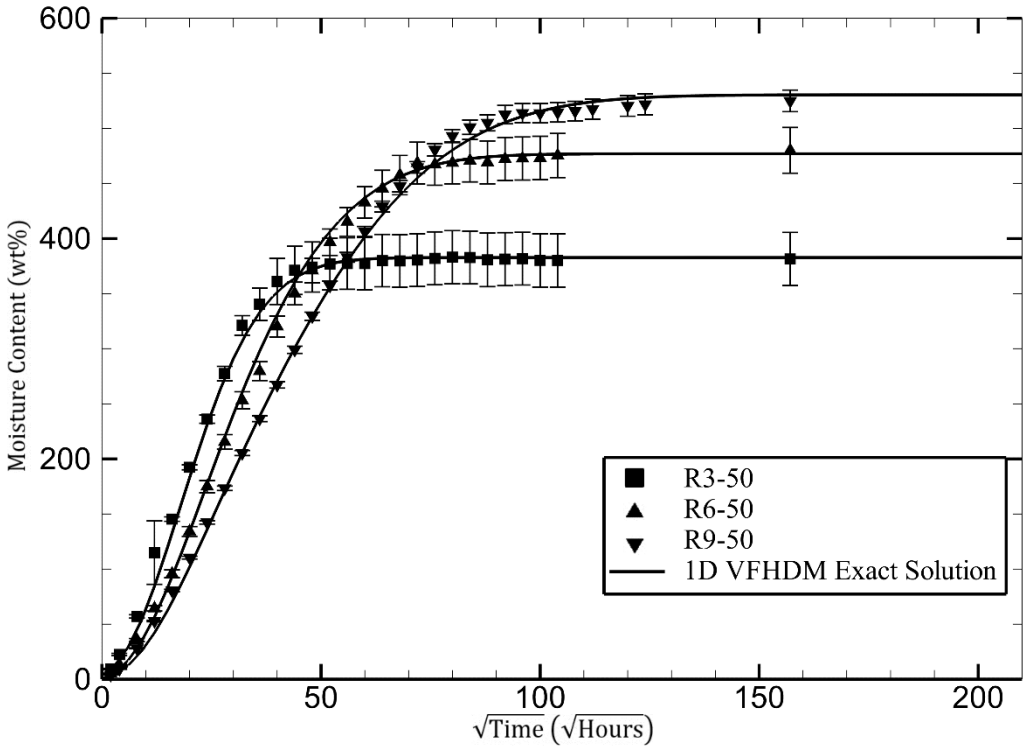


Figure 64. Mass gain data and VFHDM predictions of 3mm, 6mm, and 9mm Rohacell foams heat treated under 50 psi.

Unbound moisture absorption into foam samples heat treated under 50 psi are demonstrated in Figure 65a. Just like in other foam samples, the difference in unbound moisture absorption behavior and uniformity in the maximum unbound moisture content of samples with different thicknesses can be easily observed. For foam samples heat treated under 50 psi, the maximum unbound moisture content is 19.2 and 14.7 wt.% less than as-received foams and foam samples heat treated under 30 psi, respectively. This substantial difference in the maximum unbound moisture content is addressed to the change in microstructure. Unlike foam samples heat treated under 30 psi, foam samples heat treated under 50 psi underwent drastic microstructural changes as observed in SEM images in Figure 55. Cells not only compressed but also coalesced. These drastic changes would lead

to decrease in free volume but increase in free surfaces which in turn decreased the maximum unbound moisture content and increased the maximum bound moisture content.

In Figure 65b, bound moisture absorption into foam samples heat treated under 50 psi are plotted. Bound moisture absorption trend of foam samples heat treated under 50 psi are the same as the other Rohacell foams in this study. However, foam samples heat treated under 50 psi absorbed 14.4 and 5.4 wt.% more bound moisture than as-received foams and foam samples heat treated under 30 psi, respectively. The possibly increased crosslinking density and coalesced cell to become open-cell may have risen new interfaces and free surfaces for bound moisture to interact.

In Figure 65c, trapped moisture absorption of foams heat treated under 50 psi is shown. The trapped moisture predictions are sorted depending on their porosity/thickness. As the heat treatment processing pressure increases, the overall volume of the pores decreases resulting in less moisture intake.

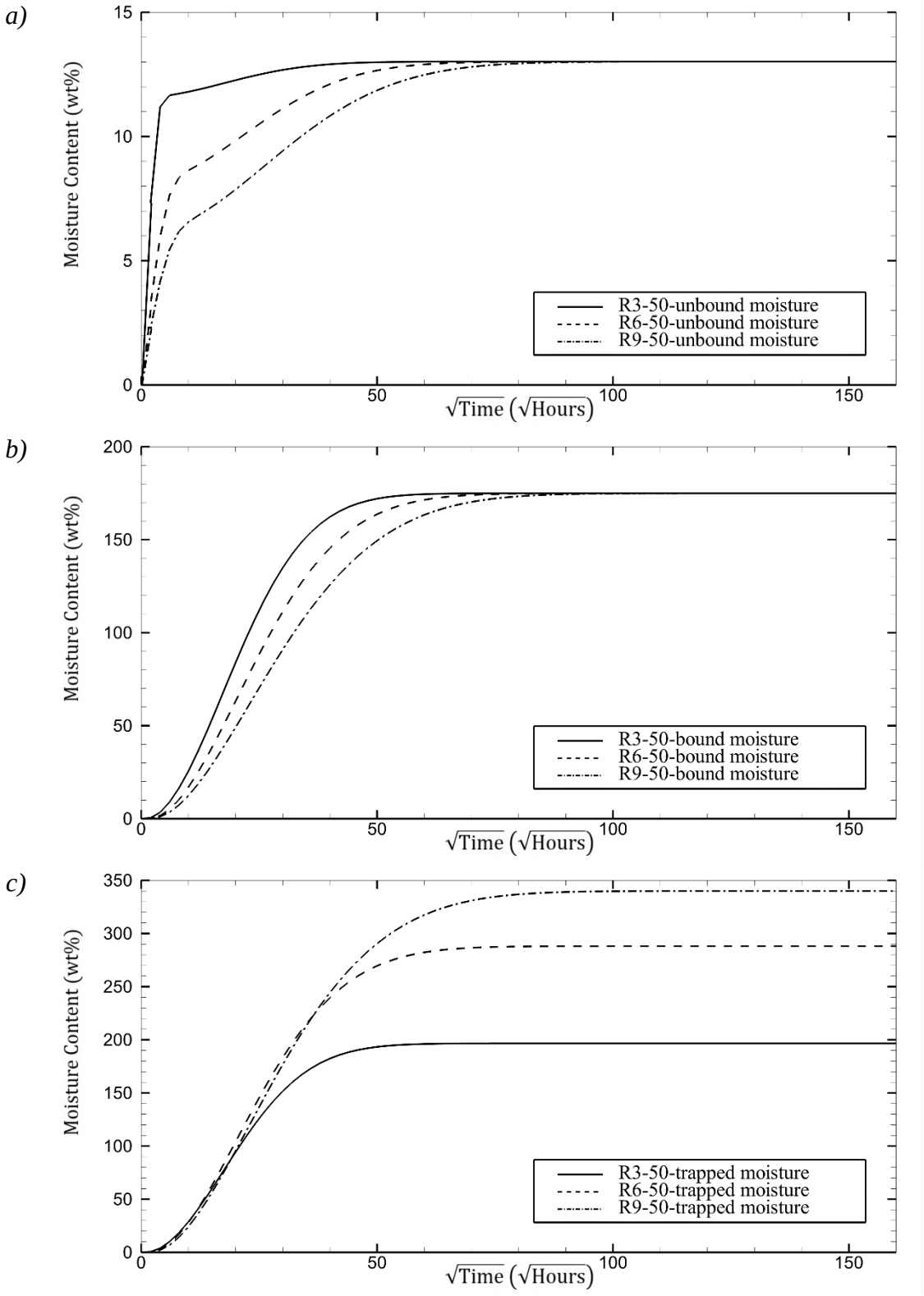


Figure 65. VFHDM predictions of *a)* unbound *b)* bound and *c)* trapped moisture absorption into Rohacell foams heat treated under 50 psi

4.4. Foam Core Sandwich Composites

Successful recovery of the moisture absorption behavior of Rohacell WF-71 closed-cell rigid foams by VFHDM lead to further investigation of the foam absorption kinetics. The closed-cell foams are commonly used as a core material in sandwich structures. In this respect, moisture absorption kinetics of a sandwich composite having a foam core of Rohacell WF-71 is investigated.

i. Materials and Sample Preparation of Rohacell Closed-Cell Structural Foam Core Sandwich Composite

Each sheet of Rohacell foam is cut into two 254 mm × 254 mm (10″ × 10″) panels. Cut panels were dried in vacuum oven at 40℃ (104°F). Tencate Ex1522/IM7, epoxy/graphite woven fabric prepreg was chosen as facesheets of the sandwich composite. Each face of the foam is covered by one ply facesheet. Then, the cure cycle of the prepreg is followed to manufacture the sandwich structure. Uncured sandwich composites were subjected to 21 MPa (30 psi) or 34 MPa (50 psi) at 127℃ (260°F) for 3 hours and further processed at 176℃ (350°F) for another 3 hours. Sandwich composites were cooled down to room temperature at a rate of 2℃/min (5°F/min) and cut into eight specimen of 51 mm × 51 mm (2″ × 2″) for absorption test. Lastly, the samples are dried in vacuum oven 43℃ (110°F) for approximately 5 days and immersed in distilled water at 25℃ (77°F).

ii. Moisture Absorption into Foam Core Sandwich Composites

For two and a half years, the sandwich composite samples are subjected to water and change in their weight is measured, periodically. The change in the weight of the composites sandwiches manufactured at 30 psi (S3-30, S6-30, S9-30), and 50 psi (S3-50, S6-50, S9-50) are illustrated in Figure 66 and Figure 67, respectively. In both figures,

variation in moisture absorption kinetics due to thickness is easily observed as in the case of absorption into foams. Distinct maximum moisture content of foams with different thicknesses are responsible for the variation in maximum moisture content of the sandwich composites. Change in absorption behavior due to manufacturing pressure is also detected from the figures. Processing pressure not only changes the absorption kinetics of the foams as observed in Section 4.3, but also changes the mass intake through the facesheets. Thus, the changes in mass gain curves are as a result of the combined effect of facesheet and foam core.

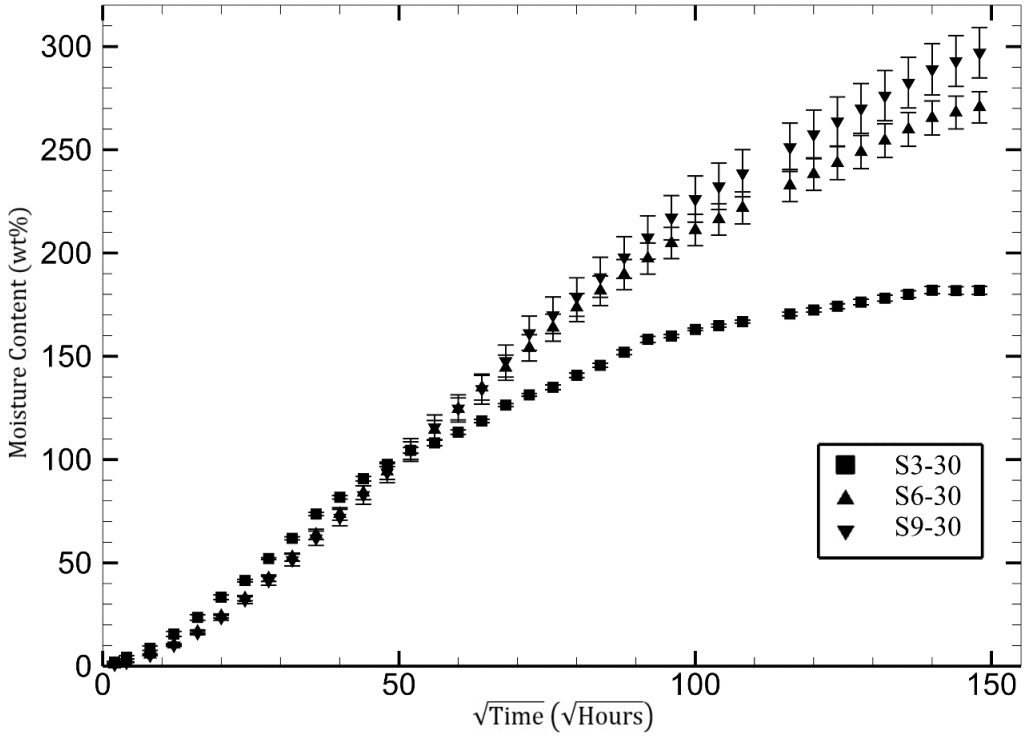


Figure 66. Mass gain data of Rohacell foam core sandwich composite manufactured under 30 psi pressure

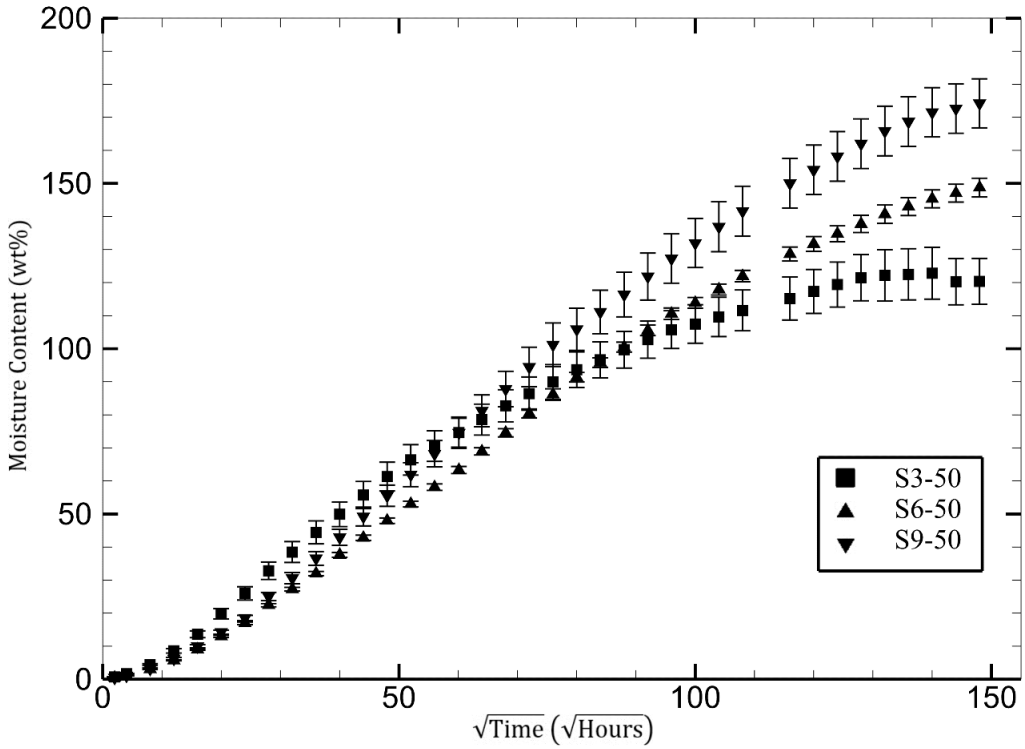


Figure 67. Mass gain data of Rohacell foam core sandwich composite manufactured under 50 psi pressure

The moisture absorption data shown in Figure 66-Figure 67 can be further processed by the combination of void filling hindered diffusion model and multilayer hindered diffusion model. However, the data for both sets of samples are still premature to recover the absorption parameters. Thus, the absorption kinetics of the sandwich structures will be recovered in the future once the subsequent data is gathered.

4.5. Conclusion

In this chapter, newly developed one-dimensional void filling hindered diffusion model (VFHDM) is introduced. VFHDM can incorporate the storage of penetrant in the porous media in addition to the chemical interactions between the matrix and penetrant and absorption due to the diffusion which both can be predicted by 1DHDM. Void filling

diffusion model (VFHDM) assumes that the penetrant can diffuse into the matrix, bind to and unbind from the matrix and be trapped inside the pores. VFHDM modifies the 1DHDM by porosity. Porosity basically scales the maximum moisture content of solid phase and unbound-to-bound transformation per unit time, in turn, generates distinctive moisture absorption.

Validation of void filling hindered diffusion model has been achieved by characterizing the microstructure and moisture absorption behavior of closed-cell Rohacell foams. Foams with different thicknesses are chosen for the absorption test. It has been observed that even though foams with different thicknesses have identical microstructure, they may have distinct densities and porosities. Open-cells at the surface of the foams change the density and porosity of the foams.

Rohacell foams are subjected to heat treatments under two different pressures (30 psi and 50 psi) to investigate the effect of microstructural changes on absorption kinetics. Heat treatment under 30 psi on Rohacell foams led to decrease in thickness, cell size, and porosity. Cells slightly elongated normal to the compression direction. Foams heat treated under 50 psi pressure has gone through more radical microstructural changes. Some cells are compressed to get smaller however, some cells coalesce to become bigger which created more variation in density, porosity, and absorbed moisture. Drastic decrease in porosity is an outcome of the coalescence of open surface cells and close-cells. As the open surface cells and closed-cells in the matrix coalesce, the new cell becomes an open-cell and does not contribute to the porosity.

Moisture absorption test on foams has shown that thickness of the foam changes the absorption behavior of the foam samples. As the foam gets thicker, the maximum moisture

content of the foam increased. VFHDM attributed this phenomenon to the porosity. The ratio of the open surface cell to the closed-cell in the matrix is higher in the thin foams. Thus, porosity of the thin foams are less than thick foams. Since open-cells cannot store moisture, it is reasonable to have lower maximum moisture content in thin samples compared to the thick samples. Increase in pores-to-solid ratio by 60% resulted in 49% more maximum moisture uptake. By attributing the excess moisture to the filling of the pores, VFHDM successfully predicted the absorption behavior of foams with various thicknesses.

Effects of foam microstructure on moisture absorption are also investigated using VFHDM. Heat treatment under 30 psi caused less amount of moisture absorption than as-received foams. Decrease in the amount of absorbed moisture is attributed to the reduction of porosity and efficiently predicted by VFHDM. In addition, VFHDM prediction of unbound, bound, and trapped moisture absorption outlined the effect of microstructural changes. Small decrease in unbound maximum moisture content and increase in bound maximum moisture content due to heat treatment are assumed to be a result of further crosslinking of the polymer chains of foam matrix. Crosslinking would presumably decrease the free volume that water molecules can diffuse to be unbound moisture and increase the bonding site to create bound moisture. Moreover, decrease in porosity due to heat treatment has shown its effect as decrease in trapped moisture.

Foams heat treated under 50 psi were underwent through drastic changes in cell size and morphology. These severe changes in the microstructure also affected the moisture absorption kinetics. These foams absorbed less amount of moisture compared to the as-received foams and foams heat treated under 30 psi. VFHDM effectually recovered the

absorption dynamics of foams heat treated under 50 psi using the calculated porosities for each thicknesses. Furthermore, VFHDM is used to describe the effect of microstructural changes on the unbound, bound, and trapped moisture absorption. Changes in unbound and bound moisture absorption are also attributed to the increase in crosslinking density. Changes in trapped moisture were predicted by the porosity.

In conclusion, one-dimensional void filling hindered diffusion model successfully predicted and explained moisture absorption behavior of foams with different porosity levels and microstructure. VFHDM defined and validated the changes in the absorbed moisture content as a function of porosity. Since foams are frequently used in high-end engineering applications as a core material in sandwich composites, VFHDM may be improved using multilayer hindered diffusion model to predict the absorption behavior of sandwich structures.

Chapter 5. Effect of Moisture Absorption on Mechanical Properties of Polymer and Polymer Composites

Increased used of polymers and polymer composites in engineering applications have led researchers to investigate environmentally induced degradation due to high humidity. Plasticization, swelling, residual stresses are the most common outcomes of moisture induced damages in polymers [11,26–31]. These physical damages result in significant loss in electrical, thermal, optical, and mechanical properties. The extent of the property loss should be considered on composite part design for mission critical systems.

Dielectric constant and loss tangent are electrical properties describing the conductivity of a polymer. As an alternative to ceramic insulators, polymers having low dielectric constant and loss tangent are investigated as insulators. However, Kumosa et al. [140], Cotinaud et al. [141] and Wang et al. [142] reported that moisture ingress into polymers significantly increases the electrical conductivity. Cotinaud et al. [141] reported a 40% increase in relative permittivity for a 1 wt.% increase in moisture content. Cotinaud et al. [141] and Wang et al. [142] showed that the dielectric properties show a slight and quasi-linear variation during initial moisture uptake. After the quasi-equilibrium moisture absorption state, a sudden increase in the dielectric constant and loss factor created continuous electric current through the polymer. Redistribution and regrouping of the water molecules occur beyond the existence of a water concentration limit leading to ionic conduction [141].

Thermal stability is another important aspect of polymers affected by the moisture absorption. Zhao and Li [143] investigated the change in thermal expansion coefficient due to water treatment of epoxy and nano alumina/epoxy composites. They reported that the

thermal expansion coefficient increases by 13% and 19% for epoxy and nano alumina/epoxy composite, respectively. However, the influence of water absorption on thermal expansion coefficient has opposite trend above glass transition temperature, T_g. Above T_g, Zhao and Li reported 13% decrease in thermal expansion coefficient by moisture absorption. Above T_g, the absorbed water has evaporated resulting in volume contractions which was counter balanced by the normal thermal expansion of materials [143].

Although polymers such as polymethyl methacrylate (PMMA), polystyrene (PS), polycarbonate (PC), styrene acrylonitrile (SAN) have been used as substitutes for glasses for optical applications, moisture absorption by these polymers may result in change in color and/or clarity of the polymer. Simar et al. [144] observed that the water absorption darkens the epoxy. During the absorption, color gradient can be observed showing the concentration gradient. Simar et al. [144] also suggested that the color change could be related to hydrolysis or oxidation of the polymer.

On the other hand, common use of polymers in structural composites influenced researches to investigate various mechanical property loss due to moisture ingress such as loss in storage modulus [117], tensile strength [26,32,35,117,118], elastic modulus [26,32,117,145], microhardness [3], transverse tensile strength [36], interlaminar shear strength [32,119], and transverse flexural strength [120] of different composites.

5.1. Mechanical Property Loss due to Moisture Ingress

Many researchers have reported the effect of moisture absorption on mechanical properties of polymers. Some of the prominent research findings on various mechanical property loss in polymers are summarized in this section.

Hu et al. [11] reported that the tensile strength of short jute fiber/Polylactide (PLA) composite material decreased by 86% and 94% after 72 and 120 hours of moisture absorption, respectively. They suggested that reliable measures of protection from moisture must be taken when such composites are used in humid environments. Similarly, Simar et al. [144] investigated the hygrothermal aging effects on mechanical properties of RTM6 epoxy. Epoxy samples lost their failure strength logarithmically with respect to immersion time. In addition, loss in Young's modulus, failure strain, and glass transition temperature is observed due to moisture ingress [144].

The viscoelastic behavior of polymers and polymer composites is also highly affected by the environmental conditions. Sarfaraz et al. [146] investigated the effect of moisture absorption on the viscoelastic behavior of epoxy film adhesive and carbon fiber reinforced epoxy. Moisture ingress led to decrease in storage modulus whereas increase in loss modulus for both CFRP composite and epoxy film. Zai et al. [147] experimented on CFRP composite of different layups. Similarly, 5 wt.% moisture absorption into CFRP composites decreased storage modulus and increased loss modulus by 17% and 40%, respectively. Comparably, increase in loss modulus and decrease in storage modulus of glass fiber reinforced polymer is observed after 60 days of moisture exposure [148]. The change in the viscoelastic behavior has been attributed to plasticization of the polymer.

Moisture induce damages, especially plasticization, also result in degradation of polymer hardness. Microhardness tests on vinylester and nanoclay/vinylester composites showed up to 17% decrease in Vickers hardness due to 650 hours of immersion [3]. Rajeesh et al. [149] also reported hardness of hectorite clay/polyamide 6 nanocomposites is reduced by 9%, 30%, 42%, and 50% under 35%, 60%, 90% relative humidity, and immersion,

respectively. Moreover, the researchers studied the fatigue behavior of hectorite clay/polyamide 6 nanocomposites under wet and humid environment [149]. Remarkably, samples conditioned at higher relative humidity showed better fatigue life. Further investigation revealed faster and smoother fracture surfaces on samples conditioned at lower relative humidity. As crack propagates, the absorbed water blunts the crack tip by increasing the chain mobility [149].

Moisture absorption affects the interlaminar shear properties of polymers, as well. Short beam test on carbon fiber/epoxy composite yields an approximately 20% decrease in interlaminar shear strength due to moisture absorption [150]. Sideridis et al. [119] also reported an interlaminar shear strength loss of glass fiber/epoxy composite by 4-23% depending on the orientation angle. Loss in interlaminar shear strength is directly related to the degradation of matrix polymer.

Micromechanical changes in polymers due to water absorption are known to affect the modulus. Cheour et al. [151] reported saturated flax fiber reinforced composite has 55% lower bending modulus than the dry one. Even though desorption of the composite samples helped the recovery of the bending modulus up to 85%, damage due to hygrothermal aging is irreversible. Similarly, Agubra et al. [117] reported 6-11% decrease in flexural modulus after 60 days of environmental degradation. Many other researchers investigated the modulus loss due to water degradation on polymers. In addition to experimental investigation of degradation in polymer, substantial efforts have been made to theoretically or computationally characterize and validate the property loss due to moisture induced damage.

5.2. Moisture Absorption and Flexure Modulus Correlation Models

i. Reimschussell's glass transition temperature model

Reimschussell developed an empirical model correlating the moisture content in polymer and change in glass transition temperature. Reimschussell's observations led the researcher to suggest that increasing the moisture content always result in a steady decrease of glass transition temperature toward a limiting value [40]. Beyond this limiting value, the glass transition temperature is no longer affected by further increase in the water content in the polymer. Reimschussell described this phenomenon by a mechanism involving the replacement of intercatenary hydrogen bonds by interaction with water.

Using experimental data, Reimschussell determined that the monotonic decrease of T_g to an finite value depends on the glass transition temperature of the dry polymer, T_{g0}, the glass transition temperature at $W = W_l$, T_{gl}, and the water concentration beyond which any increase in the water content of the polymer will not affect the glass transition temperature, W_l.

$$\frac{dT_g}{dW} = -\kappa(T_{g0}, T_{gl}, W_l)(T_g - T_{gl}) \tag{67}$$

The solution of the differential equation in Eq. (67) is found by applying boundary conditions *i)* $\frac{dT_g(T_{gl})}{dW} = 0$ and *ii)* $T_g(0) = T_{g0}$.

$$T_g(W) = \left(T_{g0} - T_{gl}\right) exp\left[-\frac{W}{W_l - \delta} In\left(T_{g0} - T_{gl}\right)\right] + T_g$$

$$\delta = W_l - \frac{W}{1 - \frac{In\left(T_g - T_{gl}\right)}{In\left(T_{g0} - T_{gl}\right)}} \tag{68}$$

Reimschussell claimed that the mechanism leading to decrease in glass transition temperature affects the elastic modulus in the same manner. Therefore, $E(W)$ may be represented in the same analogy as in $T_g(W)$:

$$E(W) = (E_0 - E_l)\, exp\left[-\frac{W}{\epsilon W_l} In(E_0 - E_l)\right] + E_l \tag{69}$$

where E_0 is the modulus of the dry polymer, E_l is the modulus of the polymer at saturation and ϵ is a constant to be determined experimentally.

ii. H-Bond dissociation model

Nissan [152] claimed that mechanical properties of hydrogen bond dominated solids are a function of hydrogen bond per unit area, N, and the function for the Young's modulus is $E = kN^{1/3}$ where k is determined by H-bond parameters. As the solid absorbs moisture, some hydrogen bonds in the solid will dissociate and form new hydrogen bonds with water. As the number of hydrogen bond in the solid diminishes, Young's modulus decreases. Nissan states that moisture absorption affects the hydrogen bond density in two different ways. *i)* Regime 1: bond dissociation takes place singly and *ii)* Regimes 2: a number of bonds appear to break cooperatively.

Regime 1 operates when $0 < w < w_c$, where w_c is the critical moisture content of BET monomolecular layer. A unimolecular reaction is defined as:

$$d(N/N_0) = -(N/N_0)d(w/W) \tag{70}$$

where N_0 is the number of hydrogen bond at dry state, W is the hypothetical quantity of water required to provide one molecule for H-donating groups, w is the water content and N is the Hydrogen bond per unit area. Applying the initial assumption that $E = kN^{1/3}$ yields:

$$\ln(E/E_0) = -{}^{1}/_{3}\,(w/W) \tag{71}$$

Regime 2 assumes when one bond forms several will form, and when one bond breaks, a whole cluster will 'dissolve'. Cluster of bond formation and dissolution occurs right after the BET monolayer forms, w_c and continues until the saturation, $w_{saturation}$, $w_c < w < w_{saturation}$. Due to cluster of bond formation and dissolution, additional term of $(\overline{C.I.})$, the average cooperative index denoting, on average, the total number of H bonds breaking, is incorporated to Eq. (70).

$$d(N/N_0) = -(\overline{C.I.})(N/N_0)d(w/W) \tag{72}$$

The solution of the differential equation, Eq. (72) is given in Eq. (73):

$$ln(E/E_0) = -{}^{1}/_{3}\,(w_c/W)[(\overline{C.I.}) - 1] - {}^{1}/_{3}\,(\overline{C.I.})\frac{w}{W} \tag{73}$$

iii. Multiscale–Multiphysics computational model

Bailakanavar et al. recently developed a coupled moisture-diffusion–mechanical-deformation computational model to predict the hygrothermal degradation of mechanical properties of polymers and polymer composites [153]. Diffusion and mechanical degradation is coupled by assuming that diffusivity was enhanced by hydrostatic strain whereas strength and stiffness were degraded by moisture ingress.

The model couples the degradation in stiffness, strength, and moisture content by Reimschussell method given in Eq. (69). The coupling between the diffusivity and the strain is governed by a concentration and deformation-dependent nonlinear diffusivity. Deformation-dependent diffusion suggests that the diffusivity increases with both mechanical strain and strain due to swelling. The non-linear diffusivity is given in the model as:

$$D = D_0\gamma(\varepsilon)\alpha e^{\beta C} \quad (74)$$

where D_0 is the initial diffusion coefficient, $\gamma(\varepsilon)$ is a function of strain which governs the deformation-dependent diffusion, ε is the strain, α and β are constants, and C is the moisture concentration. The boundary conditions of the function $\gamma(\varepsilon)$ is given as $\gamma(0) = 1$ and $\gamma(\infty) = \infty$. However, researchers did not specify how the function $\gamma(\varepsilon)$ changes with the strain.

Bailakanavar et al. used experimental data of 30% by weight filled glass fiber and carbon fiber reinforced thermoplastic composites to validate the computational model. Coupled moisture-diffusion–mechanical-deformation computational model successfully predicted the moisture absorption and stress-strain curves of various cases.

5.3. Concentration Dependent Modulus Model: Theory Development

To define the change in the modulus, all the models mentioned in the previous section uses phenomological constants or constants that are difficult to identify experimentally. However, all the models agree on the behavior and the mechanism of the modulus degradation. Modulus exponentially decreases by the moisture content. Using the framework of the previous models and experimental results, the hindered diffusion model is incorporated into a new model to predict the change in modulus.

The modulus exponentially decreases to a limiting value while moisture content is exponentially increasing to maximum moisture content. This similar but opposite behavior leads to investigate the possible correlation between the moisture content and the modulus.

Concentration difference between the medium and the solid is the driving force for the moisture absorption. The humidity level of the environment governs how much moisture the solid will absorb. Theoretically, saturation moisture content should linearly change with

the humidity level. For example, if the maximum moisture content of an immersed solid is M_∞, the maximum moisture content of a solid in 50% RH should be $0.5M_\infty$. Since M_∞ is directly correlated to $n_\infty + N_\infty$ [54], $n_\infty + N_\infty = \%RH$. This implies that each concentration level during the moisture absorption into an unsaturated solid, $n + N$, can be defined in term of maximum concentration at a lower %RH. If a relation between the maximum moisture concentration in different levels of relative humidity and modulus at that saturation level was determined, that relation would be used in terms of concentration to describe the change in modulus during transient moisture absorption. In this study, the relation between the saturation moisture content and flexural modulus of the wet thermosetting polymer is investigated.

i. Materials and Sample Preparation

The epoxy resin and curing agent used in this study is selected as EPON 862 and Epikure W (Momentive Performance Materials Inc.), respectively.

First, the epoxy resin and curing agent is mixed at a ratio of 100:26.4 by weight at 100 RPM for 15 minutes. The mixture is then degassed for an hour at room temperature to remove the trapped air. Subsequently, thin epoxy laminates are gravity-cast onto a 177.8 × 101.6 mm^2 (7 × 4 in^2) aluminum mold, preheated to 100℃ (212℉). The mold is kept at 100℃ (212℉) for 1.5 hours and then heated to 179℃ (355℉) and held constant for 2 hours. After 2 hours, the part is cooled down to room temperature at approximately 2.8℃/min to complete the cure cycle. Thirty 41.1 × 12.7 mm^2 (1.61 × 0.5 in^2) specimens were cut from the laminate. The samples are separated into five groups of six. Four group of specimens are used for absorption test in different environments. Fifth group is used to

determine the flexural modulus of the dry EPON 862. The average thickness of the each set of six specimens is 0.91 ± 0.03 mm (0.036 ± 0.001 in).

To remove the initial moisture, the samples are placed in vacuum oven at 43℃ (110°F) for approximately 5 days. Dried samples are subjected to 20%, 50%, and 80% relative humidity, and distilled water at 35℃ (95°F). Mass gain of samples due to water absorption is periodically measured for approximately 5 months. The collected mass gain data of 5 months is used to recover absorption parameters of hindered diffusion model following the aforementioned recovery procedure in Chapter 2.

ii. EPON 862 moisture absorption results

In Table 13, through-the-thickness diffusion coefficients, the hindrance coefficients, the maximum moisture content of EPON 862 at different levels of relative humidity and the root mean square error between the experimental data and model prediction per data point are presented. The decrease in diffusivity and hindrance coefficients and increase in maximum moisture content with respect to relative humidity can easily be seen. As the level of relative humidity increases, the concentration gradient between the environment and the polymer leads to higher flux of moisture into the polymer which in turn results in higher maximum moisture content in the polymer. Moreover, low root mean square error per data point values indicate an accurate recovery of the absorption behavior. The gravimetric experimental data and the one-dimensional hindered diffusion model predictions are illustrated in Figure 68.

Table 13. 1DHDM absorption parameters of EPON 862 at different relative humidity

Material Systems	D_z (mm^2/h)	β (hr^{-1})	γ (hr^{-1})	μ	M_∞ (wt.%)	RMS error (%)
EPON 862 - 20%RH	1.63×10^{-3}	8.05×10^{-4}	2.35×10^{-4}	0.292	0.44	0.26
EPON 862 - 50%RH	1.61×10^{-3}	7.61×10^{-4}	1.98×10^{-4}	0.261	0.85	0.26
EPON 862 - 80%RH	1.59×10^{-3}	7.25×10^{-4}	1.41×10^{-4}	0.194	1.62	0.26
EPON 862 - Immersion	1.57×10^{-3}	6.99×10^{-4}	1.11×10^{-4}	0.158	2.18	0.26

In Figure 68, the thermogravimetric data of EPON 862 at 20%, 50%, 80%, and 100% (distilled water immersion) relative humidity and one-dimensional hindered diffusion model predictions are shown. As in compliance with the root mean square error per data point values in Table 13, one-dimensional hindered diffusion model has predicted each case successfully. The change in the absorption behavior due to relative humidity illustrates the effects of the driving force. To further investigate the driving force effects, the change in each absorption parameters via relative humidity is plotted.

The change of diffusion coefficient with respect to the relative humidity of the environment is illustrated in Figure 69. Although an obvious linear decrease in diffusivity due to the increasing relative humidity is observed, the slope in the order of 10^{-7} suggests that the change in diffusivity may be considered negligible.

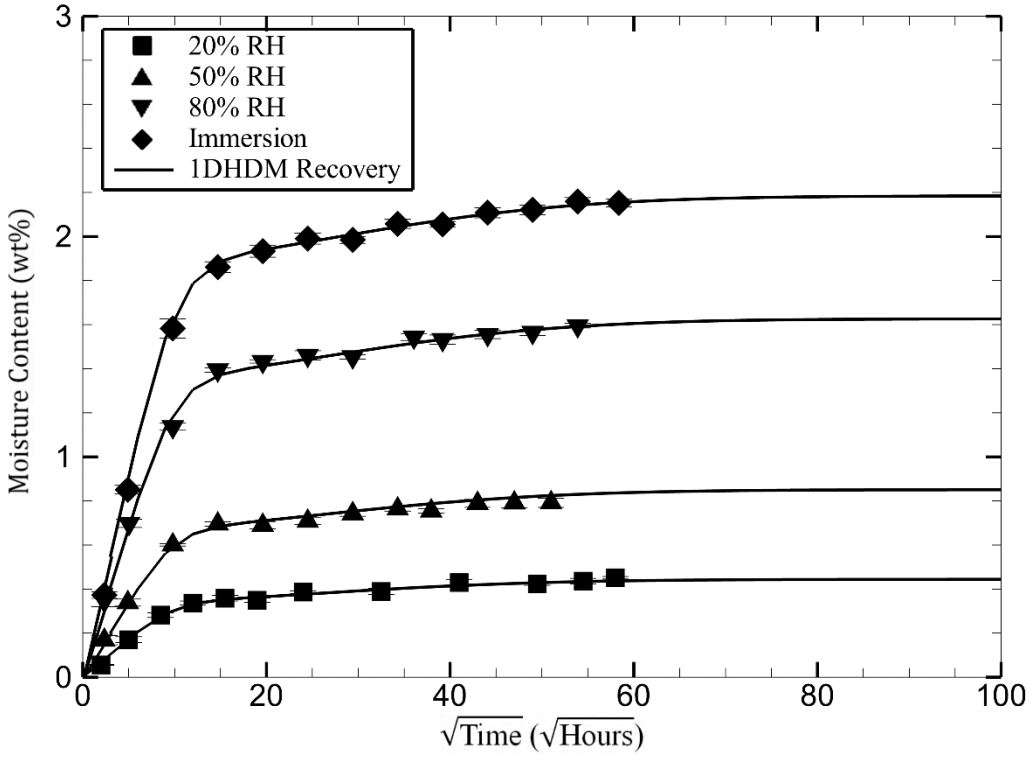


Figure 68. Mass gain data and 1DHDM predictions of EPON 862 at Different Relative Humidity

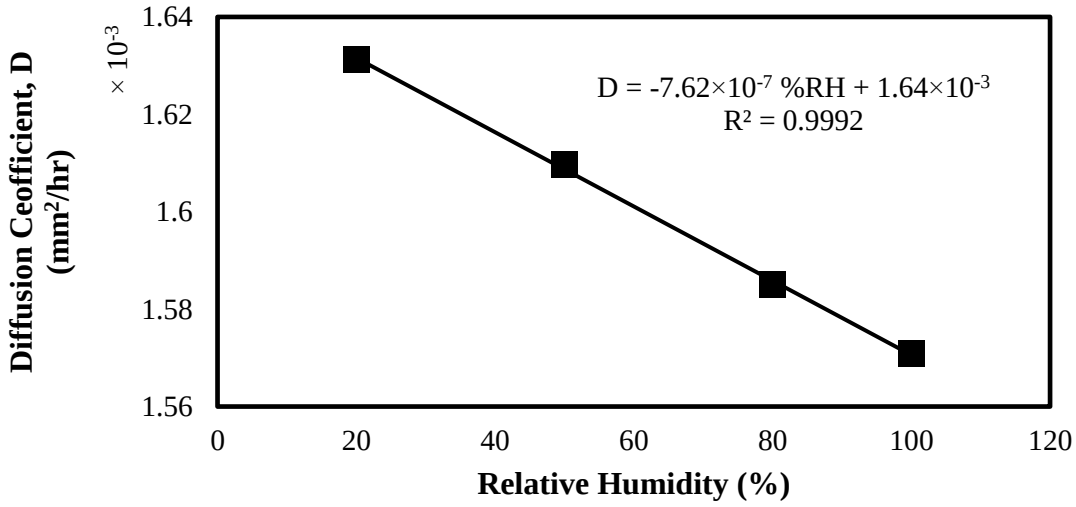


Figure 69. Change of diffusion coefficients with relative humidity

In Figure 70, the linear increase of maximum moisture content with respect to the relative humidity is illustrated. As in compliance with the suggested theory, the maximum moisture content increases linearly with increasing relative humidity. Saturation of a slab

only occurs once the flux of moisture going in to the slab from the environment is equal to the flux of moisture going out. That dynamic equilibrium is reached once the concentration of moisture molecules in the air is equal to the moisture concentration in the solid. Since the relative humidity is a measure of the moisture concentration in the air, a linear change between the relative humidity and maximum moisture content is expected. Moreover, the equation relating the maximum moisture content to relative humidity in Figure 70 shows that at 0 % RH-dry state, the maximum moisture content of the EPON 862 would be 9.82 $\times 10^{-2}$ wt.%. Theoretically, in dry state, the moisture content of the polymer must be zero. The predicted value of 9.82×10^{-2} is on the verge of the theoretical value showing the accuracy of the model predicted trend.

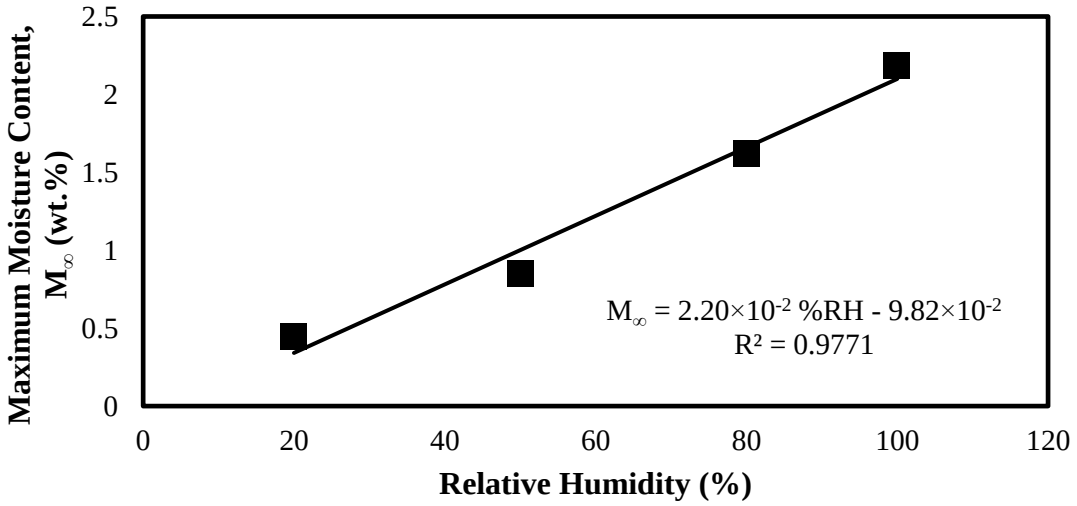


Figure 70. Change in maximum moisture content with relative humidity

Figure 71 demonstrates the variation of rate of transformations between the bound and unbound moisture molecules and hindrance coefficient by the change in relative humidity. Decreasing linear trend of hindrance coefficient suggest that as the relative humidity of the environment increases, the absorption kinetics shifts to a more Fickian behavior. The

linearity of the rate of transformations and hindrance coefficients will be further investigated.

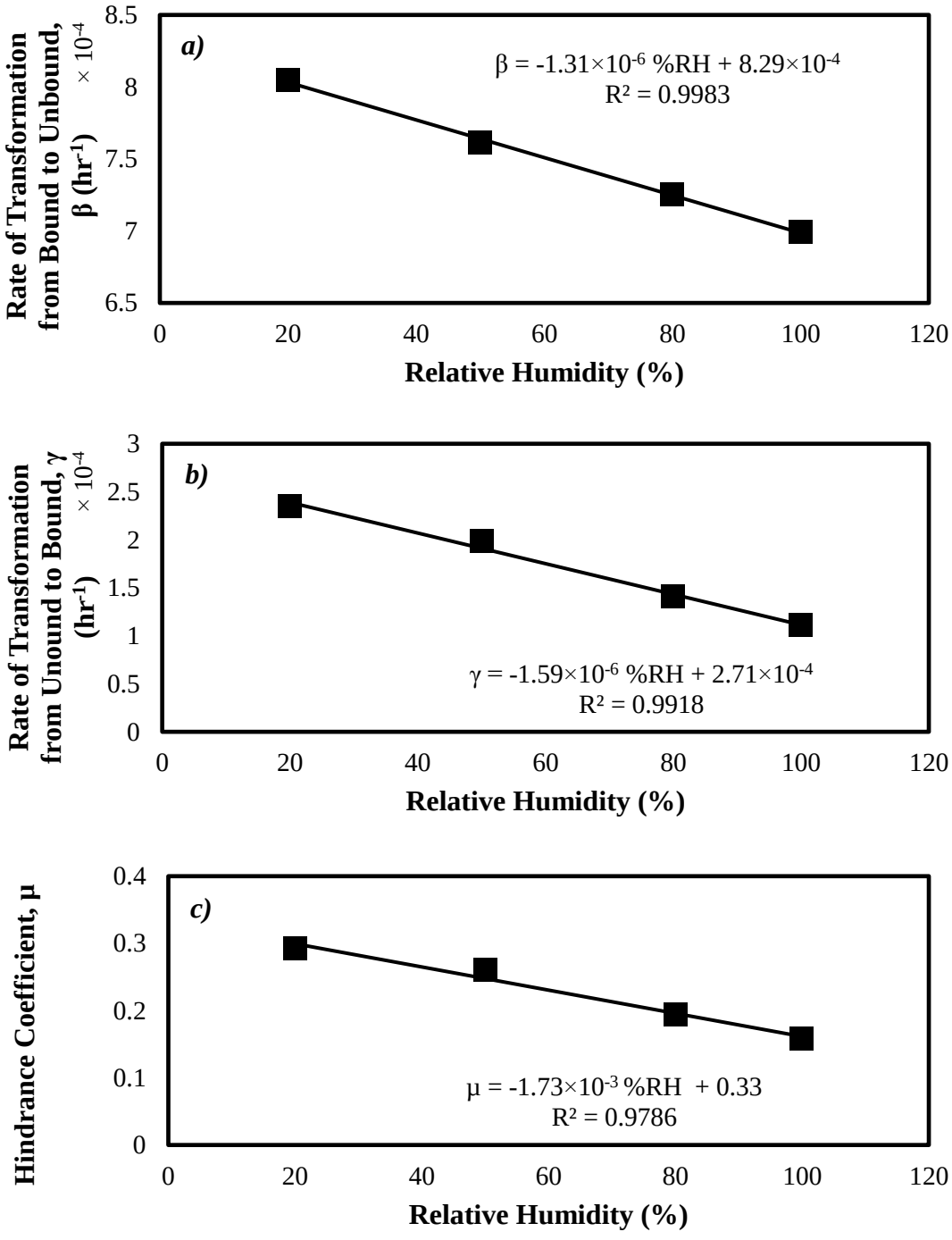


Figure 71. Change in *a)*the rate of bound molecule to become unbound *b)*the rate of unbound molecule to become bound *c)*hindrance coefficient with relative humidity

To investigate any correlation between the maximum moisture content and the flexural modulus of the samples, saturated samples were subjected to three point bending tests. Flexural tests were performed according to ASTM D790 standard to measure the flexural properties of each sample.

Figure 72 displays the flexural modulus of dry samples, samples saturated at 20%, 50%, and 80% relative humidity and saturated wet samples. The decrease in flexural modulus conforms to the literature. Plasticization effects of the absorbed moisture lead to loss in modulus [26,32,117,145,151]. Previously determined maximum moisture contents of each level of relative humidity are compared with the flexural modulus of saturated samples in Figure 73.

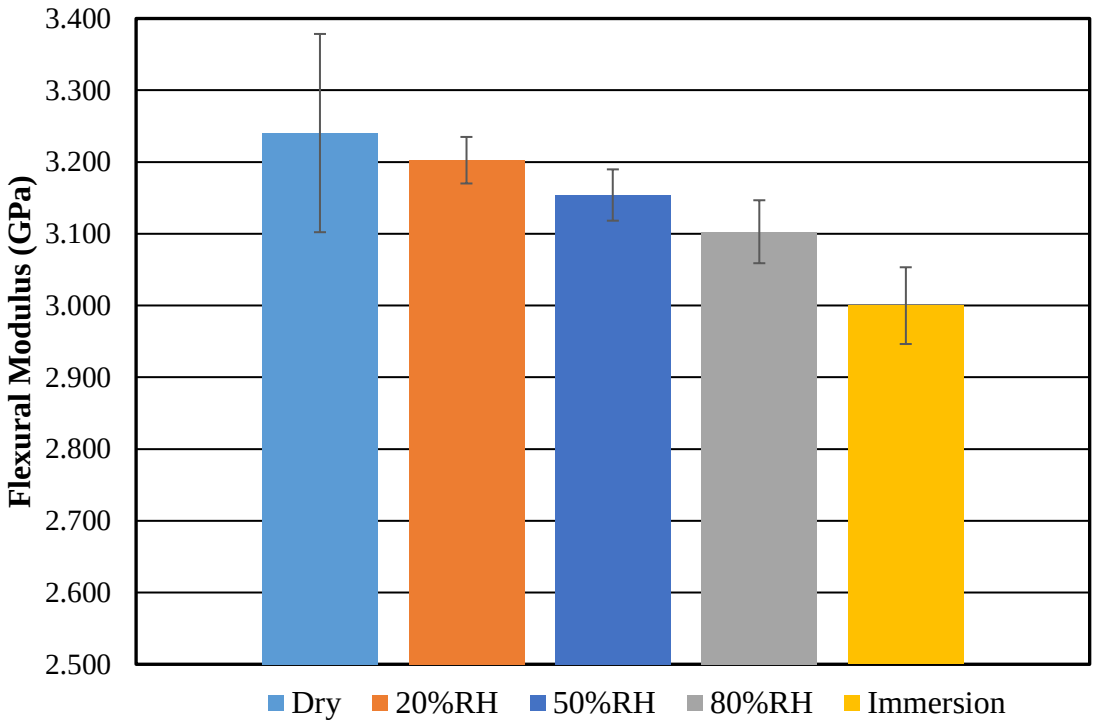


Figure 72. Flexural modulus of samples conditioned at different relative humidity levels

The comparison between the flexural modulus and the maximum moisture contents of samples surprisingly yields a linearly decreasing trend. Linear trend in Figure 73 suggests that the % plasticization in a unit volume of a solid directly depend on the moisture content in that unit volume. Since M_∞ is directly correlated to $n_\infty + N_\infty$ [54], modulus linearly changes with $n_\infty + N_\infty$ values of different relative humidity levels. Moreover, for each level of concentration, $n + N$, there is a corresponding $n_\infty + N_\infty$ at a different relative humidity. Thus, the relationship between the modulus and $n_\infty + N_\infty$ can be used in the transient concentration level, $n + N$, to predict the change in modulus during the moisture absorption.

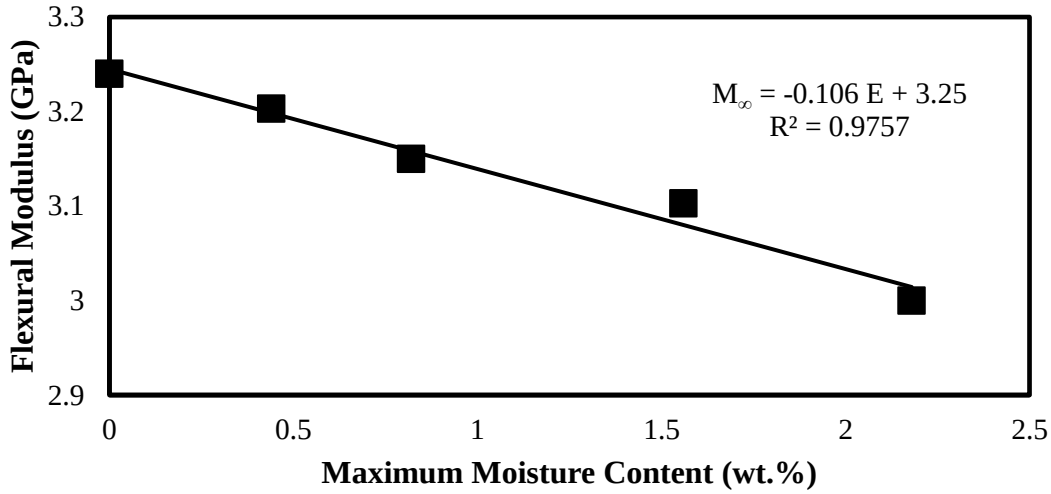


Figure 73. The correlation between the flexural modulus and maximum moisture content

5.4. Concentration Dependent Modulus Model: Model Development

The suggested linear relation between the modulus and the concentration is given as follows:

$$E(z,t) = E_0 - (E_0 - E_{@M_\infty})[n(z,t) + N(z,t)] \qquad (75)$$

$$E' = (E_0 - E_{@M_\infty})$$

i. Tensile Modulus

To find the effective Young's modulus of the thin plate having a thickness of $2h$, $E(z,t)$ is integrated over the thickness of the plate:

$$E(t) = \int_{-h}^{h} E_0 - E'\{[n(z,t) + N(z,t)]\}dz \tag{76}$$

The integration in Eq. (76) yields:

$$E(t) = E_0 - E' \left\{ \begin{array}{l} 1 - \frac{8}{\pi^2} \sum_{i=1}^{\infty(odd)} \frac{r_i^+ exp(-r_i^- t) - r_i^- exp(-r_i^+ t)}{i^2(r_i^+ - r_i^-)} + \\ \frac{8}{\pi^2}\left(K\frac{\beta}{\beta+\gamma}\right) \sum_{i=1}^{\infty(odd)} \frac{exp(-r_i^- t) - exp(-r_i^+ t)}{(r_i^+ - r_i^-)} \end{array} \right\} \tag{77}$$

$$r_i^{\pm} = \frac{1}{2}[(Ki^2 + \gamma + \beta) \pm \sqrt{(Ki^2 + \gamma + \beta)^2 - 4K\beta i^2}]$$

$$K = \frac{\pi^2 D}{h^2}$$

ii. Flexural Modulus

To find the effective flexural modulus, bending moment on a rectangular slab must be considered.

$$\mathrm{M} = \int_{-h}^{h} \sigma_x z w dz$$

$$\sigma_x = E(z,t)\frac{z}{\rho} \tag{78}$$

$$\mathrm{M} = \int_{-h}^{h} \frac{E(z,t) z^2 w dz}{\rho}$$

where M is the bending moment, σ_x is the stress along x direction, w is the width of the slab and ρ is the radius of curvature of the neutral surface during flexure.

Bending moment of a slab is also formulated in terms of flexural modulus, E_f, radius of curvature and moment of inertia, I_{yy}:

$$\mathrm{M} = \frac{E_f I_{yy}}{\rho} = \frac{E_f w h^3}{12\rho} \tag{79}$$

Equating Eq. (78) to Eq. (79) yields:

$$E_f = \frac{12\mathrm{M}\rho}{wh^3} = \frac{12}{h^3}\int_{-h}^{h} E(z,t) z^2 dz \tag{80}$$

Effective flexural modulus of a slab becomes:

$$E_f(t)$$

$$= E_0 - 24E' \left\{ \begin{array}{l} \dfrac{1}{24} - \displaystyle\sum_{i=1}^{\infty(odd)} \left[\frac{\pi^2 i^2 - 8}{\pi^4 i^4}\right] \frac{r_i^+ \, exp(-r_i^- t) - r_i^- exp(-r_i^+ t)}{(r_i^+ - r_i^-)} + \\ \left(K\dfrac{\beta}{\beta+\gamma}\right) \displaystyle\sum_{i=1}^{\infty(odd)} \left[\frac{\pi^2 i^2 - 8}{\pi^4 i^2}\right] \frac{(exp(-r_i^- t) - ex\,p(-r_i^+ t))}{(r_i^+ - r_i^-)} \end{array} \right\} \tag{81}$$

5.5. Concentration Dependent Modulus Model: Validation

Same amount of absorbed moisture in different samples does not mean that both samples have the same amount of damage. In Figure 74, maximum moisture contents of samples conditioned at 20%, 50%, and 80% relative humidity are shown as points A, B, and C on the moisture absorption curve of immersed samples. Even though the mass content of samples saturated at 20%, 50%, or 80% relative humidity, corresponding points on the mass gain curve of immersed samples are the same, they have distinct characteristics due to non-uniform diffusion kinetics during transient moisture absorption. The concentration profile at points A, B, and C and corresponding saturation concentration profiles are given in Figure 75.

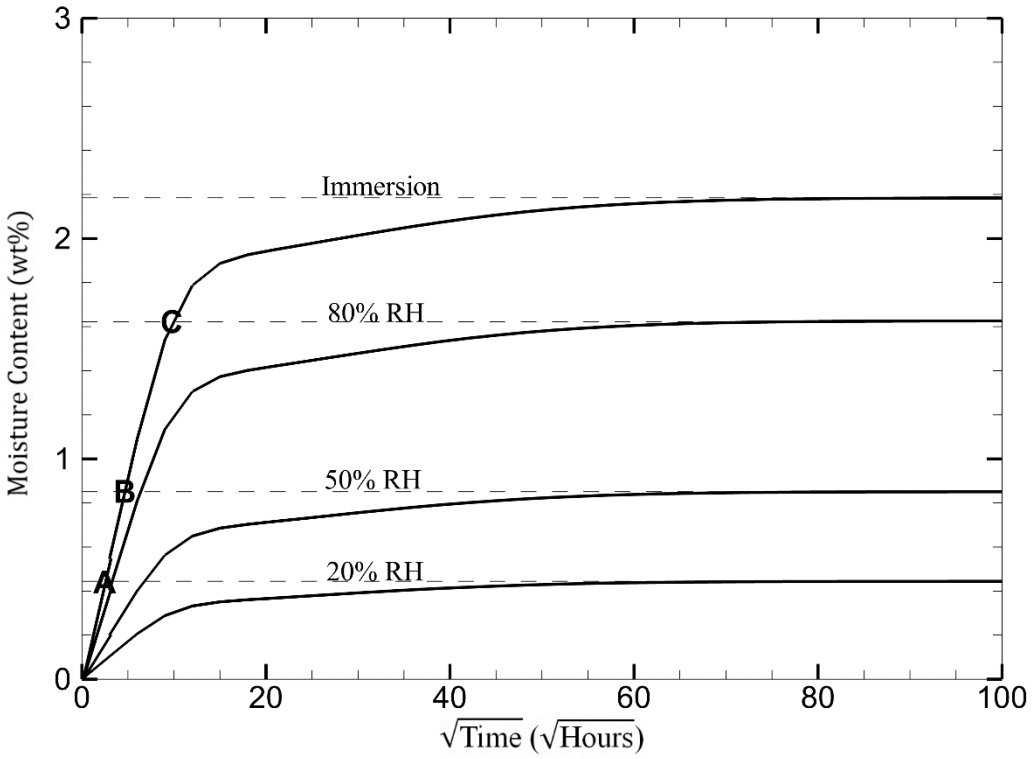


Figure 74. Maximum moisture content of samples conditioned at 20%, 50% and 80% relative humidity on the mass uptake cure of immersed samples

In Figure 75, the moisture concentration levels at point A, B, and C are compared with the saturation concentration at 20%, 50%, and 80% relative humidity, respectively. The concentration profiles are computed by one-dimensional hindered diffusion model but the calculations are extended to two dimensions for visualization. Even though both transient and corresponding saturation moisture concentration profiles have the same amount of water, transient moisture concentration profiles clearly show moisture gradient whereas the saturated moisture concentration profiles are uniform. The difference is due to the nature of moisture absorption. The driving force in moisture absorption is the concentration gradient between the polymer and the environment. The highest driving force corresponds to the surface of the polymer. Thus, the moisture absorption starts at the surfaces, creating non-uniform concentration through-out the polymer and ends when a uniform moisture distribution is reached.

Using the linear relation between the moisture concentration and the modulus in Eq. (75), the modulus distribution during the moisture absorption and at saturation are given in Figure 76. During the moisture absorption, the samples have lower modulus at the surface. As shown in Figure 75, the top and bottom surfaces of samples have higher moisture concentration than the remaining part of the samples until the saturation. The linear relation between the concentration and the modulus yields higher modulus degradation at the surfaces. Moreover, the effective flexural modulus depends on the spatial distribution of the modulus. Lower modulus at the surface decreases the flexural modulus of the sample. Samples A, B, and C have lower effective flexural modulus than the corresponding saturation level effective flexural modulus.

To compare the model prediction simulations and the actual experimental data, a set of EPON 862 samples are immersed in distilled water at 35℃ (95℉) for approximately 6 hours. After 6 hours of immersion, the samples reached to a mass content (point A) that corresponds to the saturation level moisture content at 20% relative humidity. The flexural test results of the samples indicated a lower flexural modulus than the flexural modulus of samples saturated at 20% relative humidity. The transient flexural modulus prediction by Eq. (81) and the experimental data is shown in Figure 77. The predicted effective transient flexural modulus curve accurately predicts the experimentally determined flexural modulus. The difference between the saturation level flexural modulus at 20% relative humidity ($E_f = 3.20\ GPa$) and the corresponding transient flexural modulus ($E_f = 3.14\ GPa$) shows that the moisture concentration at the surfaces clearly has a role in modulus degradation.

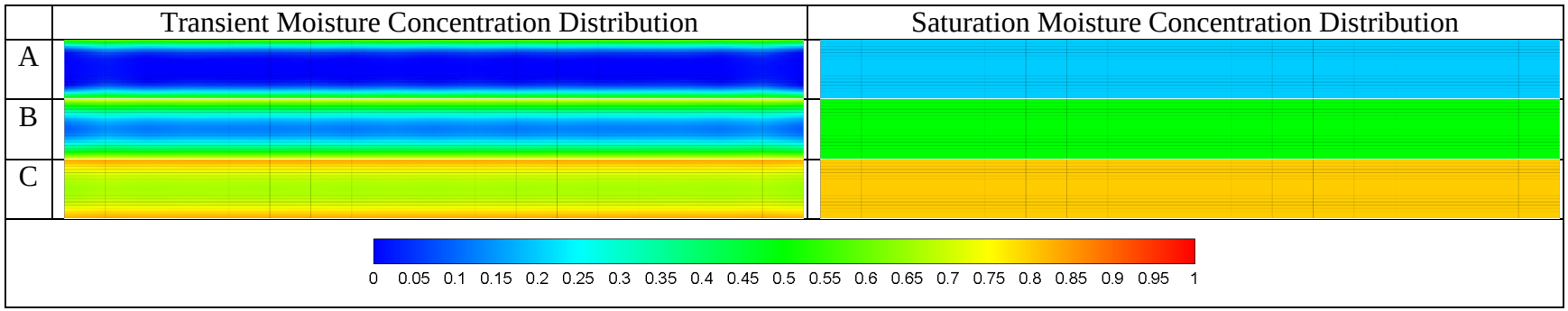


Figure 75. Comparison between the transient and saturation moisture concentration

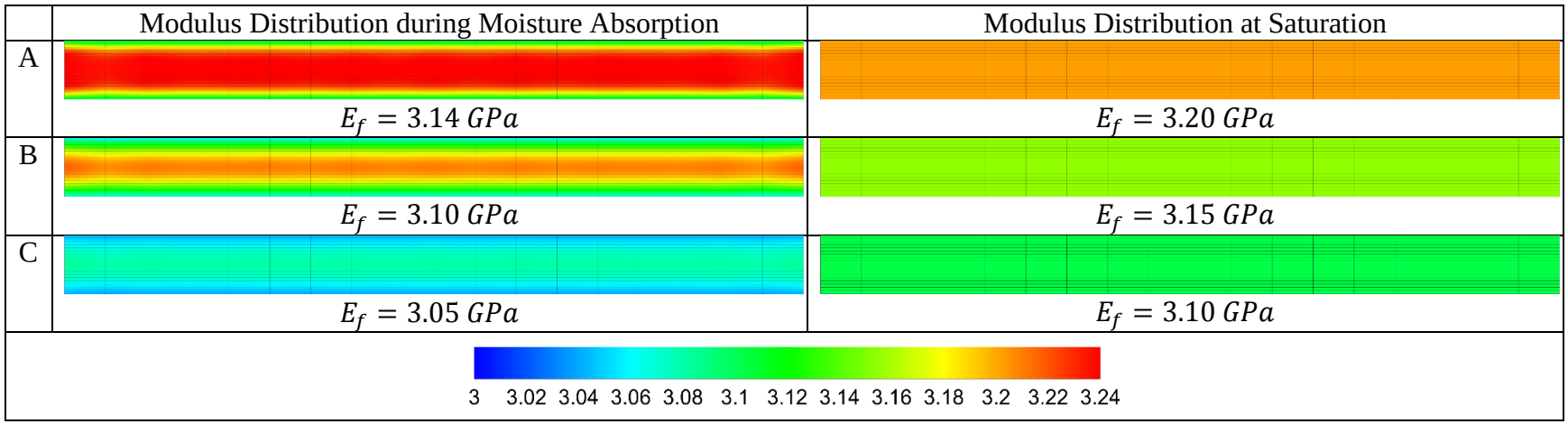


Figure 76. Comparison between the modulus distribution during moisture absorption and at corresponding saturation level

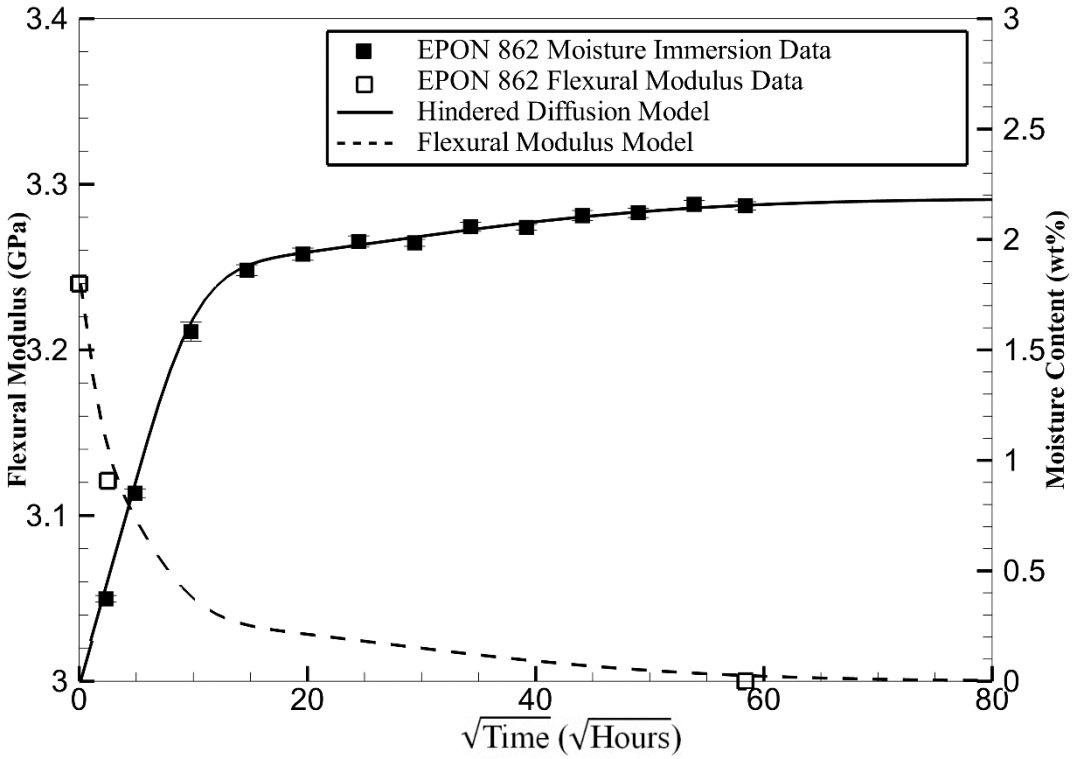


Figure 77. Variation in elastic modulus and mass gain due to moisture absorption into EPON 862

Eftekhari and Fatemi [38] used injection molded 100 × 200 × 2.8 mm^3 30 wt.% short glass fiber reinforced polyamide-6.6 (Ultramid) for moisture absorption and tensile tests. Prior the tests, PA66 specimens were dried in a vacuum chamber at 80℃ (176℉) for 24 hours. Dried PA66 samples were immersed in water at 23℃ (73℉). Weight gain of PA66 samples due to moisture absorption was periodically measured for 130 days. Tension tests were performed on the dried and wet samples based on ASTM D638.

Mass gain data obtained by Eftekhari and Fatemi [38] is used in this study to recover the 1DHDM absorption parameters. Recovered absorption parameters are used to predict the change in elastic modulus due to matrix plasticization using Eq. (77). The elastic modulus prediction is compared with experimental findings of Eftekhari and Fatemi [38]. Mass gain and elastic modulus data of PA66 samples, 1DHDM and elastic modulus predictions are given in Figure 78.

One-dimensional hindered diffusion model accurately predicts the moisture absorption behavior of polyamide 6.6. It is critical to have an accurate recovery of moisture absorption kinetics to predict the transient change in elastic modulus. Elastic modulus at the saturation must be known to calculate the elastic modulus behavior. The experimental data of Eftekhari and Fatemi [38] supply the saturation level elastic modulus. Thus, their transient elastic modulus data can be used to validate the proposed model. In Figure 78, the comparison of the transient elastic modulus data [38] and proposed elastic modulus model illustrates the predictive capabilities of the model. Only using the 1DHDM absorption parameters and the elastic modulus of dry and saturated states, the elastic modulus model successfully captured the transient change in the elastic modulus.

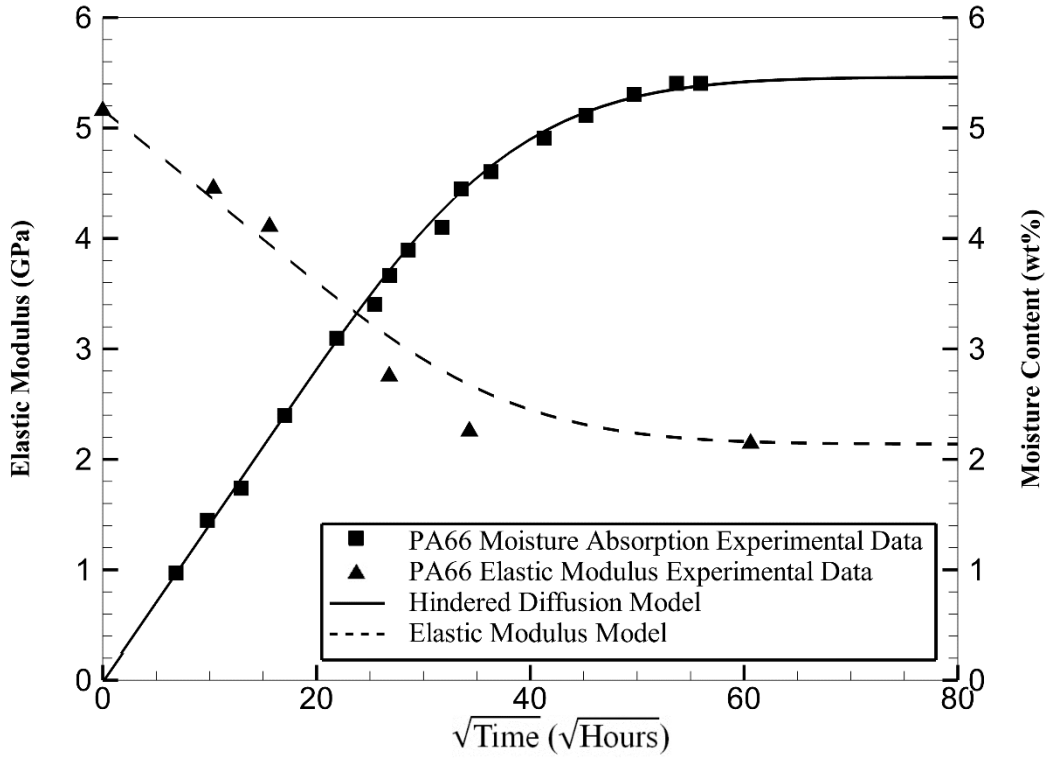


Figure 78. Variation in elastic modulus and mass gain due to moisture absorption into polyamide-6.6

Thwe and Liao [154] investigated the moisture absorption behavior of and moisture induced damage on bamboo fiber reinforced composites (BFRP) and bamboo/glass fiber reinforced hybrid composites (BGRP). Polypropylene (PP) or polypropylene/maleic anhydride polypropylene (PP/MAPP: 90/10 by weight) were used as matrix in the composite materials. Composite plates were manufactured by mixing the polymer matrix with desired short fibers and hot pressing at 190℃ (374℉) and under 3.2MPa (464 psi) pressure for 30 min. Sample notation of composite plates and their constituents are given in Table 14.

Table 14. Fiber contents and matrix type of the samples[154]

Sample	Glass fiber content (wt.%)	Bamboo fiber content (wt.%)	Matrix
B	0	30	PP
H1	10	20	PP
H2	20	10	PP
BM	0	30	PP/MAPP
HM1	10	20	PP/MAPP
HM2	20	10	PP/MAPP

Dog-bone shaped samples of BFRP and BGRP were cut from the composite plate with dimensions 60 × 12 × 3 mm^3 and were fully immersed in water at 25℃ (77℉) for up to 1600 h. The experimental data collected by Thwe and Liao [154] and one-dimensional hindered diffusion model predictions are illustrated in Figure 79.

One-dimensional hindered diffusion model accurately recovers the absorption kinetics of all 6 sample set. As explained earlier, accurate indication of the absorption behavior is dire for elastic modulus predictions. Moreover, after 1600h, no significant moisture absorption is observed in each set of samples as shown in Figure 79.

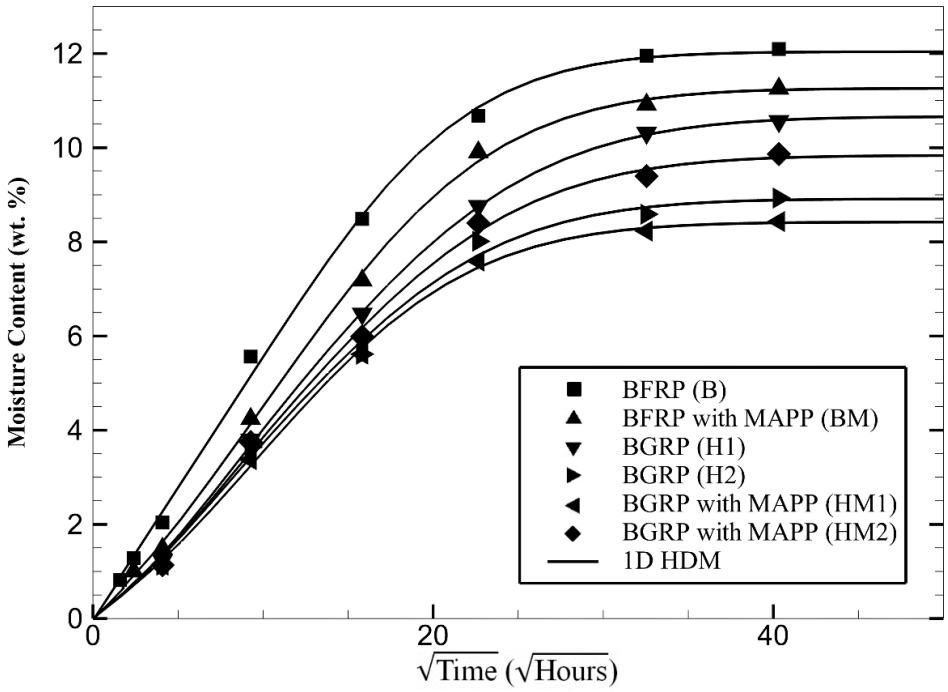


Figure 79. Mass gain data and 1DHDM predictions of BFRP and BGRP samples.

Tensile tests were performed after 520 h and 1200 h according to ASTM D638 standard to determine residual strength and modulus after aging. The resulting experimental elastic modulus data [154] and proposed model predictions are illustrated in Figure 80.

Although the latest elastic modulus measurement, taken at 1200h, is not the elastic modulus at saturation, it has been used to find the saturation level elastic modulus. One-dimensional hindered diffusion model suggests that at 1200h, the samples were approximately 98% saturated. Although the change in effective elastic modulus during the moisture absorption is not linear, between the 98% and full saturation levels, it has been assumed to change linearly to find the saturation level elastic modulus. Once the saturation level elastic modulus of the samples is determined, the elastic modulus model is incorporated. In Figure 80, it has been shown that the model and experimental effective elastic modulus of different samples are in agreement. Even though the saturation level

effective elastic modulus is determined by the assumption that between the 98% and complete saturation elastic modulus changes linearly, it may also be recovered using the experimental data [154] and Eq. (77). The differences between the recovered and determined saturation level effective elastic moduli have found to be insignificant.

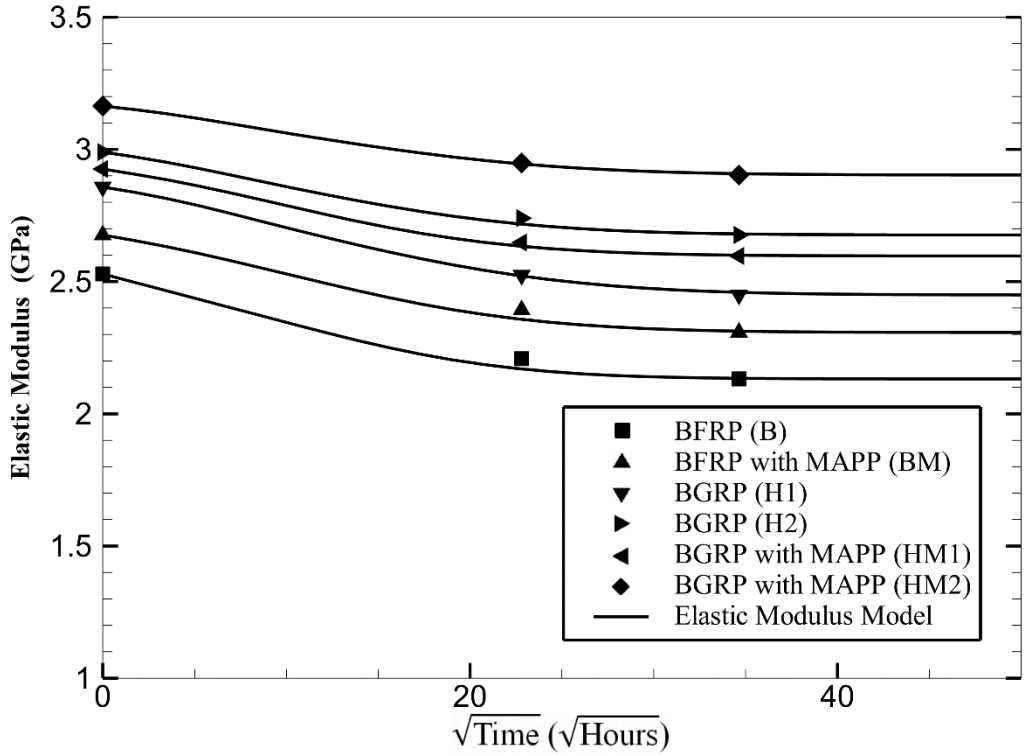


Figure 80. Transient elastic modulus data and model prediction of BFRP and BGRP composites

Kagan et al. [4] focused on moisture absorption in heat-stabilized, unfilled nylon 6 (Capron 8202 HS), a material considered homogeneous. Injection molded, 4-mm thick ISO multi-purpose tensile specimens (ISO-3167) were sealed in special bags in order to preserve their dry-as-molded state. Moisture absorption characteristics of the specimen were obtained by ISO-1110 procedure where the temperature and relative humidity were maintained at 70℃ (158℉) and 62%RH, respectively. Flexure tests were conducted according to ISO and ASTM standards by using an Instron 4505 universal testing system.

To validate the predictive abilities of flexural modulus model, 1DHDM absorption parameters is recovered and incorporated into Eq. (81). One-dimensional hindered diffusion model recovery and the moisture absorption data, and flexural modulus model and elastic modulus data of Nylon 6 samples are illustrated in Figure 81.

One-dimensional hindered diffusion model prediction suggests that the sample saturated right after 400 hours of moisture absorption. The experimental data of flexural modulus [4] is showing the saturation level flexural modulus of Nylon 6 in addition to the transient flexural modulus. Using the dry and saturation flexural moduli of the Nylon 6 and the Eq. (81), the flexural modulus model predictions are illustrated in Figure 81. The model prediction is consistent with the experimental data of flexural modulus.

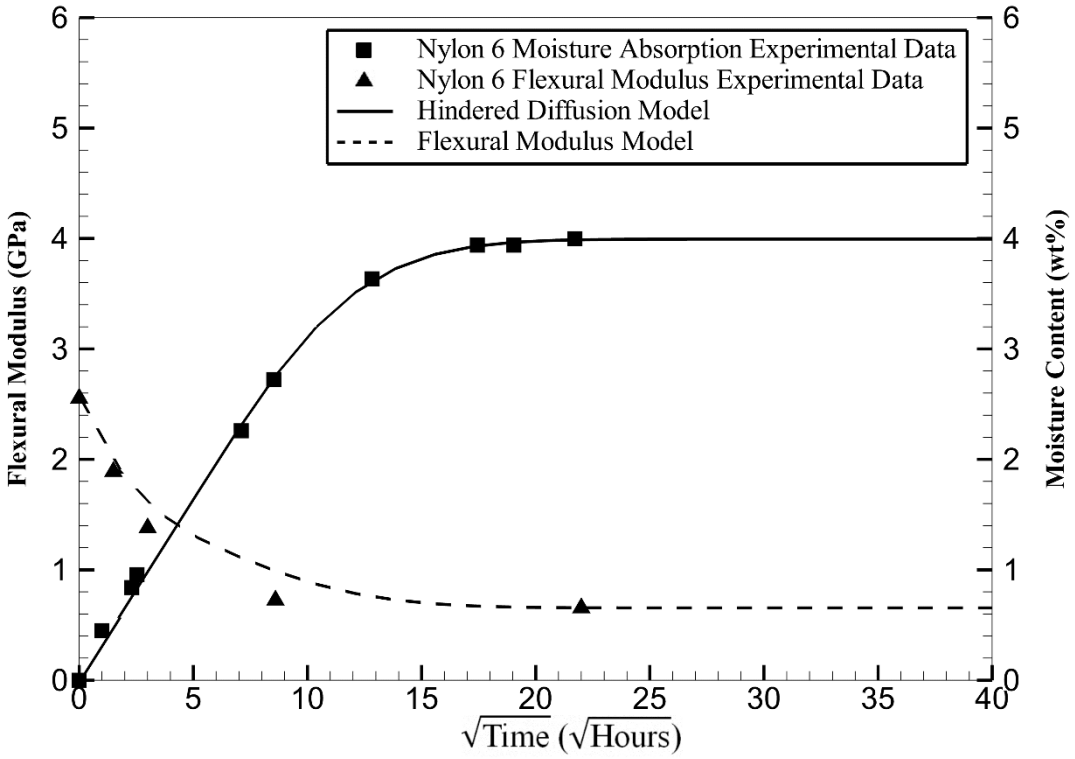


Figure 81. Variation in elastic modulus and mass gain due to moisture absorption into nylon 6

5.6. Conclusion

In this chapter, a new comprehensive elastic modulus degradation model is introduced. The model assumes that the elastic modulus varies inversely linear with the moisture concentration. Thus, each concentration level of a polymer has a corresponding modulus value. During the moisture absorption process, just like the spatial moisture concentration field, elastic modulus creates a spatially non-uniform modulus distribution. Depending on the type of the test, effective tensile or flexural modulus can be calculated using this elastic modulus distribution.

First, the linear change of modulus with concentration has been shown. Flexural tests on EPON 862 saturated at different levels of relative humidity displayed the linear relation between the modulus and the concentration.

To validate the modulus model, experimental data of tensile or flexural modulus from three different published studies are used. The modulus data from different polymers and polymeric composites were gathered during the moisture absorption until the saturation. It should be noted here that the saturation level modulus is a critical factor to determine the transient modulus values.

In the first two cases, tensile modulus data from Eftekhari and Fatemi [38] and Thwe and Liao [154] are used for validation. Both data supplied transient and saturation elastic modulus and absorption data until saturation. The absorption data is used to recover the 1DHDM absorption parameters which are used to predict the tensile modulus change in time. The tensile modulus model effectively predicted the transient elastic modulus of all material systems using only dry and saturation level elastic modulus and 1DHDM absorption parameters.

Similarly, to investigate the capabilities of flexural modulus model, absorption data, and flexural modulus of Nylon 6 [4] is used. The flexural modulus model also successfully predicted the transient effective flexural modulus of Nylon 6 during the moisture absorption process. It should be noted here that while Kagan et al. [4] tested the Nylon 6 in 5 different environmental conditions, only one set of moisture and flexural test data is used for validation purposes because only the absorption tests at 70℃ (158℉) and 62% RH were saturated.

In conclusion, elastic modulus has been experimentally shown to have an inverse linear trend with the moisture concentration. The proposed elastic modulus model has been proven valid for three separate cases. To have a complete understanding on the moisture induced property loss, other types of mechanical properties such as tensile strength, shear strength, and viscoelastic properties are suggested to be investigated in the future.

Chapter 6. Concluding Remarks

All liquid and gas molecules exhibit molecular diffusion above the absolute zero temperature. The rate and extent of diffusion depend on the environment and the molecular structure as well as the properties of both the penetrant and the medium. Polymers are known for their susceptibility to moisture ingress in highly humid environments.

Absorption of a liquid by polymers and polymeric composites causes changes in the microstructure resulting in different type and level of degradation such as swelling, residual stresses, and plasticization of the polymer. These damages lead to electrical, optical, thermal and mechanical damages, and property loss in the material which limits the design and use of polymers and polymeric composites in environmentally harsh conditions.

The one-dimensional Fickian diffusion model is the most fundamental model which is often used for predicting absorption behavior assuming reversible, random molecular motion of diffusion particles from high concentration region to low one. Even though many researchers used the Fickian diffusion model due to its simplicity and mathematical tractability, several researchers, recognizing the limitations of the Fickian theory, have proposed more realistic models for moisture absorption, in order to account for anisotropy, edge effects, and polymer-absorbent affinity.

Among the several non-Fickian models, one-dimensional hindered diffusion model predicts the absorption behavior considering the chemical interaction between the polymer and the penetrant in addition to diffusion of penetrant through the interstice. The model differentiates the absorbed penetrant as either unbound molecules or bound molecules. Coupling of polymer and the penetrant due to the intermolecular forces between them

results in bound, or immobile molecules which are no longer part of ongoing diffusion. Molecules that are free to move through the interstice are often called unbound, or mobile. Molecules diffuse into the material as unbound can either remain as unbound molecule or interact with polymer chain and become bound. Likewise, bound molecules can transform back to unbound ones. The rate of exchange between the unbound and bound moisture governs the hindrance in reaching the dynamic equilibrium and defined as hindrance coefficient, μ.

Although the amount of bound moisture is defined by the polymer-penetrant affinity, additive/fiber and matrix interface and/or voids and pores may also be considered as additional storage sites for bound, immobile molecules from a phenomenological perspective. To understand the change in absorption kinetics due to micro/nano additives and/or process induced voids and pores, experimental identification of model specific set of material properties, generally referred to as diffusion or absorption parameters, are needed to be determined. The absorption parameters can be conveniently recovered by minimizing the error between the model predictions and experimental data using the least square error function. Steepest descent gradient optimization is determined to be a convenient method to minimize the error, while recovering the model specific set of absorption parameters simultaneously.

The recovery of one-dimensional hindered diffusion model absorption parameters of I.30E nanoclay/DGEBA epoxy and I.30E nanoclay/DGEBF epoxy (EPON 862) nanocomposites, and APS treated glass sphere/DGEBA epoxy and nBS treated glass sphere/DGEBA epoxy micro additive composites yielded changes in absorption kinetics of each composite due to additive content. Addition of fillers in thermosetting polymers is

a common practice to help with the cost, mechanical, and/or other property enhancement. While the additives in polymers enhance the desired property, they would change the moisture absorption kinetics of the polymer at the macroscale.

Nanoclay or glass sphere addition in epoxy resulted in a linear decrease in diffusion coefficient with respect to the additive content following the rule of mixture. Both I.30E nanoclay and glass spheres are known to be impermeable. Impermeable additives do not absorb water, thus setting the diffusion coefficient of these additives to zero. Nonetheless, the additives occupy space in the polymer matrix and create interface at which the moisture can be stored. The decrease in the polymer content per unit volume and increase in the interface density affect the absorption kinetics.

Increasing nanoclay or glass sphere content resulted in a linear decrease in maximum moisture content of aforementioned composites. Maximum moisture content consists of unbound and bound maximum moisture content. Although there is a continuous transformation between the unbound and bound moisture, these two parameters are independent of each other. Thus, to understand the effect of additives on the maximum moisture content, its constituents are investigated.

Increasing nanoclay or glass content showed a linearly decreasing trend in the unbound maximum moisture content. As the impermeable additive content increases, the amount of epoxy in a unit volume, "free volume", decreases. Since the unbound moisture is defined to be absorbed only by the diffusion, the decrease in free volume would definitely lead to less maximum unbound moisture content. In this regard, same additive in the same epoxy system should lead to identical decrease the maximum unbound moisture content. Both APS treated glass sphere/DGEBA epoxy and nBS treated glass sphere/DGEBA epoxy

showed identical decrease in the unbound maximum moisture content with respect to the glass content since both composites have the same matrix and glass spheres size. The surface treatments on them are only affecting the interface properties.

Changes in bound maximum moisture content and hindrance coefficient are considered simultaneously since hindrance coefficient quantifies the anomalous absorption behavior due to bound moisture absorption. The effect of additive on the bound maximum moisture content and the hindrance coefficient demonstrated opposing trends in different composites. Increasing inclusion content resulted in a linear decrease in the hindrance coefficient and the maximum bound moisture content in I.30E/DGEBA epoxy whereas a linear increase in I.30E/DGEBF epoxy and both glass sphere/DGEBA epoxy composites. Moisture is known to be bound to the matrix, matrix/additive interface, and stored in voids or pores. Decrease in epoxy in unit volume by increasing additive content reduces the binding sites in the matrix. Depending on the surface chemistry of the additive/matrix interface, moisture may or may not bind to the interface. The tradeoff between the diminishing matrix binding sites and increasing/decreasing interface binding sites would govern the trend of maximum bound moisture content and the hindrance coefficient.

One-dimensional hindered diffusion model is capable of identifying the effects of additives and interface between the additive and the matrix but is not able to explain the change in absorption behavior due to different layers of polymers. Many polymers are subjected to layers of coatings to improve quality and service life. Thus, hindered diffusion model is modified to consider a continuous absorption with the discrete changes in material properties.

Changes in absorption kinetics due to additives lead to hollow glass sphere addition into epoxy to form a multilayer composite. Low density hollow spheres formed a layer of glass sphere/epoxy composite on top of the epoxy resin. Highly packed glass sphere/epoxy layer ended up absorbing more moisture than the neat epoxy layer. Even though the glass sphere/epoxy layer formation decreased the barrier capabilities of EPON 862 epoxy, multilayer hindered diffusion model, a modified version of hindered diffusion model considering the discrete change in absorption properties, successfully predicted the absorption kinetics of hollow glass sphere/epoxy-epoxy multilayer composites.

Complex fabrication processes of thermosetting polymers give rise to void formation during gelation and curing. Although voids in polymers causes loss in material properties and performance in general, pores may be introduced purposefully for a specific application. The pores, vacant sites, in foams are responsible for extreme amount of liquid absorption. Void filling hindered diffusion model is developed to illustrate the effect of porosity and microstructure on moisture absorption. Hindered diffusion model extended to void filling hindered diffusion model by incorporating porosity of foams to differentiate between the bound molecules stored in the matrix or interface and the bound molecules stored in the pores and voids. Void filling hindered diffusion model considers diffusion (unbound molecules), chemical interaction between medium and penetrant (bound molecules), and storage of molecules in voids and porous structure (trapped molecules).

ROHACELL® WF-71 rigid foam plastic based on PMI (polymethacrylimide) is a highly porous, closed-cell foam mostly used in high temperature and pressure aerospace applications. Moisture absorption tests on ROHACELL® WF-71 showed the thickness of the foam has an effect on the moisture absorption. SEM imaging and density measurements

on the ROHACELL foams having different thicknesses yielded that the open-cell on the surface to the closed-cell ratio of foams depends on the foam thickness. Thus, due to surface layer, porosity of the foams changes by the thickness of the foams. Due to the high open-cell to closed-cell ratio, thin foams are less porous than the thick foams. Void filling hindered diffusion model accurately predicted the change in absorption behavior due to thickness of the foams by integrating the porosity of the foams to the model.

Heat treatment and the pressure on the foams changed their microstructure and porosity. Hot pressed foams showed cell shrinkage and decrease in porosity and thickness. Higher pressure of hot press even resulted in cell coalescence in the foams. Decrease in porosity in foams due to hot pressing caused decrease in maximum moisture content of the foams. Void filling hindered diffusion model not only successfully recovered the absorption parameters of the hot pressed foams but attributed the decrease in maximum moisture content to the trapped moisture in the pores as well.

Hindered diffusion model and its derivatives (multilayer, void filling, and three-dimensional hindered diffusion models) can basically predict the absorption behavior of all types of thermosetting polymers and micro- and nano-polymer composites. However, moisture induced damages in polymers still cannot be quantified by the moisture absorption models. Absorption models may explain but cannot predict the extent of the property loss.

Theoretically, each concentration level can be related to the saturation moisture content at various relative humidity conditions. If there is a relation between the saturation moisture content at different relative humidity conditions and the loss in material property, that relation may be used to predict the transient property change during the immersion or in

other environments with transient relative humidity. Absorption tests in various relative humidity on EPON 862 showed a linear trend between saturation moisture content and corresponding flexural modulus.

A new comprehensive modulus degradation model where the modulus varies inversely linear with the moisture concentration is introduced. Linearly decreasing trend of modulus creates a spatial modulus distribution during the moisture immersion. The change in effective modulus is presumed to be found by using the modulus distribution.

Experimental data of tensile or flexural modulus and moisture absorption from three different published studies are used to validate the modulus model. Knowing the dry and saturation level modulus, the change in between is assumed linear. Using the recovered absorption parameters and using the modulus data, both elastic modulus model and flexural modulus model accurately represented the transient change in the modulus.

6.1. Research Proposals

Capabilities of hindered diffusion model and its extensions to predict the absorption behavior of various polymers and polymeric composites unfold further questions about the model. The absorption parameters that governs the rate of exchange between the unbound and bound molecules, γ and β, should be investigated in depth. The chemical reaction rate of becoming bound or unbound molecule may help explain the change in γ and β. Alternatively, the rate of exchange between the unbound and bound molecules may be investigated following a probabilistic approach following the entropy equation. Either way the nature of rate of exchange between the unbound and bound molecules, γ and β, is worth exploring.

As the trapped moisture is differentiated from the bound moisture using the void filling hindered diffusion model, bound moisture at the additive matrix interface may be distinguished using the interface properties. Linear changes of absorption parameters with respect to the additive content suggest a relation between the interface density and the absorption parameters. Moreover, the change in the slope for different material systems may be defined in terms of interface properties such as surface tension and chemical potential.

Multilayer hindered diffusion model effectively predicted the absorption behavior of glass sphere/epoxy-epoxy multilayer composites. Even though the barrier properties of the glass sphere/epoxy are unfavorable, multilayer hindered diffusion model may be used to predict what type of reinforcement or coating would be needed to improve the water resistance. The model can be used to design a coating for protection against moisture absorption.

Foams are frequently used in high-end engineering applications as a core material in sandwich composites. As a core material, foams increase the flexural strength of the sandwich structure without a compromise from the weight. A merger between the void filling hindered diffusion model and multilayer hindered diffusion model might be useful to predict the absorption behavior of sandwich composites. Often sandwich composites have less absorbent facesheets. However, barrier properties of the facesheets does not change the fact that the foam core will eventually start absorbing moisture and the mass gain of the foams would be significant. Thus, the overall absorption behavior of the foam core sandwich composites should be investigated to predict the durability of the material.

Lastly, the capabilities of the modulus model can be extended to other types of mechanical or electrical properties. Change in desired property should be investigated by saturating the material in various relative humidity conditions. If a meaningful relation between the saturation moisture content and the property is determined, transient property change can be investigated.

References

[1] Guloglu G.E., Hamidi Y.K. and Altan M.C. "Fast recovery of non- fickian moisture absorption parameters for polymers and polymer composites". *Polymer Engineering & Science*, 2016;57:921–31.

[2] Glaskova T. and Aniskevich A. "Moisture absorption by epoxy/montmorillonite nanocomposite". *Composites Science and Technology*, 2009;69:2711–5.

[3] Sridhar R., Narasimha Murthy H.N., Karthik B., Vishnu Mahesh K.R., Krishna M. and Ratna P. "Moisture diffusion through nanoclay/vinylester processed using twin- screw extrusion". *Journal of Vinyl and Additive Technology*, 2014;20:152–9.

[4] Jia N., Fraenkel H.A. and Kagan V.A. "Effects of moisture conditioning methods on mechanical properties of injection molded nylon 6". *Journal of Reinforced Plastics and Composites*, 2004;23:729–37.

[5] Czél G. and Czigány T. "A study of water absorption and mechanical properties of glass fiber/polyester composite pipes - Effects of specimen geometry and preparation". *Journal of Composite Materials*, 2008;42:2815–27.

[6] Thwe M.M. and Liao K. "Environmental effects on bamboo-glass/polypropylene hybrid composites". *Journal of Materials Science*, 2003;38:363–76.

[7] Beg M.D.H. and Pickering K.L. "Mechanical performance of Kraft fibre reinforced polypropylene composites: Influence of fibre length, fibre beating and hygrothermal ageing". *Composites Part A: Applied Science and Manufacturing*, 2008;39:1748–55.

[8] Hargitai H., Rácz I. and Anandjiwala R.D. "Development of HEMP fiber reinforced polypropylene composites". *Journal of Thermoplastic Composite Materials*, 2008;21:165–74.

[9] Yu Y., Yang X., Wang L. and Liu H. "Hygrothermal aging on pultruded carbon fiber/vinyl ester resin composite for sucker rod application". *Journal of Reinforced Plastics and Composites*, 2006;25:149–60.

[10] Popineau S., Rondeau-Mouro C., Sulpice-Gaillet C. and Shanahan M.E.R. "Free/bound water absorption in an epoxy adhesive". *Polymer*, 2005;46:10733–40.

[11] Hu R.-H., Sun M.-Y. and Lim J.-K. "Moisture absorption, tensile strength and microstructure evolution of short jute fiber/polylactide composite in hygrothermal environment". *Materials and Design*, 2010;31:3167–73.

[12] Errajhi O.A.Z., Osborne J.R.F., Richardson M.O.W. and Dhakal H.N. "Water absorption characteristics of aluminised E-glass fibre reinforced unsaturated polyester composites". *Composite Structures*, 2005;71:333–6.

[13] Sajna V., Mohanty S. and Nayak S.K. "Moisture absorption behavior of hybrid bionanocomposites of polylactic acid and evaluation of physicochemical properties". *Journal of Thermoplastic Composite Materials*, 2017;30:521–44.

[14] Scott P. and Lees J.M. "Water, salt water, and alkaline solution uptake in epoxy thin films". *Journal of Applied Polymer Science*, 2013;130:1898–908.

[15] Loos A.C. and Springer G.S. "Moisture Absorption of Graphite-Epoxy Composites Immersed in Liquids and in Humid Air". *Journal of Composite Materials*, 1979;13:131–47.

[16] Dana H.R., Perronnet A., Fréour S., Casari P. and Jacquemin F. "Identification of moisture diffusion parameters in organic matrix composites". *Journal of Composite Materials*, 2013;47:1081–92.

[17] Dhakal H.N., Zhang Z.Y., Bennett N., Lopez-Arraiza A. and Vallejo F.J. "Effects of water immersion ageing on the mechanical properties of flax and jute fibre biocomposites evaluated by nanoindentation and flexural testing". *Journal of Composite Materials*, 2014;48:1399–406.

[18] Shah A.P., Gupta R.K., Gangarao H.V.S. and Powell C.E. "Moisture diffusion through vinyl ester nanocomposites made with montmorillonite clay". *Polymer Engineering and Science*, 2002;42:1852–63.

[19] Grace L.R. "Projecting long-term non-Fickian diffusion behavior in polymeric composites based on short-term data: a 5-year validation study". *Journal of Materials Science*, 2016;51:845–53.

[20] Joliff Y., Belec L. and Chailan J.F. "Modified water diffusion kinetics in an unidirectional glass/fibre composite due to the interphase area: Experimental, analytical and numerical approach". *Composite Structures*, 2013;97:296–303.

[21] Helmroth I.E., Dekker M. and Hankemeier T. "Additive diffusion from LDPE slabs into contacting solvents as a function of solvent absorption". *Journal of Applied Polymer Science*, 2003;90:1609–17.

[22] Moffet M.L. and La Saponara V. "Rheological properties of neat epoxy exposed to in-service aerospace contaminants". *Journal of Applied Polymer Science*, 2013;130:3961–71.

[23] La Saponara V. "Environmental and chemical degradation of carbon/epoxy and structural adhesive for aerospace applications: Fickian and anomalous diffusion, Arrhenius kinetics". *Composite Structures*, 2011;93:2180–95.

[24] Hamidi Y., Altan M. and Grady P.B. Polymer Composites. In: Encyclopedia of Chemical Processing. 2005.

[25] Rodriguez F. and Rodriguez F. "Principles of polymer systems" 2003.

[26] Kim D.H. and Kim H.S. "Waterproof characteristics of nanoclay/epoxy nanocomposite in adhesively bonded joints". *Composites Part B: Engineering*, 2013;55:86–95.

[27] Sugita Y., Winkelmann C. and La Saponara V. "Environmental and chemical degradation of carbon/epoxy lap joints for aerospace applications, and effects on their mechanical performance". *Composites Science and Technology*, 2010;70:829–39.

[28] Akil H.M., Santulli C., Sarasini F., Tirillò J. and Valente T. "Environmental effects on the mechanical behaviour of pultruded jute/glass fibre-reinforced polyester hybrid composites". *Composites Science and Technology*, 2014;94:62–70.

[29] Adhikary K.B., Pang S. and Staiger M.P. "Long-term moisture absorption and thickness swelling behaviour of recycled thermoplastics reinforced with Pinus radiata sawdust". *Chemical Engineering Journal*, 2008;142:190–8.

[30] Abhilash A.S., Joshi S.P., Mukherjee A. and Mishnaevsky L. "Micromechanics of diffusion-induced damage evolution in reinforced polymers". *Composites Science and Technology*, 2011;71:333–42.

[31] Visco A.M., Brancato V. and Campo N. "Degradation effects in polyester and vinyl ester resins induced by accelerated aging in seawater". *Journal of Composite Materials*, 2012;46:2025–40.

[32] Pérez-Pacheco E., Cauich-Cupul J.I., Valadez-González A. and Herrera-Franco P.J. "Effect of moisture absorption on the mechanical behavior of carbon fiber/epoxy matrix composites". *Journal of Materials Science*, 2013;48:1873–82.

[33] Aktas L., Hamidi Y. and Altan M.C. "Effect of moisture on the mechanical properties of resin transfer molded composites - Part II: Desorption". *Journal of Materials Processing and Manufacturing Science*, 2002;10:255–67.

[34] Aktas L., Hamidi Y. and Altan M. "Effect of Moisture on the Mechanical Properties of Resin Transfer Molded Composites - Part I: Absorption". *Journal of Materials Processing & Manufacturing Science - J MATER PROCESS MANUF SCI*, 2002;10:239–54.

[35] Selzer R. and Friedrich K. "Mechanical properties and failure behaviour of carbon fibre-reinforced polymer composites under the influence of moisture". *Composites Part A: Applied Science and Manufacturing*, 1997;28:595–604.

[36] Pomies F. and Carlsson L.A. "Analysis of Modulus and Strength of Dry and Wet Thermoset and Thermoplastic Composites Loaded in Transverse Tension". *Journal of Composite Materials*, 1994;28:22–35.

[37] Regazzi A., Léger R., Corn S. and Ienny P. "Modeling of hydrothermal aging of short flax fiber reinforced composites". *Composites Part A: Applied Science and*

Manufacturing, 2016;90:559–66.

[38] Eftekhari M. and Fatemi A. "Tensile behavior of thermoplastic composites including temperature, moisture, and hygrothermal effects". *Polymer Testing*, 2016;51:151–64.

[39] Peret T., Clement A., Freour S. and Jacquemin F. "Numerical transient hygro-elastic analyses of reinforced Fickian and non-Fickian polymers". *Composite Structures*, 2014;116:395–403.

[40] Reimschuessel H.K. and Chemical A. "Relationships on the effect of water on glass transition temperature and young ' s modulus of nylon 6". *Journal of Polymer Science: Polymer Chemisrty Edition*, 1978;16:1229–36.

[41] Youssef Z., Jacquemin F., Gloaguen D. and Guillén R. "A multiscale hygroviscoelastic approach to predicting the internal stresses in composite materials". *Mechanics of Composite Materials*, 2010;46:201–10.

[42] Fick A. "Ueber Difusion;". *Annalen Der Physik*, 1855.

[43] Shen C.-H. and Springer G.S. "Moisture Absorption and Desorption of Composite Materials". *Journal of Composite Materials*, 1976;10:2–20.

[44] Joliff Y., Belec L., Heman M.B. and Chailan J.F. "Experimental, analytical and numerical study of water diffusion in unidirectional composite materials - Interphase impact". *Computational Materials Science*, 2012;64:141–5.

[45] Rao R.M.V.G.K., Chanda M. and Balasubramanian N. "A Fickian Diffusion Model for Permeable Fibre Polymer Composites". *Journal of Reinforced Plastics and Composites*, 1983;2:289–99.

[46] Hayward D., Hollins E., Johncock P., McEwan I., Pethrick R.A. and Pollock E.A. "The cure and diffusion of water in halogen containing epoxy/amine thermosets". *Polymer*, 1997;38:1151–68.

[47] Al-Harthi M., Loughlin K. and Kahraman R. "Moisture diffusion into epoxy adhesive: Testing and modeling". *Adsorption*, 2007;13:115–20.

[48] Mensitieri G., Lavorgna M., Musto P. and Ragosta G. "Water transport in densely crosslinked networks: A comparison between epoxy systems having different interactive characters". *Polymer*, 2006;47:8326–36.

[49] Roy S., Xu W.X., Park S.J. and Liechti K.M. "Anomalous Moisture Diffusion in Viscoelastic Polymers: Modeling and Testing". *Journal of Applied Mechanics*, 2000;67:391.

[50] Jacobs P.M. and Jones E.R. "Diffusion of moisture into two-phase polymers - Part 2 Styrenated polyester resins". *Journal of Materials Science*, 1989;24:2343–7.

[51] Maggana C. and Pissis P. "Water Sorption and Diffusion in an Epoxy Resin System". *Journal Of Polymer Science Part B-Polymer Physics*, 1999;37:1165–82.

[52] Berens A.R. and Hopfenberg H.B. "Diffusion and relaxation in glassy polymer powders: 2. Separation of diffusion and relaxation parameters". *Polymer*, 1978;19:489–96.

[53] Berens A.R. "Induction and Measurement of Glassy-State Relaxations by Vapor Sorption Techniques". *Journal of Polymer Science*, 1979;17:1757–70.

[54] Carter H.G. and Kibler K.G. "Langmuir-Type Model for Anomalous Moisture Diffusion In Composite Resins". *Journal of Composite Materials*, 1978;12:118–31.

[55] Grace L.R. and Altan M.C. "Non- Fickian three-dimensional hindered moisture absorption in polymeric composites: Model development and validation". *Polymer Composites*, 2013;34:1144–57.

[56] Lee M.C. and Peppas N.A. "Water transport in epoxy resins". *Progress in Polymer Science*, 1993;18:947–61.

[57] Grace L.R. and Altan M.C. "Characterization of anisotropic moisture absorption in polymeric composites using hindered diffusion model". *Composites Part A: Applied Science and Manufacturing*, 2012;43:1187–96.

[58] Vanlandingham M.R., Eduljee R.F. and Gillespie J.W. "Relationships between Stoichiometry, Microstructure, and Properties for Amine-Cured Epoxies" 2001:699–712.

[59] Yosomiya R., Morimoto K., Nakajima A., Ikaka Y. and Suzuki T. Adhesion and Bonding in Composites. Taylor & Francis; 1989.

[60] Arao Y., Koyanagi J., Hatta H. and Kawada H. "Analysis of Time-Dependent Deformation of CFRP Considering the Anisotropy of Moisture Diffusion". *Advanced Composite Materials*, 2008;17:359–72.

[61] Aktas L., Hamidi Y.K. and Altan M.C. "Combined Edge and Anisotropy Effects on Fickian Mass Diffusion in Polymer Composites". *Journal of Engineering Materials and Technology*, 2004;126:427.

[62] Guloglu G.E., Hurdelbrink K.R., Anderson J.P. and Altan M.C. "Experimental and theoretical investigation of non-Fickian moisture absorption of quartz/BMI laminates fabricated by preconditioned prepregs" 2016;120012:120012.

[63] Glaskova T.I., Guedes R.M., Morais J.J. and Aniskevich A.N. "A comparative analysis of moisture transport models as applied to an epoxy binder". *Mechanics of Composite Materials*, 2007;43:377–88.

[64] Boukhoulda F.B., Guillaumat L., Lataillade J.L., Adda-Bedia E. and Lousdad A.

"Aging-impact coupling based analysis upon glass/polyester composite material in hygrothermal environment". *Materials and Design*, 2011;32:4080–7.

[65] Grace L.R. and Altan M.C. "Three- dimensional anisotropic moisture absorption in quartz- reinforced bismaleimide laminates". *Polymer Engineering & Science*, 2013;54:137–46.

[66] Aronhime M.T., Peng X., Gillham J.K. and Small R.D. "Effect of time- temperature path of cure on the water absorption of high Tgepoxy resins". *Journal of Applied Polymer Science*, 1986;32:3589–626.

[67] LaPlante G. and Lee-Sullivan P. "Moisture effects on FM300 structural film adhesive: Stress relaxation, fracture toughness, and dynamic mechanical analysis". *Journal of Applied Polymer Science*, 2005;95:1285–94.

[68] Liu W., Hoa S. V. and Pugh M. "Water uptake of epoxy-clay nanocomposites: Model development". *Composites Science and Technology*, 2008;68:156–63.

[69] Eslami S. and Taheri F. "Effects of perforation size on the response of perforated GFRP composites aged in acidic media". *Corrosion Science*, 2013;69:262–9.

[70] Li Y., Miranda J. and Sije H. "Moisture Diffusion Behavior in Bismaleimide Resin Subjected to Hygrotherrnal Cycling". *Polymer Engineering and Sciencengineering and Science*, 2002;42:375–81.

[71] Barink M., Mavinkurve A. and Janssen J. "Predicting non-Fickian moisture diffusion in EMCs for application in micro-electronic devices". *Microelectronics Reliability*, 2016;62:45–9.

[72] Noamen G., Nader H., Khaled E. and Ferid A.H. "Effect of filler addition and weathering conditions on the performance of PVC/CaCO3 composites". *Polymer Composites*, 2015;37:2171–83.

[73] Garg M., Sharma S. and Mehta R. "Carbon nanotube-reinforced glass fiber epoxy composite laminates exposed to hygrothermal conditioning". *Journal of Materials Science*, 2016;51:8562–78.

[74] Kotrotsos A., Vavouliotis A., Tsantzalis S. and Kostopoulos V. "Effect of CNT modified matrix of epoxy CFRPs on hydrothermal behaviour of material. Evaluation of water uptake using electrical resistance measurements". *Plastics, Rubber and Composites*, 2014;43:122–9.

[75] van Soestbergen M. and Mavinkurve A. "Anomalous water absorption by microelectronic encapsulants due to hygrothermal- induced degradation". *Journal of Applied Polymer Science*, 2014;131.

[76] Starkova O., Buschhorn S.T., Mannov E., Schulte K. and Aniskevich A. "Water transport in epoxy/MWCNT composites". *European Polymer Journal*,

2013;49:2138–48.

[77] Korobkov V.A., Krylova Y.E., Kasatkina T.B., Levashov A.S., Gorokhov R.V., Bukov N.N., et al. "Diffusion of moisture in an epoxy coating with a disperse mineral filler". *Polymer Science - Series D*, 2016;9:351–7.

[78] Drozdov A.D., Christiansen J., Gupta R.K., Shah A.P. and Virginia W. "Model for Anomalous Moisture Diffusion through a Polymer – Clay Nanocomposite" 2002:476–92.

[79] Kumar A. and Roy S. "Modeling of anomalous moisture diffusion in nanographene reinforced thermoset polymers". *Composite Structures*, 2015;122:1–7.

[80] Al-Qadhi M., Merah N. and Gasem Z.M. "Mechanical properties and water uptake of epoxy-clay nanocomposites containing different clay loadings". *Journal of Materials Science*, 2013;48:3798–804.

[81] Kawaguchi T. and Pearson R.A. "The effect of particle-matrix adhesion on the mechanical behavior of glass filled epoxies: Part 1. A study on yield behavior and cohesive strength". *Polymer*, 2003;44:4229–38.

[82] Gauvin F. and Robert M. "Durability study of vinylester/silicate nanocomposites for civil engineering applications". *Polymer Degradation and Stability*, 2015;121:359–68.

[83] Jefferson G.D., Farah B., Hempowicz M.L. and Hsiao K.T. "Influence of hygrothermal aging on carbon nanofiber enhanced polyester material systems". *Composites Part B: Engineering*, 2015;78:319–23.

[84] Shen L., Phang I.Y., Chen L., Liu T. and Zeng K. "Nanoindentation and morphological studies on nylon 66 nanocomposites. I. Effect of clay loading". *Polymer*, 2004;45:3341–9.

[85] Haque A., Shamsuzzoha M., Hussain F. and Dean D. "S2-glass/epoxy polymer nanocomposites: Manufacturing, structures, thermal and mechanical properties". *Journal of Composite Materials*, 2003;37:1821–38.

[86] Hosur M., Mahdi T.H., Islam M.E. and Jeelani S. "Mechanical and viscoelastic properties of epoxy nanocomposites reinforced with carbon nanotubes, nanoclay, and binary nanoparticles". *Journal of Reinforced Plastics and Composites*, 2017;36:667–84.

[87] Lei Y., Wu Q., Clemons C.M., Yao F. and Xu Y. "Influence of nanoclay on properties of HDPE/wood composites". *Journal of Applied Polymer Science*, 2007;106:3958–66.

[88] Haq M., Burgueño R., Mohanty A.K. and Misra M. "Hybrid bio-based composites from UPE/EML blends, natural fibers, and nanoclay". *Macromolecular Materials*

and Engineering, 2014;299:1306–15.

[89] Costa M.L., De Almeida S.F.M. and Rezende M.C. "Critical Void Content for Polymer Composite Laminates". *AIAA Journal*, 2005;43:1336–41.

[90] Loos A.C. and Springer G.S. "Curing of Epoxy Matrix Composites". *Journal of Composite Materials*, 1983;17:135–69.

[91] Harper B.D., Staab G.H. and Chen R.S. "A Note on the Effects of Voids Upon the Hygral and Mechanical Properties of AS4/3502 Graphite/Epoxy". *Journal of Composite Materials*, 1987;21:280–9.

[92] de Almeida S.F.M. and Neto Z.D.S.N. "Effect of Void Content on the Strength of Composite Laminates". *Composite Structures*, 1994;28:139–48.

[93] Liu H., Cui H., Wen W., Su X., Kang H. and Engler-Pinto C. "The effect of voids on the quasi-static tensile properties of carbon fiber/polymer-laminated composites". *Journal of Composite Materials*, 2017.

[94] Zhang A., Lu H. and Zhang D. "Effects of voids on residual tensile strength after impact of hygrothermal conditioned CFRP laminates". *Composite Structures*, 2013;95:322–7.

[95] Costa M.L., Rezende M.C. and De Almeida S.F.M. "Strength of hygrothermally conditioned polymer composites with voids". *Journal of Composite Materials*, 2005;39:1943–61.

[96] Lu Z., Xian G. and Li H. "Effects of thermal aging on the water uptake behavior of pultruded BFRP plates". *Polymer Degradation and Stability*, 2014;110:216–24.

[97] Bao L.R. and Yee A.F. "Moisture diffusion and hygrothermal aging in bismaleimide matrix carbon fiber composites: Part II-woven and hybrid composites". *Composites Science and Technology*, 2002;62:2111–9.

[98] Ahern A., Verbist G., Weaire D., Phelan R. and Fleurent H. "The conductivity of foams: A generalisation of the electrical to the thermal case". *Colloids and Surfaces A: Physicochemical and Engineering Aspects*, 2005;263:275–9.

[99] Amaral C., Vicente R., Ferreira V.M. and Silva T. "Polyurethane foams with microencapsulated phase change material: Comparative analysis of thermal conductivity characterization approaches". *Energy and Buildings*, 2017;153:392–402.

[100] Yuan H., Xiong Y., Luo G., Li M., Shen Q. and Zhang L. "Microstructure and electrical conductivity of CNTs/PMMA nanocomposite foams foaming by supercritical carbon dioxide". *Journal Wuhan University of Technology, Materials Science Edition*, 2016;31:481–6.

[101] Vizzini A.J. "Lightweight Sandwich Structures". *Aerospace Engineering*, 2010:1–10.

[102] Mouritz A.P. "Ultrasonic and Interlaminar Properties of Highly Porous Composites". *Journal of Composite Materials*, 2000;34:218–39.

[103] Huo Z., Mohamed M., Nicholas J.R. and Wang X. "Experimentation and simulation of moisture diffusion in foam-cored polyurethane sandwich structure". *Journal of Sandwich Structures and Materials*, 2016;18:30–49.

[104] Gueribiz D., Rahmani M., Jacquemin F., Fréour S., Guillen R. and Loucif K. "Homogenization of Moisture Diffusing Behavior of Composite Materials with Impermeable or Permeable Fibers — Application to Porous Composite Materials". *Journal of Composite Materials*, 2009;43:1391–408.

[105] Youssef Z., Jacquemin F., Gloaguen D. and Guillén R. "Hygro-elastic Internal Stresses in Porous Composite Materials: A Multi-scale Analysis". *Journal of Reinforced Plastics and Composites*, 2007;26:1865–80.

[106] Bennacer R., Mohamad A.A. and El Ganaoui M. "Analytical and numerical investigation of double diffusion in thermally anisotropy multilayer porous medium". *Heat and Mass Transfer/Waerme- Und Stoffuebertragung*, 2005;41:298–305.

[107] Prakotmak P., Soponronnarit S. and Prachayawarakorn S. "Modelling of moisture diffusion in pores of banana foam mat using a 2-D stochastic pore network: Determination of moisture diffusion coefficient during adsorption process". *Journal of Food Engineering*, 2010;96:119–26.

[108] Chen L., Chu H.W. and Fan X. "A convection-diffusion porous media model for moisture transport in polymer composites: Model development and validation". *Journal of Polymer Science, Part B: Polymer Physics*, 2015;53:1440–9.

[109] Piggott M. and Woo M. "Water Absorption of Resins and Composites: IV. Water Transport in Fiber Reinforced Plastics". *Journal of Composites, Technology and Research*, 1988;10:20–4.

[110] Crank J. "the Mathematics of Diffusion" 1975.

[111] Blikstad R. "Three-Dimensional Moisture Diffusion in Graphite / Epoxy Laminates Pthin" 1986;5:9–18.

[112] Aronhime M.T., Neumann S. and Marom G. "The anisotropic diffusion of water in Kevlar-epoxy composites". *Journal of Materials Science*, 1987;22:2435–46.

[113] Pierron F., Poirette Y. and Vautrin A. "A Novel Procedure for Identification of 3D Moisture Diffusion Parameters on Thick Composites: Theory, Validation and Experimental Results". *Journal of Composite Materials*, 2002;36:2219–43.

[114] Weitsman Y. "Diffusion With Time-Varying Diffusivity, With Application to Moisture-Sorption in Composites". *Journal of Composite Materials*, 1976;10:193–204.

[115] Gersappe D. "Molecular Mechanisms of Failure in Polymer Nanocomposites". *Physical Review Letters*, 2002;89:1–4.

[116] Shah D., Maiti P., Jiang D.D., Batt C.A. and Giannelis E.P. "Effect of nanoparticle mobility on toughness of polymer nanocomposites". *Advanced Materials*, 2005;17:525–8.

[117] Agubra V.A. and Mahesh H. V. "Environmental degradation of E-glass/nanocomposite under the combined effect of UV radiation, moisture, and rain". *Journal of Polymer Science, Part B: Polymer Physics*, 2014;52:1024–9.

[118] Bradley W. and Grant T. "The effect of the moisture absorption on the interfacial strength of polymeric matrix composites". *Journal of Materials Science*, 1995;30:5537–42.

[119] Sideridis E.P. and Bikakis G.S. "Shear properties and load–deflection response of cross–ply glass–epoxy composite short–beams subjected to three-point-bending tests, and the effect of moisture absorption". *Journal of Applied Polymer Science*, 2013;129:2244–52.

[120] Bullions T.A., Loos A.C. and McGrath J.E. "Moisture Sorption Effects on and Properties of a Carbon Fiber-reinforced Phenylethynyl-terminated Poly(etherimide)". *Journal of Composite Materials*, 2003;37:791–809.

[121] Bentzl R.W. and Neville H.A. "Water Content of Hydrophilic Phenol-Formaldehyde Resins : Vapor Pressure-Temperature Relationships" 1949;IV:673–88.

[122] Reynolds J.G., Johnston C.T. and Agnew S.F. "A molality-based bet equation for modeling the activity of water sorbed on clay minerals". *Clays and Clay Minerals*, 2012;60:599–609.

[123] Bai J., Liao X., Huang E., Luo Y., Yang Q. and Li G. "Control of the cell structure of microcellular silicone rubber/nanographite foam for enhanced mechanical performance". *Materials and Design*, 2017;133:288–98.

[124] Park E.-S. "Mechanical properties and antibacterial activity of peroxide-cured silicone rubber foams". *Journal of Applied Polymer Science*, 2008;110:1723–9.

[125] Klempner D., Sendijarevic V. and Aseeva R.M. Handbook of polymeric foams and foam technology. Munich; Cincinnati: Hanser Publishers ; Hanser Gardener [i.e. Gardner] Publications; 2004.

[126] Verdejo R., Stämpfli R., Alvarez-Lainez M., Mourad S., Rodriguez-Perez M.A., Brühwiler P.A., et al. "Enhanced acoustic damping in flexible polyurethane foams

filled with carbon nanotubes". *Composites Science and Technology*, 2009;69:1564–9.

[127] Zhang C., Li J., Hu Z., Zhu F. and Huang Y. "Correlation between the acoustic and porous cell morphology of polyurethane foam: Effect of interconnected porosity". *Materials and Design*, 2012;41:319–25.

[128] Ridha M. and Shim V.P.W. "Microstructure and Tensile Mechanical Properties of Anisotropic Rigid Polyurethane Foam". *Experimental Mechanics*, 2008;48:763–76.

[129] Gibson L.J. and Ashby M.F. Cellular Solids: Structure and Properties. 2nd ed. Cambridge: Cambridge University Press; 1997.

[130] Chen Y., Das R. and Battley M. "Effects of cell size and cell wall thickness variations on the strength of closed-cell foams". *International Journal of Engineering Science*, 2017;120:220–40.

[131] Siriruk A., Penumadu D. and Sharma A. "Effects of Seawater and Low Temperatures on Polymeric Foam Core Material". *Experimental Mechanics*, 2012;52:25–36.

[132] Fesmire J.E., Coffman B.E., Sass J.P., Williams M.K., Smith T.M. and Meneghelli B.J. "Cryogenic Moisture Uptake in Foam Insulation for Space Launch Vehicles". *Journal of Spacecraft and Rockets*, 2012;49:220–30.

[133] Manujesh B.J., Rao V. and Aan M.P.S. "Moisture absorption and mechanical degradation studies of polyurethane foam cored E-glass-reinforced vinyl-ester sandwich composites". *Journal of Reinforced Plastics and Composites*, 2014;33:479–92.

[134] Singh A.K. and Davidson B.D. "Effects of temperature, seawater and impact on the strength, stiffness, and life of sandwich composites". *Journal of Reinforced Plastics and Composites*, 2011;30:269–77.

[135] Avilés F. and Aguilar-Montero M. "Moisture absorption in foam-cored composite sandwich structures". *Polymer Composites*, 2009;31:714–22.

[136] Earl J.S. and Shenoi R.A. "Determination of the moisture uptake mechanism in closed cell polymeric structural foam during hygrothermal exposure". *Journal of Composite Materials*, 2004;38:1345–65.

[137] Li X. and Weitsman Y.J. "Sea-water effects on foam-cored composite sandwich lay-ups". *Composites Part B: Engineering*, 2004;35:451–9.

[138] Sabbahi A. and Vergnaud J.M. "Absorption of water at 100°C by polyurethane foam" 1991;27:845–50.

[139] Georjon O. and Galy J. "Effects of crosslink density on the volumetric properties of

high Tg polyurethane networks. Consequences on moisture absorption". *Polymer*, 1998;39:339–45.

[140] Kumosa L., Benedikt B., Armentrout D. and Kumosa M. "Moisture absorption properties of unidirectional glass/polymer composites used in composite (non-ceramic) insulators". *Composites Part A: Applied Science and Manufacturing*, 2004;35:1049–63.

[141] Cotinaud M., Bonniau P. and Bunsell A.R. "The effect of water absorption on the electrical properties of glass-fibre reinforced epoxy composites". *Journal of Materials Science*, 1982;17:867–77.

[142] Wang W., Sain M. and Cooper P.A. "Study of moisture absorption in natural fiber plastic composites". *Composites Science and Technology*, 2006;66:379–86.

[143] Zhao H. and Li R.K.Y. "Effect of water absorption on the mechanical and dielectric properties of nano-alumina filled epoxy nanocomposites". *Composites Part A: Applied Science and Manufacturing*, 2008;39:602–11.

[144] Simar A., Gigliotti M., Grandidier J.C. and Ammar-Khodja I. "Evidence of thermo-oxidation phenomena occurring during hygrothermal aging of thermosetting resins for RTM composite applications". *Composites Part A: Applied Science and Manufacturing*, 2014;66:175–82.

[145] Silva L., Tognana S. and Salgueiro W. "Study of the water absorption and its influence on the Young's modulus in a commercial polyamide". *Polymer Testing*, 2013;32:158–64.

[146] Sarfaraz R., Canal L.P., Violakis G., Botsis J., Michaud V. and Limberger H.G. "An experimental-numerical investigation of hydrothermal response in adhesively bonded composite structures". *Composites Part A: Applied Science and Manufacturing*, 2015;73:176–85.

[147] Zai B.A., Park M.K., Choi H.S., Mehboob H. and Ali R. "Effect of moisture absorption on damping and dynamic stiffness of carbon fiber/epoxy composites". *Journal of Mechanical Science and Technology*, 2010;23:2998–3004.

[148] Botelho E.C., Costa M.L., Pardini L.C. and Rezende M.C. "Processing and hygrothermal effects on viscoelastic behavior of glass fiber/epoxy composites". *Journal of Materials Science*, 2005;40:3615–23.

[149] Rajeesh K.R., Gnanamoorthy R. and Velmurugan R. "Effect of humidity on the indentation hardness and flexural fatigue behavior of polyamide 6 nanocomposite". *Materials Science and Engineering A*, 2010;527:2826–30.

[150] Botelho E.C., Pardini L.C. and Rezende M.C. "Hygrothermal effects on the shear properties of carbon fiber/epoxy composites". *Journal of Materials Science*, 2006;41:7111–8.

[151] Cheour K., Assarar M., Scida D., Ayad R. and Gong X.L. "Effect of water ageing on the mechanical and damping properties of flax-fibre reinforced composite materials". *Composite Structures*, 2016;152:259–66.

[152] Nissan A.H. "H-Bond Dissociation in Hydrogen Bond Dominated Solids". *Macromolecules*, 1976;9:840–50.

[153] Bailakanavar M., Fish J., Aitharaju V. and Rodgers W. "Computational coupling of moisture diffusion and mechanical deformation in polymer matrix composites". *International Journal for Numerical Methods in Engineering*, 2014;98:859–80.

[154] Thwe M.M. and Liao K. "Effects of environmental aging on the mechanical properties of bamboo-glass fiber reinforced polymer matrix hybrid composites". *Composites - Part A: Applied Science and Manufacturing*, 2002;33:43–52.

Appendix

Material Systems	D_z (mm^2/h)	β (hr^{-1})	γ (hr^{-1})	M_∞ (wt.%)	E_0 (GPa)	$E_{@M_\infty}$ (GPa)
PA 66 [38]	1.03×10^{-3}	1.07×10^{-2}	2.96×10^{-5}	5.46	5.16	2.14
B [154]	3.77×10^{-3}	1.09×10^{-2}	6.99×10^{-6}	12.04	2.53	2.13
H1 [154]	2.02×10^{-2}	5.64×10^{-3}	1.27×10^{-2}	11.26	2.68	2.30
H2 [154]	5.92×10^{-3}	2.72×10^{-2}	2.94×10^{-2}	10.66	2.86	2.44
BM [154]	5.97×10^{-3}	3.20×10^{-2}	2.48×10^{-2}	8.91	2.99	2.67
HM1 [154]	1.63×10^{-2}	7.17×10^{-3}	1.32×10^{-2}	8.42	2.93	2.59
HM2 [154]	6.01×10^{-3}	3.19×10^{-2}	3.22×10^{-2}	9.84	3.16	2.90
Nylon 6 [4]	2.11×10^{-2}	1.23×10^{-2}	1.54×10^{-6}	3.99	2.55	0.65

Table 15. Absorption parameters of polymers used to validate the elastic modulus models